Casimir Effect and Interaction between Surface Plasmons

Francesco Intravaia

Laboratoire Kastler-Brossel **Université Pierre et Marie Curie**

Thèse de doctorat de l'Université Paris VI
Spécialité : Physique Quantique

présentée par

Francesco Intravaia

Pour obtenir le grade de DOCTEUR de l'UNIVERSITÉ PARIS 6

Effet Casimir et interaction entre plasmons de surface

Soutenue le 21 Juin 2005 devant le jury composé de :

M. Daniel BLOCH ..... *Rapporteur*
M. Jean-Michel COURTY ..... *Examinateur*
M. Jacques LAFAIT ..... *Président du jury*
Mme Astrid LAMBRECHT ..... *Directrice de thèse*
M. Roberto ONOFRIO ..... *Rapporteur*
M. Serge REYNAUD ..... *Examinateur*

Abstract-Résumé

In this thesis we discuss the influence of surface plasmons on the Casimir effect between two plane parallel metallic mirrors at arbitrary distances. Using the plasma model to describe the optical response of the metal, we express the Casimir energy as a sum of contributions associated with evanescent surface plasmon modes and propagative cavity modes. In contrast to expectations, the plasmonic mode contribution is essential at all distances in order to ensure the correct result for the Casimir energy. One of the two plasmonic modes gives rise to a repulsive contribution, balancing the attractive contributions from propagating cavity modes, while both contributions taken separately are much larger than the actual value of the Casimir energy. This also suggests possibilities to tailor the sign of the Casimir force via surface plasmons.

Keywords: Casimir Effect, vacuum fluctuations, optical networks, scattering amplitudes, hydrodynamic model, surface plasmons, logarithmic argument theorem, cavity modes, repulsive Casimir force.

Dans cette thèse on discute l'influence des plasmons de surfaces sur l'effet Casimir entre deux miroirs métalliques plans et parallèles placés à une distance arbitraire. En utilisant le model plasma pour décrire la réponse optique du métal, on exprime l'énergie de Casimir comme une somme des contributions associées aux modes évanescents relatifs aux plasmons de surface et aux modes propagatifs de la cavité. Contrairement à une ce qu'on pouvait attendre, la contribution des modes plasmoniques est essentielle à toute distance afin d'assurer le correct résultat pour l'énergie de Casimir. Un des deux modes plasmoniques génère une contribution répulsive qui compense la contribution attractive provenant des modes propagatifs de la cavité, alors que les deux contributions, prises séparément, sont beaucoup plus importantes que la valeur réelle pour l'énergie de Casimir. Cela suggère qu'il est possible d'ajuster le signe de la force de Casimir en manipulant les plasmons de surface.

Mots-clé : Effet Casimir, fluctuations du vide, réseaux optiques, amplitudes de diffusion, modèle hydrodynamique, plasmons de surface, théorème de l'argument du logarithme, modes de cavité, force de Casimir répulsive

Acknowledgements

Je vous avoue que j'ai longuement réfléchi à la langue à utiliser pour les remerciements : une thèse écrite en anglais, par un italien, dans un laboratoire français... bref, à mes yeux ce n'était pas la chose la plus évidente. Enfin, ne sachant pas me décider, en demandant conseil autour de moi et au prix de me faire traiter de frimeur j'ai décidé de faire un petit mélange...

Conversely to what one might naively think the PhD is not the result of only one person. Of course there is only one person who, during five months or more, spends all his time in front of a PC trying to explain something in the simplest, but not simplistic, manner he can do, trying to make a picture, a plot and so on. But this is only a little bit of the PhD period.

The PhD thesis is the result of a group work where more or less all the people contribute as they can to the achievement of the final goal. Each one has brought his little, medium, or huge stone to the building and I would like to thank everybody but I think that all the manuscript pages would be not enough for this.

Nevertheless, some people have played an essential role.

First of all I wish to thank very much Astrid for the scientific and the human support. She trusted in me even when I was not so confident. This stimulated me to overcome my limits and reach results I did not guess. She took with me a lot of often unusual bets, last between them the redaction in English of the manuscript. Thank you very much Astrid!

A great MERCI to Serge who supervised my work during my first year and played a crucial role in last part of it. I wish to thank him for his advices, his patience (I confess that sometimes I am very difficult to understand) and his help even during the weekend!!

I wish also to thank the remanent of my PhD board of examiners: Jacques Lafait, Jean-Michel Courty, Daniel Bloch and Roberto Onofrio. A particular thank to those last two to have been the referees of my manuscript. Grazie a Roberto per avermi sempre consigliato e sostenuto.

As I said previously the PhD thesis is the result of a work of a group of persons which has its hard core in the Fluctuation and Relativity group at the Kastler-Brossel Laboratory in the Jussieu site. With Astrid and Serge this group is composed by three PhD students and by a just confirmed permanent member (et oui!!). During my PhD I have found in these guys real friends.

Je voulais tout d'abord remercier beaucoup le plus âgé d'entre eux, Brahim (il s'avère purtant qu'il est même plus jeune que moi ! !). Il a été plus que précieux pendant toutes

mes années de thèse. Il a toujours été disponible pour tout et j'ai pu compter sur lui à chaque moment et pour n'importe quelle raison, scientifique et non.

Je remercie énormément Rémy pour m'avoir supporté dans mes petites manies (tapoter sur le bureau , faire le cents pas, etc.) mais aussi et surtout pour avoir su m'écouter quand j'avais besoin de parler pendant des moments difficiles.

Enfin merci aux deux derniers qui ont rejoint l'équipe au début de ma dernière année de thèse : François-Xavier (mieux connu comme FX !) et Guillaume avec lesquels on s'est entendu tout de suite super bien.

Le laboratoire a été pour moi une grande famille. Le climat amical qui y règne a été plus que bénéfique pour mon travail. J'ai pu trouver un répondant à tous les niveaux : techniciens, administratifs, chercheurs, doctorants, visiteurs, vraiment tous.

Évidemment c'est principalement au niveau des doctorants que j'ai tissu les liens les plus forts.

Non so come ringraziare il mitico Martino che con la sua amicizia mi ha aiutato ad attraversare uno periodo molto difficile per me. Una parsona con un cuore grande quanto una casa. Lo stesso vale per Julien (Super Juju!) che completa la piccola cricca dei dottorandi puramente teorici de la pyramide. Per quante volte l'abbia potuto disturbare non mi ha mai detto di no! Merci Juju!!!

Je voulais aussi remercier the great Sylvain in Vienna, in USA et un peu partout dans le monde, et Vincent : eux aussi ont été toujours disponibles pour un coup de main et pleins de bonnes idées.

Merci beaucoup aussi à tous les autres doctorants du laboratoire ! !

Certains chercheurs en blaguant ont suggéré d'italianiser le nom du laboratoire : Laboratorio Kastlero-Brossello, ils disent. C'est dû a la forte composante italienne de ses membres.

Tra loro Alberto, che nonostante il fatto che tifi Milan e che venga da Arcore (ognuno ha i suoi difetti!) è una persona simpaticissima, e Marco, uno spettacolare toscanaccio D.O.C.. Con loro ho diviso con piacere e per molto tempo il ghetto italiano della Torre 12. Alcuni amici transalpini hanno bravato i limiti di questo territorio con il risultato che ora parlano un franco-ritale di qualità! Tra loro Augustin, Vincent, Aurélien et Charles. Ho potuto constatare che il povero Jean che pensavo si fosse salvato invece presenta purtroppo anche lui tutti i sintomi della ritalizzazione.

Le laboratoire a été un carrefour des chemins incroyable. J'ai pu rencontrer et tisser des rapports d'amitié avec des personnes venant d'un peu partout. En particulier il y a eu Riccardo, Antonino, Sophie et en fin Estefania. Malgré leur bref séjour j'ai partagé avec eux "les joies et les douleur" d'un thésitif. Je suis particulièrement reconnaissant à Estefania et Sophie pour l'amitié qu'elles m'ont offert.

Thanks a lot to Claude, Nicolas, Thomas, Jean-Pierre, Jean-Philippe, Antoine, François, François 2, Paul, Éric-Olivier, Benoit, Amouri, Dominique and, in general, to all researchers of the laboratory for their advices, their kindness and their availability. A special thank to Michel for all he did for me.

Je voulais remercier beaucoup Monique et Laetitia pour toutes les fois (et elles sont beaucoup ! !) que j'ai imposé ma présence au secrétariat entre une marche péripatétique

et une autre, pour les cinq minutes de détente que je prenais avec elles en parlant de tout et de rien. Merci en particulier à Monique pour son amitié et pour m'avoir aidé en énormément de choses.

Merci beaucoup aussi à nos informaticiens et en particulier à Serge qui m'a dépanné un nombre incalculable de fois.

Vu que heureusement je n'ai pas passé tout mon temps au laboratoire...enfin sauf les cinq derniers mois de la thèse...bref, vu que j'avais une vie aussi au dehors de la physique je voulais remercier tout le monde qui avec son affection et son amitié m'a fourni une couette chaude dans laquelle me blottir dans les moments difficiles (et il y en a toujours dans la vie d'un thésard ! !).

Merci donc à Armelle, Cécile, Christelle, Rim, Audrey, Marco et Pauline pour l'encouragement et l'aide dans tout ce qui a concerné la gestion de l'association dont on fait tous partie. Marco il a même poussé les limite jusqu' à s'impliquer dans l'organisation de mon pot de thèse. Un gros merci aussi à Laure, que j'ai embeté pas mal de fois, mais qui n'a jamais hésité à m'aider.

Thank a lot also to Nadia and Jeff. I promise you: I am going to come to Bordeaux as soon as possible!!!

Grazie anche a Marcello che spesso mi ha accompagnato via intenet nelle lunghe giornate e serate passate davanti al pc.

Enfin je voulais remercier "le mie donne", les trois soeurs Chaib, qui pendant ces trois dernières années ont étés plus que des amies : elles ont étés ma famille. Sans elles ma vie à Paris, et ma vie tout court, aurait été très grise. Merci énormément à Kinda sans laquelle ma vie n'aurait pas été pareille et pour s'être prise la tête pour l'organisation du pot avec Jamila, Brahim, Marco, Vincent et FX.

Un grazie sentito va ai miei genitori che mi hanno sempre accordato moltissima fiducia e su cui sapevo di poter contare quando ne avevo bisogno. Anche mio fratello Ludovico è stato un valido supporto: grazie Vico!

Per finire volevo ringraziare tutti i miei amici in italia che ho sfortunatamente trascurato in questi tre anni di tesi . Grazie ragazzi !!!

Évidemment ceux que je viens de citer ne représente qu'une petite partie des personnes qui ont fait partie de ma vie de doctorant et qui donc, peut-être malgré eux, ont influencé en quelques mesure mon doctorat.

À ceux-la et à tous les autres, encore une fois, MERCI BEAUCOUP ! ! !

Francesco Intravaia
(Paris le 11 Juillet 2005)

Contents

Effet Casimir et interaction entre plasmons de surface **I**

Introduction **1**

1 The Casimir Effect and the Theory of Quantum Optical Network **9**
1.1 Introduction . . . 10
1.2 The Casimir effect in its original formulation . . . 10
1.3 Physical meaning of the regularization procedure . . . 14
1.3.1 The substraction of $\mathcal{E}(L \to \infty)$ . . . 14
1.3.2 The introduction of a cutoff function. . . . 15
1.3.3 The limitation of Casimir's approach . . . 15
1.4 The Quantum Optical Network Theory . . . 15
1.4.1 The Scattering and Transfer Matrices . . . 16
1.4.2 Elementary networks . . . 18
1.4.2.1 Reciprocity . . . 20
1.4.2.2 A useful example: The dielectric slab . . . 20
1.4.3 Quantum scattering . . . 21
1.4.3.1 Theoretical background . . . 22
1.4.3.2 Noise in scattering and transfer approach . . . 22
1.4.3.3 Composition of dissipative networks . . . 24
1.4.4 The Cavity Matrix: The Airy function . . . 25
1.5 The Casimir force: a radiation pressure difference . . . 26
1.5.1 Electromagnetic stress tensor and radiation pressure . . . 26
1.5.2 The Casimir force as an integral over real and imaginary frequencies 29
1.6 Conclusions . . . 32

2 The Casimir effect and the Plasmons **33**
2.1 Introduction . . . 33
2.2 The Casimir effect within the Hydrodynamic model of a metal . . . 34
2.2.1 The hydrodynamic model and the plasmons . . . 35
2.2.2 The metallic bulk . . . 37

2.2.3 The non-retarded zero point interaction between two bulks 41
2.3 The Casimir energy: the plasma model 44
2.3.1 The long distances limit: recovering the perfect mirrors case 46
2.3.2 The short distances limit: Coulomb interaction between surface plasmons 47
2.4 Conclusions and Comments 48

3 The Casimir energy as sum over the Cavity Frequency Modes 51
3.1 Introduction 51
3.2 The Casimir energy as a sum over the frequency modes of a real cavity . . . 53
3.3 Mode analysis with the plasma model 56
3.3.1 Equation for the cavity modes 57
3.3.1.1 Propagative modes 57
3.3.1.2 Evanescent modes 58
3.3.2 TE-modes 59
3.3.3 The TM-modes 61
3.3.3.1 The propagative modes 62
3.3.3.2 The evanescent modes 64
3.4 Conclusion and comments 67

4 Plasmonic and Photonic Modes Contributions to the Casimir energy 69
4.1 Introduction 69
4.2 Equation for the cavity modes 70
4.3 Photonic and Plasmonic modes contributions 74
4.4 The contribution of the Plasmonic modes to the Casimir energy 75
4.4.1 Convergence 75
4.4.2 Derivation of a simpler expression 76
4.4.3 Explicit calculation 77
4.5 Sum of the propagative modes and the bulk limit 83
4.6 Sum of the TE-propagative modes and asymptotic behavior 85
4.7 The difference between the TM- and TE-propagative modes 87
4.7.1 Recasting the first term of Eq.(4.7.10) 89
4.7.2 Recasting the second term of Eq.(4.7.10) 92
4.7.3 Result for $\Delta\eta_{ph}$ and asymptotic behaviors 92
4.8 Discussion of the results 94

Conclusion 101

A Complement on the general derivation of the Casimir effect 105
A.1 Regularization in Casimir's approach 105
A.2 Radiation pressure on a plane mirror 107
A.2.1 Pressure on a Mirror oriented in the (x, y)-plane. 108
A.2.2 Diagonal terms 108
A.2.3 Non-diagonal terms 109

A.2.4 Evaluation of $\pi^{\rightarrow\leftarrow}_{m,m'}$ . . . 110
A.3 The Logarithmic argument theorem . . . 111
A.3.1 Demonstration . . . 111
A.3.2 Some mathematical considerations: the branching points . . . 112

B The hydrodynamic model with boundary conditions 115
B.1 Bulk shape . . . 115
B.2 Two facing bulks . . . 118

C Complements to the mode decomposition 121
C.1 The propagative and the evanescent waves . . . 121
C.1.1 Polarization of the evanescent and propagative waves. . . . 123
C.1.2 Reflection and transmission coefficients . . . 125
C.2 The bulk approximation . . . 126
C.2.1 The contribution of the bulk region . . . 127

D Complements to the photonic and plasmonic mode contribution 131
D.1 Higher orders developments in Ω_p . . . 131
D.1.1 Analysis of the integrand of η_{ev} . . . 132
D.1.2 Alternative method . . . 132
D.1.3 Improving calculations . . . 133
D.1.4 Comparison with the previous results . . . 135
D.1.5 On the small distances behavior of $\Delta\eta_{ph}$ . . . 136
D.2 Evanescent and Propagative contribution . . . 136
D.2.1 TE-modes: no evanescent contribution . . . 137
D.2.2 TM-modes: evanescent and ordinary contribution . . . 138

Effet Casimir et interaction entre plasmons de surface

"Natura Abhorret a Vacuo"

Quand Aristote introduit sa théorie de l'"*horror vacui*" dans le quatrième livre de la "*Physique*", il ne pouvait imaginer comment le concept du "*vide*" évoluerait jusqu'à nos jours.

Le développement de la physique classique était basé sur un espace idéalisé qui pouvait être pensé comme totalement vide. Cette idéalisation classique n'a pas pu être maintenue, même en tant que cas limite, après la naissance de la mécanique statistique et de la théorie quantique. L'avènement de la théorie quantique a, en particulier, profondément changé notre conception de l'espace en nous obligeant a concevoir le "vide " comme rempli de fluctuations irréductibles de champs. Dans le contexte de la théorie quantique le vide devient un concept parfaitement bien défini.

L'idéalisation classique d'un espace absolument vide avait été déjà mise en cause dans les premiers travaux de Planck sur le rayonnement du corps noir. C'est précisément en essayant d'expliquer les propriétés de ce rayonnement que Planck introduit sa première loi en 1900 [1]. Cette loi donne l'énergie électromagnétique moyenne E par mode de fréquence ω comme l'énergie d'un photon $\hbar\omega$ multipliée par le nombre de photons n contenus dans le mode :

$$E = n\hbar\omega, \quad \text{avec} \quad n = \frac{1}{e^{\frac{\hbar\omega}{k_B T}} - 1}.$$

Cette loi est valable à l'équilibre thermodynamique à une température T, k_B et $\hbar$ étant respectivement la constante de Boltzmann et la constante de Planck. Dans la limite de température nulle, le nombre de photons par mode tend vers zéro pour toutes les fréquences. Par conséquent, en 1900 il est encore possible de considérer un espace complètement vide, sans matière ni rayonnement. Il est intéressant de remarquer que pour dériver sa première loi, Planck n'introduit aucune quantification : le fait de considérer l'énergie moyenne comme étant composée de paquets de valeur $\hbar\omega$ a été pour Planck une simple astuce mathématique, "un acte désespéré" [2] comme il l'a avoué lui-même.

Insatisfait de sa première dérivation, Planck, en 1912, dérive sa seconde loi :

$$E = \left(n + \frac{1}{2}\right)\hbar\omega.$$

La différence entre les deux formules correspond à ce que l'on appelle aujourd'hui "fluctuations du vide" ou "énergie de point zéro". Si la première loi permettait de considérer un espace vidé de rayonnement dans la limite de température nulle, la deuxième loi décrit dans la même limite un espace rempli d'une énergie résiduelle correspondant à l'énergie d'un demi photon par mode. Les travaux de Planck ont été, depuis le début, pris en considération par de nombreux physiciens : parmi eux, Einstein et Stern, ont observé que la deuxième loi, contrairement à la première, donnait le bon comportement dans la limite des hautes températures [3] :

$$\left(\frac{1}{2} + n\right)\hbar\omega = k_B T + \mathcal{O}\left(\frac{1}{T}\right) \qquad T \to \infty.$$

Debye affirme en 1914 que les fluctuations de point zéro des oscillateurs matériels doivent avoir des effets observables, en discutant les modifications des pics d'intensité de diffraction [4]. Mulliken donne la première preuve expérimentale de l'existence des fluctuations du vide en étudiant les spectres de vibration des molécules [5].

Dans un premier temps, la plupart des physiciens préfèrent attribuer les fluctuations quantiques à des objets matériels. Nernst [6] est le premier, en 1916, à affirmer clairement que de telles fluctuations doivent aussi exister pour les modes du champ électromagnétique. Par conséquent, l'idée que le vide absolu pouvait être atteint en éliminant toute la matière et en baissant la température jusqu'au zéro absolu, doit être définitivement abandonnée

Nernst fut aussi le premier à soulever un problème lié à la présence des fluctuations du vide. Le vide est rempli de fluctuations de point zéro du champ électromagnétique et correspond à l'état du champ où l'énergie est minimale. Ceci interdit l'utilisation de cette énergie dans le mouvement perpétuel, préservant ainsi les lois de la thermodynamique. Néanmoins, ceci conduit à une difficulté qu'on peut nommer "catastrophe du vide " en analogie avec la "catastrophe ultraviolette " résolue par Planck en 1900 pour le rayonnement du corps noir. En effet, quand on calcule l'énergie du vide en ajoutant les énergies $\hbar\omega/2$ de tous les modes de champ, on obtient une valeur infinie. En introduisant formellement une coupure à hautes fréquences ω_{max} sur le spectre des fluctuations du vide, on obtient pour la densité moyenne d'énergie ρ

$$\rho = \frac{\hbar}{160\pi^2 c^3}(20\omega_{\mathrm{max}}^4 + \theta^4) \quad \text{avec} \quad \theta = \frac{2\pi k_B T}{\hbar}$$

Le second terme, proportionnel à θ^4, où θ est la température mesurée comme une fréquence, est la densité d'énergie par unité de volume associée aux fluctuations thermiques dans la première loi de Planck. Cette expression est finie et correspond à la loi de Stefan-Boltzmann. Cependant, le premier terme, proportionnel à ω_{max}^4 - c'est-à-dire la densité d'énergie du vide par unité de volume - diverge quand $\omega_{max\to\infty}$. Ce problème n'est pas seulement formel : la valeur calculée est considérablement plus grande que l'énergie

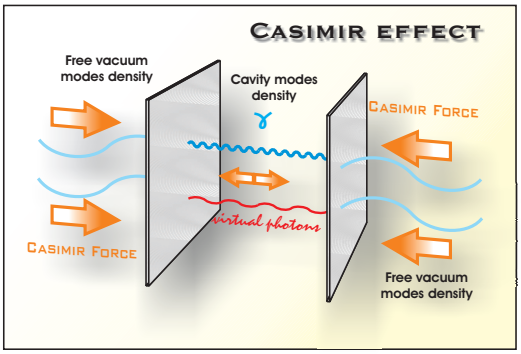

Fig. 1 : Une vision d'artiste de l'effet Casimir. Deux miroirs plan, parallèles, en face l'un de l'autre, s'attirent. L'effet Casimir résulte de la compétition entre la pression de rayonnement exercée par les fluctuations du vide à l'intérieur et à l'extérieur de la cavité.

moyenne du vide observée dans le monde qui nous entoure pour les phénomènes gravitationnels et ce, pour n'importe quel choix de la fréquence de coupure ω_{max} qui préserve les lois de la théorie quantique aux énergies où elles sont bien vérifiées [7]. Ce problème est aussi connu sous le nom de "problème de la constante cosmologique" du fait de ses connections avec le problème de la constante cosmologique dans les équations d'Einstein [8, 9].

Dans les années mêmes où une théorie quantique se construisait, London donnait une interprétation des forces de Van der Waals [10] dans les termes de la mécanique quantique [11]. Ces forces décrivent l'interaction entre des molécules ou des atomes neutres et jouent un rôle crucial dans des nombreux phénomènes biologiques et physico-chimiques. Elles déterminent en particulier l'attraction entre les colloïdes, déterminant ainsi la stabilité des protéines [12]. En étudiant spécifiquement ce problème, Overbeck observe un désaccord entre la théorie de London et ses mesures. En remarquant que la théorie de London était basée sur une interaction électromagnétique instantanée, il demande à son collègue, Henrik Casimir, d'étudier l'influence de la vitesse finie de la lumière sur les forces de Van der Waals [13]. En collaboration avec son étudiant, Dirk Polder, Casimir réussit à donner une description de la force de Van der Waals qui tenait compte des effets de retard [14]. Il comprit ensuite que son résultat pouvait être interprété en termes de fluctuations du vide [15]. Il observa de plus que les fluctuations du vide quantique pouvaient avoir des effets macroscopiques observables sur deux miroirs formant une cavité Fabry - Perot.

Casimir considère alors une cavité formée par deux miroirs parfaitement plans et parallèles entre eux (voir figure1) [16]. La surface A des miroirs est supposée beaucoup plus grande que le carré de la distance L entre eux afin de pouvoir négliger les effets de diffraction aux bords. Dans le cas de miroirs parfaitement réfléchissants, Casimir calcula que les fluctuations du vide produisent une force et une énergie égales à

$$F_{\text{Cas}} = \frac{\hbar c \pi^2 A}{240 L^4}, \quad E_{\text{Cas}} = -\frac{\hbar c \pi^2 A}{720 L^3} \quad (A \gg L^2)$$

La force de Casimir est attractive et l'énergie correspond à une énergie de liaison. Il est remarquable que dans le cas de miroirs parfaits cette force dépend uniquement des paramètres géométriques du système et de deux constantes fondamentales, la constante de Planck $\hbar$ - mettant en évidence le caractère quantique de l'effet - et la vitesse de la lumière

c. Les expressions précédentes, contrairement aux forces de van der Waals, ne dépendent pas des constantes atomiques. L'universalité de la force et de l'énergie de Casimir dans la configuration de miroirs parfaits correspond à une saturation de la réflectivité des miroirs qui ne peuvent réfléchir plus de 100% de la lumière incidente.

Même si l'effet Casimir est profondément ancré dans l'électrodynamique quantique, il existe des effets analogues en physique classique. Un exemple est illustré en 1836 dans l'*Album du Marin* [17] de P. C. Caussé (voir figure 2). Celui-ci décrit une mystérieuse force attractive entre deux bateaux placés l'un à coté de l'autre, force qui pouvait porter à des conséquences désastreuses. Récemment, Boersma [18] a suggéré une explication physique de ce phénomène en termes de différence de pression exercée par les vagues autour des deux bateaux et entre eux. L'extraordinaire découverte de H.B.G. Casimir a consisté à montrer qu'une telle force était présente même dans le vide à la température du zéro absolu.

Fig. 2 : Un analogue marin de l'effet Casimir. A l'époque des navires, les marins remarquaient que, sous certaines conditions, deux bateaux placés l'un à coté de l'autre s'attiraient mystérieusement. Ce phénomène a été expliqué en analogie avec l'effet Casimir, en 1990 seulement. (Figure tirée de ref [17])

La force de Casimir est relativement petite : ainsi, pour deux miroirs d'une surface de $1cm^2$ chacun, séparés par une distance d'un micromètre, la force est égale à $0,1\mu N$. Néanmoins, elle a été expérimentalement observée peu après sa prédiction théorique [19, 20, 21, 22, 23, 24, 25, 26, 27, 28, 29, 30, 31, 32, 33, 34, 35]. Dans les dernières années, elle a été de nouveau mesurée en exploitant des techniques expérimentales plus modernes. Beaucoup de ces expériences ont atteint une précision dans le domaine du % en mesurant, avec un pendule de torsion ou un microscope à force atomique, la force entre une surface plane et une sphère [36,37,38,39] ou encore entre deux cylindres [40]. Des expériences similaires ont été effectuées sur des systèmes micro-éléctro-mécaniques (MEMS) [41,42]. Les MEMS sont des systèmes microscopiques ou sub-microscopiques contenants des éléments métalliques mobiles. Ils sont très prometteurs au niveau technologique et ont déjà été utilisés comme senseurs de pression dans la construction des airbags. Du fait des distances très courtes entre ses composants, les MEMS sont particulièrement sensibles à la force de Casimir qui pourrait nuire à leur bon fonctionnement [43]. Dans le même temps, la force de Casimir pourrait aussi être utilisée pour les contrôler [42].

Les difficultés liées au parallélisme des deux surfaces planes rendent difficile toute mesure expérimentale de la force de Casimir dans la géométrie plan-plan. La seule expérience où ces difficultés ont été dépassées avec succès a été effectuée à l'Université de Padoue (Italie) [44]. Une revue des expériences récentes se trouve dans les références [45, 46].

Cette nouvelle génération d'expériences et la précision expérimentale accrue sont aussi à l'origine d'un renouveau des études théoriques sur l'effet Casimir. Afin de pouvoir comparer précisément théorie et expérience il faut prendre en considération les différences entre le cas

idéal considéré par Casimir et les situations expérimentales réelles. Lifshitz a été le premier à développer une théorie de l'effet Casimir entre deux miroirs diélectriques [47,48]. Depuis, un nombre croissant des travaux théoriques ont été consacrés à cet effet, dans différentes configurations [49, 50, 51, 52, 53].

La force de Casimir est la conséquence macroscopique des fluctuations du vide la plus accessible du point de vue expérimental. Mesurer l'effet Casimir signifie donc tester la théorie quantique des champs. Les problèmes liés à l'énergie du vide, expliqués plus haut constituent, donc une grande motivation pour ces tests. Une autre motivation pour une comparaison de plus en plus précise entre la théorie et l'expérience vient des théories des champs modernes de grande unification qui prédisent l'existence de nouvelles forces pour des distances entre le nanomètre et le millimètre [54, 55, 56, 57, 58, 59, 60, 61]. Pour ces distances, la force de Casimir est l'interaction la plus importante entre deux objets neutres non magnétiques. Ces nouvelles forces pourraient alors se manifester dans une comparaison entre les données expérimentales et les résultats théoriques. C'est pour cette raison que la précision, à la fois des expériences et des calculs théoriques, joue un rôle fondamental [62].

Dans un calcul précis de la force de Casimir, il faut tenir compte de la situation réelle rencontrée dans les expériences par rapport à la situation idéale étudiée par Casimir. Il considère en effet des miroirs parfaitement réfléchissants, tandis que dans la plupart des expériences on utilise des miroirs métalliques qui se comportent comme des réflecteurs presque parfaits uniquement dans le cas de fréquences inférieures à la fréquence plasma caractéristique du métal. De plus, les expériences sont effectuées à température ambiante où les effets de la pression de radiation du champ thermique se superposent à ceux des fluctuations du vide. Ces dernières années en particulier, ce dernier point a été au centre d'une vive polémique [63, 64, 65, 66, 67, 68, 69, 70, 71, 72, 73]. La plupart des mesures récentes ont été effectuées dans la géométrie plan - sphère, mais malheureusement aucun résultat exact n'est disponible pour cette géométrie. L'expression de la force est donc dérivée en utilisant l'approximation de proximité [74] qui consiste à additionner toutes les contributions correspondantes aux plans qui forment la sphère comme si elles étaient indépendantes. Etant donné qu'une des particularités de la force de Casimir est de ne pas être additive, l'hypothèse précédente n'est qu'une approximation. Les résultats disponibles dans la géométrie plan-sphère [75,76,77] montrent que l'approximation est bonne quand le rayon de la sphère est grand par rapport a la distance minimale entre le deux objets. Par contre, l'emploi de l'approximation de proximité s'avère beaucoup plus délicat pour la correction due à la rugosité des surfaces. Dans ce cas, l'approximation sous estime

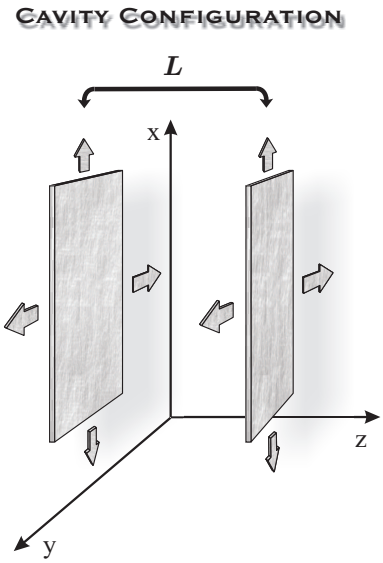

Fig. 3 : La configuration de la cavité pour le calcul de l'effet Casimir. La surface A des miroirs est supposée être très grande par rapport à la distance L entre eux afin de pouvoir négliger les effets de diffraction aux bords.

la vraie correction [45, 78, 79, 80].

Ce travail de thèse s'inscrit dans une étude de l'effet Casimir entre des miroirs métalliques et en particulier à l'étude de l'influence des plasmons de surface sur la force de Casimir.

Revenons d'abord à la formulation initiale de l'effet, donnée par Casimir lui-même : il dérive son résultat en additionnant les énergies de point zéro correspondantes aux modes propres de la cavité pour des miroirs parfaits. Dans ce cas, les fréquences propres de la cavité ont une expression relativement simple :

$$\omega_n = c\sqrt{|\mathbf{k}|^2 + \left(\frac{\pi}{L}n\right)^2} \qquad l, n = 0, 1, 2....\infty \quad \mathbf{k} \equiv (k_x, k_y)$$

Casimir rénormalisa l'énergie ainsi obtenue en soustrayant les résultats correspondants à une distance finie et infinie, en introduisant une fonction de coupure et en appliquant la formule d'Euler-Mclaurin [16, 81, 82]. Notons déjà que pour des miroirs réels, les fréquences propres de la cavité ont généralement une expression mathématiquement compliquée et ne sont pas connues sous une forme explicite.

Lifshitz fut le premier à donner une formulation alternative de l'effet Casimir [47, 48]. La dérivation qu'il en donna présente l'inconvénient de n'être valable que dans le cas de miroirs non dissipatifs. Depuis, de nombreuses formulations et généralisations de l'effet ont été proposées.

Dans la première partie de cette thèse, je décris la dérivation de l'énergie et de la force de Casimir dans le cadre de la théorie des Réseaux Optiques Quantiques [83, 84]. Cette méthode est basée sur le fait que les fluctuations du vide quantique obéissent aux lois de l'optique. Ainsi les diffuseurs peuvent être simplement caractérisés par leurs amplitudes de diffusion et nous pouvons utiliser des matrices de diffusion et de transfert afin de calculer la transformation des fluctuations du vide par des réflexions successives sur les miroirs. En suivant cette procédure on peut dériver les relations de commutation des champs à l'intérieur de la cavité en fonction des propriétés des champs libres à l'extérieur. La force de Casimir peut ainsi être déduite comme la différence des pressions de radiation entre les faces externe et interne des miroirs. La force peut s'écrire comme une intégrale régulière sur toutes les fréquences ω et les vecteurs d'onde transverses $\mathbf{k}$ d'une expression qui contient les coefficients de réflexion des miroirs de la cavité. Le résultat final pour la force et l'énergie de Casimir est obtenu en sommant sur les deux polarisations du champ $p = TE,\ TM$:

$$F = A\frac{\hbar}{\pi}\sum_p \int_{\mathbb{R}^2} \frac{d^2\mathbf{k}}{(2\pi)^2} \int_0^\infty d\omega\ Im\left[\kappa \frac{r_{\mathbf{k}}^p[\omega]^2 e^{-2\kappa L}}{1 - r_{\mathbf{k}}^p[\omega]^2 e^{-2\kappa L}}\right]$$

$$E = A\frac{\hbar}{2\pi}\sum_p \int_{\mathbb{R}^2} \frac{d^2\mathbf{k}}{(2\pi)^2} \int_0^\infty d\omega\ Im\left[\ln\left(1 - r_{\mathbf{k}}^p[\omega]^2 e^{-2\kappa L}\right)\right]$$

avec $\kappa = \sqrt{|\mathbf{k}|^2 - \omega^2/c^2}$. La formule finale a une portée plus générale que le résultat de Lifshitz et peut être légitimement utilisée avec des coefficients de réflexion dissipatifs.

La dérivation de l'effet Casimir à travers la théorie des réseaux optiques montre clairement l'importance des ondes évanescentes dans la dérivation du résultat final [85]. Les ondes évanescentes contribuent au même titre que les ondes propagatives à la pression de rayonnement et donc à la force et à l'énergie de Casimir. Elles jouent un rôle essentiel dans la détermination de l'effet dans le cas des miroirs réels.

Afin de calculer la force de Casimir, il faut maintenant connaître les coefficients de réflexion des miroirs, liés aux propriétés des matériaux utilisés. Les miroirs métalliques sont souvent décrits par le modèle hydrodynamique [86,87,88] que j'expose dans le chapitre 2 de cette thèse. Ce modèle décrit un métal comme un gaz d'électrons libres sur un fond d'ions positifs statiques [89] conduisant à une fonction diélectrique $\epsilon[\omega]$

$$\epsilon[\omega] = 1 - \frac{\omega_p^2}{\omega^2}$$

où ω_p est la fréquence de plasma du métal. Même si ce modèle n'est pas suffisant pour expliquer tous les comportements d'un métal, à cause de sa simplicité même, il se révèle particulièrement adéquat pour une description qualitative de l'effet Casimir.

En moyenne, le système est neutre mais il est possible, par exemple à cause des fluctuations thermiques, qu'apparaisse localement un excès de charge. L'effet combiné de l'attraction/répulsion électrique et de l'énergie cinétique des électrons peut donner lieu à des oscillations dans le gaz électronique. Ces oscillations, appelées oscillations de plasma, génèrent un champ électromagnétique qui peut coupler la dynamique du gaz à l'intérieur du métal avec celle d'un autre métal placé en face du premier. Il en résulte donc une interaction et donc une force entre les deux métaux. En appliquant les conditions aux limites spatiales du système, le model hydrodynamique prévoit que le gaz électronique vibre comme une superposition de modes normaux appelés plasmons [86,87,88]. Ces plasmons se divisent en plasmons de *bulk* et plasmons de surface, ces derniers étant fortement localisés à l'interface entre le métal et le vide [86]. Ces vibrations peuvent être quantifiées de façon équivalente au champ électromagnétique.

La mécanique quantique fournit une source de fluctuations intrinsèque aux oscillations de plasma présente même au zéro absolu. A courtes distances, on montre que la force qui s'exerce entre les deux métaux peut être dérivée du décalage de l'énergie de point zéro des plasmons de surface, induit par leur couplage coulombien [86, 87, 88]. Ce décalage est mesuré par rapport à la configuration où les deux métaux sont placés à une distance infinie où ils n'interagissent pas. A une distance infinie, les fréquences des plasmons de surface couplés, ω_+ et ω_-, tendent vers la fréquence du plasmon de surface d'un métal isolé ω_{sp},

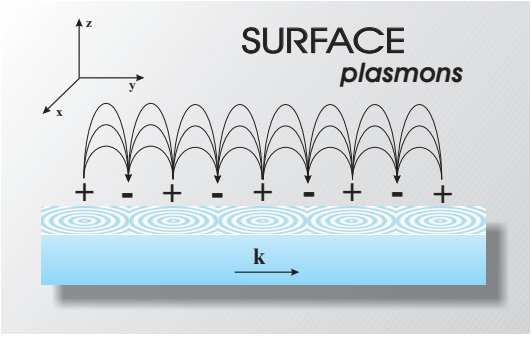

Fig. 4 : Une vision d'artiste des plasmons de surface à l'interface vide/metal.

$$E = cA \int \frac{d^2\mathbf{k}}{(2\pi)^2} \frac{\hbar}{2} \left[\omega_+ + \omega_-\right]_{L\to\infty}^{L} = cA \int \frac{d^2\mathbf{k}}{(2\pi)^2} \frac{\hbar}{2} \left(\omega_+ + \omega_- - 2\omega_{sp}\right)$$

où $\omega_{sp}^2 = \omega_p^2/2$ et $\omega_\pm^2 = \omega_{sp}^2 \left(1 \pm e^{-|\mathbf{k}|L}\right)$. Je montrerai plus loin, en utilisant le modèle plasma, que cette énergie n'est rien d'autre que l'énergie de Casimir établissant ainsi une interprétation de l'effet à l'interface entre la physique de la matière condensée et la théorie des champs [81]. Naturellement, cette connexion est seulement possible dans le cadre d'une théorie qui considère les propriétés réelles des miroirs.

Dans la dernière partie du second chapitre, j'étudie quelques caractéristiques de la force de Casimir entre deux miroirs métalliques décrits par le modèle plasma. A courtes distances, à savoir pour $L \ll \lambda_p$ où λ_p est la longueur d'onde plasma du métal, la force et l'énergie de Casimir sont proportionnelles respectivement à L^{-3} et L^{-2} [90,91]. Ceci est dû au fait qu'à courte distance le comportement à haute fréquence des miroirs est dominant. Or, tout miroir réel devient transparent à haute fréquence et par conséquent la force de Casimir est beaucoup plus petite entre deux miroirs réels qu'entre deux miroirs parfaits. Par contre, à longue distance, $L \gg \lambda_p$, la formule obtenue à travers la théorie des réseaux optiques restitue le résultat des miroirs parfaits et donc une dépendance en L^{-4} pour la force et en L^{-3} pour l'énergie. Ce changement de loi de puissance vérifiée expérimentalement rappelle le changement analogue dans les interactions de Casimir-Polder entre atomes. Finalement, dans la limite des courtes distances l'expression intégrale de l'énergie de Casimir retrouve une forme qui rappelle la formulation originale de l'effet Casimir comme étant la somme sur l'énergie de point zéro des modes de la cavité. Or, il s'avère qu'à courte distance, les seuls modes propres de la cavité qui donnent une contribution à l'énergie sont les plasmons de surface. Ceux-ci donnent lieu à des ondes évanescentes, tandis que la contribution des ondes propagatives peut être négligée à courte distance. Ceci met encore une fois en évidence le rôle important des ondes évanescentes pour l'effet Casimir.

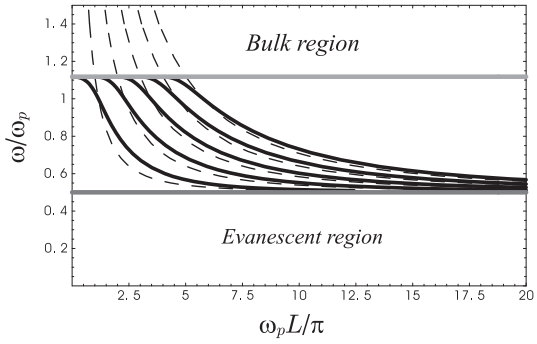

Fig. 5 : Les fréquences des modes propagatifs pour la polarisation TM dans le cas des miroirs métalliques décrits par le modèle plasma. Les courbes par traits représentent les modes, dans le cas des miroirs parfaits.

Dans la suite de ma thèse, je généralise ces arguments pour des distances arbitraires. Dans le troisième chapitre, je calcule les modes propres d'une cavité faite par deux miroirs métalliques décrits par le modèle plasma. Comme je l'ai dit précédemment, les fréquences propres ne sont plus, dans ce cas, connues sous une forme explicite. Les figures 5 et 6 montrent une analyse graphique de modes propagatifs de la cavité pour les deux polarisations TM et TE en fonction de la longueur de la cavité. Les courbes en traits correspondent aux modes propres pour des miroirs parfaits. Il apparaît clairement que les modes entre deux miroirs métalliques sont déplacés par rapport au cas idéal. Par ailleurs, leurs fréquences maximales sont bornées du fait de la transparence, à hautes fréquences,

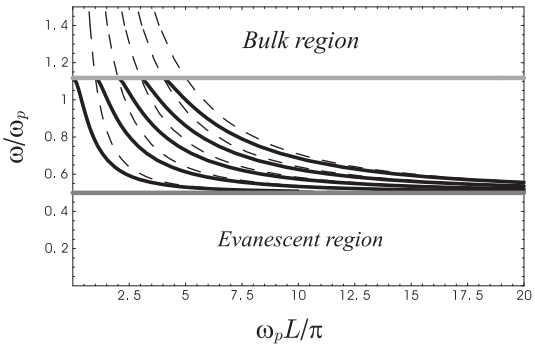

Fig. 6 : Les fréquences des modes propagatifs pour la polarisation TE dans le cas des miroirs métalliques décrits par le modèle plasma. Les courbes par traits représentent les modes dans le cas des miroirs parfaits.

des miroirs réels. En plus des modes propagatifs, il existe aussi deux modes évanescents, nommés ω_+ et ω_-, qui sont les généralisations des plasmons de surfaces sur régime retardé, c'est-à-dire pour des distances arbitraires. La figure 7 montre leurs fréquences en fonction de la longueur de la cavité L. Le mode ω_- reste borné au secteur évanescent,

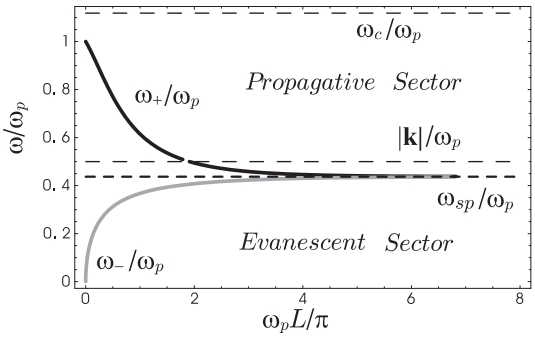

Fig. 7 : Représentation des deux modes plasmoniques ω_+ et ω_- en fonction de la longueur de la cavité. Le mode ω_- reste borné dans le secteur évanescent, tandis que le mode ω_+ est propagatif ou évanescent en fonction de L. Pour $L \to \infty$ les fréquences des deux modes dégénèrent et deviennent égales a la fréquence du plasmon de surface d'un métal isolé ω_{sp}.

tandis que le mode ω_+ est propagatif ou évanescent en fonction de L et $\mathbf{k}$. La classification en terme de modes propagatifs et évanescent n'est plus adaptée au vu des propriétés du mode ω_+. Les modes ω_- et ω_+ n'ont pas d'équivalent dans le cas de miroirs parfaits. Les modes photoniques ont la caractéristique d'être propagatifs quelle que soit la distance et ils tendent vers les fréquences des modes propres des miroirs parfaits dans la limite des longues distances. Cette décomposition en modes propres, me permet de généraliser, dans le quatrième chapitre, la formulation originale de Casimir pour des miroirs parfaits aux miroirs métalliques. Il m'est ainsi possible d'écrire l'énergie de Casimir comme une somme de l'énergie de point zéro sur tous les modes de la cavité à une distance L, en faisant ensuite la différence avec la même énergie obtenue à une distance qui tend vers l'infini

$$E = \sum_{p,\mathbf{k}} \left[\sum_n \frac{\hbar\omega_n^p}{2} \right]_{L\to\infty}^{L} = \underbrace{\sum_{\mathbf{k}} \left[\frac{\hbar\omega_+}{2} + \frac{\hbar\omega_-}{2} \right]_{L\to\infty}^{L}}_{\text{Contribution plasmonique } (E_{pl})} + \underbrace{\sum_{p,\mathbf{k}} \left[\sum_n \frac{\hbar\omega_n^p}{2} \right]_{L\to\infty}^{L}}_{\text{Contribution photonique } (E_{ph})}$$

La somme sur les modes propres se sépare ensuite en une somme sur les modes plasmoniques et une somme sur les modes photoniques.

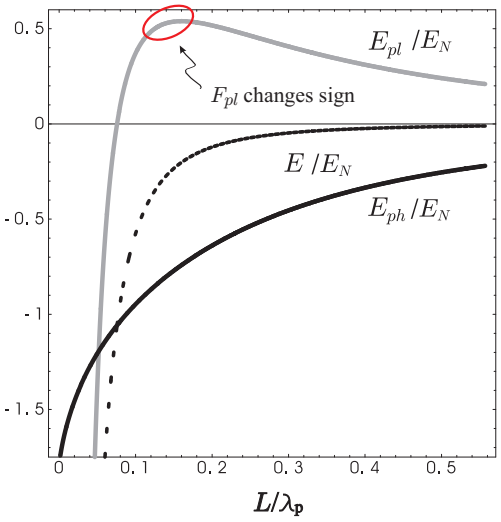

Fig. 8 : L'énergie plasmonique E_{pl}, photonique E_{ph} et l'énergie Casimir totale E normalisées par la valeur $E_N = (2\pi)^3 \frac{\hbar c \pi^2 A}{720 \lambda_p^3}$. E_{pl} montre un maximum pour $L/\lambda_p \sim 0.16$ (la force correspondante F_{pl} change de signe). L'énergie photonique E_{ph}, au contraire, tend de façon monotone à zéro (La force correspondante F_{ph} reste toujours attractive).

Dans la partie finale de cette thèse, je développe une technique pour calculer ces deux contributions séparément. Le résultat de cette analyse est illustré dans la figure 8. Elle montre que, dans la limite des courtes distances, l'effet Casimir est dominé par la contribution des modes plasmoniques ce qui confirme l'interprétation de l'effet comme interaction électrostatique entre les plasmons de surfaces. Le comportement asymptotique de l'énergie plasmonique, dans la limite des courtes distances, montre exactement le même changement des lois de puissance comme commenté précédemment. La contribution des modes photoniques est proportionnelle à $(L/\lambda_p)^3$ et elle peut être négligée au niveau de 1% jusqu'à $L/\lambda_p \sim 0.2$. A des distance plus grandes, l'énergie photonique E_{ph} augmente tandis que l'énergie plasmonique E_{pl} devient positive et change de pente à une distance de l'ordre $L/\lambda_p \sim 1/4\pi$: ceci correspond à une contribution répulsive à la force de Casimir.

Je démontre que ce comportement vient du mode ω_+, dont la contribution à la force de Casimir est répulsive à toute distance. Par exemple, pour $L \approx \lambda_p$, les contributions plasmonique et photonique à l'énergie de Casimir sont toutes les deux environ 36 fois plus grandes que l'énergie de Casimir totale, obtenue comme somme des deux contributions. Les deux contributions ont un signe opposé et la contribution photonique est légèrement plus grande que la contribution plasmonique. Il en résulte une énergie de Casimir totale toujours attractive, venant d'une compensation entre une énergie photonique négative et une énergie plasmonique positive. Ces résultats montrent clairement l'importance cruciale des plasmons de surface non seulement à courtes distances où ils dominent l'effet Casimir mais aussi à longues distances. Par conséquent, pour des miroirs métalliques, les plasmons de surface ne correspondent pas à une correction comme il a été suggéré en [92]. Un seul mode plasmonique assure la consistance de la force entre des miroirs métalliques avec son expression pour les miroirs parfaits. Si l'effet Casimir avait été calculé en considérant seulement les modes photoniques, on aurait obtenu un résultat complètement différent de la valeur réelle. L'énergie de Casimir résulte donc d'une fine compétition entre la contribution plasmonique et photonique.

La dérivation de l'effet Casimir en termes de réseaux optiques a aussi permis de montrer que la force de Casimir entre deux miroirs plans et parallèles est toujours attractive [84], correspondant donc à une énergie de liaison. Les résultats de ma thèse laissent espérer de pouvoir changer le signe de la force en modifiant la géométrie afin d'amplifier la contribution plasmonique par rapport à la contribution photonique. Ceci peut s'envisager par exemple en utilisant des miroirs avec des surfaces nano-structurées ou des surfaces avec des réseaux de trous qui ont été récemment utilisées pour amplifier la transmission de la lumière à travers des structures métalliques [93, 94, 95]. Il est clair qu'un tel changement dans le signe de la force de Casimir serait d'intérêt considérable dans la technologie des MEMS [42, 43].

Casimir Effect and Interaction between Surface Plasmons

Introduction

"Natura Abhorret a Vacuo"

When in the fourth book of the "*Physics*" Aristotle discussed his theory of the "*horror vacui*" he could not have imagined how the concept of vacuum would change over the time until nowadays.

The development of classical physics was based on the idealization that space can be thought as being absolutely empty. This classical idealization could not be maintained, not even as a limiting case, when it was realized that space is always filled with freely propagating radiation fields after the birth of statistical mechanics and then of quantum mechanics. Indeed, the advent of the quantum theory has deeply changed our idea of empty space by obliging us to conceive the vacuum as filled with quantum fluctuations of the electromagnetic field. In quantum theory, vacuum becomes a well defined notion.

The classical idealization of space as being absolutely empty was already affected by the advent of statistical mechanics when it was realized that space is filled with blackbody radiation which exerts a pressure on the boundaries of any cavity. It is precisely to explain the properties of blackbody radiation that Planck introduces his first law in 1900 [1]. In modern terms this law gives the energy E per electromagnetic field mode as the product of the energy of a photon $\hbar\omega$ by a number of photons n per mode

$$E = n\hbar\omega, \quad \text{with} \quad n = \frac{1}{e^{\frac{\hbar\omega}{k_B T}} - 1}.$$

This law is valid at thermodynamic equilibrium at a temperature T, k_B is the Boltzmann constant and $\hbar$ the Planck constant. The number of photons per mode tends towards zero for all frequencies in the limit of zero temperature. In 1900, it is thus still possible to consider a completely empty space, disencumbered by pumping of all matter, then of any radiation by lowering the temperature towards the absolute zero. In order to give this law "a real physical meaning" (citations in this paragraph are from [2]), Planck begun what he later described as a "a few weeks of the most strenuous work of my life" which culminated in the birth of the quantum theory. Historically, it is amusing that in his derivation he did not introduce any quantization of radiation or matter. The idea that the energy was split into discrete packets of value $\hbar\omega$ was for Plank a simple mathematical device, an "act of desperation" needed to derive the previous formula.

Unsatisfied with his first derivation, Planck resumed his work in 1912 and derived a different result where the energy contains an extra term [96]

$$E = \left(\frac{1}{2} + n\right)\hbar\omega$$

The difference between these two laws of Planck is precisely what we call today "vacuum fluctuations" or "zero point fluctuations". Whereas the first law describes a cavity entirely emptied out of radiation in the limit of zero temperature, the second law tells us that there remain field fluctuations corresponding to half the energy of a photon per mode. The history of the two Planck laws and the debates they generated are discussed in a certain number of articles [2,97,98,99]. It is interesting to recall that many physicists took Planck's work very seriously right from the beginning. Among them, Einstein and Stern noticed already in 1913 that the second Planck law, in contrast to the first, has the correct classical limit at high temperature [3]

$$\left(\frac{1}{2} + n\right)\hbar\omega = k_B T + \mathcal{O}\left(\frac{1}{T}\right) \qquad T \to \infty.$$

Debye affirms in 1914 that zero point fluctuations must also have observable effects on material oscillators by discussing their effect on the intensities of diffraction peaks [4]. Mulliken provides in 1924 the first experimental evidence of these fluctuations by studying vibration spectra of molecules [5]. The majority of physicists preferred to attribute quantum fluctuations to material oscillators rather than to fields. Of course, Einstein constitutes an exception with his famous paper of 1905 on the nature of radiation [100], his description of the photon statistics [101] or of the atomic emission and absorption coefficients [102] (see [103] for a discussion of these contributions) up to the discovery of the Bose-Einstein statistics in 1924 [104, 105, 106]. Nernst has to be credited as being the first in 1916 to affirm clearly that zero point fluctuations must also exist for the modes of the electromagnetic field [6], which dismisses the classical idea that absolutely empty space exists and may be attained by removing all matter from an enclosure and lowering its temperature down to zero. At this point we may emphasize that these discussions took place before the existence of vacuum fluctuations was confirmed by a fully consistent quantum theory [107, 108, 109].

We now come to a serious difficulty which Nernst noticed already in his 1916 paper. Vacuum is permanently filled with electromagnetic field fluctuations and it corresponds to the field state where the energy of field fluctuations is minimal. This prevents us from using this energy to build up perpetual motions violating the laws of thermodynamics. However, this leads to a serious problem which can be named "vacuum catastrophe" in analogy to the "ultraviolet catastrophe", this latter being solved by Planck in 1900 for blackbody radiation. When the total energy of quantum vacuum is calculated by adding the energies of all field modes in the vacuum state, an infinite value is obtained. When a high frequency cutoff ω_{max} is introduced, the energy density ρ reads

$$\rho = \frac{\hbar}{160\pi^2 c^3}(20\omega_{max}^4 + \theta^4) \quad \text{with} \quad \theta = \frac{2\pi k_B T}{\hbar}$$

The first term, proportional to ω_{max}^4 is the vacuum energy density per unit volume and it diverges when $\omega_{max} \to \infty$. The second term is the Stefan Boltzmann energy density of blackbody radiation at a temperature θ measured as a frequency. This terms is proportional to θ^4 and it remains always finite. The divergence of the cutoff term is not a mere formal difficulty. In fact, the calculated vacuum energy density is tremendously larger than the mean vacuum energy observed in the world around us through gravitational phenomena. And this is not only true when ω_{max} is chosen as the Planck frequency. The problem persists for any value of the cutoff which preserves the laws of quantum theory at the energies where they are well tested.

Vacuum energy should as any energy in general relativity contribute to the gravitational field. Supposing the universe to be filled with vacuum fluctuations, they should therefore produce for example an effect on planetary motion. As a consequence, astrophysical and cosmological observations can be used to impose an upper bound for the vacuum energy density. The limiting value which can be deduced in this manner is by many orders of magnitude smaller than the theoretical prediction using a reasonable cutoff frequency. The discrepancy is such that it is sometimes called the largest discrepancy ever observed in physics [7]. This problem is know as the "cosmological constant problem" because of its obvious connection with the introduction of a cosmological constant in Einstein's gravitation equations [8,9]. It has remained unsolved during the twentieth century despite considerable efforts for proposing solutions [110].

In these same years when a self consistent quantum theory is built up, London [11] gives a quantum interpretation of the interaction forces between neutral atoms or molecules, which were known since the work of Van der Waals [10]. Van der Waals forces are important for a great number of phenomena. They play a crucial role in biology, in adhesion processes or in the chemistry of colloids, where the van der Waals attraction between colloids determines the stability properties [12]. While studying this subject, Overbeek observed a disagreement between the London theory and his measurements. Noticing that the London theory is based on instantaneous interactions, he asks his colleague Henrik Casimir to study the influence of a finite speed of light on the Van der Waals force [13]. With Dirk Polder, Casimir gives a complete expression of the Van der Waals force taking into account retarded interaction due to the finite field propagation velocity [14]. Very quickly, Casimir realizes that his results can be interpreted by starting from the concept of vacuum fluctuations [15]. Prolonging his analysis, Casimir observes that vacuum fluctuations should also produce observable physical effects on macroscopic mirrors thus predicting for the first time a macroscopic mechanical effect of vacuum fluctuations [16].

Casimir considered a cavity formed by two perfectly plane parallel mirrors facing each other as shown in figure 9. The surface A of the mirrors is supposed much larger than the square of the distance L in order to be able to neglect any effect of diffraction on the edges of the mirrors. Considering the special case of perfectly reflecting mirrors, Casimir calculates the mechanical force exerted by vacuum fluctuations on these mirrors and obtains the following expressions for the force and the energy

$$F_{\text{Cas}} = \frac{\hbar c \pi^2 A}{240 L^4}, \quad E_{\text{Cas}} = -\frac{\hbar c \pi^2 A}{720 L^3} \quad \left(A \gg L^2\right)$$

The Casimir force is an attractive force and the Casimir energy a binding energy. It is interesting to note that in this ideal case of the perfectly reflective mirrors, the expressions of the force and energy depend only on geometrical parameters and two fundamental constants: the speed of the light c and the Planck's constant $\hbar$, the latter clearly showing the quantum character of the Casimir effect. These expressions are independent of atomic constants in contrast to the Van der Waals forces. This universality property of the Casimir force and energy between two perfectly reflecting mirrors corresponds, as shown by Lifshitz [47, 48], to the saturation of the mirrors response which cannot reflect more than 100% of the incident field.

Although the Casimir effect is deeply rooted in quantum field theory, there are analogous effects in classical physics. A striking example is discussed in 1836 by P.C. Caussée in his *L'Album du Marin* [17] (see fig.10). Caussée there reports a mysteriously strong attractive force that can arise between two ships floating side by side - a force that can lead to disastrous consequences. A physical explanation of this force was recently offered by Boersma [18] who suggested that it has its origin in a pressure difference exerted by the sea waves between the ships and around them.

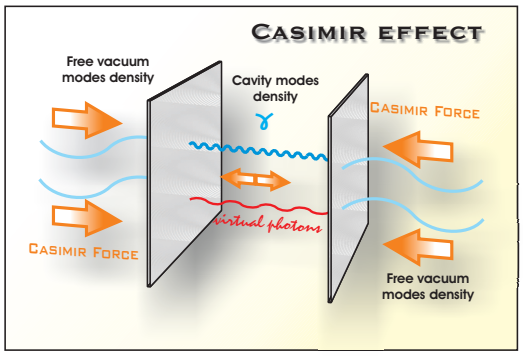

Figure 9 : An artist view of the Casimir effect. Two flat plan parallel mirrors, which are facing each other in quantum vacuum, are attracted to each other. As we will see later, the Casimir effect is the result of the competition between the intracavity and external vacuum radiation pressure. The intracavity spectral density is modified by the presence of the mirrors with respect to the external one.

The Casimir force is comparably small: for two mirrors with a surface of 1cm^2, separated by a distance of 1μm, it equals 0.1μN. Nevertheless, it was observed experimentally shortly after its theoretical prediction [19, 20, 21, 22, 23, 24, 25, 26, 27, 28, 29, 30, 31, 32, 33, 34, 35]. During the last years, it has been remeasured with modern experimental techniques. Several experiments reached an accuracy in the % range by measuring the force between a plane and a sphere [36,37,38,39] or two cylinders [40] using either torsion-pendula or atomic force microscopes. Similar experiments were also performed with Micro-Electro-Mechanical Systems (MEMS) [41, 42]. MEMS are tiny devices containing metallic elements on a micron and submicron scale. They have very promising performances being already used as pressure sensors in air-bags. Due to the small distances between its elements, the Casimir force becomes very important for these systems. It may for example produces sticking between them [43], but it may also be used to control the MEMS [42]. The only experiment which studied the plane-plane geometry considered by Casimir has been performed at the University of Padova (Italy). In this experiment the specific experimental difficulties associated with the plane-plane geometry had to be faced and were successfully mastered [44]. For more reviews of recent experiments see [45, 46].

This new generation of experiments of high precision is to a very large extent at the

origin of a revival of the theoretical studies on the Casimir effect. To compare precisely the experimental results with the theoretical predictions, it is necessary to take into account the differences between the ideal case considered by Casimir and the real situations of the experiments. Lifshitz has first developed a theory of the Casimir effect between dielectric mirrors [47, 48]. Since then, a great number of theoretical papers has been dedicated to the Casimir effect in various configurations. With regard to this work, we just cite the review articles or books in which hundreds of references are quoted [49, 50, 51, 52, 53].

Figure 10 : A Casimir-like effect at sea. In the days of square-riggers, sailors noticed that under certain conditions, ships lying close to one other would be mysteriously drawn together, with various unhappy out comes. Only in the 1990s was the phenomenon explained as a maritime analogy of the Casimir effect. (Image from ref [17])

The Casimir force is the most accessible experimental consequence of vacuum fluctuations in the macroscopic world. The problems related to vacuum energy constitute a serious reason for testing with great care the predictions of Quantum Field Theory concerning the Casimir effect. Furthermore, an accurate comparison with theory of the measured Casimir force is a key point for the experiments searching for new short range weak forces predicted in theoretical unification models [54, 55, 56, 57, 58, 59, 60, 61]. Since the Casimir force is the dominant effect between two neutral objects at distances between the nanometer and the millimeter, any search for a new force in this range is basically a comparison between experimental measurements and theoretical expectations of this force. For comparisons of this kind, the accuracy of theoretical calculations is as crucial as the precision of experiments [62].

In this context, it is essential to account for the differences between the ideal case considered by Casimir and the real situations encountered in experiments. Casimir considered perfectly reflecting mirrors whereas the experiments are performed with real reflectors, for example metallic mirrors which show perfect reflection only at frequencies below their plasma frequency. Then, the ideal Casimir formula corresponds to the limit of zero temperature, whereas experiments are performed at room temperature, with the effect of thermal fluctuations superimposed to that of vacuum fluctuations. The evaluation of the Casimir force between imperfect lossy mirrors at non zero temperature has given rise to a burst of controversial results [63, 64, 65, 66, 67, 68, 69, 70, 71, 72] which were discussed in detail in [73]. In the most accurate experiments, the force is measured between a plane and a sphere, and not between two parallel planes. Since no exact result is available for the former geometry, the force is derived from the Proximity Force Approximation (PFA) [74] often called in a somewhat improper manner the proximity force theorem. This approximation amounts to summing up the force contributions corresponding to the various inter-plate distances as if these contributions were independent and additive. However, the Casimir force is in general not additive and the previous method is only an approximation, the accuracy of which is not really mastered. The results available for the plane-sphere geometry [75, 76, 77] show that the PFA leads to correct results when the radius R of the sphere is much larger than

the distance L of closest approach. Finally, the surface state of the plates, in particular their roughness, also affects the force, which is again often given a simple approximate evaluation through the proximity force approximation [45]. However, in contrast to the geometry problem, obviously the diffraction of electromagnetic field by a rough surface cannot be treated as the sum of the diffractions at different distances [78, 79, 80].

After the discussion of the different corrections to the Casimir force let us now come back to Casimir's original derivation. Casimir obtained the Casimir energy for perfect mirrors by summing the zero-point energies $\frac{\hbar\omega}{2}$ of the cavity eigenmodes, subtracting the result for finite and infinite separation, and extracting the regular expression by inserting a formal high-energy cutoff and using the Euler-McLaurin formula [81, 82]. In his seminal paper [16], Casimir noticed that the energy should be a finite expression, without the need of any regularization, provided one takes into account the high frequency transparency of real mirrors. The idea was implemented by Lifshitz who calculated the Casimir energy for mirrors characterized by dielectric functions [47, 48]. For metallic mirrors he recovered expression for perfectly reflecting plates for separations L much larger than the plasma wavelength λ_{p} associated with the metal, as metals are very good reflectors at frequencies much smaller than the plasma frequency ω_{p}. At shorter separations in contrast, the Casimir effect probes the optical response of metals at frequencies where they are poor reflectors and the Casimir energy is reduced with respect to the ideal case. This reduction has been studied in great detail recently ([83, 84] and references therein) since it plays a central role in the comparison of theoretical predictions with experimental results as mentioned before.

In the limit of small separations $L \ll \lambda_{\mathrm{p}}$, the Casimir effect has another interpretation establishing a bridge between quantum field theory of vacuum fluctuations and condensed matter theory of forces between two metallic bulks. It can indeed be understood as resulting from the Coulomb interaction between surface plasmons, that is the collective electron excitations propagating on the interface between each bulk and the intracavity vacuum [88, 87, 86, 111]. The corresponding field modes are evanescent waves and have an imaginary longitudinal wavevector. We will call them plasmonic modes at arbitrary distances as they coincide with the surface plasmon modes at small distances. Plasmonic modes have to be seen in contrast to ordinary propagating cavity modes, which have a real longitudinal wavevector. For simplicity we will call those in the following photonic modes. Photonic modes are usually considered in quantum field theory of the Casimir effect [81] and are thought to determine the Casimir effect at large distances where the mirrors can be treated as perfect reflectors. At short distances, plasmonic modes are known to dominate the interaction [90, 91].

In this thesis I will study extensively the mode decomposition of the Casimir effect and the respective influence of photonic and plasmonic modes on the Casimir energy. They will turn out to be quite different than usually anticipated.

In chapter 1 I will first recall the original derivation of the Casimir effect between two perfect mirrors under ideal conditions as the sum of the cavity eigenmodes. This method needs of course regularization procedures that I will discuss in the following. After a discussion of the limitations of such an approach I will then present the theory of the Casimir

effect within the framework of the Quantum Optical Networks (QON) theory [84] where regularization procedures are not necessary anymore. The starting point of the QON derivation is the fact that vacuum fluctuations obey optics laws. Recalling the theory of Scattering and Transfer matrices, we will derive the general expression of the Casimir force and energy between two dielectric mirrors at zero temperature in the plane-plane geometry. The result then contains the information about the real mirrors properties through their reflection coefficients. We will show that evanescent waves appear naturally in the QON derivation when considering dielectric mirrors.

In chapter 2 I will then introduce the plasma model to describe the optical properties of metallic mirrors developed in the framework of the more general hydrodynamic model. The latter model describes the metal as if the electrons formed a continuous fluid moving on a static uniform positive background. Neglecting spatial dispersion, the corresponding dielectric function is then given by the plasma model. Even if this model is not sufficient for an accurate evaluation of the Casimir effect at the percent level, its simplicity and its mathematical properties will allow us to describe qualitatively and quantitatively the influence of plasmonic and photonic modes to the Casimir energy. Indeed, an important prediction of the hydrodynamic model is the existence of electron plasma oscillations or surface plasmons, the properties of which I will sketch rapidly. Using the plasma model for the dielectric function, I then calculate the non retarded Casimir force and show that it can be interpreted as the electrostatic (Coulomb) interaction between the plasmons living on the surface of each metallic mirror.

In Chapter 3, we will decompose the Casimir energy as a sum of zero-point energies $\frac{\hbar\omega}{2}$ over the whole set of modes of the cavity with its two mirrors described by a plasma model. In contrast to perfectly reflecting mirrors, this set will contain surface plasmon modes as well as ordinary cavity modes. Surface plasmon modes correspond to evanescent waves which do not propagate between the two mirrors. They do not have an equivalent in the perfect mirrors case. Plasmonic modes are the generalization to all distances of the surface plasmon modes at short distances. On the other hand, ordinary cavity modes or photonic modes are simply the generalization of the perfect cavity modes to the case, where mirrors have real material properties, and they propagate between the two mirrors.

The differences in the propagation properties of the plasmonic and photonic modes suggest to separately evaluate their contribution to the Casimir energy. This will be done in Chapter 4 after a discussion of the physical meaning of the definition of the plasmonic and photonic energy. In order to evaluate explicitly the two contributions we will develop a mathematical technique allowing us to circumvent the problem that the cavity eigenmodes are not known as explicit functions. The calculation is lengthy and tedious, but will be presented for completeness. We will also derive a simplified mathematical expression for the plasmonic and photonic mode contribution to the Casimir energy, which will allow us to evaluate the asymptotic behaviors in the long distance and short distance limit. As expected from [90,91], the contributions of plasmonic modes will be found to dominate the Casimir effect for small separations corresponding to Coulomb interaction between surface

plasmons. However, plasmonic modes will turn out to have a much greater importance than usually appreciated. Contrary to naive expectations, they will be found not to vanish for large separations. For distances larger than about $\lambda_p/4\pi$ ($\sim$10nm for typical metals) they even give rise to a contribution having simultaneously a negative sign and a too large magnitude with respect to the Casimir formula. The repulsive character can be attributed to one of the two plasmonic modes as will be discussed in detail. The main result of these calculations and its physical discussion is presented in the Letter appended at the end of this chapter.

CHAPTER 1

The Casimir Effect and the Theory of Quantum Optical Network

In this chapter I give an overview of the theoretical derivation of the Casimir effect theory. I begin in the first section with the original formulation of the effect between two perfect mirrors and discuss the limitations of such an approach. This allows us to familiarize with some mathematical features of such an effect which will be useful in all this thesis. I describe then in the second section a derivation of the Casimir force which is based on quantum optical methods and in particular on the Quantum Optical Network Theory (QON). This will lead (third section) to a general expression of the Casimir force and energy between two dielectric mirrors at zero temperature in the plane-plane geometry. I emphasize the necessity to take into account the evanescent waves when we deal with dielectric mirrors.

Contents

1.1 Introduction **10**
1.2 The Casimir effect in its original formulation **10**
1.3 Physical meaning of the regularization procedure **14**
1.3.1 The substraction of $\mathcal{E}(L \to \infty)$ 14
1.3.2 The introduction of a cutoff function. 15
1.3.3 The limitation of Casimir's approach 15
1.4 The Quantum Optical Network Theory **15**
1.4.1 The Scattering and Transfer Matrices 16
1.4.2 Elementary networks 18
1.4.3 Quantum scattering 21
1.4.4 The Cavity Matrix: The Airy function 25
1.5 The Casimir force: a radiation pressure difference **26**
1.5.1 Electromagnetic stress tensor and radiation pressure 26
1.5.2 The Casimir force as an integral over real and imaginary frequencies 29
1.6 Conclusions **32**

1.1 Introduction

This effect was first predicted by H. Casimir in 1948 [16] between two perfect mirrors and soon observed in different experiments which confirmed its existence [19, 20, 21, 22, 36, 37, 42]. The result obtained by Casimir was independent of any real characteristic of the mirrors. It was derived via the modification of space geometry due to the presence of perfect boundaries, which modify indeed the spectral distribution of vacuum fluctuations in the limited zone between them. This leads a vacuum energy depending on the mirrors distance and thus to a force between them.

Since then several other geometrical configurations [112] were explored and different techniques developed to calculate the Casimir force under real experimental conditions, showing a strong dependence on boundary conditions but also on any element of "reality" of the system (finite conductivity of the mirrors, non zero temperature, etc.) [45,47,48,88,84].

The most realistic prediction of the Casimir effect has been made in the framework of the Quantum Optical Networks Theory (QON) [84]. Defining scattering and transfer matrices for elementary networks (like the interface between two media or the propagation through a given medium) it is possible to deduce the matrices associated with composed networks. An opportune generalization of such concepts to the case of quantum fields allows to relate the spectral density inside a Fabry-Perot like cavity to the reflection coefficients amplitudes seen by the intracavity field. Through the spectral density it is possible to deduce the Casimir effect which then is fully related to the "real reflection properties" of the cavity mirrors.

1.2 The Casimir effect in its original formulation

In order to illustrate Casimir's derivation of the attractive force between two perfect mirrors [113,16], let us consider a cavity made by perfect walls/mirrors with edges a, b and L along the x, y and z direction respectively. Continuity conditions for the electromagnetic field at the vacuum/mirror interface impose that the electromagnetic field must vanish on the wall

$$\mathbf{E} = \mathbf{H} = 0. \tag{1.2.1}$$

Inside the cavity, only particular field frequencies are allowed. Those are given by the relation

$$\omega^{p}_{l,m,n} = c\sqrt{\left(\frac{\pi}{a}l\right)^2 + \left(\frac{\pi}{b}m\right)^2 + \left(\frac{\pi}{L}n\right)^2} \qquad l,\ m,\ n = 0, 1, 2....\infty \tag{1.2.2}$$

The superscript p distinguishes between the two polarizations of the light[1] and c is the speed of light. The quantities

$$k_x = \frac{\pi}{a}l, \quad k_y = \frac{\pi}{b}m, \quad k_z = \frac{\pi}{L}n, \tag{1.2.3}$$

[1] In the perfect mirrors case the frequencies do not depend on the polarization which explain why p does not appear in the righthand of Eq.(1.2.2). This, however, is not true in the general case and we prefer to introduce such a notation since now.

are the components of the wavevector of the electromagnetic field vibrating inside the cavity.

Each frequency corresponds to a particular mode of the field and a generic field can be written as a linear combination of such modes. The quantization procedure associates to each mode a quantum oscillator with a frequency $\omega_{l,\,m,\,n}$, the momentum and the position of the particle being replaced by the magnetic and the electric field. As for a normal oscillator we get the quantum energy of a mode given by

$$E^p_{l,m,n} = \hbar\omega^p_{l,m,n}(N^p_{l,m,n} + \frac{1}{2}) \tag{1.2.4}$$

$N^p_{l,m,n}$ represents the number of quanta (photons) contained in the mode labeled by $p,\ l,\ m,\ n$. As for the quantum oscillator the energy per mode has a low bound value, its zero point energy, which is different from zero and equal to

$$\frac{\hbar}{2}\omega^p_{l,m,n} \tag{1.2.5}$$

This fundamental result of quantum theory is derived directly from the Heisenberg principle which, in the case of the electromagnetic field, reflects the impossibility to measure the electric and the magnetic field simultaneously with an *ad libitum* precision. Alternatively the zero point energy shows the existence of irreducible fluctuations of the electromagnetic field around a zero mean value.

The total zero point energy of the electromagnetic inside the cavity is

$$\mathcal{E} = \sum_{p,l,m,n}{}' \frac{\hbar}{2}\omega^p_{l,m,n} \tag{1.2.6}$$

p runs from 1 to 2 and the prime on the summation symbol implies that a factor $1/2$ should be inserted if one of the integers $(l,\ m,\ n)$ is zero, for then we have just one independent polarization [113]. The weirdness of this last calculation is that the result is an infinite quantity: the sum involved in the definition of $\mathcal{E}$ irremediably diverges.

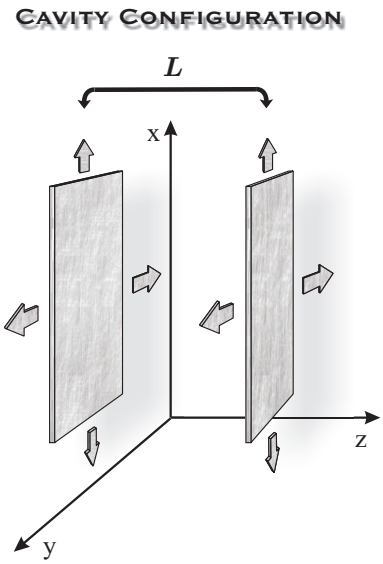

Figure 1.1 : The cavity configuration for the calculation of the Casimir effect. The plate dimensions along the x- and y-direction, a and b respectively, are supposed much larger than the distance L along the z-direction.)

For simplicity let us suppose that $a,\ b, \gg L$ (this is the case in the situation of physical interest) we may replace the sums over l and m in Eq.(1.2.6) by integrals:

$$\sum_{p,l,m,n}{}' = \sum_{p,n}{}' \frac{ab}{\pi^2}\int_0^\infty dk_x\, dk_y = \sum_{p,n}{}' A\int_{\mathbb{R}^2}\frac{d^2\mathbf{k}}{(2\pi)^2} \equiv \sum_{p,n}{}'\sum_{\mathbf{k}} \tag{1.2.7}$$

where A is the area of the mirrors separated by a distance L and $\mathbf{k} \equiv (k_x, k_y)$ is the transverse electromagnetic wavevector. Eq.(1.2.6) now reads as

$$\mathcal{E}(L) = \sum_{p,n}{}' \sum_{\mathbf{k}} \frac{\hbar}{2}\omega_n^p(\mathbf{k}), \quad \text{with} \quad \omega_n^p(\mathbf{k}) = c\sqrt{|\mathbf{k}|^2 + \left(\frac{n\pi}{L}\right)^2}. \tag{1.2.8}$$

$\mathcal{E}(L)$ is still an infinite quantity as the number of vacuum modes is infinite. To extract from this expression a physical quantity Casimir proposed the following procedure. He states that the quantity which has a physical sense arises from the difference

$$E(L) = \mathcal{E}(L) - \mathcal{E}(L \to \infty) \tag{1.2.9}$$

$\mathcal{E}(L \to \infty)$ is the asymptotic function of $\mathcal{E}(L)$ evaluated in the limit $L \to \infty$. This limit implies a replacement of the sum over n by an integral and we get

$$\mathcal{E}(L \to \infty) = \frac{L}{\pi}\int_0^\infty dk_z \sum_p \sum_{\mathbf{k}} \frac{\hbar}{2} c\sqrt{|k|^2 + k_z^2} \tag{1.2.10}$$

which is still an infinite quantity.

$E(L)$ is then a difference between two infinite quantities and in order to extract a finite result Casimir proposed to introduce a function $f(\omega/\omega_{cut})$ which is unity for $\omega \ll \omega_{cut}$ but tends to zero sufficiently rapidly for $\omega/\omega_{cut} \to \infty$. He justified this by saying: "*The physical meaning* [of this function] *is obvious: for very short waves (X-rays e.g.) our plate is hardly an obstacle at all and therefore the zero point energy of these waves will not be influenced by the position of this plate*" [16].

With some algebra and a change of variable Eq.(1.2.9) can then be rewritten as

$$E(L) = \lim_{\Omega_{cut}\to\infty} \frac{\hbar c\pi^2 A}{4L^3}\left(\sum_{n=0}{}' F(n) - \int_0^\infty F(x)dx\right) \tag{1.2.11}$$

where

$$F(x) = \int_0^\infty dk^2\sqrt{k^2+x^2} f\left(\frac{\sqrt{k^2+x^2}}{\Omega_{cut}}\right), \quad \Omega_{cut} = \frac{\omega_{cut}L}{c} \tag{1.2.12}$$

We can now apply the Euler-Maclaurin formula [82]

$$\sum_{n=0}{}' F(n) - \int_0^\infty dx F(x) = -\sum_{m=1}^\infty \frac{B_{2m}}{(2m)!}F^{(2m-1)}(0) \tag{1.2.13}$$

with B_m the Bernoulli numbers defined by [82, 114]

$$B_m = \frac{m!}{2\pi\imath}\oint_C \frac{z}{e^z-1}\frac{dz}{z^{m+1}} \quad \text{or} \quad \frac{z}{e^z-1} = \sum_{m=0} B_m \frac{z^m}{m!} \tag{1.2.14}$$

The contour C encloses the origin, has radius less than 2π (to avoid the poles at $\pm 2\pi\imath$), and is followed in the counterclockwise direction. To apply the Euler-Maclaurin formula in Eq.(1.2.13) we have exploited the fact that $F(x) \xrightarrow{x\to\infty} 0$.

$$F(x) = \int_{x^2}^{\infty} dw\sqrt{w} f(\frac{\sqrt{w}}{\Omega_{cut}}) \Rightarrow F^{(1)}(x) = -2x^2 f(\frac{x}{\Omega_{cut}})$$

$$F^{(1)}(0) = 0 \ (m=1), \quad F^{(3)}(0) = -4 \ (m=2),$$
$$F^{(2m-1)}(0) = -2\frac{(2m-2)!}{(2m-4)!}\frac{f^{(2m-4)}(0)}{\Omega_{cut}^{(2m-4)}}, \ m \geq 3$$

Taking the limit $\Omega \to \infty$ and using

$$-\frac{B_{2m}}{(2m)!}_{|m=2} = \frac{1}{720} \tag{1.2.15}$$

we get the expression derived by Casimir [16]

$$E_{Cas}(L) = -\frac{\hbar c \pi^2}{720}\frac{A}{L^3}. \tag{1.2.16}$$

Assuming that all the derivatives of the cutoff function vanish at $\omega = 0$, one can show that all the derivatives $F^{(2m-1)}(0) = 0$ vanish for $m \geq 3$. From (1.2.16) by a simple derivation we get

$$F_{Cas}(L) = \frac{dE_{Cas}(L)}{dL} = \frac{\hbar c \pi^2}{240}\frac{A}{L^4} \tag{1.2.17}$$

which is the expression of the Casimir force given in [16]. The signs have been chosen to fit the thermodynamical convention with the minus sign of the energy E_{Cas} corresponding to a binding energy and a positive force to an attraction.

As already said the expressions given in Eq.(1.2.16) and (1.2.17) depend only on the Planck's $\hbar$ constant, the speed of the light c and the geometric properties of the system A, L showing that in the perfect mirrors case the Casimir effect seems a pure geometrical effect connected to the presence of some boundary conditions in vacuum [115]. One can show that a sort of classical Casimir effect arises in the same geometry if we deal with the classical electromagnetic field at non zero temperature [116]. However, at room temperature, even if the thermal and vacuum contributions are considered simultaneously one can show that, for distances (L) in the nanometric/micrometric domain the vacuum contribution dominates the thermal effect. Then the Casimir effect remains a quantum vacuum effect even at room temperature [117, 115].

In the following sections we are going to see that the properties of real mirrors sensibly modify the expression of the Casimir force. At this point, we want to discuss in more detail the regularization technique introduced by Casimir, one of the ancestors of renormalization.

1.3 Physical meaning of the regularization procedure

In the previous paragraph we deduced the Casimir energy and force between two perfect facing mirrors placed at relative distance L in vacuum at zero temperature. This finite result has been derived from infinite quantities through a procedure which can be summed up in two steps:

1. The substraction of $\mathcal{E}(L \to \infty)$
2. The introduction of a cutoff function

I will now give a physical meaning of this procedure.

1.3.1 The substraction of $\mathcal{E}(L \to \infty)$

To understand the meaning of this step we need to know what the Casimir effect is a measure of. There are different ways of answering this question, one for each way to understand the Casimir effect.

The Casimir energy measures the shift in the zero point energy of the electromagnetic field due to the modification of the boundary conditions. The energy shift is measured between the configuration with the plates a distance L apart and the configuration with the plates at infinite distance (empty space). When the two mirrors are truly present imposing new boundary conditions, they modify the vacuum spectral density which becomes sharply peaked at the cavity modes frequencies. The corresponding energy is given by $\mathcal{E}(L)$ in Eq.(1.2.8). Without the mirrors the same volume would be filled by free vacuum energy. One can easily show that the free vacuum energy density is given by

$$\varrho = \int_{\mathbb{R}^3} \frac{d^3\mathbf{K}}{(2\pi)^3} \frac{\hbar}{2} \omega(\mathbf{K}), \quad \mathbf{K} = (\mathbf{k}, k_z) \tag{1.3.1}$$

where $\omega(\mathbf{K})^2 = c^2 K^2$ is the dispersion relation of the electromagnetic waves in the vacuum. The volume of the cavity is given by $V = LA$ and then the vacuum free energy which would fill this volume is found to be

$$\mathcal{E}(L \to \infty) = V\varrho \equiv \frac{\hbar c A L}{2\pi} \int_{\mathbb{R}^2} \frac{d^2\mathbf{k}}{(2\pi)^2} \int_0^\infty dk_z \sqrt{|\mathbf{k}|^2 + k_z^2} \tag{1.3.2}$$

The Casimir energy is then given by the energy shift

$$\Delta\mathcal{E}(L) = \mathcal{E}(L) - \mathcal{E}(L \to \infty) \equiv E_{Cas}(L) \tag{1.3.3}$$

which is the expression given in Eq.(1.2.9).

A more clear picture of this procedure arises in the interpretation of the Casimir force as a net radiation pressure exerted on the mirrors forming the cavity (see the last section of this chapter, Appendix A.1 and Chapter 3 for more details) [84, 113].

1.3.2 The introduction of a cutoff function.

Mathematically speaking the introduction of a cutoff function $f(\omega/\omega_{cut})$ in Eq.(1.2.9) has the unique aim to make the integral involved in the definition of $\mathcal{E}(L)$ and of $\mathcal{E}(L \to \infty)$ convergent. This way the differences in Eq.(1.2.9) can be easily evaluated, applying for example in the perfect mirrors case the Euler-Maclaurin summation formula [82]. The cutoff has the physically intuitive meaning to cut the integral at frequencies $\sim \omega_{cut}$ where any real mirror becomes transparent.

We have however to point out that despite this regularization the only physical meaningful quantities are the whole differences given in Eq.(1.2.9) and Eq.(1.2.17). Therefore is not surprising that the term $\mathcal{E}(L)$ or $\mathcal{F}(L)$ alone is divergent. The important thing is that the result of the difference is finite.

1.3.3 The limitation of Casimir's approach

The first limitation of Casimir's calculation is its dependence on the renormalization procedure: all renormalization techniques must deliver the same end result. Although this is the case for the plane-plane configuration, this point is not evident in spherical geometries [112].

Secondly, real experiments inevitably need the generalization of the result to a case where the mirrors are not perfect. They are generally made of dielectric materials the properties of which depend on the incoming radiation characteristics (frequency and wavevector). This response is causal but non local which means that the value of the electromagnetic field at a given time can depend on the values of the field in the previous instants [85].

An important consequence is that the conditions given in Eq.(1.2.1) are not satisfied. The electromagnetic spectral density is no longer delta peaked on some particular frequencies (given by Eq.(1.2.2)) but it is still sharply peaked on some frequencies, the vibration modes of the cavity. Those frequencies are connected with the mirrors reflection properties.

Some fundamental difficulties arise also when dissipation is taken into account [48]. We are going to see that these difficulties can be circumvented using another approach based on the theory of the Quantum Optical Network (QON). The starting point of this derivation is the fact that vacuum fluctuations obey optics laws. Introducing the theory of the Scattering and Transfer matrices we will be able to get the general expression of the Casimir force and energy for two mirrors at zero temperature in the plane-plane geometry and in the dissipative case.

1.4 The Quantum Optical Network Theory

We introduce in this section some fundamental concepts concerning the Quantum Optical Networks Theory (QON) [84, 118]. This theory is the optical version of an equivalent theory developed for electronic circuits [119].

Disregarding the detail of their microscopic structure, the mirrors and the cavity they enclose are indeed treated as a sort of "box" (network) which transforms the input field

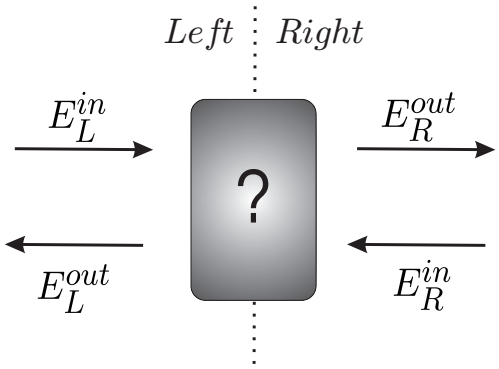

Figure 1.2 : A schematic representation of a general network. It transforms the input in the output field following some well defined transformation rules deeply connected with its own physical properties and those of the surrounding media.

in an output field following some well defined transformation rules (see figure 1.2). The mirrors can be lossy and characterized by a frequency dependent optical response.

Elementary networks are for example interfaces between two media or the propagation over a length in a medium. Each elementary network is characterized by its scattering and transfer matrices. We will be able to deduce the scattering and transfer matrices associated with composed networks, such as the optical slab, the multilayer mirror or a cavity from the elementary ones. The output field leaving an elementary or composed network can then be deduced from the input field through simple matrix manipulations.

In the following I will introduce scattering and transfer matrices for elementary networks. We define the network summation rules as well as the definition of some elementary network. We generalize then the formalism to the quantum case taking into account the effect of vacuum fluctuations.

1.4.1 The Scattering and Transfer Matrices

Let us consider the interface volume between two zones of the space, which we label "Left" (L) and "Right" (R), having some well defined dielectric properties[2]. Since now we assume also that the medium has no magnetic properties. This interface region can have a finite volume as well as it can reduce to a simple surface. The field incoming on the interface will be partially reflected and partially transmitted. In the framework of a linear model [85] the reflected and transmitted amplitude for a plane monochromatic wave are given by

$$E^{tr} = t\ E^{in} \quad E^{rf} = r\ E^{in} \tag{1.4.1}$$

where E is the complex electromagnetic field at just outside the interface volume and t, r are the so called transmission and reflection coefficients. They are in general complex functions dependent on the optical properties of the involved media as well as on the interface volume. For simplicity we omit frequency, wavevector and polarization dependence in all quantities, showing it only when it is necessary.

As the time dependent response of medium has to be real ($r(t)$ and $t(t)\ \in \mathbb{R}$) we

[2]Metals are included in the definition of dielectric mirrors.

deduce for the frequency dependent response functions:

$$r^*[\omega] = r[-\omega], \quad t^*[\omega] = t[-\omega] \tag{1.4.2}$$

Moreover those amplitudes should verify the high frequency transparency property, i.e. the fact that any realistic medium becomes transparent to a high frequency radiation

$$r[\omega] \xrightarrow{\omega\to\infty} 0 \tag{1.4.3}$$

The field interface continuity conditions impose that [85]

$$\begin{cases} E_L^{out} = r_L\ E_L^{in} + t_R\ E_R^{in} \\ E_R^{out} = t_L\ E_L^{in} + r_R\ E_R^{in} \end{cases} \tag{1.4.4}$$

where $E_i^{in/out}$ mean the incoming/outgoing field propagating in the medium i while r_i and t_i are the transmission and the reflection coefficient seen from the medium i. These relations can be cast in a more compact matrix relation

$$\mathbf{E}^{out} = \mathrm{S}\ \mathbf{E}^{in} \tag{1.4.5}$$

where

$$\mathbf{E}^{out} = \begin{pmatrix} E_L^{out} \\ E_R^{out} \end{pmatrix}, \quad \mathbf{E}^{in} = \begin{pmatrix} E_L^{in} \\ E_R^{in} \end{pmatrix}, \quad \mathrm{S} = \begin{pmatrix} r_L & t_R \\ t_L & r_R \end{pmatrix} \tag{1.4.6}$$

S is the scattering matrix of the system.

Using the scattering matrix, it is straightforward to write down the energy balance of the system. From Eq.(1.4.5) we have that

$$\left|\mathbf{E}^{out}\right|^2 = \left(\mathbf{E}^{in}\right)^\dagger \mathrm{S}^\dagger\mathrm{S}\ \mathbf{E}^{in} \tag{1.4.7}$$

For a system without dissipation the incoming energy $\left|\mathbf{E}^{in}\right|^2$ must be equal to the outgoing one $\left|\mathbf{E}^{out}\right|^2$. Therefore we necessarily must have that

$$\mathrm{S}^\dagger\mathrm{S} = \mathrm{S}\mathrm{S}^\dagger = 1 \tag{1.4.8}$$

which means that in the lossless systems the scattering matrix corresponds to unitary transformation of the field. From condition given in Eq.(1.4.8) we find in particular [85]

$$|r_i|^2 + |t_i|^2 = 1 \tag{1.4.9}$$

For a dissipative system $\left|\mathbf{E}^{out}\right|^2 < \left|\mathbf{E}^{in}\right|^2$ and the condition given in Eq.(1.4.8) fails. We have in general that [85]

$$|r_i|^2 + |t_i|^2 < 1 \tag{1.4.10}$$

The S-matrix gives the outgoing fields as a function of the incoming ones. For different purpose it may be advantageous to adopt a different point of view and considering the Right/Left transfer of the field. Defining

$$\mathbf{E}^L = \begin{pmatrix} E_L^{in} \\ E_L^{out} \end{pmatrix}, \quad \mathbf{E}^R = \begin{pmatrix} E_R^{in} \\ E_R^{out} \end{pmatrix} \tag{1.4.11}$$

we may look for a transfer matrix T relating the left side field to the right side one:

$$\mathbf{E}_L = \mathrm{T}\ \mathbf{E}_L \tag{1.4.12}$$

Its matrix elements can be derived directly from the scattering matrix elements. If we introduce the two projection and a swap matrices

$$\pi_+ = \begin{pmatrix} 1 & 0 \\ 0 & 0 \end{pmatrix}, \quad \pi_- = \begin{pmatrix} 0 & 0 \\ 0 & 1 \end{pmatrix}, \quad \eta = \begin{pmatrix} 0 & 1 \\ 1 & 0 \end{pmatrix} \tag{1.4.13}$$

one can show that [84] the following relations between the S-matrix and the T-matrix formalism

$$\mathrm{T} = -(\pi_- - \eta \mathrm{S} \pi_+)^{-1}(\pi_+ - \eta \mathrm{S} \pi_-) \tag{1.4.14a}$$

$$\mathrm{S} = -\eta(\pi_- - \mathrm{T} \pi_+)^{-1}(\pi_+ - \mathrm{T} \pi_-) \tag{1.4.14b}$$

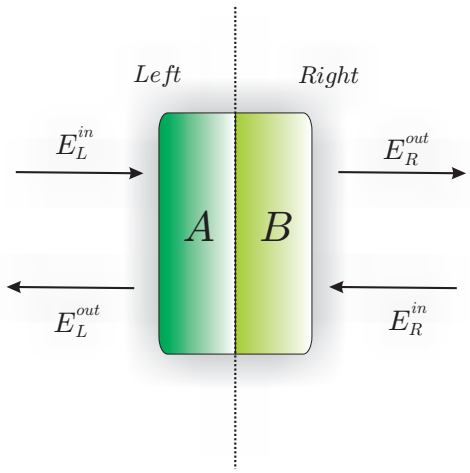

Figure 1.3 : A composite network corresponding to the piling up of two different elementary networks A and B. The whole network T-matrix is just given by the product of the T-matrices for the network A and the network B.

While the energetic considerations are more tedious in the T-matrix point of view, the transfer matrix is particular well suited for composed networks. We may obtain the T-matrix for a composite network by "piling up" the T-matrices of elementary network. For example if the composite network is made of a multilayer dielectric, we have a corresponding T-matrix, T_i, for each interface i. The global T-matrix of the multilayer network $\mathrm{T}_{mult}[\omega]$ is simply given by

$$\mathrm{T}_{mult} = \prod_i \mathrm{T}_i \tag{1.4.15}$$

The global scattering matrix S_{mult} can be then obtained exploiting the relation given in Eq.(1.4.14b). To deduce the property given in Eq.(1.4.15) we have assumed the dielectric layers (elementary networks) to be in the immediate vicinity of each other but without any electronic exchange between them.

1.4.2 Elementary networks

We now study in more detail two elementary networks, that is the traversal of an interface and the propagation over a given length inside a dielectric medium.

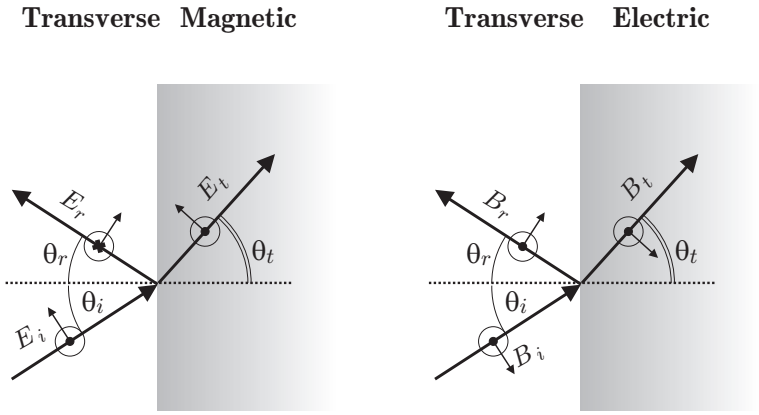

Figure 1.4 : A schematic representation of the reflection-transmission process for a plane wave incoming on an interface between two dielectric media. The TE and the TM modes have been represented separately. For the TE mode the electric vector is orthogonal to the incidence plane while for the TM mode it lays inside the incidence plane.

For the scattering at the plane interface between two media with indices $n_L = \sqrt{\epsilon_L}$ on the left and $n_R = \sqrt{\epsilon_R}$ on the right, ϵ_i being the dielectric response function[3], we write the reflection and transmission amplitudes as the Fresnel scattering amplitudes [85].

They are obtained from characteristic impedances Z^p defined for plane waves with polarization p in each medium and from the continuity equations at the interface:

$$r_L^p = -r_R^p = \frac{1 - Z^p}{1 + Z^p} \tag{1.4.16a}$$

$$\sqrt{\frac{\kappa_R}{\kappa_L}} t_L^p = \sqrt{\frac{\kappa_L}{\kappa_R}} t_R^p = \sqrt{1 - \left(r_{int}^p\right)^2} \tag{1.4.16b}$$

$$Z^{TE} = \frac{\kappa_R}{\kappa_L}, \quad Z^{TM} = \frac{\epsilon_R}{\epsilon_L}\frac{\kappa_L}{\kappa_R} \tag{1.4.16c}$$

$$\kappa_i = \sqrt{|\mathbf{k}|^2 - \epsilon_i[\omega]\frac{\omega^2}{c^2}} \tag{1.4.16d}$$

where TE denotes the Transverse Electric mode and TM the Transverse Magnetic mode (see paragraph 1.5.1 page 26). Those definitions can be written in a compact way in the corresponding T-matrix for the interface, T_{int}^p

$$T_{int}^p = \sqrt{\frac{\kappa_R}{\kappa_L}} \frac{1}{\sqrt{2\sinh\beta^p}} \begin{pmatrix} e^{\frac{\beta^p}{2}} & -e^{-\frac{\beta^p}{2}} \\ -e^{-\frac{\beta^p}{2}} & e^{\frac{\beta^p}{2}} \end{pmatrix}, \quad \beta^p = \ln\frac{Z^p - 1}{Z^p + 1} \tag{1.4.17}$$

[3] In general the optical response may depend on the plane wave frequency, wavevector and direction inside the medium.

We now consider the process of field propagation over a propagation length d, inside a dielectric medium characterized by a permittivity ϵ_m. For this elementary network, the T-matrix is given by

$$\mathrm{T}_{prop} = \begin{pmatrix} e^{\alpha_m} & 0 \\ 0 & e^{-\alpha_m} \end{pmatrix}, \quad \alpha = \kappa_m \, d \tag{1.4.18}$$

where κ_m is defined as in Eqs.(1.4.16). The function α does not depend on the polarization. It represents the spatial phase gained by the electromagnetic field during the propagation through the medium[4].

1.4.2.1 Reciprocity

In this section we discuss the reciprocity property of dielectric multilayers, i.e. networks obtained by piling up interfaces and propagations. To this aim, we first remark that from the relation given in Eq.(1.4.14a) we get

$$\det(\mathrm{T}) = \frac{\det(\pi_{-}\mathrm{S})}{\det(\pi_{+}\mathrm{S})} = \frac{t_R}{t_L} \tag{1.4.19}$$

If the T-matrix describe the properties of an interface between two dielectric we have from Eqs.(1.4.16) that

$$\det(\mathrm{T}_{int}) = \frac{\kappa_R}{\kappa_L} \tag{1.4.20}$$

Now if we deal with a multilayer dielectric network having its two "Left" and "Right" ports corresponding to vacuum, which is the case for a mirror, the values of κ_j are equal on its two sides. From the Eq.(1.4.20) and Eq.(1.4.15) it is clear that

$$\det(\mathrm{T}_{mult}) = 1 \;\Rightarrow\; t_R = t_L \tag{1.4.21}$$

Note that this reciprocity property corresponds to a symmetrical S matrix and has to be distinguished from the spatial symmetry of the network with respect to its median plane which entails $r_L = r_R$.

1.4.2.2 A useful example: The dielectric slab

As an example of the S- and T-Matrix formalism let us evaluate those matrices for homogenous dielectric slab of width d. The slab is obtained by piling up a vacuum/matter/vacuum interface with indices $n_1 = 1 \mid n_2 = n \mid n_1 = 1$ plus a propagation over a length d inside matter. As a consequence of the composition law given in Eq.(1.4.15) and exploiting Eq.(**??**) we get

$$\mathrm{T}_{slb} = \mathrm{T}_{int}\mathrm{T}_{prop}\mathrm{T}_{int}^{-1} \tag{1.4.22}$$

Though the definitions given in Eqs.(1.4.17) and (1.4.18) we deduce

$$\mathrm{S}_{slb} = \frac{1}{\sinh\beta}\begin{pmatrix} \sin[\alpha+\beta] & \sinh\alpha \\ -\sinh\alpha & \sin[\alpha-\beta] \end{pmatrix} \tag{1.4.23}$$

[4]The sign of the square root have to be chosen to assure the right physical behavior in the dissipative case.

(we have dropped for simplicity the m subscript for α). We can now evaluate the corresponding S-Matrix with the help of the relation given in Eq.(1.4.14b) which leads to

$$\mathrm{S}_{slb} = \frac{1}{\sinh[\alpha+\beta]} \begin{pmatrix} -\sinh\alpha & \sin\beta \\ \sin\beta & -\sinh\alpha \end{pmatrix} \tag{1.4.24}$$

It is interesting to discuss limit cases. The first one occurs for $\alpha \to 0$. In this case the T-Matrix becomes the identity matrix, the propagation through the medium can be forgotten and the interface effects compensate each other. It is important to remark that $\alpha \to 0$ is realized either for $\kappa \to 0$ or $d \to 0$. In the first situation the medium becomes transparent[5] while in the second case it is extremely thin.

The second case correspond to the so called bulk limit $d \to \infty$. When the medium is dissipative case κ is a complex quantity with a non negative real part, which in general diverge in the bulk limit: $Re[\kappa_m d] \xrightarrow{d\to\infty} \infty$. The matrix transforms then into

$$T_{bulk} = \begin{pmatrix} e^{-\beta p} & 0 \\ 0 & e^{-\beta p} \end{pmatrix} \tag{1.4.25}$$

This limit corresponds to a total extinction of the field inside the medium. Note that experiments are performed with metallic mirrors having a thickness much larger than the plasma wavelength. This is why the limit of a total extinction of the field through the medium is assumed in most calculations.

It is worth to underline however that the bulk limit rises several delicate problems. First of all it is not possible to define a corresponding T-Matrix. Secondly the bulk limit cannot occur in general in the non dissipative case and even in the dissipative case it may happen that despite $d \to \infty$, $\kappa \to 0$ leading to a transparent slab in contrast with the result of the bulk limit.

1.4.3 Quantum scattering

Up to now we have performed a classical analysis of the S- and T- Matrices. This formalism is not sufficient when we want to take into account quantum vacuum fluctuations. Despite the fact that the quantum mean values behave like the corresponding classical quantities, other important properties as for example correlation functions are contained in the noise characteristic. Moreover when dissipation is taken into account the noise properties are modified by the interaction with the environment. The connection is established by the well known fluctuation dissipation theorem [120].

In the following we see how to extend the scattering and transfer matrices to the scattering of quantum fluctuations. We shall assume that the scattering is restricted to the modes of interest and still fulfills the symmetry of the plane mirrors. This amounts to neglect multiple scattering process which could couple different modes through their coupling with noise modes.

[5] It may happen just for one frequency as well as for a frequency domain.

1.4.3.1 Theoretical background

In this paragraph we give a quick and non exhaustive review of the basic concepts of the interaction between a quantum system and the quantum environment. For further detail one can refers to articles, books cited in [121, 122, 123, 124, 125, 126, 127] and references therein.

Let us consider a typical quantum system, an harmonic oscillator coupled with an heat bath in the thermal equilibrium. Under the assumption of a linear response[6] the environment can be represented by a set of quantum harmonic oscillators [125]. Therefore our whole system is an ensemble of coupled oscillators: we are interested in the dynamics of one of them indexed by "0", while the others are in the thermal equilibrium. The oscillator is subject to a quantum equivalent of the Langevin equation

$$\ddot{\hat{x}}_0(t) + \imath\gamma\dot{\hat{x}}_0(t) = -\omega_0^2\hat{x}_0(t) + \hat{F}(t) \tag{1.4.26}$$

$\hat{x}_0$ is the position operator, ω_0 the free oscillation frequency, the dot represents the time derivative, and γ is the dissipation coefficient. The operator $\hat{F}(t)$ is the noise operator given by a linear combination of the bath oscillators. At thermal equilibrium the noise spectral properties are connected to the dissipation function by the relation

$$\Delta[\omega] \propto \gamma \coth\left(\frac{\hbar\omega}{2k_BT}\right) \tag{1.4.27}$$

where k_B is the Boltzmann constant, $\Delta[\omega]$ is the Fourier transformation of the symmetric correlation function of the noise $\hat{F}(t)$. The expression (1.4.27) is nothing but the fluctuations-dissipation theorem [120].

The interesting feature of the dynamics described in Eq.(1.4.26) is that a quantum oscillator coupled to a thermal bath behaves more or less like a classical dissipative oscillator. The main difference is due to the presence of a noise operator. $\hat{F}(t)$ has a zero mean value at the thermal equilibrium and therefore it is responsible (even at zero temperature) of the addition of further fluctuations to the system dynamics.

Remark that the relation given in Eq.(1.4.27) establishes a connection between the environment-induced fluctuations and the dissipative behavior of our system. Since the whole system is closed, it is subject to a unitary evolution and the total energy is conserved. This is of course not the case for the single zero-oscillator (without considering the noise line). The unitary evolution can be recovered only including the noise which compensates the losses.

This is the starting point to generalize the scattering and transfer matrix formalism to the quantum case.

1.4.3.2 Noise in scattering and transfer approach

The previous arguments suggest a simple way to generalize the transformation described in Eqs.(1.4.4). The quantum equivalent of the complex field E is the annihilation operator

[6] This assumption is always fulfilled in the case of small deviation form the equilibrium point, i.e. assuming for example a weak coupling.

$\hat{a}$. We can therefore account for the losses by replacing Eqs.(1.4.4) by the more general transformations

$$\begin{cases} \hat{a}_L^{out} = r_L\ \hat{a}_L^{in} + t_R\ \hat{a}_R^{in} + \hat{F}_1 \\ \hat{a}_R^{out} = t_L\ \hat{a}_L^{in} + r_R\ \hat{a}_R^{in} + \hat{F}_2 \end{cases} \tag{1.4.28}$$

Here $\hat{F}_1[\omega]$ and $\hat{F}_2[\omega]$ are the quantum fluctuations added due to the dissipative nature of the system. Again we can cast the previous system in a matrix form

$$\hat{\mathbf{a}}^{out} = \mathrm{S}\ \hat{\mathbf{a}}^{in} + \hat{\mathbf{F}} \tag{1.4.29}$$

where the S matrix has the same form as defined in Eq.(1.4.6) while we have

$$\hat{\mathbf{a}}^{out} = \begin{pmatrix} \hat{a}_L^{out} \\ \hat{a}_R^{out} \end{pmatrix} \quad \hat{\mathbf{a}}^{in} = \begin{pmatrix} \hat{a}_L^{in} \\ \hat{a}_R^{in} \end{pmatrix} \quad \text{and} \quad \hat{\mathbf{F}} = \begin{pmatrix} \hat{F}_1 \\ \hat{F}_2 \end{pmatrix} \tag{1.4.30}$$

For the reasons discussed above the transformation described by the matrix S can not be unitary because of the dissipation. In order to see this more clearly let us consider a general transformation of the form

$$\hat{\mathbf{b}} = \sum_i \Theta_i \hat{\mathbf{c}}_i \tag{1.4.31}$$

and define the symbol $[\hat{\mathbf{b}}, \hat{\mathbf{b}}^\dagger]$ as follows

$$[\hat{\mathbf{b}}, \hat{\mathbf{b}}^\dagger]_{i,j} \equiv [\hat{b}_i, \hat{b}_j^\dagger] \tag{1.4.32}$$

Therefore the symbol $[\hat{\mathbf{b}}, \hat{\mathbf{b}}^\dagger]$ is a matrix having as elements all the possible commutation relations between the operators $\hat{b}_1$, $\hat{b}_2$ and their hermitian conjugates.

Starting from this definition and from the transformation (1.4.31) one can show

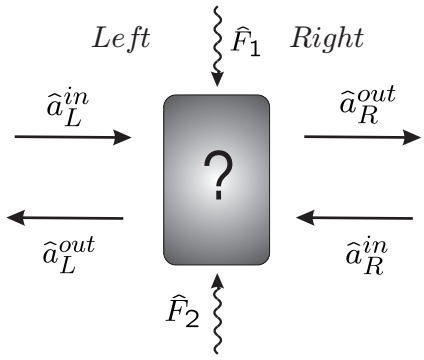

Figure 1.5 : A schematic representation of a dissipative network. The fluctuation-dissipation theorem imposes to include in the description of a dissipative system some auxiliary noise lines represented here by the operator $\hat{F}_1$ and $\hat{F}_2$.

$$[\hat{\mathbf{b}}, \hat{\mathbf{b}}^\dagger] = \sum_i \Theta_i [\hat{\mathbf{c}}_i, \hat{\mathbf{c}}_i^\dagger] \Theta_i^\dagger \tag{1.4.33}$$

In Eq.(1.4.33) we have assumed that the operator vectors with a different subscript commute, i.e. $[\hat{\mathbf{c}}_i, \hat{\mathbf{c}}_j^\dagger] = \delta_{i,j} 1$ where 1 is the identity matrix.

Let us now represent the additional fluctuations $\hat{\mathbf{F}}$ in Eq.(1.4.29) by introducing auxiliary noise modes $\hat{\mathbf{f}}$ and auxiliary noise amplitudes gathered in a noise scattering matrix S′

$$\hat{\mathbf{F}} = \mathrm{S}' \hat{\mathbf{f}}[\omega] \quad \text{with } \mathrm{S}' = \begin{pmatrix} r'_L & t'_R \\ t'_L & r'_R \end{pmatrix} \tag{1.4.34}$$

The input and output fields are free electromagnetic quantum fields.

$$[\hat{\mathbf{a}}^{out}, (\hat{\mathbf{a}}^{out})^{\dagger}] = [\hat{\mathbf{a}}^{in}, (\hat{\mathbf{a}}^{in})^{\dagger}] = 1 \tag{1.4.35}$$

We define the input and output noise modes to have the same canonical commutation relation

$$[\hat{\mathbf{f}}, \left(\hat{\mathbf{f}}\right)^{\dagger}] = 1 \tag{1.4.36}$$

In such a way they are defined up to an ambiguity: any canonical transformation of the noise modes leads to an equivalent representation of the additional fluctuations, which corresponds to a different form for the noise amplitudes, while leading to the same physical results.

Exploiting the relation (1.4.33) we deduce

$$1 = \mathrm{S}\mathrm{S}^{\dagger} + \mathrm{S}'\mathrm{S}'^{\dagger} \tag{1.4.37}$$

This relation shows in a simple way the unitarity of the whole system (mirror+environment) evolution. At the same time another application of Eq.(1.4.33) leads to

$$\left[\hat{\mathbf{F}}, \hat{\mathbf{F}}^{\dagger}\right] = \mathrm{S}'\mathrm{S}'^{\dagger} = 1 - \mathrm{S}\mathrm{S}^{\dagger} \tag{1.4.38}$$

which determines in a unique way all the commutation properties of the added noises [118].

1.4.3.3 Composition of dissipative networks

We may also express the effect of the noise lines in the transfer matrix approach:

$$\hat{\mathbf{a}}_L = \mathrm{T}\ \hat{\mathbf{a}}_R + \mathrm{T}'\ \hat{\mathbf{f}} \tag{1.4.39}$$

where the noise transfer matrix T' can again be obtained from the S' using the relation given in Eq.(1.4.14a) and [84]

$$\mathrm{T}' = (\pi_- - \eta\mathrm{S}\pi_+)^{-1}\eta\mathrm{S}' = (\pi_- - \mathrm{T}\pi_+)\eta\mathrm{S}' \tag{1.4.40}$$

The matrix T' has an useful computational property [84]

$$\mathrm{T}'\mathrm{T}'^{\dagger} = \mathrm{T}\Phi\mathrm{T} - \Phi, \quad \text{with } \Phi = \pi_+ - \pi_- \tag{1.4.41}$$

Because of the introduction of the noise lines the composition law have not the simple form described in Eq.(1.4.15) any more. Physically speaking the final result shows a "classical transferred" part plus a noise part. This statement becomes in the case of a multilayer network [84]

$$\hat{\mathbf{a}}_L = \mathrm{T}_{mult}\ \hat{\mathbf{a}}_R + \mathrm{T}'_{mult}\ \hat{\mathbf{f}}_{mult} \tag{1.4.42}$$

where T_{mult} is obtained as in Eq.(1.4.15). Considering the case of two layers A and B, the following identity holds:

$$\mathrm{T}'_{mult}\ \hat{\mathbf{f}}_{mult} = \mathrm{T}'_A\ \hat{\mathbf{f}}_A + \mathrm{T}_A\ \mathrm{T}'_B\ \hat{\mathbf{f}}_B \tag{1.4.43}$$

This relation means that two noises lines, $\hat{\mathbf{f}}_A$ and $\hat{\mathbf{f}}_B$, and the two transfer amplitudes have been rewritten in terms of a new noise line $\hat{\mathbf{f}}_{mult}$ and noise amplitudes T'_{mult}. From Eq.(1.4.33) we then get

$$\mathrm{T}'_{mult}\mathrm{T}'^{\dagger}_{mult} = \mathrm{T}'_A\mathrm{T}'^{\dagger}_A + \mathrm{T}_A\mathrm{T}'_B\left(\mathrm{T}_A\mathrm{T}'_B\right)^{\dagger} = \mathrm{T}_{mult}\Phi\mathrm{T}_{mult} - \Phi \tag{1.4.44}$$

Equivalently one can show that deriving the matrices S_{mult} from the T_{mult} via the Eq.(1.4.14b) and S'_{mult} from the T'_{mult} they obey the relation

$$1 = \mathrm{S}_{mult}\mathrm{S}^{\dagger}_{mult} + \mathrm{S}'_{mult}\mathrm{S}'^{\dagger}_{mult} \tag{1.4.45}$$

which, as already said, shows the unitarity of the whole scattering process.

1.4.4 The Cavity Matrix: The Airy function

The central problem in the calculation of the Casimir effect is the characterization of the properties of the electromagnetic field inside the Fabry-Perot cavity. In Casimir's calculation this characterization was simplified by the fact that we dealt with perfect mirrors. In a more realistic situation such a description may be done through the formalism described in the previous paragraphs.

The quantum field inside the cavity is totally characterized by the commutations rules of its quantum creator ($\hat{\mathbf{a}}^{\dagger}_C$) and annihilation ($\hat{\mathbf{a}}_C$) operators. The properties of $\hat{\mathbf{a}}_C$ depend in general on the incoming field $\hat{\mathbf{a}}^{in}$ and the noise lines corresponding to the two mirrors, say $\hat{\mathbf{f}}_{M_1}$ and $\hat{\mathbf{f}}_{M_2}$. Our aim is to determine the transformation which connects all those quantities in function of the properties of the mirrors.

Without loss of generality we expect a transformation of the form

$$\hat{\mathbf{a}}_C = \mathrm{R}\ \hat{\mathbf{a}}^{in} + \mathrm{R}_1\ \hat{\mathbf{f}}_{M_1} + \mathrm{R}_2\ \hat{\mathbf{f}}_{M_2} \tag{1.4.46}$$

If we choose $\hat{\mathbf{f}}_{M_1}$ and $\hat{\mathbf{f}}_{M_2}$ having the canonical commutation rules we get from Eq.(1.4.33) that

$$\left[\hat{\mathbf{a}}_C, \hat{\mathbf{a}}^{\dagger}_C\right] = \mathrm{RR} + \mathrm{R}_1\mathrm{R}^{\dagger}_1 + \mathrm{R}_2\mathrm{R}^{\dagger}_2 = \mathcal{G} \tag{1.4.47}$$

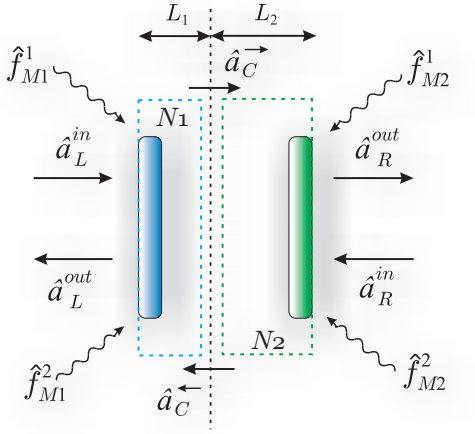

Figure 1.6 : A scheme of the Fabry-Perot cavity as a Quantum Optical Network. Each mirror at the same time transforms the incoming field and inject an environmental noise because of its dissipative nature. The cavity field can be obtained as the result of all those contributions.

With the help of the projection and the swap matrices defined in Eq.(1.4.13), the form of the matrices R, R_1 and R_2 can be deduced from the S- and the T- matrices corresponding to the composite networks $N1$ and $N2$ [84]. Those last ones are made by multilayer slabs representing the mirror and a part of the free propagation along a distance L_1 and L_2

$(L_1 + L_2 = L)$ of the electromagnetic field inside the cavity. The field $\hat{\mathbf{a}}_C$ is calculated on the interface surface between the two networks (see fig.1.7). The calculation leads to [84]

$$\mathcal{G} = 1 + \frac{1}{D}\begin{pmatrix} r_R^{M_1} r_L^{M_2}\ e^{-2\alpha} & r_R^{M_1}\ e^{-2\alpha_1} \\ r_R^{M_2}\ e^{-2\alpha_2} & r_R^{M_1} r_L^{M_2}\ e^{-2\alpha} \end{pmatrix} + h.c., \text{ with } \quad D = 1 - r_R^{M_1} r_L^{M_2}\ e^{-2\alpha} \quad (1.4.48)$$

where $\alpha_i = \kappa L_i$ and $r_R^{M_i}$ and $r_L^{M_i}$ are the reflection coefficients for the mirror M_i seen from their intracavity sides. As a consequence, the intracavity field commutators depend only on the inner reflection coefficients. For this reason, the indices R and L will be dropped in the following.

The expression of the matrix $\mathcal{G}$ means that the commutators of the intracavity fields are not the same as those of the input/output field. This difference is due to the feedback provided by the cavity; the operator $\hat{a}_C^{\rightarrow}$ depends on $\hat{a}_C^{\leftarrow}$ due to the boundary conditions at mirror M_1, but the operator $\hat{a}_C^{\leftarrow}$, in turn, depends on $\hat{a}_C^{\rightarrow}$ because of the boundary conditions at mirror M_2. This feedback is responsible for the denominator D which may be interpreted as arising from a sum over multiple reflections at the two mirrors [118].

In particular the diagonal commutators are independent of the position inside the cavity

$$\left[\hat{a}_C^{\rightarrow}, (\hat{a}_C^{\rightarrow})^\dagger\right] = \left[\hat{a}_C^{\leftarrow}, (\hat{a}_C^{\leftarrow})^\dagger\right] = g \quad (1.4.49)$$

where g is nothing but the Airy function of the cavity:

$$g = 1 + f + f^*, \quad f = \frac{r^{M_1} r^{M_2}\ e^{-2\alpha}}{1 - r^{M_1} r^{M_2}\ e^{-2\alpha}} \quad (1.4.50)$$

The commutation rules (1.4.49) are equivalent to a modification of the spectral density of the intracavity electromagnetic field. They represent the central result of the Quantum Optical Network Theory for the derivation of the Casimir effect.

1.5 The Casimir force: a radiation pressure difference

I will now derive the Casimir force as the difference between the outer vacuum radiation pressure and the inner cavity radiation pressure acting on the surface of a mirror forming the cavity. The net result is indeed a force which pushes each mirror towards the other.

To this aim I will use the results obtained in the previous section to give an expression of the force which allows to include realistic experimental conditions.

1.5.1 Electromagnetic stress tensor and radiation pressure

Let us choose the Coulomb gauge, $\nabla \cdot \mathbf{A}(\mathbf{r}, t) = 0$ [113]. Moreover let us separate the right-ward z-propagation from the left-ward one. Therefore the field decomposes itself in two parts which differ according to the sign of k_z. Introducing a new variable $\phi = \pm 1$ which defines the sign of k_z we obtain the expressions of the quantum electromagnetic

field propagating in the vacuum [84, 113]:

$$\hat{\mathbf{E}} = \sqrt{cZ_{vac}} \sum_{m,\phi} \sqrt{\frac{\hbar\omega_m}{2}} \left(\imath \hat{a}_m^\phi \boldsymbol{\epsilon}_m^\phi e^{-\imath(\omega t - \mathbf{k}\cdot\boldsymbol{\rho} - \phi k_z z)} + h.c; \right) \tag{1.5.1a}$$

$$\hat{\mathbf{B}} = \sqrt{\frac{Z_{vac}}{c}} \sum_{m,\phi} \sqrt{\frac{\hbar\omega_m}{2}} \left(\imath \hat{a}_m^\phi \boldsymbol{\beta}_m^\phi e^{-\imath(\omega t - \mathbf{k}\cdot\boldsymbol{\rho} - \phi k_z z)} + h.c. \right) \tag{1.5.1b}$$

$\boldsymbol{\rho}$ as well as $\mathbf{k}$ are transverse vectors lying in the plane (x, y). Substituting the expressions given in Eqs.(1.5.1) in the respective wave equations we get the following consistency condition between the three-dimensional wavevector $\mathbf{K} \equiv (\mathbf{k}, k_z)$ and the frequency:

$$K = \sqrt{|\mathbf{k}|^2 + k_z^2} = \frac{\omega}{c} \tag{1.5.2}$$

which is nothing but the dispersion relation of the electromagnetic field in the vacuum. In Eqs.(1.5.1) we have also defined

$$\sum_{m,\phi} = \sum_{\phi} \sum_{p} \int \frac{d^3\mathbf{K}}{(2\pi)^3} \int_0^\infty d\omega \; \delta\left(\omega - cK\right) \tag{1.5.3}$$

The variable m stands for $(\omega, \mathbf{K}, p)$ where p is the field mode polarization. The unit vectors $\boldsymbol{\epsilon}$ and $\boldsymbol{\beta}$ specify the polarization of the field component. They are transverse with respect to the direction of propagation

$$\mathbf{K} \cdot \boldsymbol{\epsilon}[\mathbf{K}] = \mathbf{K} \cdot \boldsymbol{\beta}[\mathbf{K}] = 0 \text{ (transversality condition)}, \quad \boldsymbol{\beta}[\mathbf{K}] = \mathbf{K} \times \boldsymbol{\epsilon}([\mathbf{K}] \tag{1.5.4a}$$

and normalized

$$\boldsymbol{\epsilon} \cdot \boldsymbol{\epsilon} = \boldsymbol{\beta} \cdot \boldsymbol{\beta} = 1 \tag{1.5.4b}$$

The conditions given in Eqs.(1.5.4a) and (1.5.4b) however do not define univocally those vectors. We choose $\boldsymbol{\epsilon}^{TE}$ contained in the plane (x, y) which implies $\epsilon_z^{TE} = 0$, where as usual TE is the Transverse Electric polarization. Equivalently TM denote the Transverse Magnetic polarization, for which the magnetic field is orthogonal to the incidence plane.

We use also the vacuum impedance Z_{vac} in place of the electromagnetic constants in the vacuum

$$Z_{vac} = c\mu_0 = \frac{1}{c\varepsilon_0} \tag{1.5.4c}$$

In the following the symbol ϵ will be used as a relative permittivity so that its values in vacuum will be unity.

Now Poynting theorem allows an extension to the fields of the momentum conservation law [85] (see Appendix A.2). In particular if the Maxwell stress tensor $\mathbb{T}$ is defined by

$$\|\mathbb{T}\|_{i,j} = T = \frac{1}{Z_{vac}} \left[E_i E_j + c^2 B_i B_j - \frac{1}{2} \left(E^2 + c^2 B^2 \right) \delta_{i,j} \right] \tag{1.5.5}$$

then the product $\mathbb{T} \cdot \mathbf{n}$ represents the momentum vector flux which enter the volume through a surface element oriented along the direction $\mathbf{n}$. The tensor $\mathbb{T}$ has the dimension

of a pressure and can be used to determine the module of the pressure exerted by the field upon boundaries.

Let us now consider two mirrors (M_1 and M_2) facing each other placed orthogonally to the z-axis. We wish to calculate the net average pressure exerted by the vacuum field upon M_1. Since the surface is orthogonal to the z-direction $\mathbf{n} = \mathbf{z}$, where $\mathbf{z}$ is the unit vector in z direction, one can show from the Poynting theorem that the average pressure is given by

$$P_1 = \langle T_{z,z} \Big|_{\Sigma_{out}}^{\Sigma_{in}} \rangle \tag{1.5.6}$$

where the symbol $\langle \cdots \rangle$ means at the same time the surface average and the quantum average. The surfaces Σ_{out} and Σ_{in} are the external and internal surfaces of the cavity. $T_{z,z}$ is the $i = z,\ j = z$ component of the stress tensor

$$T_{z,z} = -\frac{1}{2Z_{vac}} \left(\mathbf{E} \cdot \mathbb{G} \cdot \mathbf{E} + c^2 \mathbf{B} \cdot \mathbb{G} \cdot \mathbf{B} \right), \qquad \mathbb{G} = 1 - 2\mathbf{zz} \text{ (dyadic form)} \tag{1.5.7}$$

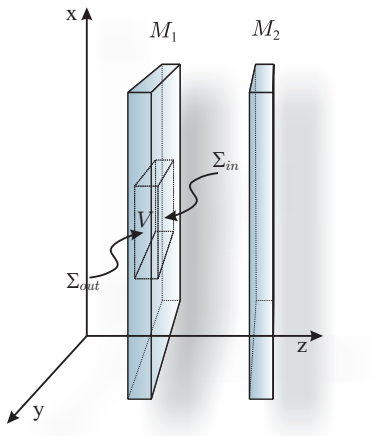

Figure 1.7 : A scheme for the calculation of the net vacuum radiation pressure on the mirror M_1 through the Poynting theorem. The surfaces Σ_{out} and Σ_{in} are the mirror external and internal surfaces.

The surface and quantum average of this quantity in the vacuum state leads to a contraction over the modes resulting in

$$P_1 = \langle T_{z,z} \Big|_{\Sigma_{out}}^{\Sigma_{in}} \rangle = -\sum_{m,\phi} \cos^2 \theta_m \frac{\hbar \omega_m}{2} \langle \hat{a}_m^{\phi} \left(\hat{a}_m^{\phi} \right)^{\dagger} \Big|_{\Sigma_{out}}^{\Sigma_{in}} \rangle_{vac} \tag{1.5.8}$$

where θ_m is the incidence angle, i.e. the angle between the wave vector $\mathbf{K}$ and the z-axis direction. The complete calculation is given in Appendix A.2.

Now we have to calculate the difference between the intracavity field operators acting on the mirror surface Σ_{in} and the external field operators acting on the external surface Σ_{out}. For the mirror M_1 we get

$$P_1 = \sum_m \cos^2 \theta_m \frac{\hbar \omega_m}{2} \langle \hat{\mathbf{a}}_{m,L} \cdot \hat{\mathbf{a}}_{m,L}^{\dagger} - \hat{\mathbf{a}}_{m,C} \cdot \hat{\mathbf{a}}_{m,C}^{\dagger} \rangle_{vac} \tag{1.5.9}$$

The quantum average on the vacuum state of the operators can be easily evaluated using

$$\langle \hat{\mathbf{a}} \cdot \hat{\mathbf{a}}^{\dagger} \rangle_{vac} = \frac{1}{2} Tr \left[\hat{\mathbf{a}}, \hat{\mathbf{a}}^{\dagger} \right] \tag{1.5.10}$$

For the outer fields the diagonal commutators are equal to the unity. For the intracavity field waves, relation (1.4.49) entails that the diagonal commutators are equal to the Airy function g. Therefore we get for the radiation pressure on the mirror M_1

$$P_1 = \sum_m \cos^2 \theta_m \hbar \omega_m \left(1 - g_m \right) \tag{1.5.11}$$

Repeating the calculation for the mirror M_2 one shows that the averaged pressure has opposite values on the two mirrors: $P_1 = -P_2 = P$. This entails that the global force exerted by the vacuum upon the the cavity vanishes, in consistency with the translational invariance of the vacuum. Conversely a non zero force exists between the mirrors and it has magnitude given by

$$F = AP = A \sum_m \cos^2 \theta_m \hbar \omega_m \left(1 - g_m\right) \tag{1.5.12}$$

where A is the surface of the mirrors. The sign convention used here is that a positive value of the force corresponds to an attraction.

We still need to have a deeper look at the integration domain in the definition of the force (1.5.12). We will see that this point is of crucial importance.

1.5.2 The Casimir force as an integral over real and imaginary frequencies

The net force (1.5.12) can be rewritten as

$$F = -A \sum_p \int \frac{d^2\mathbf{k}}{(2\pi)^2} \int_0^\infty \frac{d\omega}{2\pi} \, k_z \left(1 - g_{\mathbf{k}}^p[\omega]\right) \tag{1.5.13}$$

where we have exploited the fact that

$$k_z = \frac{\omega}{c} \cos\theta = \sqrt{\frac{\omega^2}{c^2} - |\mathbf{k}|^2} \tag{1.5.14}$$

At this point we still have to define the domain of integration. k_z may be a real or imaginary quantity, giving rise to propagative or evanescent waves respectively. The properties of evanescent waves can be obtained through analytical continuation of those of the propagative waves (see Appendix C.1). Of course those properties have to be represented by a function which is already analytic in the propagative domain. This is not the case for the whole Airy function. But this is the case for the function

$$f[\omega] = \frac{\rho[\omega]}{1 - \rho[\omega]}, \quad \rho[\omega] = r^{M_1}[\omega] r^{M_2}[\omega] \; e^{-2\alpha[\omega]} \tag{1.5.15}$$

The function $\rho[\omega]$ is the so called "open loop function" whereas the function $f[\omega]$ is the "closed loop function". The open loop function describes a reflection on the mirror M_1, a reflection on the mirror M_2 as well as a propagation forth and back along the full cavity length. In other words $\rho[\omega]$ describe one round trip for a light beam inside the cavity. The closed loop function is nothing but the result of the addition of the infinite round trips performed by the light beam inside the cavity

$$f[\omega] = \sum_{m=1}^{\infty} \rho[\omega]^m \tag{1.5.16}$$

Passivity condition [128] ensures $|\rho[\omega]| < 1$ and then the convergence of the series.

The analytical properties of the closed loop function can be then directly reconnected to those of the reflection coefficients and the phaseshift term. Causality [85] ensures the analyticity of the reflection coefficient in the upper part of the ω-complex plane ($Im\,[\omega] > 0$). The choice of a particular branch of the square-roots involved in the definitions given in Eqs.(1.4.16) has to deal with the choice of a domain where it is possible to isolate a monodronomic branch of the square root [129]. This point is the origin of several misunderstandings in some mathematical developments around the Casimir effect. At the moment we choose the branch of the square root so that for κ_i as defined in Eq.(1.4.16d) we have $Re\,[\kappa_i] > 0$ and $Im\,[\kappa_i] < 0$ in $Im\,[\omega] > 0$ [7]. This automatically sets also the analyticity properties of the phaseshift term similarly to those of the reflection coefficients.

Therefore the closed loop function is an analytical function in the upper ω-complex plane. For this reason it is better to rewrite Eq.(1.5.17) as

$$F = \mathfrak{F} + \mathfrak{F}^* \tag{1.5.17}$$

The integral $\mathfrak{F}$ has an integrand with analytical properties which allows us to describe the effect of the evanescent wave via an analytical continuation of the expression. We can write ($k_z = \imath\kappa$):

$$\mathfrak{F} = A\frac{\hbar}{2\pi\imath}\sum_p \int_{\mathbb{R}^2} \frac{d^2\mathbf{k}}{(2\pi)^2} \int_0^\infty d\omega\ \kappa f[\omega] \tag{1.5.18}$$

In the evanescent sector (see Appendix C.1), the closed loop function $f[\omega]$ is written in terms of the reflection amplitudes calculated for the evanescent waves and an exponential factor corresponding to the evanescent propagation through the cavity. This means that it describes the "frustration" of the total reflection on a mirror due to the presence of the other. This explains why the radiation pressure of the evanescent waves is not identical on the two sides of a given mirror and, therefore, how evanescent waves have a non-null contribution to the Casimir force.

Finally we can give the main results of this chapter: two dielectric mirrors forming a Fabry-Perot cavity placed in the vacuum experience a force, the Casimir Force, given by the expression

$$F = A\frac{\hbar}{\pi}\sum_p \int_{\mathbb{R}^2} \frac{d^2\mathbf{k}}{(2\pi)^2} \int_0^\infty d\omega\ Im\left[\kappa f_{\mathbf{k}}^p[\omega]\right] \tag{1.5.19}$$

The previous expression is a convergent integral as soon as the reflection coefficients obey the physical assumptions: causality, passivity and high frequency-transparency for each mirror. Those assumptions imply that the force F is attractive for dielectric mirrors (no magnetic permittivity) [84].

Remark that the expression in Eq.(1.5.19) is quite different form the an analog expression which can be given for perfectly reflecting mirrors [113] (see Appendix A.1). This is essentially due to the necessity to take into account the evanescent waves and then to

[7] Despite those conditions we have still to fix some degrees of freedom to uniquely isolate a monodromic branch and a domain of analyticity. This problem will be discussed with more detail in the forthcoming chapters and in appendix A.3.

introduce the concept of analytical continuation. In the perfect mirror case there is only propagative wave and we could stop our derivation at the expression given in Eq.(1.5.12).

The expression in Eq.(1.5.19) was first obtained by Lifshitz [47,48] in a particular case. The expression (1.5.19) has a wider range of applicability, when dissipation is considered. This is a non trivial result because we have seen that dealing with dissipative systems is quite delicate.

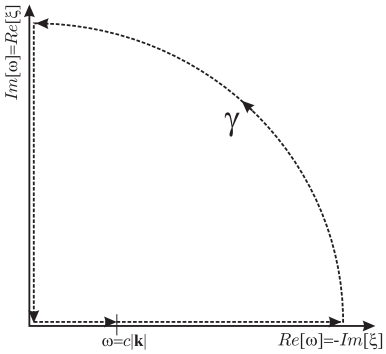

Figure 1.8 : A representation of the contour C in the complex omega plane. C encloses the first quarter of the ω-complex plane, i.e. $(Re\,[\omega] > 0, Im\,[\omega] > 0)$. The path consists in the ω-real positive axe and the ω-imaginary positive axe and is closed at the infinity by the arc γ

Eq.(1.5.19) gives the Casimir force as an integral over real frequencies. For some calculations it is advantageous to change the integration domain to imaginary frequencies. To this aim we come back to Eq.(1.5.18). The closed loop function $f^p_{\mathbf{k}}[\omega]$ is analytical in the upper ω-complex plane. From the Cauchy's theorem [129], the ω-complex integral along any closed path contained in the upper plane is automatically zero. Let us consider a contour C which encloses the first quarter of the ω-complex plane (see fig. 1.8), i.e. $(Re\,[\omega] > 0, Im\,[\omega] > 0)$. The path consists in the ω-real positive axe and the ω-imaginary positive axe and is closed at infinity by the arc γ.

$$\oint_C d\omega\ \kappa f[\omega] = \left(\int_0^\infty d\omega\ + \int_\gamma d\omega\ + \int_{\imath\infty}^0 d\omega\right) \kappa f[\omega] = 0 \tag{1.5.20}$$

Now the integral on the arc γ goes to zero because the high frequency-transparency property of the mirrors

$$\lim_{|\omega|\to\infty} \kappa f[\omega] = 0 \tag{1.5.21}$$

Introducing an imaginary frequency ξ with $\omega = \imath\xi$ we obtain

$$\int_0^\infty d\omega\ \kappa f[\omega] = \int_0^{\imath\infty} d\omega \kappa f[\omega] = \imath \int_0^\infty d\xi \kappa f[\imath\xi] \tag{1.5.22}$$

leading to a Casimir force

$$F = 2\mathfrak{F} = A\frac{\hbar}{\pi}\sum_p \int_{\mathbb{R}^2} \frac{d^2\mathbf{k}}{(2\pi)^2} \int_0^\infty d\xi \kappa f^p_{\mathbf{k}}[\imath\xi] \tag{1.5.23}$$

We have used the fact that $\mathfrak{F}$ is real and then equal to $\mathfrak{F}^*$. The advantage of this expression is indeed that the integrand is a real function of ξ. In particular we find from Eqs.(1.4.2) for the reflection coefficients

$$r^*[\omega] = r[-\omega] \Rightarrow r[\imath\xi] \in \mathbb{R},\ \forall \xi \in \mathbb{R} \tag{1.5.24}$$

The expression given in Eq.(1.5.23) is mathematically equivalent to the one given in Eq.(1.5.19) but often it is more handy for computation. It gives a non divergent expression for the Casimir force which does not need any further regularization procedure. The cutoff

is automatically supplied by the mirrors frequency-dependent reflection coefficients. One can also see easily that $F \xrightarrow{L\to\infty} 0$ or that it reduces to the perfect mirror case expression (1.2.17) when setting $r = 1$. The limiting case $r \to 1$ is discussed in detail in Appendix A.1.

From Eq.(1.5.23) we deduce the expression for the Casimir energy

$$E = A\frac{\hbar}{2\pi}\sum_p \int_{\mathbb{R}^2} \frac{d^2\mathbf{k}}{(2\pi)^2} \int_0^\infty d\xi \ln\left(1 - \rho^p_{\mathbf{k}}[\imath\xi]\right) \tag{1.5.25}$$

Following backwards the contour integral argument we get the expression for the real frequencies

$$E = A\frac{\hbar}{2\pi}\sum_p \int_{\mathbb{R}^2} \frac{d^2\mathbf{k}}{(2\pi)^2} \int_0^\infty d\omega Im\left[\ln\left(1 - \rho^p_{\mathbf{k}}[\omega]\right)\right] \tag{1.5.26}$$

Deriving such an expression directly from Eq.(1.5.19) would lead to some difficulties in dealing with the limit $L \to \infty$. The dependence on L is given indeed by the phaseshift term in the open loop function. This term for the propagative waves does not admit a limit for $L \to \infty$. The problem is solved considering the limit of the appropriate physical analytic continuation in the upper ω-complex plane[8] which is the same argument leading to the expression given in Eq.(1.5.26).

1.6 Conclusions

In this chapter I gave an overview of the theory of the Casimir effect at zero temperature, first in its original formulation, then using a more general treatment which allows to take into account frequency-dependent reflection coefficients in the dissipative case.

I stressed some features which are often misunderstood and which will be extensively exploited in the remainder of this thesis. I showed how a treatment of the Casimir effect involving dielectric mirrors, needs the inclusion of evanescent waves in the calculation. I will show in the rest of this thesis that the evanescent waves represent as the propagative wave an essential feature of the Casimir effect: the two concepts are deeply entangled.

This separation of the integration domain leads naturally to questions whether it is possible to evaluate separately the evanescent part of the Casimir force/energy and the propagative part or what is the physical meaning of this separation. In the rest of this thesis I will answer those questions and this will lead us to some unexpected and interesting results.

[8] We shall discuss this point in the following in more details. In some sense this can be considered a sort of renormalization procedure similar for example to the one involved in the Riemann's zeta function technique.

CHAPTER 2

The Casimir effect and the Plasmons

In this second chapter I give an introduction to the concept of plasmons as developed in the frame of the hydrodynamic model of a metal [86]. A particular case of this model, in which dispersion is neglected, leads to the simple plasma model.

I will calculate the Casimir energy using this model to take into account the mirrors frequency-dependent reflection coefficients. Only in the large distance limit the Casimir effect reproduces the ideal configuration result. At short distances I show that the Casimir energy can be expressed as the zero-point energy shift due to the electrostatic coupling between the surface plasmons, living on the surface of each metallic mirror.

Contents

2.1 Introduction 33
2.2 The Casimir effect within the Hydrodynamic model of a metal 34
2.2.1 The hydrodynamic model and the plasmons 35
2.2.2 The metallic bulk 37
2.2.3 The non-retarded zero point interaction between two bulks . . . 41
2.3 The Casimir energy: the plasma model 44
2.3.1 The long distances limit: recovering the perfect mirrors case . . . 46
2.3.2 The short distances limit: Coulomb interaction between surface plasmons 47
2.4 Conclusions and Comments 48

2.1 Introduction

In the previous chapter I presented the formalism that has been developed to express the Casimir effect via vacuum radiation pressure between real mirrors. Those mirrors are described by frequency-dependent reflection coefficients, characterized typically by the dielectric function of the material.

In this Chapter we will concentrate on the description of the mirrors. In all recent experiments the mirrors were made of metal, typically Au (gold) or Cu (copper). A

possible description of those may be given within the hydrodynamic model of a metal [87, 86, 130, 131], which consider the valence electrons as an electronic-gas. When dissipation and viscosity are negligible, the model reduces to the plasma model. Although very simple, this model turns out to be well adapted to our specific purpose.

In the following I will first evaluate the Casimir energy in the framework of the hydrodynamic model and in the electrostatic approximation. We will show that this expression notably differs from the perfect case showing some similarities with the atom-atom Casimir-Polder interactions [14, 132]. At the same time it recalls the perfect case expression because the result can be expressed as a sum over the zero point energy of the cavity eigenmodes.

We will then exploit the result given at the end of the previous chapter to calculate Casimir energy for a cavity formed by two identical metallic mirrors described by the plasma model. Some mathematical considerations will allow us to evaluate the long distances and short distances approximation of the Casimir energy. We shall see that in the limit of long distance the Casimir energy reproduces the perfect mirrors value. Conversely in the short distance limit we will recover the result obtained in the context of the hydrodynamic model.

2.2 The Casimir effect within the Hydrodynamic model of a metal

In a heuristic vision the van der Waals interactions between a couple of atom arise from the fluctuations of the the electronic cloud surrounding the nucleus: the fluctuations of the first atom cloud generate an electromagnetic field which induces a dipole in the second which at the same time induces a dipole in the first. The induced-dipole induced-dipole interaction is sufficient to give a first understanding of the van der Waals force. The great contribution of H.B.G. Casimir was to include in this vision the retardation effect due to the finiteness of the speed of light. He then showed that those interactions "*may also be derived through studying by means of classical electrodynamic the change of the zero point energy*" of the system [16].

Now let us transfer this argument to the case of a metallic bulk described by means of the hydrodynamic model. There the metal is described as an electronic cloud moving on a static ionic background. The charge density of background and electron cloud together is on the average zero. If electron charge density in some region is reduced below the neutral average, for example due to the thermal fluctuations, the positive background is no longer neutralized in that region and the resulting positive charge attracts the neighbouring electrons. This tends to restore charge neutrality, but the attracted electrons acquire momentum and so overshoot the mark. This produces an excess of negative charge which causes the electrons to be repelled out-wards again. Oscillations are set up which are commonly called plasma oscillations [89].

Let us suppose now that two bulks are facing each other a distance L apart. The plasma oscillations/fluctuations in one bulk must couple the dynamic of the electronic cloud of one bulk with the cloud of the other. Like for the atoms in the case of the van der Waals forces, an interaction between the two bulk is then established which leads to a force. Because of this analogy, we will talk in both cases of van der Waals interactions.

In the previous cases we claimed the thermal motion as the responsible of the fluctuations of the system. Quantum mechanics provides an alternative origin which has the property to exist even at the absolute zero.

In the following sections we concentrate on the plasma oscillation of a metallic bulk described by the hydrodynamic model. We show that those oscillations can be decomposed over a set of orthogonal modes with well defined frequencies. The system can be quantized as for the electromagnetic field and the respective quanta, called plasmons, have an energy proportional to the plasmon mode frequency. As for the electromagnetic field a non null zero point energy exists. Starting from there we describe the interaction between two metallic bulks as the shift in plasmons zero point energy due to their coupling via a quasi-electrostatic field.

2.2.1 The hydrodynamic model and the plasmons

The existence of the plasmons was experimentally shown by Ritchie [133]. If a beam of high energy electrons is shot through a thin aluminium film the energy-loss spectrum of the electrons after the film shows peaks which occur at intervals of approximately 15 eV [133, 89]. This has been recognized as the signature of the plasmons excitation in the metal.

To understand the physical origin of this phenomenon let us consider the metal described by the hydrodynamic model. The free electrons are described as a fluid moving over a positive uniform background. It is worth to stress here that the electrons are free in the sense that they are not bounded in an atom but can move in the whole metal. Still electrons feel each other through the Coulomb interaction.

Let us suppose that $\varrho_e(\mathbf{r}, t)$ represents the density of the electrons at the position $\mathbf{r}$ at time t, so that, if $-e$ is the charge of an electron, the electronic charge density is given by $-e\varrho_e$. If we indicate with $\langle\varrho\rangle$ the average density of the electrons the neutrality condition of the whole system impose that the charge of the uniform static background is given by $e\langle\varrho_e\rangle$. Therefore the excess of positive charge is given by $e\Delta\varrho_e(\mathbf{r}, t) = e(\langle\varrho_e\rangle - \varrho_e(\mathbf{r}, t))$ and the Poisson equation leads to

$$\nabla \cdot \mathbf{E} = 4\pi\Delta\varrho_e e \tag{2.2.1}$$

where $\mathbf{E}$ is the electric field. As usually in fluidodynamic theories [134] we can write the continuity equation

$$-\partial_t\varrho_e = \nabla \cdot (\varrho_e\mathbf{v}) \tag{2.2.2}$$

where $\mathbf{v}(\mathbf{r}, t)$ is the fluid velocity.

Now let us assume that the displacement $\boldsymbol{\zeta}(\mathbf{r}, t)$ from the equilibrium position of the fluid is small corresponding to plasma oscillations of small amplitude. The fluid velocity is then given by $\mathbf{v} = \partial_t\boldsymbol{\zeta}$. Under this assumption the continuity equation can be written in its linearized form

$$-\partial_t\varrho_e = \langle\varrho_e\rangle\nabla \cdot (\partial_t\boldsymbol{\zeta}) \tag{2.2.3}$$

Integrating with respect to the time and considering as initial values the equilibrium

($\varrho_e(\mathbf{r}, t_0) = \langle\varrho_e\rangle$ and $\boldsymbol{\zeta}(\mathbf{r}, t_0) = 0$) we get

$$\langle\varrho_e\rangle - \varrho = \Delta\varrho_e = \langle\varrho_e\rangle\nabla\cdot\boldsymbol{\zeta} \tag{2.2.4}$$

and therefore, inserting this result in Eq.(2.2.1),

$$\nabla\cdot\mathbf{E} = 4\pi\langle\varrho_e\rangle\nabla\cdot\boldsymbol{\zeta} \Rightarrow \mathbf{E} = 4\pi\langle\varrho_e\rangle e\boldsymbol{\zeta} \tag{2.2.5}$$

i.e. the electric field is proportional to the fluid displacement vector.

If we neglect magnetic effects and fluid vorticity (i.e. $\nabla\times\mathbf{v} = 0$) [134] the force per unit of volume on the electron gas is given by

$$\mathbf{F} = -e\langle\varrho_e\rangle\mathbf{E} + \nabla(\Delta P) \tag{2.2.6}$$

The scalar function $\Delta P(\mathbf{r}, t) = P(\mathbf{r}, t) - \langle P\rangle$ is the deviation of the hydrodynamic pressure $P(\mathbf{r}, t)$ from its equilibrium value $\langle P\rangle$. In the limit of small displacements [134] we find the pressure variation as a function of the displacement

$$\partial_t P = -m_e\langle\varrho_e\rangle\beta^2\nabla\cdot\mathbf{v} \Rightarrow \Delta P = -m_e\langle\varrho_e\rangle\beta\nabla\cdot\boldsymbol{\zeta} \tag{2.2.7}$$

where we have again integrated with respect to the time with equilibrium as initial value ($P(\mathbf{r}, t_0) = \langle P\rangle$ and $\boldsymbol{\zeta}(\mathbf{r}, t_0) = 0$). The constant β would be the sound velocity if the medium were neutral. It is introduced in the model as a parameter responsible for dispersion.

Exploiting relation (2.2.5) the equation of motion of the electron gas then turns out to be

$$\begin{aligned} m_e\langle\varrho_e\rangle\partial_t^2\boldsymbol{\zeta} = -e\langle\varrho_e\rangle\mathbf{E} + \nabla(\Delta P) \quad &\Rightarrow \quad \partial_t^2\boldsymbol{\zeta} = -\frac{4\pi\langle\varrho_e\rangle e^2}{m_e}\boldsymbol{\zeta} + \beta^2\nabla(\nabla\cdot\boldsymbol{\zeta}) \\ &\Rightarrow \quad \beta^2\nabla^2\boldsymbol{\zeta} - \partial_t^2\boldsymbol{\zeta} - \omega_p^2\boldsymbol{\zeta} = 0 \end{aligned} \tag{2.2.8}$$

where we have introduced the plasma frequency defined as

$$\omega_p^2 = \frac{4\pi\langle\varrho_e\rangle e^2}{m_e} \tag{2.2.9}$$

and exploited the irrotationality of the fluid.

When $\beta \neq 0$ the last equation is a vectorial equivalent of the Klein-Gordon wave equation for a massive field [81] the "mass" being proportional to the plasma frequency. It describes the propagation of a perturbation with a dispersion relation given by

$$\omega[K] = \sqrt{\omega_p^2 + \beta^2K^2} \tag{2.2.10}$$

with ω and K the wave frequency and the modulus of the wavevector respectively. Because of the non neutral nature of the medium, a perturbation propagates with a group velocity given by

$$\frac{d\omega[K]}{dK} = \frac{\beta^2K}{\sqrt{\omega_p^2 + \beta^2K^2}} \leq \beta \tag{2.2.11}$$

If we now consider an external electromagnetic field $\mathbf{E}_{ext}$ instead of the one produced by the displacement and take the Fourier transformation of the equation of motion we obtain

$$\boldsymbol{\zeta}[\omega, \mathbf{K}] = \frac{e}{m_e} \frac{\mathbf{E}_{ext}[\omega, \mathbf{K}]}{\omega^2 - \beta^2 K^2} \tag{2.2.12}$$

The vector dipole density associated with this displacement is given by

$$\mathbf{d} = -e\boldsymbol{\zeta} \Rightarrow \mathbf{d}[\omega, \mathbf{K}] = -\frac{e^2}{m_e} \frac{\mathbf{E}_{ext}[\omega, \mathbf{K}]}{\omega^2 - \beta^2 K^2} = \alpha[\omega, \mathbf{K}]\mathbf{E}_{ext}[\omega, \mathbf{K}] \tag{2.2.13a}$$

$$\alpha[\omega, \mathbf{K}] = -\frac{e^2}{m_e} \frac{1}{\omega^2 - \beta^2 K^2} \tag{2.2.13b}$$

The function $\alpha[\omega, \mathbf{K}]$ is nothing but the dispersive polarizibility of the electronic gas leading immediately to the dielectric function [85]

$$\epsilon[\omega, \mathbf{K}] = 1 + 4\pi\alpha[\omega, \mathbf{K}] = 1 - \frac{\omega_p^2}{\omega^2 - \beta^2 K^2} \tag{2.2.14}$$

This is the dispersive plasma model. The non dispersive case can be recovered in the limit $\beta \to 0$. In this limit, equation given in Eq.(2.2.8) describes a simple harmonic motion of an electron gas oscillating with a frequency given by the plasma frequency ω_p [89].

The dispersive plasma model takes into account effects coming from the non local response of the metal. These effects, however, manifest themselves only at extremely short distances (below 10nm [135, 136, 137]) which are at the moment out of the experimental reach of Casimir effect measurements.

Until now we did not give any restriction on the metal shape and the electron gas was allowed to fill the whole space. In the next section we consider the metal bulk, which imposes some spatial limitations on the electron gas motion. In this case the system vibrates as a superposition of modes with a well defined frequency. This consideration will allow me to introduce the concept of plasmon.

2.2.2 The metallic bulk

Let us consider that our electronic fluid with its positive background extends throughout the half-space $z \leq 0$. This imposes the following boundary conditions of the displacement field

$$\zeta_z(z = 0) = 0 \quad \text{and} \quad \zeta_z(z \to -\infty) < \infty \tag{2.2.15}$$

The normal component of the displacement (and hence the velocity since $\mathbf{v} = \partial_t \boldsymbol{\zeta}$) vanishes on the interface of the bulk with vacuum and the displacement remains finite to (minus) infinite.

If the fluid is irrotational ($\nabla \times \mathbf{v} = 0$) [134] the displacement can be derived as the gradient of a scalar potential $\Psi(\mathbf{r}, t)$ while, in the electrostatic limit ($c \to \infty$), the electric field can be deduced from the scalar potential $\Phi(\mathbf{r}, t)$

$$\boldsymbol{\zeta} = -\nabla\Psi \quad \text{and} \quad \mathbf{E} = -\nabla\Phi \tag{2.2.16}$$

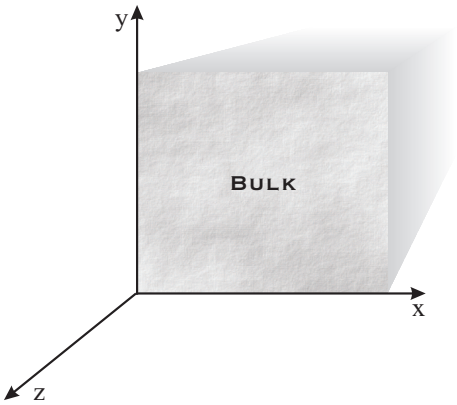

Figure 2.1 : Bulk mirror configuration. The electronic fluid with its positive background extends throughout the half-space $z \leq 0$.

One can show (see Appendix B) that in the frequency domain the hydrodynamic model impose that these two potentials have to satisfy the following equations

$$\nabla^2 \left(\beta^2 \nabla^2 + \omega^2 - \omega_p^2\right) \Psi = 0 \quad \text{and} \quad \Phi = -\frac{m_e}{e} \left(\beta^2 \nabla^2 + \omega^2\right) \Psi \quad (z \leq 0) \tag{2.2.17}$$

Because of the spatial boundary conditions typical of a bulk shape the hydrodynamic model predicts that the gas of free electrons vibrates as a superposition of normal modes with frequencies given by $\omega_{sp}[\mathbf{k}]$ and $\omega_B[\mathbf{k}, k_b]$ (see Appendix B)

$$\Psi(\mathbf{r}, t) = \sum_{\mathbf{k}} \alpha_{\mathbf{k}} \psi_{|\mathbf{k}|}(z) e^{\imath(\mathbf{k}\cdot\boldsymbol{\rho} - \omega_{sp}[\mathbf{k}]t)} + \sum_{|\mathbf{k}|, k_b} \alpha_{\mathbf{k}, k_b} \psi_{\mathbf{k}, k_b}(z) e^{\imath(\mathbf{k}\cdot\boldsymbol{\rho} - \omega_B[\mathbf{k}, k_b]t)} + c.c. \tag{2.2.18}$$

with $\boldsymbol{\rho} = (x, y)$ and $\mathbf{k} = (k_x, k_y)$ and where synthetically we wrote

$$\sum_{\mathbf{k}} \equiv cA \int_{\mathbb{R}^2} \frac{d^2\mathbf{k}}{(2\pi)^2} \quad \text{and} \quad \sum_{\mathbf{k}, k_B} \equiv cA \int_{\mathbb{R}^2} \frac{d^2\mathbf{k}}{(2\pi)^2} \int_0^\infty \frac{dk_b}{\pi} \tag{2.2.19}$$

A is the surface of vacuum/bulk interface. For simplicity hereafter I will measure all frequencies as wavevectors, i.e. ω stands for $\frac{\omega}{c}$

The modes belong to two different ensembles depending on whether $\omega^2 < \omega_p^2 + \beta |\mathbf{k}|^2$ or $\omega^2 > \omega_p^2 + \beta |\mathbf{k}|^2$ (see Appendix B).

Surface modes: $\omega^2 < \omega_p^2 + \beta |\mathbf{k}|^2$.

The first ensemble describes modes in which the electrons oscillations are strongly localized near the interface vacuum/bulk and propagate in a direction parallel to it

$$\psi_{|\mathbf{k}|}(z) = N_{|\mathbf{k}|} \left(\kappa_{sp}[\omega]\ e^{|\mathbf{k}|z} - |\mathbf{k}|\ e^{\kappa_{sp}[\omega]z}\right) \quad (z \leq 0) \tag{2.2.20}$$

where $N_{|\mathbf{k}|}$ is a constant. The electric field associated to such a charge motion propagates also along the surface and exponentially decreases when we move from the surface, corresponding to evanescent waves.

The electric potential outside the bulk has the form

$$\phi_k(z) = C_{|\mathbf{k}|} e^{-|\mathbf{k}|z} \tag{2.2.21}$$

Supposing β fixed the unknown variables of our system are $N_{|\mathbf{k}|}$, $C_{|\mathbf{k}|}$, ω, $|\mathbf{k}|$. The constant $N_{|\mathbf{k}|}$ can be fixed by normalization of $\psi_{|\mathbf{k}|}(z)$ (see the quantification of the plasma oscillation in the following). The boundary conditions leave only one unfixed variable, the others being defined as functions of it. In particular if we chose $|\mathbf{k}|$ as the free variable we deduce (see Appendix B)

$$\omega = \omega_{sp}[\mathbf{k}] = \frac{\omega_p^2 + \beta^2 |\mathbf{k}|^2 + \beta |\mathbf{k}| \sqrt{2\omega_p^2 + \beta^2 |\mathbf{k}|^2}}{2} \xrightarrow{\beta \to 0} \frac{\omega_p^2}{2} \tag{2.2.22}$$

defining the dispersion relation for these modes.

Bulk modes: $\omega^2 > \omega_p^2 + \beta |\mathbf{k}|^2$.

The second ensemble describes a continuum of modes labeled by k_B which propagate inside the bulk. Imposing boundary conditions the corresponding modes have the following form

$$\psi_{|\mathbf{k}|,k_B}(z) = A_{|\mathbf{k}|,k_b} \cos\left[k_B z + \varphi_{|\mathbf{k}|,k_B}\right] + B_{|\mathbf{k}|,k_B b} e^{|\mathbf{k}|z} \tag{2.2.23}$$

where the phase $\left|\varphi_{|\mathbf{k}|,k_B}\right| < \frac{\pi}{2}$.

All the unknown constants can be expressed as function of two free variables. In particular we can write

$$\omega = \omega_B[\mathbf{k}, k_B] \tag{2.2.24}$$

If we suppose that the bulk has a finite thickness $\zeta_z(z = -d) = 0$, $d \gg 1$ we find also

$$\omega^2 = \omega_B^2[\mathbf{k}, n] \equiv \omega_p^2 + \beta^2 |\mathbf{k}|^2 + \left(\beta \frac{n\pi}{d} - \beta \frac{\varphi_{|\mathbf{k}|,n}}{d}\right)^2 \quad n = 1, 2.... \tag{2.2.25}$$

This is an infinite but discrete number of frequency modes (see Appendix B). In the following paragraphs, we shall see that it can be mathematically advantageous to deal with a finite bulk thickness and take the limit $d \to \infty$ only at the end of the calculation. In this case we have a discrete number of modes becoming continuous in the limit $d \to \infty$.

Since $\left|\varphi_{|\mathbf{k}|,n}\right| < \frac{\pi}{2}$ we see from Eq.(2.2.25)

$$\omega_B^2[\mathbf{k}, n] \xrightarrow{\beta \to 0} \omega_p^2 \tag{2.2.26}$$

Evidently the result remains valid also in the limit $d \to \infty$. This result was already encountered in the previous paragraph.

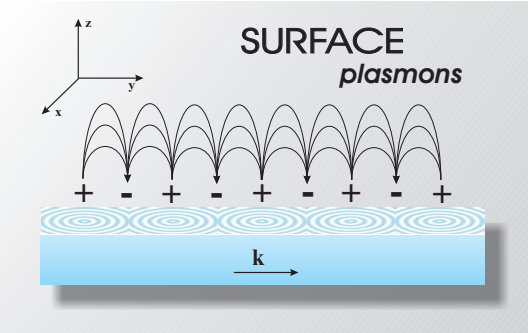

Figure 2.2 : An artist view of the surface plasmon at the metal/ vacuum interface . They are oscillations of the plasma which propagate parallel to the interface, strongly localized near this last and which exponentially decreases as far as we move inside the bulk.

The whole system can be quantized as the electromagnetic field [81]. This leads to the substitutions

$$\alpha_{\mathbf{k}} \rightarrow \hat{a}_{\mathbf{k}} \quad \text{and} \quad \alpha_{\mathbf{k},k_B} \rightarrow \hat{a}_{\mathbf{k},k_B} \tag{2.2.27}$$

$$\left[\hat{a}_{\mathbf{k}}, \hat{a}^{\dagger}_{\mathbf{k}'}\right] = \delta\left(\mathbf{k}-\mathbf{k}'\right) \quad \text{and} \quad \left[\hat{a}_{\mathbf{k},k_B}, \hat{a}^{\dagger}_{\mathbf{k}',k'_B}\right] = \delta\left(\mathbf{k}-\mathbf{k}'\right)\delta\left(k_B-k'_B\right) \tag{2.2.28}$$

Choosing conventionally the normalization constants [113,81], we can write the Hamiltonian associated to motion of the electronic fluid as

$$\hat{H} = \sum_{\mathbf{k}} \hbar\omega_{sp}\left(\hat{N}_{\mathbf{k}} + \frac{1}{2}\right) + \sum_{\mathbf{k},k_B} \hbar\omega_B\left(\hat{N}_{\mathbf{k},k_B} + \frac{1}{2}\right) \tag{2.2.29}$$

In complete analogy with the quantum electromagnetic field the operators $\hat{N}_{\mathbf{k}} = \hat{a}^{\dagger}_{\mathbf{k}}\hat{a}_{\mathbf{k}}$ and $\hat{N}_{\mathbf{k},k_B} = \hat{a}^{\dagger}_{\mathbf{k},k_B}\hat{a}_{\mathbf{k},k_B}$ give the number of plasmons, contained in the surface mode designed by $\mathbf{k}$ and in the bulk mode $(\mathbf{k}, k_B)$. The respective quanta energies are $\hbar\omega_{sp}[\mathbf{k}]$ for the surface mode and $\hbar\omega_B[\mathbf{k}, k_B]$ for the bulk mode. Roughly speaking, since $\omega_{sp}[\mathbf{k}], \omega_B[\mathbf{k}, k_B] \sim \omega_p$ those energies are of the order of $\hbar\omega_p \approx 16eV$ for aluminium. In comparison the kinetic energy of an electron in a metal at room temperature is of the order of the Fermi's energy $\mu_F \approx 3eV$ (Fermi's temperature $\Theta_F \sim 35000K$ and velocity $v_F \sim 10^6$ m/s) [138]. This means that usually the plasmons are not excited at room temperature and the system can be considered in its ground state . The zero-point energy of the system is given by

$$\langle\hat{H}\rangle_{ground} = \sum_{\mathbf{k}} \frac{\hbar\omega_{sp}}{2} + \sum_{\mathbf{k},k_B} \frac{\hbar\omega_B}{2} \tag{2.2.30}$$

Since their discovery [133] plasmons and in particular surface plasmons have been of continuous interest in solid state research physics [139]. Recently they have played a central role in understanding the phenomenon transmission of light through sub-wavelenght hole arrays in optical metal films [93, 94]. Very recently the group headed by Woerdman has experimentally shown [140, 95] that it was possible to transfer entanglement to surface plasmons confirming their quantum nature and proving that they could be used for quantum information applications.

2.2.3 The non-retarded zero point interaction between two bulks

Let us consider now two metallic bulks facing each other in the electrostatic limit. The bulk on the left extends for $-\infty \leq z \leq -L/2$ while the one on right for $L/2 \leq z \leq \infty$.

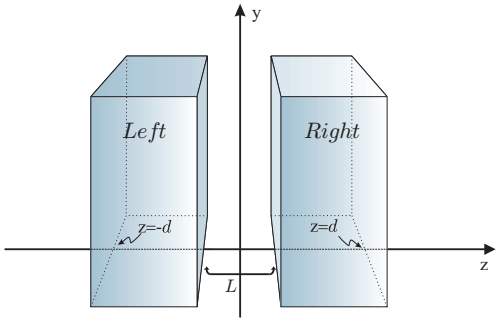

Figure 2.3 : Two metallic bulks facing. The bulk on the left ($Left$) extends for $-d \leq z \leq -L/2$ while the one on right ($Right$) for $L/2 \leq z \leq d$

There is a non-zero electric field outside the bulk associated to the dynamic of the electron fluid. As a consequence, the plasma oscillations in the two bulks are electrostatically coupled:

$$\hat{H}_c = \hat{H}_{Left} + \hat{H}_{Right} + \hat{H}_{Int} \qquad (2.2.31)$$

$\hat{H}_{Left}$ and $\hat{H}_{Right}$ are the corresponding free hamiltonians for the left and right bulks with a form like in Eq.(2.2.29) while $\hat{H}_{Int}$ represent the interaction between them. For simplicity we evaluate directly the exact mode frequencies of the composite system rather than obtain them from a diagonalization of the hamiltonian $\hat{H}_c$.

The principal difference with the one bulk case resides in the solutions for the electric potential Ψ outside the two bulks. The electric potential now has to be continuous with the z component of the electric field across two different vacuum/bulk interfaces (see Eq.(B.1.5) in the Appendix B), namely $z = -L/2$ and $z = L/2$.

Because of the translational symmetry of the whole system the specular symmetry with respect to the plane $z = 0$ we have (see Appendix B)

$$\phi^{\pm}_{|\mathbf{k}|}(z) = C^{\pm}_{|\mathbf{k}|}\left(e^{|\mathbf{k}|z} \pm e^{-|\mathbf{k}|z}\right) \quad (|z| \leq \frac{L}{2}) \qquad (2.2.32)$$

The even (+) and odd (-) solution corresponds to a particular $\psi^{\pm}_{|\mathbf{k}|}(z)$ in the left bulk and in the right one. Again because of the specular symmetry it is sufficient to consider solutions only in one half space, say, the left half-space ($z \leq -\frac{L}{2}$). Again, the solutions split into two classes depending on whether $\beta\kappa_{\pm} = \sqrt{\omega_p^2 + \beta^2 |\mathbf{k}|^2 - \omega^2}$ is a real or a pure imaginary number.

For the **coupled surface modes** we obtain

$$\psi^{\pm}_{|\mathbf{k}|}(z) = N^{\pm}_{|\mathbf{k}|}\left(\kappa_{\pm}\, e^{|\mathbf{k}|\left(z+\frac{L}{2}\right)} - |\mathbf{k}|\; e^{\kappa_{\pm}\left(z+\frac{L}{2}\right)}\right) \quad (z \leq -\frac{L}{2}) \qquad (2.2.33)$$

They are still oscillations strongly localized near the interface vacuum/bulk and propagating in a direction parallel to it. In this case the application of the boundary conditions leads to

$$\omega^2_{\pm}[\mathbf{k}] \xrightarrow{\beta \to 0} \frac{\omega_p^2}{2}\left(1 \pm e^{-|\mathbf{k}|L}\right) \qquad (2.2.34)$$

For simplicity, we consider only the non-dispersive limit for the frequency mode.

Coupled bulk modes still propagate inside the bulk

$$\psi^{\pm}_{k,k^{\pm}_B}(z) = A^{\pm}_{|\mathbf{k}|,k^{\pm}_B} \cos\left[k^{\pm}_B\left(z+\frac{L}{2}\right)+\varphi^{\pm}_{|\mathbf{k}|,k^{\pm}_B}\right] + B^{\pm}_{|\mathbf{k}|,k^{\pm}_B} e^{|\mathbf{k}|\left(z+\frac{L}{2}\right)} \tag{2.2.35}$$

Again the infiniteness of the bulks (see Appendix B) leads to a continuum of modes with frequencies given by $\omega^{\pm}_B\left[\mathbf{k},k^{\pm}_B\right]$. The discretization of the bulk modes is now obtained imposing that $\zeta_{Left}(z=-d)=\zeta_{Right}(z=d)=0$. For a large enough d we get

$$k^{\pm}_B d+\varphi^{\pm}_{|\mathbf{k}|,k^{\pm}_B}=n\pi \Rightarrow k^{\pm}_B=\frac{n\pi}{d}-\frac{\varphi^{\pm}_{|\mathbf{k}|,n}}{d} \quad n=1,2.... \tag{2.2.36}$$

and consequently

$$\omega^2 \equiv \omega^{\pm}_B[\mathbf{k},n]^2=\omega_p^2+\beta^2|\mathbf{k}|+\left(\beta\frac{n\pi}{d}-\beta\frac{\varphi^{\pm}_{|\mathbf{k}|,n}}{d}\right)^2 \quad n=1,2.... \tag{2.2.37}$$

This is an infinite but discrete number of frequency modes.

Remark that the splitting of the frequency modes had to be expected from the form of the interaction hamiltonian. Classically in the electrostatic approximation it has the form [85]

$$H_{Int}=-\frac{e}{2}\left(\int_{z\leq -L/2} d^3\mathbf{r}\Delta\varrho_{Left}\Phi_{Right}+\int_{z\geq L/2} d^3\mathbf{r}\Delta\varrho_{Right}\Phi_{Left}\right) \tag{2.2.38}$$

where $\Delta\varrho_{Left}(\Delta\varrho_{Right})$ represents the variation of the electronic charge density from the equilibrium value in the left(right) bulk and $\Phi_{Left}(\Phi_{Right})$ is the external electric potential generated by the bulk placed on the right(left). Each integral runs over one half-space. The interaction hamiltonian can be rewritten in terms of the functions Ψ and Φ and then in terms of the corresponding quantum operators $\hat{\Psi}$ and $\hat{\Phi}$ (see Appendix B)

$$\hat{H}_{Int}=\frac{e\langle\varrho_e\rangle}{2}\left(\int_{z\leq -L/2}\hat{\Phi}_{Right}\nabla^2\hat{\Psi}_{Left}\ d^3\mathbf{r}+\int_{z\geq L/2}\hat{\Phi}_{Left}\nabla^2\hat{\Psi}_{Right}\ d^3\mathbf{r}\right) \tag{2.2.39}$$

Since the potential $\hat{\Phi}_{Left}\left(\hat{\Phi}_{Right}\right)$ can be expressed in terms of $\hat{\Psi}_{Left}\left(\hat{\Psi}_{Right}\right)$, this hamiltonian describes a linear coupling between the electronic gases of the two bulks. The interaction depends on the distance L between the bulks and vanishes for an infinite distance.

After diagonalization the hamiltonian (2.2.31) describing the coupled bulks system takes the form

$$\hat{H}_c=\sum_i\left[\sum_{\mathbf{k}}\hbar\omega_i\left(\hat{N}^i_{\mathbf{k}}+\frac{1}{2}\right)+\sum_{\mathbf{k},k^i_B}\hbar\omega^i_B\left(\hat{N}^i_{\mathbf{k},k^i_B}+\frac{1}{2}\right)\right], \quad i=\pm \tag{2.2.40}$$

where $\hat{N}^i$ and $\hat{N}^i_{\mathbf{k},k^i_B}$ are the operators giving the number of surface and bulk coupled plasmons in the mode $\hbar\omega_i$ and ω^i_B respectively. The corresponding ground energy can be written

$$\langle \hat{H}_c \rangle_{ground} = \sum_i \left[\sum_{\mathbf{k}} \frac{\hbar\omega_i}{2} + \sum_{\mathbf{k},k^i_B} \frac{\hbar\omega^i_B}{2} \right], \quad i = \pm \tag{2.2.41}$$

In complete analogy to the Casimir energy, we may now calculate the energy difference between the two bulks, being at distance L and being infinitely far away from each other

$$E = \left[\langle \hat{H}_c \rangle_{ground} \right]^L_{L\to\infty} = \langle \hat{H}_c \rangle_{ground} - 2\langle \hat{H} \rangle_{ground} \tag{2.2.42}$$

The last identity holds because the interaction operator vanishes for infinite distances. One can then easily show that expression (2.2.42) decomposes into

$$E = \underbrace{\sum_{\mathbf{k}} \frac{\hbar}{2} \left(\omega_+ + \omega_- - 2\omega_{sp} \right)}_{\text{Surface plasmons shift}} + \underbrace{\left[\sum_{\mathbf{k},k^i_b} \frac{\hbar\omega^i_B}{2} \right]^L_{L\to\infty}}_{\text{Bulk plasmons shift}} \quad (i = \pm) \tag{2.2.43}$$

Assuming a finite but very large thickness for the bulks from Eqs.(2.2.37) and (2.2.25) and defining

$$q = \frac{n\pi}{L} \quad \text{and} \quad \omega^2[\mathbf{k}, q] = \omega_p^2 + \beta^2 |\mathbf{k}| + \beta^2 q \tag{2.2.44}$$

we can write

$$\omega^\pm_B[\mathbf{k}, n]^2 \approx \omega^2[\mathbf{k}, q] - 2\beta^2 q \frac{\varphi^\pm_{|\mathbf{k}|,q}}{d}, \quad \omega_B[\mathbf{k}, n]^2 \approx \omega^2[\mathbf{k}, q] - 2\beta^2 q \frac{\varphi_{|\mathbf{k}|,q}}{d} \tag{2.2.45}$$

$$\left[\omega^\pm_B[\mathbf{k}, n] \right]^L_{L\to\infty} = \omega^\pm_B[\mathbf{k}, n] - \omega_B[\mathbf{k}, n] = -\frac{\beta^2 q}{\omega[\mathbf{k}, q] d} \left(\varphi^\pm_{|\mathbf{k}|,q} - \varphi_{|\mathbf{k}|,q} \right) \tag{2.2.46}$$

Now we have just to write the discretized version of the bulk plasmons shift and take the limit $d \to \infty$ at the end

$$\begin{aligned} \left[\sum_{\mathbf{k},k^i_B} \frac{\hbar\omega^i_B}{2} \right]^L_{L\to\infty} &\to \lim_{d\to\infty} \frac{\hbar}{2} \sum_{\mathbf{k},n} \left[\omega^i_B \right]^L_{L\to\infty} \\ &= -\beta^2 \sum_{\mathbf{k}} \int_0^\infty \frac{dq}{\pi} \frac{q}{\omega[\mathbf{k}, q]} \left(\varphi^+_{k,q} + \varphi^+_{|\mathbf{k}|,q} - 2\varphi_{|\mathbf{k}|,q} \right) \end{aligned} \tag{2.2.47}$$

Since the double integral in the last term is convergent in the limit $\beta \to 0$ the whole contribution vanishes in the same limit. This behavior reveals the so called decoupling of the bulk plasmons from the exterior [86]. One can indeed show that the electric potential and the electric field associated to the bulk modes vanish outside the medium in the limit $\beta \to 0$. The propagative modes of the two bulks cannot be coupled and they do not

contribute to the zero point energy shift. In the dispersive limit ($\beta \to 0$) the energy difference is therefore given by

$$E \approx cA \int \frac{d^2\mathbf{k}}{(2\pi)^2} \frac{\hbar}{2} \left(\omega_+ + \omega_- - 2\omega_{sp}\right) \tag{2.2.48}$$

where we put $\omega_{sp}^2 = \omega_p^2/2$ and $\omega_\pm^2 = \omega_{sp}^2 \left(1 \pm e^{-|\mathbf{k}|L}\right)$.

2.3 The Casimir energy: the plasma model

In Chapter 1 we have shown that Casimir force results from the radiation pressure exerted by vacuum fluctuations upon the two mirrors which form a Fabry-Perot cavity. The force is the result of the balance between the radiation pressure of the resonant and non resonant modes which push the mirrors respectively towards the outer and inner sides of the cavity. This balance includes not only the contributions of ordinary waves propagating freely outside the cavity with a frequency ω larger than the bound $c\,|\mathbf{k}|$ fixed by the norm of the transverse vector but also that of evanescent waves which correspond to frequencies ω smaller than $c\,|\mathbf{k}|$. These waves are fed by additional fluctuations coming from the noise lines [118] into the dielectric medium and propagating with an incidence angle larger than the limit angle. They are thus transformed into evanescent waves decreasing exponentially when the distance from the interface increases.

This method always leads to a finite result for Casimir force and energy as a consequence of the causality properties and high-frequency transparency of real mirrors [84]. In other words, the properties of real mirror are enough to obtain a regular expression of the Casimir force, despite the infiniteness of the vacuum energy.

Imperfectly reflecting mirrors can be indeed described by scattering amplitudes which depend on the frequency, wavevector and polarization while obeying general properties of stability, high-frequency transparency and causality (see Chap. 1 and [84]).

In a geometrical configuration where two plane parallel mirrors, at zero temperature are placed a distance L apart from each other, the area A of the mirrors being much larger than the squared distance($A \gg L^2$) the general expression of the Casimir's force and energy can be written (see Chap. 1 and [84]) as

$$F = \frac{\hbar A c}{\pi} \sum_p \int \frac{d^2\mathbf{k}}{(2\pi)^2} \int_0^\infty d\xi \kappa \frac{\rho_{\mathbf{k}}^p[\imath\xi]}{1 - \rho_{\mathbf{k}}^p[\imath\xi]} \tag{2.3.1a}$$

$$E = \frac{\hbar A c}{2\pi} \sum_p \int \frac{d^2\mathbf{k}}{(2\pi)^2} \int_0^\infty d\xi \ln[1 - \rho_{\mathbf{k}}^p[\imath\xi]] \tag{2.3.1b}$$

where

$$\kappa = \sqrt{\xi^2 + |\mathbf{k}|^2} \quad \text{and} \quad \rho_{\mathbf{k}}^p[\imath\xi] = r_{\mathbf{k}}^p[\imath\xi]^2 e^{-2\kappa L} \tag{2.3.2}$$

The function $r_{\mathbf{k}}^p[\imath\xi]$ represents the reflection coefficient of the cavity mirrors (seen from inside the cavity) while $\rho_{\mathbf{k}}^p[\imath\xi]$ is the open loop function (see Chapter 1). The sum on

p stands for the two possible polarizations (TE, TM) of the electromagnetic field. For simplicity I measure all frequencies as wavevectors, i.e. ω stands for $\frac{\omega}{c}$ and ξ stands for $\frac{\xi}{c}$.

Expressions given in Eqs.(2.3.1) are mathematically equivalent to more intuitive but mathematically less convenient expressions where the integral is taken on the frequency ω. Eqs.(2.3.1) give Casimir force and energy between real mirrors described by arbitrary frequency dependent reflection amplitudes. They are regular integrals as these amplitude respect causality, high frequency transparency, stability conditions and hold both for dissipative and lossless mirrors (see Chap. 1 and [84]).

In the simplest model the mirror can be described by a metallic bulk[1] with an optical response described by non-dispersive plasma model (see previous paragraph). In this case the reflection coefficient is simple given by Fresnel laws corresponding to vacuum/metal interface [48, 85]

$$r_{\mathbf{k}}^{p}[\imath\xi] = \frac{1 - Z_{\mathbf{k}}^{p}[\imath\xi]}{1 + Z_{\mathbf{k}}^{p}[\imath\xi]} \tag{2.3.3a}$$

For $p = TM, TE$ we have [85, 48]

$$Z_{\mathbf{k}}^{TE} = \frac{\kappa_m}{\kappa}, \quad Z_{\mathbf{k}}^{TM} = \epsilon\frac{\kappa}{\kappa_m} \quad \text{where} \quad \kappa_m = \sqrt{\epsilon[\imath\xi]\xi^2 + |\mathbf{k}|^2} \tag{2.3.3b}$$

$\epsilon[\imath\xi]$ is the dielectric constant of the metal, describing its optical response. In the non-dispersive limit it takes the form

$$\epsilon[\imath\xi] = 1 + \frac{\omega_p^2}{\xi^2}. \tag{2.3.4}$$

ω_p is the plasma frequency. Equivalently we may also use the plasma wavelength $\lambda_p = 2\pi/\omega_p$

Thanks to its particular simple expression and to its mathematical properties we are able to put in evidence some qualitative and quantitative features of the Casimir effect. In particular, introducing the definition given for $\epsilon[\imath\xi]$ in Eq.(2.3.4) we get $\kappa_m = \sqrt{\omega_p^2 + \kappa^2}$.

For mathematical purpose it is useful to introduce a corrective factor η which describes the Casimir energy with respect to its value in the perfect mirrors case

$$E = \eta E_{cas}, \quad E_{Cas} = -\frac{\hbar c \pi^2 A}{720 L^3}, \tag{2.3.5}$$

The corrective coefficient is still a function of the cavity length L. Always to simplify mathematics it is useful to work with dimensionless variables defined by

$$\Omega_p = \omega_p L, \quad \Xi = \xi L, \quad K = \kappa L, \quad k = |\mathbf{k}|\, L \tag{2.3.6}$$

In terms of those variables the corrective coefficient can be written as

$$\eta = \frac{180}{\pi^4} \sum_p \int_0^\infty dk \int_0^\infty d\Xi \ln[1 - \rho^p[\imath\Xi, K]] \tag{2.3.7}$$

[1] In Chapter 1 we already briefly discussed the difficulties connected with the bulk approximation. Here we make this approximation without further comments. A more detailed analysis of the implication of this approximation is done in Chapter 3 and in Appendix C.2.

2.3.1 The long distances limit: recovering the perfect mirrors case

Let us consider the case where $L \gg \lambda_p$. Using normalized variables this distance range corresponds to the limit $\Omega_p \gg 1$. From an inspection of the open loop function one can show that the most significant contribution to the integrals involved in the definition of η given in Eq.(2.3.7) arises for $K \sim 1$. In the large distances limit ($\Omega_p \gg 1$) the short frequency behavior reflection coefficient is dominant. At low frequencies metals are reals perfect reflectors ($r^p \sim 1$) and one can show that for $\Omega_p \gg 1$ and $K \sim 1$

$$r^{TE}[\imath\Xi, K]^2 - 1 \approx -\frac{4K}{\Omega_p} \quad \text{and} \quad r^{TM}[\imath\Xi, K]^2 - 1 \approx -\frac{4K}{\Omega_p}\frac{\Xi^2}{K^2} \tag{2.3.8a}$$

We can then develop the expression of η as:

$$\eta \approx \frac{180}{\pi^4}\sum_p \int_0^\infty dk \int_0^\infty d\xi \left(\ln[1-e^{-2K}] + \frac{1}{1-e^{2K}}\left[r^p[\imath\Xi, K]^2 - 1\right]\right) \tag{2.3.9}$$

Substituting Eq.(2.3.8) into (2.3.9) an performing the integration we derive that

$$\eta \approx 1 - \frac{4}{\Omega_p} = 1 - 8\pi\frac{\lambda_p}{L} \quad L \gg \lambda_p \Rightarrow \Omega_p \gg 1 \tag{2.3.10}$$

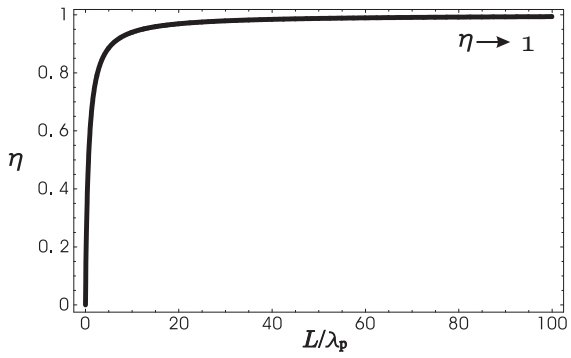

Figure 2.4 : A plot of the corrective coefficient η as function of L/λ_p. The plot shows that in the long distances limit ($L \gg \lambda_p$) when the metal is described by the plasma model the Casimir energy tends towards the value between perfect mirrors.

The result is sketched in figure 2.4. Clearly in the long distances limit ($L \gg \lambda_p$) the Casimir energy tends towards its value between two perfect mirrors case [90, 141].

Physically speaking this result is not surprising. Looking at the dielectric function, we see that the mirrors are good reflectors for frequency lower than the plasma frequency. In this range of frequencies they can be approximated as perfect reflectors. We saw that in the perfect mirrors case the cavity frequency modes are given by

$$\omega_n = \sqrt{|\mathbf{k}|^2 + \left(\frac{n\pi}{L}\right)^2} \tag{2.3.11}$$

Therefore the number of modes n_c in the range of frequency where the perfect mirrors approximation is valid is roughly give by $n_c \sim \Omega_p/\pi$. We can say that in the limit $\Omega_p \gg 1$ the large number of perfect modes leads the Casimir energy to reach the limit of perfect mirrors.

2.3.2 The short distances limit: Coulomb interaction between surface plasmons

More interesting is the distance range given by $L \ll \lambda_p \Rightarrow \Omega_p \ll 1$. Under this approximation Eq.(2.3.1b) takes a simpler form. Since $L \ll \lambda_p$, an evaluation of the significant contribution to the integral together with the condition for non-vanishing value of the reflection coefficients in Eq.(2.3.1a) leads to

$$\begin{cases} \kappa L \sim 1 \\ \xi \leq \omega_p \end{cases} \rightarrow \begin{cases} \kappa\lambda_p \gg 1 \\ \frac{\xi}{\omega_p} = \frac{\xi\lambda_p}{2\pi} \leq 1 \end{cases} \rightarrow \begin{cases} \kappa \gg \frac{\omega_p}{2\pi} \\ \xi \leq \omega_p \end{cases} \Rightarrow |\mathbf{k}| \gg \xi \quad \text{(evanescent region)} \tag{2.3.12}$$

Those last relations imply that κ and κ_m are both approximately equal to $|\mathbf{k}|$. From the definitions given in Eqs.(2.3.3) one can show that for these range of parameters $r_{\mathbf{k}}^{TE}$ becomes negligible whereas $r_{\mathbf{k}}^{TM}$ takes the form

$$Z_{\mathbf{k}}^{TM} \approx \epsilon[\imath\xi] \Rightarrow r_{\mathbf{k}}^{TM} \approx \frac{1-\epsilon[\imath\xi]}{1-\epsilon[\imath\xi]} = -\frac{\omega_{sp}^2}{\xi^2+\omega_{sp}^2}, \quad \omega_{sp}^2 = \frac{\omega_p^2}{2} \tag{2.3.13}$$

The closed loop function can then be written as

$$\kappa f_{\mathbf{k}}^{TM}[\imath\xi] \approx \mp\frac{1}{2}\frac{\omega_+^2-\omega_-^2}{[\xi^2+\omega_+^2][\xi^2+\omega_-^2]}\frac{d}{dL}\omega_\pm^2 = \sum_i \frac{\omega_i}{\xi^2+\omega_i^2}\frac{d}{dL}\omega_i, \qquad i=\pm \tag{2.3.14}$$

where we put $\omega_\pm^2 = \omega_{sp}^2\left(1 \pm e^{-|\mathbf{k}|L}\right)$. Performing the integral over the imaginary frequencies

$$F \approx \frac{\hbar cA}{\pi}\int\frac{d^2\mathbf{k}}{(2\pi)^2}\int_0^\infty d\xi \sum_i \frac{\omega_i}{\xi^2+\omega_i^2}\frac{d}{dL}\omega_i = cA\frac{\hbar}{2}\int\frac{d^2\mathbf{k}}{(2\pi)^2}\sum_i\frac{d}{dL}\omega_i, \qquad i=\pm \tag{2.3.15}$$

and remembering that the force and the energy are connected by an integral over the cavity length L (see Chapter 1)

$$E(L) = -\int_L^\infty F(l)dl \tag{2.3.16}$$

we find the following approximated form for Casimir energy for $L \ll \lambda_p$ [90]

$$E \approx cA\int\frac{d^2\mathbf{k}}{(2\pi)^2}\frac{\hbar}{2}\left(\omega_+ + \omega_- - 2\omega_{sp}\right) \tag{2.3.17}$$

This expression corresponds precisely to Eq.(2.4.1), which gave the electrostatic interaction between the surface plasmons in the hydrodynamic model. In other words, at short distances the Casimir energy may be expressed as the Coulomb interaction between the two surface plasmons ω_+ and ω_- living on the surface of each mirror. Indeed, for small distances $L \ll \lambda_p$ ($\sim$100nm for typical metals) we may neglect any retardation effect coming from the finite speed of the light.

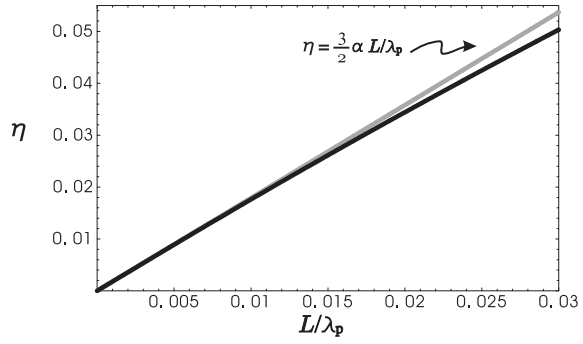

Figure 2.5 : A plot of the corrective coefficient η as function of L/λ_p. The graphics shows that in the short distances limit ($L \ll \lambda_p$) when the metal is described by the plasma model the corrective factor linearly depends on the rapport L/λ_p (see the gray curve). The change in the power law of the Casimir energy generated in the limit $L \ll \lambda_p$ by corrective factor recalls Casimir-Polder-Van der Waals interactions behavior.

Using the explicit expression for the coupled surface plasmon frequencies, $\omega_\pm$ and exploiting the definition of the dimensionless variables, we can derive the correction coefficient for the Casimir energy at short distances:

$$\eta \approx \frac{3}{4\pi}\alpha\ \Omega_p = \frac{3}{2}\alpha\frac{L}{\lambda_p} \quad L \ll \lambda_p \Rightarrow \Omega_p \ll 1 \tag{2.3.18}$$

$$\alpha = -\frac{120\sqrt{2}}{\pi^2}\int_0^\infty k\left(\sqrt{1+e^{-k}} + \sqrt{1-e^{-k}} - 2\right)dk \tag{2.3.19}$$

where numerically $\alpha = 1.193..$ [90].

At short distances, the energy does not scales with $1/L^3$ anymore, but with $1/L^2$. It is worth comparing the variation with distance of the Casimir force with that of the Van der Waals force between two atoms in vacuum. Casimir and Polder [14, 132] indeed showed that the latter force obeys power laws in the two limits of short and long distances, with the exponent being changed by one unit when going from one limit to the other and the crossover taking place when the interatomic distance L crosses the typical atomic wavelength λ_A. The same behavior is also observed for the Casimir force between two metallic mirrors with the plasma wavelength λ_p playing the role of λ_A. This change of exponent in the power laws is effectively similar in the Casimir and Casimir-Polder cases : the Casimir energy scales as $\frac{1}{L^3}$ at large distance and as $\frac{1}{\lambda_p L^2}$ at short distances while the Casimir-Polder energy scales as $\frac{1}{L^7}$ at large distances and as $\frac{1}{\lambda_A L^6}$ at short distances[2].

2.4 Conclusions and Comments

When we describe the metal as a electron fluid moving on a positive uniform static background, we find it to exhibit oscillations. Moreover when boundary conditions are imposed on the spatial distribution of the gas it can vibrate only as a linear combinations of normal modes. In average the gas charge density neutralizes the positive background but because

[2]The difference in the power exponent between Casimir-Polder and Casimir laws can be traced back to the efficiency of the coupling in the case of facing plane mirrors [90]. Indeed it follows from the point-like character of atoms that their mutual coupling through the field is less efficient than for mirrors. In other words, the two atoms form a poor-finesse cavity so that the higher order interferences terms, which play an important role in the Fabry-Perot cavity, can be disregarded in the two-atoms problem [90].

of the oscillations locally it may appear a net charge and consequently an electric field. Therefore it is not surprising that considering a system formed by two metallic bulk the hydrodynamic model predicts an interaction between them.

Now quantum mechanics provides the vibration source. If the fluid motion is quantized like the electromagnetic field the gas shows zero-point fluctuations. This means that the quantized version of the hydrodynamic model predicts an interaction between two facing metallic bulks even at zero temperature. This interaction produces a shift in the value of the zero-point energy of the whole system. In Chapter 1 we saw that this shift is nothing but the Casimir energy. Because of the modes decomposition of the electronic fluid vibration the system zero-point energy looks like a sum of terms like $\hbar\omega_n/2$ where ω_n is the mode frequency. The Casimir energy looks like $E = [\sum_n \hbar\omega_n/2]_{L\to\infty}^{L}$, L being the distance between the two bulks.

In this chapter we proved that in the electrostatic approximation and in the non-dispersive limit the interaction produce a energy shift which can be written as

$$E = cA \int \frac{d^2\mathbf{k}}{(2\pi)^2} \frac{\hbar}{2} \left(\omega_+ + \omega_- - 2\omega_{sp}\right) \tag{2.4.1}$$

$\omega_\pm$ and ω_{sp} are respectively the electrostatic coupled and uncoupled surface plasmons frequency, oscillations of the plasma which propagate parallel to the interface, strongly localized close to it and which exponentially decreases when we move inside the bulk.

We showed that the previous expression coincides exactly with the short distance ($L \ll \lambda_p$) asymptotic expression of the Casimir energy derived at the end of the Chapter 1 when the optical response of mirrors can be described by the plasma model. Eq.(2.4.1) gives a description of the Casimir effect which establishes a connection between the condensed matter theory and the quantum electromagnetic field theory. In this limit the Casimir energy exhibits a change in the power law similar to the one of the Casimir-Polder energy between two atoms.

Exploiting the bulk limit expression for the reflection coefficients we also showed that the long ($L \gg \lambda_p$) distances asymptotic expressions for the Casimir energy reproduces the perfect mirrors behavior.

CHAPTER 3

The Casimir energy as sum over the Cavity Frequency Modes

In this chapter I will perform the decomposition of the Casimir energy into a sum of the cavity modes. I will then analyze explicitly these modes by using the plasma model for the mirrors material properties. Two sets of modes will appear, propagative cavity modes and evanescent modes. Their characteristics will be discussed in detail.

Contents

3.1 Introduction 51
3.2 The Casimir energy as a sum over the frequency modes of a real cavity 53
3.3 Mode analysis with the plasma model 56
3.3.1 Equation for the cavity modes 57
3.3.2 TE-modes 59
3.3.3 The TM-modes 61
3.4 Conclusion and comments 67

3.1 Introduction

Historically the Casimir energy was derived between perfect mirrors as the sum of the zero-point energies $\frac{\hbar\omega}{2}$ of the cavity eigenmodes, subtracting the result for finite and infinite separation, and extracting the regular expression by inserting a formal high-frequencies cutoff [82](see Chap.1)

$$E_{Cas} = -\frac{\hbar c \pi^2 A}{720 L^3}. \tag{3.1.1}$$

In Chapter 1 we have also derived the Casimir effect by adopting another point of view which leads to a generalization of the result to more realistic configurations. The Casimir force is seen as the net result between the intracavity and the external vacuum radiation

pressure. The Casimir force and energy can be written as an integral over frequencies and transverse wavevectors. The perfect mirrors result is then recovered by setting the reflection coefficients of the mirrors to unity.

In the previous Chapter we calculated the Casimir effect between metallic mirrors using the plasma model. Even if this model is not sufficient for an accurate evaluation of Casimir effect at the order of the 1% for precise theory-experiment comparisons [62], its simplicity allow us to describe qualitatively and quantitatively some interesting physical features. We showed that the Casimir effect has another interpretation establishing a bridge between quantum field theory of vacuum fluctuations and condensed matter theory of forces between two metallic bulks. In the limit of small separations $L \ll \lambda_p$ the Casimir effect can be understood as resulting from the Coulomb interaction between surface plasmons. We derived the following approximated form for Casimir energy [90]

$$E \approx A \int \frac{d^2\mathbf{k}}{(2\pi)^2} \left(\frac{\hbar\omega_+}{2} + \frac{\hbar\omega_-}{2} - 2\frac{\hbar\omega_{sp}}{2} \right) \tag{3.1.2}$$

where $\omega_\pm^2 = \omega_{sp}^2 \left(1 \pm e^{-|\mathbf{k}|L}\right)$ denote the two coupled plasmons frequencies. This expression is a particular case of an expression obtained by Barton [86] and Heinrichs [87] starting from a dispersive hydrodynamic model for metal mirrors and neglecting retardation effects ($c \to \infty$) of electromagnetic field. Under those approximations ω_{sp} is the surface plasmons frequency whereas $\omega_\pm$ show how the surface plasmon corresponding to the two mirrors are displaced because of their coupling. Casimir effect thus appears as resulting from the "electrostatic" shift of the quanta corresponding to a collective vibrations of the electrons at the surface of the metal mirrors.

We saw that for the surface plasmons a collective motion of a large number of electrons [140] is associated with oscillating modes electromagnetic fields, strongly localized at the surface of a metal (evanescent waves). This means that at short distances the Casimir effect is a pure evanescent effect, i.e. is totally due to the evanescent field inside the cavity. This particular feature stresses the importance of including the evanescent sector in the evaluation of the Casimir effect.

These two points of view for describing the Casimir energy, namely Coulomb interaction between surface plasmons at short distances and sum over the cavity eigenmodes at long distances (that is between perfect mirrors) seem to be totally disconnected and even incompatible with each other. Yet they describe the same physical phenomenon.

In this chapter we are going to generalize Casimir's original formulation and show that the Casimir energy can be rewritten as a sum over the cavity eigenmodes for mirrors described by non absorbing dielectric function. We will then calculate explicitly the cavity eigenmodes in the case of the plasma model. This modes will be identified as the two surface plasmons mode corresponding to evanescent waves as well as an ensemble of propagative cavity modes. Our analysis will therefore connect the points of view in a common and more general formulation of the Casimir energy as a sum over cavity modes between real mirrors.

The chapter is organized as follows: in the first section we show how the expression of the Casimir energy (1.5.26) can be expressed as a sum over the eigenfrequencies of a

real cavity. In the second section we analyze the characteristic of those modes. In the last section we give some conclusions and comments.

3.2 The Casimir energy as a sum over the frequency modes of a real cavity

We start from the expression of the force and the energy as integrals over imaginary frequencies and transverse wavevectors

$$F = A\frac{\hbar c}{\pi}\sum_{p}\int_{\mathbb{R}^2}\frac{d^2\mathbf{k}}{(2\pi)^2}\int_0^\infty d\xi\kappa f^p_{\mathbf{k}}[\imath\xi] \tag{3.2.1a}$$

$$E = A\frac{\hbar c}{2\pi}\sum_{p}\int_{\mathbb{R}^2}\frac{d^2\mathbf{k}}{(2\pi)^2}\int_0^\infty d\xi \ln\left(1-\rho^p_{\mathbf{k}}[\imath\xi]\right) \tag{3.2.1b}$$

where p differentiates the two polarizations of the electromagnetic field, A is the mirror surface and $\mathbf{k}\equiv(k_x,k_y)$ is the transverse wavevector. For simplicity all the frequencies - real and imaginary - are measured as wavevectors, i.e. ω stands for $\frac{\omega}{c}$ and ξ stands for $\frac{\xi}{c}$.

We may rewrite the force in the following form:

$$F = \sum_{p,\mathbf{k}}\frac{\hbar}{2}\Delta^p_{\mathbf{k}} \quad \text{with} \quad \Delta^p_{\mathbf{k}} = \frac{2}{\pi}\int_0^\infty d\xi\kappa\frac{\rho^p_{\mathbf{k}}[\imath\xi]}{1-\rho^p_{\mathbf{k}}[\imath\xi]} \tag{3.2.2}$$

The functions $f^p_{\mathbf{k}}[\imath\xi]$ and $\rho^p_{\mathbf{k}}[\imath\xi]$ are respectively the closed and the open loop functions discussed in Chap.1:

$$\rho^p_{\mathbf{k}}[\imath\xi] = r^p_{\mathbf{k}}[\imath\xi]^2\ e^{-2\kappa L} \tag{3.2.3}$$

The mirrors reflection coefficient is determined in the bulk limit through the impedance functions (see Chap. 1 and 2).

To eliminate the problem with the branch points (see Appendix A.3) I reintroduce the thickness of the mirror (d) and come back to the bulk case ($d\to\infty$) only at the end of the calculation as proposed by Schram [111]. The impedance function then writes

$$Z^p_s[\imath\xi] = Z^p_{\mathbf{k}}[\imath\xi]\coth\left[\kappa_m d\right] \tag{3.2.4}$$

where the subscript "s" denotes mirrors of finite thickness (slab) (see fig.3.1).

The expression for $\Delta^p_{\mathbf{k}}$ is then transformed into

$$\Delta^p_s = \frac{1}{\pi}\int_0^\infty\left(\mathfrak{g}^p_s[\imath\xi,L]-\kappa\right)d\xi \tag{3.2.5}$$

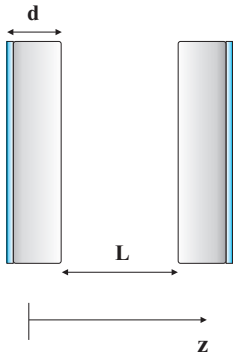

Figure 3.1 : The cavity mirrors configuration with two dielectric slabs of finite thickness d parallel to the (x,y) plane and separated by a vacuum gap of width L.

with

$$\mathfrak{g}_s^p[\imath\xi, L] = \kappa \frac{1+\rho_s^p[\imath\xi]}{1-\rho_s^p[\imath\xi]} \quad \text{with} \quad \rho_s^p[\imath\xi] = \left(\frac{1-Z_s^p[\imath\xi]}{1+Z_s^p[\imath\xi]}\right)^2 e^{-2\kappa L} \tag{3.2.6}$$

One can verify that the integrand is an even function of κ_m and then suffers only of the branch points due to κ [129]. Let us remind that in this formulation we may connect $\mathfrak{g}_s^p$ with the radiation pressure exerted by the electromagnetic field inside the cavity while κ can be reconnected to the radiation pressure exerted by the external vacuum. From Eq.(3.2.6) we notice that in the limit of infinite distances $\mathfrak{g}_s^p$ tends to κ:

$$\mathfrak{g}_s^p[\imath\xi, L \to \infty] \to \kappa \tag{3.2.7}$$

Exploiting the explicit expression for $\mathfrak{g}_s^p$ one shows that

$$\mathfrak{g}_s^p[\imath\xi, L] = \kappa \frac{e^{\kappa L}(1+Z_s^p[\imath\xi])^2 + (1-Z_s^p[\imath\xi])^2 e^{-\kappa L}}{e^{\kappa L}(1+Z_s^p[\imath\xi])^2 - (1-Z_s^p[\imath\xi])^2 e^{-\kappa L}} = \partial_L \ln G_s^p[\imath\xi, L] \tag{3.2.8}$$

with

$$G_s^p[\imath\xi, L] = \kappa \left[e^{\kappa L}(1+Z_s^p[\imath\xi])^2 - (1-Z_s^p[\imath\xi])^2 e^{-\kappa L}\right] \tag{3.2.9}$$

The function $G_s^p[\imath\xi, L]$ has the particular property to be an even function of both κ and κ_m and then it does not show any branch points. $G_s^p[\imath\xi, L]$ is a meromorphic function independently from the choice of the square root determination.

Exploiting the parity properties typical of non-dissipative models for the dielectric function ($\rho_s^p[\imath\xi] = \rho_s^p[-\imath\xi]$) [85] and using high frequency transparency ($\rho_s^p[\imath\xi] \xrightarrow{|\xi|\to\infty} 0$) we rewrite Eq.(4.7.10) integrating by parts:

$$\Delta_s^p = \frac{1}{2\pi}\int_{-\infty}^{\infty} [\mathfrak{g}_s^p]_{L\to\infty}^L \, d\xi = -\frac{1}{2\pi}\partial_L \int_{-\infty}^{\infty} \left[\frac{\xi \partial_\xi G_s^p}{G_s^p}\right]_{L\to\infty}^L d\xi \tag{3.2.10}$$

We have used the fact that we can exchange the derivation, the $[\cdots]_{L\to\infty}^L$ and the integral symbol thanks to the uniform convergence in L of the integral in the previous equation. Using the high frequency transparency[1] we rewrite Eq.(3.2.10) as a complex contour integral

$$\Delta_s^p = -\frac{1}{2\pi}\partial_L \oint_C \left[\frac{\xi \partial_\xi G_s^p}{G_s^p}\right]_{L\to\infty}^L d\xi \tag{3.2.11}$$

where C is a path enclosing all the domain $Im[\xi] \leq 0$ which has to be closed in the clockwise sense. Using the logarithm argument theorem (see Appendix A.3) we get

$$\Delta_s^p = \partial_L \left[\sum_n \imath\bar{\xi}_n^p\right]_{L\to\infty}^L = \partial_L \left[\sum_n \bar{\omega}_n^p\right]_{L\to\infty}^L \tag{3.2.12}$$

[1] Some problems can occur for the validity of the high frequency transparency condition along the the imaginary ξ-axis. Adopting the Schram's modification of the surface impedence the function $\rho_s^p[\imath\xi]$ could not vanish in the point of the path C which corresponds to $\xi \to -\imath\infty$. This problem can be solved by the introduction of a renormalizing function [111]. Note however that this problem occurs only in one point of the part of the path C which is located at infinity. In such a point the value of the function can be redefined to get the right behavior.

where we have put $\imath\bar{\xi}_n^p = \bar{\omega}_n^p$. The $\bar{\xi}_n^p$ are the zeros of $G_s^p[\imath\xi, L]$ or alternatively the solutions of the equation

$$1 - \rho_s^p[\imath\xi] = 0 \tag{3.2.13}$$

contained in the domain enclosed by C ($Im\,[\xi] < 0$).

Here, as in Chapter 1, each sum may becomes infinite due to the infiniteness of vacuum energy and has to be understood as a regularized quantity, while only the difference is physically meaningful.

Taking the bulk limit one gets

$$\Delta_{\mathbf{k}}^p = \lim_{d\to\infty} \Delta_s^p = \partial_L \left[\sum_n \omega_n^p\right]_{L\to\infty}^{L} \tag{3.2.14}$$

where ω_n^p are now the solutions of

$$1 - \rho_{\mathbf{k}}^p[\omega_n^p] = 0 \tag{3.2.15}$$

and therefore precisely the resonance frequencies of the cavity.

Parity and causality properties allow us to show that these frequencies ω_n^p are positive real quantities or, equivalently, that the zeros of $G_{\mathbf{k}}^p[\imath\xi, L]$ are all placed along the imaginary ξ-axis. Causality indeed imposes that $G_{\mathbf{k}}^p[\imath\xi, L]$ is an analytic function on $Re\,[\xi] > 0$ while parity extend this characteristic to $Re\,[\xi] < 0$. This means that poles must lay on $Re\,[\xi] = 0$, i.e. on the real ω-axis. The choice of the path C allows to take into account only the positive part of this axis.

The energy is obtained by an integration of the force over L

$$E = -\int_L^\infty F dL = \sum_{p,\mathbf{k}} \left[\sum_n \frac{\hbar}{2}\omega_n^p\right]_{L\to\infty}^{L} \tag{3.2.16}$$

The limit of infinite distances corresponds to the work done by vacuum radiation pressure outside the cavity to carry a mirror from L to infinity (see Appendix A.1). To illustrate this let us take into consideration the limit of perfect mirrors for which the cavity resonance frequencies are

$$\omega_n^p = \sqrt{|\mathbf{k}|^2 + \left(\frac{n\pi}{L}\right)^2},\ n = 0...\infty \tag{3.2.17a}$$

The sum over all the cavity modes for infinite distances can be transformed into a continuous integral

$$\frac{\hbar}{2}\left[{\sum_{n=0}}' \sqrt{|\mathbf{k}|^2 + \left(\frac{n\pi}{L}\right)^2}\right]_{L\to\infty} = \frac{\hbar}{2}\frac{L}{\pi}\int_0^\infty \sqrt{|\mathbf{k}|^2 + k_z^2}dk_z \tag{3.2.17b}$$

where we have used the quantification of the longitudinal wavevector $k_z = n\pi/L$. One thus recovers Casimir's original result [16]

$$E_{Cas} = \sum_{p,\mathbf{k}} \left({\sum_{m=0}}' \sqrt{|\mathbf{k}|^2 + \left(\frac{m\pi}{L}\right)^2} - \frac{\hbar c}{2}\frac{L}{\pi}\int_0^\infty \sqrt{|\mathbf{k}|^2 + k_z^2}dk_z\right) \tag{3.2.17c}$$

Remark that in the previous procedure we did not need to specify the analytic form of the dielectric function and we have just exploited its analyticity and parity properties. This means the previous result is still valid for any non dissipative optical response model [86, 87, 135, 136, 137].

It is worth noting that Eq.(3.2.16) establishes a connection between the modern derivations of the Casimir effect ([113,84,47,45,142] and Chap.1) and the initial derivation given by Casimir himself in his seminal paper [16]. With this equation, we now dispose of the decomposition of the Casimir energy into a set of cavity modes. We now study those modes when the mirrors are described by the plasma model.

3.3 Mode analysis with the plasma model

The starting point of the analysis of the cavity modes with the plasma model, is equation (3.2.15). The cavity modes correspond to the zeros of Eq.(3.2.15) and therefore to the poles of the closed loop function $f^p_{\mathbf{k}}[\imath\xi]$ defined in Eq.(3.2.3). Generally speaking the closed loop function shows peaks in correspondence with the frequencies which represent the cavity modes. It is worth to stress that equation (3.2.15) does not contradict the passivity condition $\rho^p_{\mathbf{k}}[\omega] < 1$ discussed briefly in the Chap.1. This consideration must be verified only in the upper part of the ω-complex plane, i.e. in the domain of analyticity for $f^p_{\mathbf{k}}[\imath\xi]$. This means that the poles of $f^p_{\mathbf{k}}[\imath\xi]$ have to be situated in the lower part of the complex ω-plane or at most on the frontier of this domain. This is the case, for example, for the plasma model which situate the poles of $f^p_{\mathbf{k}}[\imath\xi]$ on the real ω-axis. The plasma model can also be considered as the limiting case of a dissipative model in the limit of vanishing dissipation, the poles on the real axis being limits of poles laying in the lower ω-complex plane.

The solutions are functions of the transverse wavevector $|\mathbf{k}|$, of the polarization p and of the cavity length L. Except in a few cases, the frequencies ω^p_n can not be expressed as a combination of elementary functions. Nevertheless it is possible to extract all the results we need in the following.

The reflection amplitudes are calculated for a metallic bulk with the optical response of metals described by the plasma model with the dielectric constant

$$\epsilon[\omega] = 1 - \frac{\omega_p^2}{\omega^2} \tag{3.3.1}$$

ω_p is the plasma frequency, a constant which can be relied to the specific physical properties of the dielectric. For $\omega \lesssim \omega_p$ the dielectric constant differs from unity differentiating the behavior of the dielectric from the surrounding vacuum. For $\omega \gg \omega_p$ the dielectric constant approaches the unity and the dielectric becomes transparent. This is nothing but the high frequencies-transparency phenomenon in the case of the plasma model.

The reflection amplitudes can be rewritten in terms of real frequencies as it follows

$$r^{TE} = \frac{\kappa - \kappa_m}{\kappa + \kappa_m}, \quad r^{TM} = \frac{\kappa_m - \epsilon[\omega]\kappa}{\kappa_m + \epsilon[\omega]\kappa} \tag{3.3.2}$$

where we have defined

$$\kappa = \sqrt{|\mathbf{k}|^2 - \omega^2} \tag{3.3.3a}$$

$$\kappa_m = \sqrt{|\mathbf{k}|^2 - \epsilon[\omega]\omega^2} = \sqrt{|\mathbf{k}|^2 - \omega^2 + \omega_p^2} = \sqrt{\kappa^2 + \omega_p^2} \tag{3.3.3b}$$

The determination of the square root is chosen in function of the physical analytical continuation of the closed loop function (see par.1.5.2 Chap.1): we have $Re\,[\kappa_i] > 0$ and $Im\,[\kappa_i] < 0$ in $Im\,[\omega] > 0$.

3.3.1 Equation for the cavity modes

Eq.(3.2.15) leads to the following equation for the cavity modes

$$r_{\mathbf{k}}^p[\omega]^2 e^{-2\kappa L} = 1 \tag{3.3.4}$$

As the solutions of those equations have to be searched on the real ω-axis, κ (see Eq.(3.3.3)) could be a positive real or a pure imaginary number. This defines two distinct ensembles of poles called *evanescent* and *propagative* because the corresponding field is evanescent or propagative respectively. The frequency domain is split in two regions (see Appendix C.1):

- **the evanescent region**: is the region for which $|\mathbf{k}| > \omega$ and then $\kappa = \sqrt{\mathbf{k}^2 - \omega^2}$ is a positive real. The electromagnetic field propagates on the vacuum/mirror interface and exponentially decreases far away from the surface .
- **the propagative (ordinary) region**: is the region for which $|\mathbf{k}| < \omega$ an then where $\kappa = \sqrt{\mathbf{k}^2 - \omega^2}$ is imaginary. The electromagnetic field propagates inside the cavity.

3.3.1.1 Propagative modes

In the propagative sector the longitudinal wavevector $k_z = \imath\kappa$ is real (κ is pure imaginary), the phase factor e^{2ik_zL} has a unit modulus. Therefore, reflection amplitudes have a unit modulus $\left|r_{\mathbf{k}}^p\right| = 1$ at the cavity resonance frequencies and the effect of mirrors is reduced to a dephasing

$$\delta_{\mathbf{k}}^p[\omega] \equiv \frac{1}{2} \arg r_{\mathbf{k}}^p[\omega]^2 \tag{3.3.5}$$

The modes are described by the resonance condition as usually for a Fabry-Perot cavity

$$k_z L + \delta_{\mathbf{k}}^p[\omega] = n\pi \tag{3.3.6a}$$

$k_z L$ would correspond to an integer number of π for the n-th mode of a cavity with perfect mirrors (n is the order of the cavity mode); the dephasing δ is responsible for a shift of the position of the cavity mode due to the imperfect reflection. This equation can be rewritten

$$\frac{k_z L}{\pi} + \frac{\delta_{\mathbf{k}}^p[\omega]}{\pi} = n \tag{3.3.6b}$$

where $\frac{\delta^p_{\mathbf{k}}[\omega]}{\pi}$ measures the mode-shift as a fraction of the "free spectral range" of the cavity.

We may distinguish two different regions in the ordinary sector, depending on the sign of κ_m^2:

- $0 < k_z \leq \omega_p$: κ_m is a positive real quantity and therefore $\left|r^p_{\mathbf{k}}\right| = 1$. The mirrors remain perfectly reflecting.

- $0 < \omega_p < k_z$: κ_m is imaginary and then $\left|r^p_{\mathbf{k}}\right| < 1$. In this domain in contrast, the mirrors show imperfect reflection, and no solution exists anymore for either polarizations.

$$k_z > \omega_p \Rightarrow \omega > \omega_c = \sqrt{|\mathbf{k}|^2 + \omega_p^2}. \tag{3.3.7}$$

This means that all modes lie in the first domain and the their frequency is limited by

$$\omega_n^p \leq \omega_c \tag{3.3.8}$$

This cutoff phenomenon is a direct consequence of the high frequency-transparency property of real mirrors. We could say that photons with frequencies higher than ω_c cannot be trapped in the cavity and pass in the bulk where they propagate "freely" , with a speed depending on $\epsilon[\omega]$, because of the infinite thickness of the bulk itself. For this reason we call the frequency range $\omega > \omega_c$ bulk region. We come back on this point in the following.

3.3.1.2 Evanescent modes

In the evanescent sector, κ is real and positive, so that the phase factor $e^{-2\kappa L}$ has a modulus smaller than unity. Hence to satisfy Eq.(3.2.15) the modes have to correspond to an amplitude $r^p_{\mathbf{k}}$ with a modulus larger than unity. Since κ_m in the evanescent sector is real and positive, $r^{TE}_{\mathbf{k}}$ cannot meet this condition, which forbids the existence of evanescent TE modes.

Conversely, $r^{TM}_{\mathbf{k}}$ may show in the evanescent sector a modulus larger than unity depending on the sign of the dielectric function $\epsilon[\omega]$:

$$r^{TM} = \frac{\kappa_m - \epsilon[\omega]\kappa}{\kappa_m + \epsilon[\omega]\kappa} \quad \Rightarrow \begin{cases} \left|r^{TM}\right| > 1 \quad \text{for} \quad \epsilon[\omega] < 0 \Rightarrow 0 < \omega < \omega_p \\ \\ \left|r^{TM}\right| < 1 \quad \text{for} \quad \epsilon[\omega] > 0 \Rightarrow \omega > \omega_p \end{cases} \tag{3.3.9}$$

All evanescent modes lie in the first domain $0 < \omega < \omega_p$. In the forthcoming evaluations, they are described by the modulus condition

$$\kappa L = \frac{1}{2}\ln r^2 \quad \text{or, equivalently,} \quad \frac{\kappa L}{\pi} = -\rho, \quad \rho = -\frac{1}{2\pi}\ln r^2 \tag{3.3.10}$$

This condition may be described as an analytical continuation in the complex plane of the phase condition written for ordinary modes.

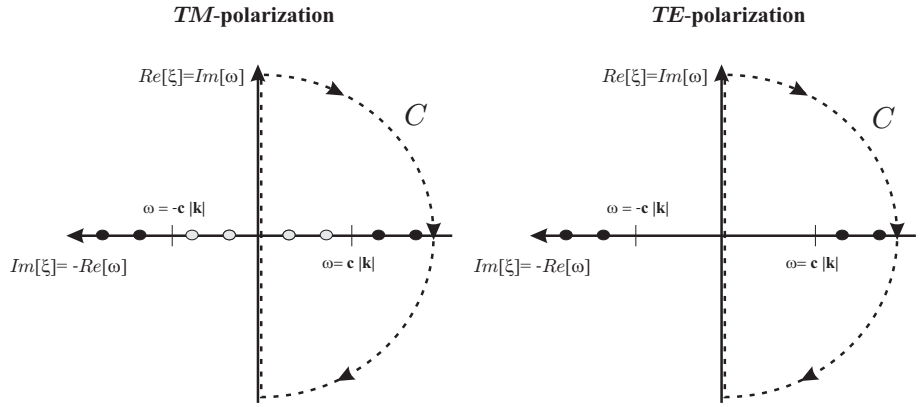

Figure 3.2 : A schematic representation of the distribution of the poles of the closed loop function in the complex ω-plane for a fixed transverse wavevector. Propagative cavity mode are printed in black, evanescent modes in gray. The two polarization show important difference in the evanescent zone ($|\omega| < |\mathbf{k}|$): only the TM polarization allows for evanescent frequency modes.

3.3.2 TE-modes

In the previous paragraph we saw that for $p = TE$ Eq.(3.2.15) cannot admit solutions in the evanescent region.

As the modes lie in the domain where the mirrors reflection amplitude has modulus equal to unity, we may use the parametrization

$$k_z = \omega_p \sin\left(\frac{\pi}{2}t\right) \;\Rightarrow \sqrt{\omega_p^2 - k_z^2} = \omega_p \cos\left(\frac{\pi}{2}t\right) \quad \text{with } 0 < t < 1 \tag{3.3.11}$$

which allows to rewrite the reflection coefficient

$$r^{TE} = \frac{-\imath k_z - \sqrt{\omega_p^2 - k_z^2}}{-\imath k_z + \sqrt{\omega_p^2 - k_z^2}} = -e^{\imath\pi t} \tag{3.3.12}$$

This implies a phase shift $\delta^{TE} = \pi t$.

Using the dimensionless variables

$$x = \frac{\omega_p L}{\pi}, \quad y = \frac{k_z L}{\pi} \tag{3.3.13}$$

the TE-modes are implicitly described through their wavevector-length relation. We get the following ensemble of parametric curves $y = \nu_n(x)$

$$y = \nu_n(x) \rightarrow \left(x(t) = \frac{n-t}{\sin\left(\frac{\pi}{2}t\right)},\ y(t) = n - t \right) \qquad t \in [0,1] \quad n = 1, 2, 3... \tag{3.3.14}$$

which is plotted in fig.3.3. All cavity modes correspond to solid black lines. Each mode tends to $(x \rightarrow \infty, y = n)$ when $t \rightarrow 0$. Those asymptotes correspond to the limit of perfect

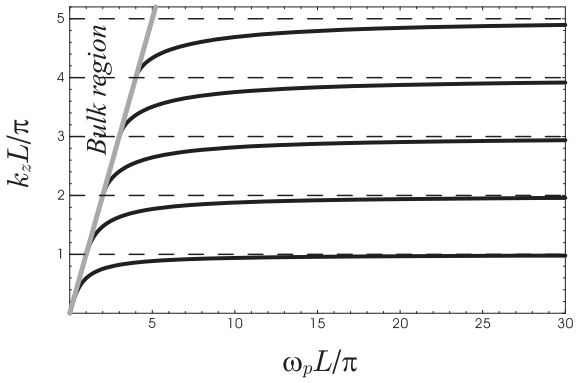

Figure 3.3 : Representation of the TE-propagative modes through their wavevector-length relation. Each curve tends to $k_zL/\pi = n$ when $L \to \infty$. Those asymptotes correspond to the modes in the limit of perfect mirrors where n is the order n of the mode of the Fabry-Perot cavity. The mode coincide on the diagonal corresponding to $k_z = \omega_p$.

mirrors with y equal to the order n of the Fabry-Perot cavity. Non vanishing values of t represent the shift of the mode which results from the dephasing on the mirror due to the plasma model. On the other end $t \to 1$ of the segment on which t is defined, the shift is just equal to the range between two modes of the perfect Fabry-Perot. The corresponding points $y = x = n - 1$ are aligned on the diagonal. On a curve corresponding to a given n, the slope is calculated by writing

$$dx = \frac{1}{\sin\left(\frac{\pi}{2}t\right)}dy - \frac{\pi}{2}\frac{\cos\left(\frac{\pi}{2}t\right)}{\sin^2\left(\frac{\pi}{2}t\right)}dt, \quad dy = -dt \tag{3.3.15a}$$

which leads to

$$\frac{d}{dx}\nu_n(x) = \frac{dy}{dx} = \frac{y}{x}\frac{1}{1 + \frac{\pi}{2}\sqrt{x^2 - y^2}} \tag{3.3.15b}$$

An important result of this calculation is that

$$\frac{d}{dx}\nu_n(x) = \frac{dy}{dx} \xrightarrow{t\to 1} 1 \tag{3.3.15c}$$

This means that all the modes are tangent to the diagonal $k_z = \omega_p$ (or equivalently $\omega = \omega_c$). Consequently, they may be continued by the diagonal. This trick allows us to have the number of modes preserved when L varies, while ensuring continuity of the solution and of its derivative.

It is also instructive to study the mode via their frequency-length relation. To this aim we use another parametric representation

$$x = \frac{\omega_p L}{\pi}, \quad y = \frac{\omega}{\omega_p} = \sqrt{\frac{|\mathbf{k}|^2}{\omega_p^2} + \frac{k_z^2}{\omega_p^2}} \tag{3.3.16}$$

The mode ensemble is then represented by

$$\left(x(t) = \frac{n - t}{\sin\left(\frac{\pi}{2}t\right)},\ y(t) = \sqrt{s^2 + \sin^2\left(\frac{\pi}{2}t\right)}\right) \qquad s = \frac{|\mathbf{k}|}{\omega_p},\ t \in [0,1] \quad n = 1, 2, 3.... \tag{3.3.17}$$

Of course this representation depends on the value of the transverse wave vector $|\mathbf{k}|$ through the parameter s. The result of a plot for $s = 0.5$ is shown in fig. 3.4. Again all modes are

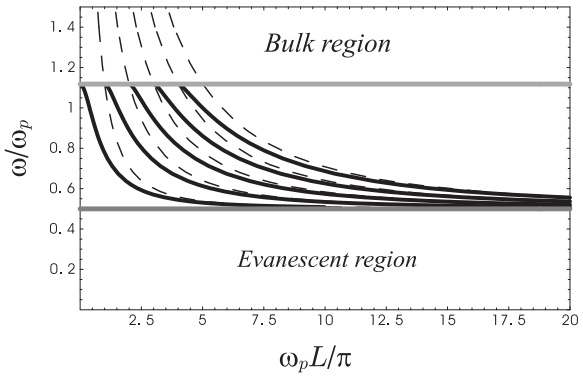

Figure 3.4 : Frequencies of the TE-propagative modes as a function of the cavity length for $s = 0.5$. The dashed lines correspond to the perfect mirror case. We see that the propagative cavity modes exist between the bulk and the evanescent region. The perfect cavity corresponds to the dashed lines.

represented by solid black lines, while the modes for the perfect cavity corresponds to the dashed lines.

The slope is deduced from the following relations

$$y = \sqrt{s^2 + \left[\frac{\nu_n(x)}{x}\right]^2} \Rightarrow \frac{dy}{dx} = \frac{1}{y}\frac{\nu_n(x)}{x}\frac{[x\nu_n'(x) - \nu_n(x)]}{x^2} \tag{3.3.18}$$

and

$$\frac{\nu_n(x)}{x} \xrightarrow{t\to 0} 0, \quad \nu_n(x) \xrightarrow{t\to 1} x, \quad \text{and } \nu_n'(x) \xrightarrow{t\to 1} 1 \tag{3.3.19}$$

We deduce that all the curves have a common asymptote $y = \frac{\omega}{\omega_p} = s$ (i.e. $\omega = k$) at $t \to 0$ and that they are tangent to the same line $y = \frac{\omega}{\omega_p} = \sqrt{s^2+1}$ (i.e. $\omega = \sqrt{\omega_p^2 + |\mathbf{k}|^2}$) at $t \to 1$. Again those expressions can be continued along $\omega = \omega_c = \sqrt{\omega_p^2 + |\mathbf{k}|^2}$.

It is worth to stress that those continuations do not affect the expression of the energy because since they do not depend on L they disappear in the difference between the finite and the infinite distances. Nevertheless this trick leads to a clearer interpretation of the expression of the Casimir energy as sum over the cavity modes given in Eq.(3.2.16). All the modes indeed can be thought as if they were coalescing at the frequency $\omega = \omega_c$ from where they detach with increasing distance L. Fig. 3.4 shows that compared to the cavity with perfect mirrors, the metallic properties induce a decrease of the frequencies of the cavity modes.

3.3.3 The TM-modes

From the discussion of the previous paragraphs one can easily understand that the study of the TM-modes is more complicated than the one of the TE modes. The first remarkable difference arises from the fact that Eq.(3.2.15) allows for solution in the evanescent zone where the z-component of the field wavevector becomes a pure imaginary number. We therefore have to separately study the behavior of propagative and evanescent modes.

Here we give first a description of the modes in terms of parametric curves which allow to study the features of the TM modes as a function of the distance L.

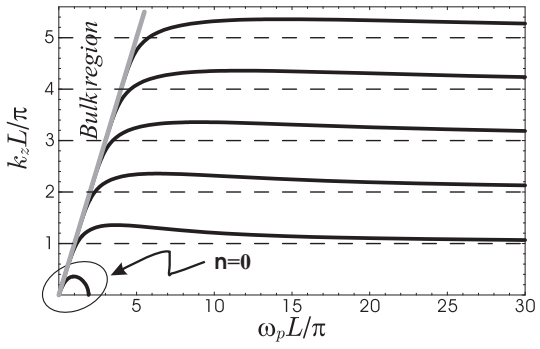

Figure 3.5 : Representation of the TM-propagative modes through their wavevector-length relation. Each curve tends to $k_zL = n\pi$ when $L \to \infty$. Those asymptotes correspond to the limit of perfect mirrors where n is the order of the Fabry-Perot cavity. The points $k_z = \omega_p L = \pi(n-1)$ are aligned on the diagonal corresponding to the frequency ω_c. The mode $n = 0$ shows a different behavior.

3.3.3.1 The propagative modes

As for the TE-modes let us parameterize k_z as

$$k_z = \omega_p \sin\left(\frac{\pi}{2}t\right) \quad \text{with } t \in [0,1] \tag{3.3.20}$$

Again this allows us to take into account the cutoff condition in Eq.(3.3.8). The TM reflection coefficient can be written as

$$r^{TM} = \frac{\cos\left(\frac{\pi}{2}t\right) + \imath\epsilon[s,t]\sin\left(\frac{\pi}{2}t\right)}{\cos\left(\frac{\pi}{2}t\right) + \imath\epsilon[s,t]\sin\left(\frac{\pi}{2}t\right)} \tag{3.3.21}$$

where, because of the parameterizations, the dielectric constant $\epsilon[s,t]$ has the form

$$\epsilon[s,t] = 1 - \frac{\omega_p^2}{|\mathbf{k}|^2 + k_z^2} = 1 - \frac{1}{s^2 + \sin^2\frac{\pi t}{2}}, \quad \text{with } s = \frac{|\mathbf{k}|}{\omega_p} \tag{3.3.22}$$

The dephasing δ^{TM} is now a more complicated function of t and s:

$$\delta^{TM} = \frac{1}{2}\arg\left(r^{TM}\right)^2 = \arg\left(r^{TM}\right) = \pi u[s,t] \tag{3.3.23a}$$

$$u\left[s,t\right] = \frac{2}{\pi}\arctan\left[\left(1 - \frac{1}{s^2 + \sin^2\left(\frac{\pi}{2}t\right)}\right)\tan\left(\frac{\pi}{2}t\right)\right] \tag{3.3.23b}$$

The dependence of k_z on the transverse wavevector is introduced by the dependence of δ^{TM} on s. Note however that in that limit $s \to \infty$ i.e. $|\mathbf{k}| \to \infty$ we have $\delta^{TM} \to t$ recovering the TE modes behavior (this is seen more clearly in Chap. 4).

Let us now fix s and set again

$$x = \frac{\omega_p L}{\pi}, \quad y = \frac{k_z L}{\pi} \tag{3.3.24}$$

in order to characterize the TM-modes through their wavevector-length L relation. We get the following ensemble of parametric curves $y = \nu_n(x, sx)$

$$y = \nu_n(x, sx) \to \left(x(t) = \frac{n - u\left[s,t\right]}{\sin\left(\frac{\pi}{2}t\right)},\ y(t) = n - u\left[s,t\right]\right) \qquad t \in [0,1] \tag{3.3.25}$$

the plot of which is shown in fig. 3.5. Solid black lines correspond to TM modes with the plasma model, dashed lines to the perfect mirrors case. The behaviors of those curves is very similar to the TE case. Each curve with $n \neq 0$ tends to $(x \to \infty, y = n)$ when $t \to 0$. This asymptote corresponds to the limit of perfect mirrors with y equal to the order n of the Fabry-Perot cavity. Again, non vanishing values of t represent the shift of the mode which results from the dephasing on the mirror. In the same manner when we consider the limit $t \to 1$ the corresponding points are aligned on the diagonal $y = x = n - 1$ ($u[s,t] \xrightarrow{t\to 1} 1$).

Let us evaluate again the slope in the limit $t \to 1$. We have

$$dx = \frac{1}{\sin\left(\frac{\pi}{2}t\right)}dy - \frac{\pi}{2}\frac{\cos\left(\frac{\pi}{2}t\right)}{\sin^2\left(\frac{\pi}{2}t\right)}dt \quad dy = -du \tag{3.3.26a}$$

which lead

$$\frac{d}{dx}\nu_n(x, sx) = \frac{dy}{dx} = \frac{y}{x}\frac{1}{1 + \frac{\pi}{2}\sqrt{x^2 - y^2}\frac{dt}{du}} \tag{3.3.26b}$$

Since again $y \xrightarrow{t\to 1} x$ we have

$$\lim_{t\to 1}\left|\frac{dt}{du}\right| = \frac{s^2}{(1+s^2)} < \infty \quad \Rightarrow \frac{d}{dx}\nu_n(x, sx) \xrightarrow{t\to 1} 1 \tag{3.3.26c}$$

This means that the curves are tangent to the diagonal and that the conclusions derived from this property for the TE modes are still valid for the TM ones.

It is particularly interesting to follow the behavior of the mode $n = 0$. Under the following equivalent conditions

$$u\,[s,t] < 0 \quad \Longleftrightarrow \quad \epsilon\,[s,t] < 0 \quad \Longleftrightarrow \quad \sin^2\frac{\pi t}{2} < 1 - s^2 \tag{3.3.27}$$

a particular mode appears. This condition can be met only for $s < 1$ and, in this case, on the limited range $0 < \sin\left(\frac{\pi}{2}t\right) < \sqrt{1-s^2}$. For $n = 0$ this mode tends to $\left(x = \frac{2}{\pi}\left[\frac{1}{s^2} - 1\right], y = 0\right)$ when $t \to 0$. Since $y = 0 \Rightarrow k_z = 0$ those values correspond to the frontier between the propagative and the evanescent region. From the $t \to 0$ result we deduce that this mode exists in the propagative sector when

$$\frac{\omega_p L}{\pi} \leq x(t \to 0) = \frac{2}{\pi}\left[\frac{1}{s^2} - 1\right] \Rightarrow |\mathbf{k}| \leq \frac{k_p}{L} = \frac{1}{L}\sqrt{\frac{2\omega_p^2 L^2}{1 + \omega_p L}} \tag{3.3.28}$$

To illustrate the extra-mode more clearly let us consider now the representation in terms of the frequency-length L relation:

$$x = \frac{\omega_p L}{\pi}, \quad y = \frac{\omega}{\omega_p} = \sqrt{\frac{|\mathbf{k}|^2}{\omega_p^2} + \frac{k_z^2}{\omega_p^2}} \tag{3.3.29}$$

The mode ensemble is then represented by

$$\left(x(t) = \frac{n - u\,[s,t]}{\sin\left(\frac{\pi}{2}t\right)},\ y(t) = \sqrt{s^2 + \sin^2\left(\frac{\pi}{2}t\right)}\right) \qquad s = \frac{|\mathbf{k}|}{\omega_p},\ t \in [0,1] \tag{3.3.30}$$

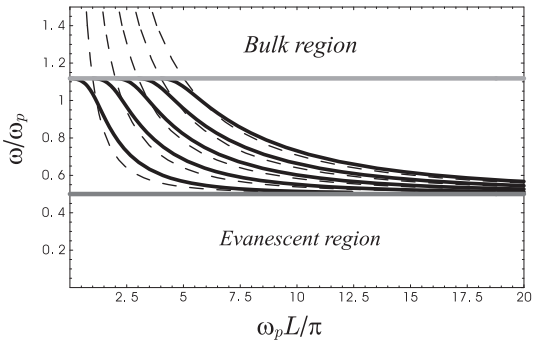

Figure 3.6 : Plot of the frequencies of the TM-propagative modes as a function of the cavity length L for $s = 0.5$. The dashed lines correspond to the perfect mirror case.

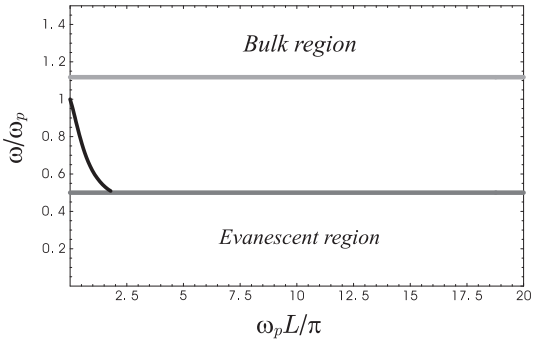

Figure 3.7 : Plot of the frequency-length relation of the TM-propagative $n = 0$ mode for $s = 0.5$. This mode behaves differently from the others: it starts at $(L = 0, \omega = \omega_p)$ and stops at $\omega_p L = 2\ \frac{1}{s^2} - 1\ , \omega = |\mathbf{k}|$.

In fig.3.6 the ensemble of TM modes frequencies with the plasma model is shown as solid black lines as a function of cavity length. Only the modes with $n \neq 0$ are plotted. Dashed lines corresponds again to perfectly reflecting mirrors. All curves have $y = s$ $(\omega = |\mathbf{k}|)$ as common asymptote and are tangent to $y = \sqrt{s^2 + 1}$ $(\omega = \sqrt{\omega_p^2 + |\mathbf{k}|^2})$. In contrast to the TE modes, we see that for TM modes mirrors which have their properties described by the plasma model, have the frequencies of the cavity modes increased with respect to the perfect mirrors case.

The mode corresponding to $n = 0$ behaves differently: the limitation $\epsilon[s,t] < 0$ entails that this mode starts at $(x = 0, y = 1)$ and stops at $\left(x = \frac{2}{\pi}\left[\frac{1}{s^2} - 1\right], y = s\right)$ as shown in fig.3.7. We will study this mode in more detail in the next paragraph.

3.3.3.2 The evanescent modes

The evanescent mode properties can be obtained as an analytic continuation of the propagative modes properties. The z-component of the field wavevector becomes a pure imaginary number $k_z = \imath\kappa$. The phaseshift transforms into decreasing exponential factor $e^{-2\kappa L}$, which drastically modify the behavior of the mode solutions both as function of the transverse wavevector $|\mathbf{k}|$ and of the distance L. We already saw that the frequency of those solutions lies in $0 < \omega_n^{TM} < \omega_p$ $(\epsilon[\omega] < 0)$. From Eq.(3.2.15) we deduce the asymptotic behavior of the solution in the limit $|\mathbf{k}| \gg \omega$

$$\frac{1}{\left(r^{TM}\right)^2} = e^{-2\kappa L} \xrightarrow{|\mathbf{k}| \gg \omega} \left(\frac{1+\epsilon[\omega]}{1+\epsilon[\omega]}\right) \approx e^{-2|\mathbf{k}|L} \Rightarrow \omega_{\pm}[\mathbf{k}] \approx \frac{\omega_p}{\sqrt{2}}\sqrt{1 \pm e^{-|\mathbf{k}|L}} \tag{3.3.31}$$

The frequencies $\omega_{\pm}[\mathbf{k}]$ are precisely the surface plasmons frequencies in the electrostatic ($c \to \infty$) non dispersive limit ($\beta \to 0$) introduced in Chapter 2 [87, 86]. Those solutions are degenerate in the limit $|\mathbf{k}|\, L \to \infty$ in the value $\omega_p/\sqrt{2}$. Indeed, the electrostatic limit is recovered in the short distance condition

$$c \to \infty \Longleftrightarrow |\mathbf{k}| \gg \omega \tag{3.3.32}$$

Let us consider now the limit $L \to \infty$. Physically, this corresponds to the case where the mirrors are so far away that they can be considered isolated in vacuum. In the evanescent domain this limit solution corresponds to the surface plasmons of a metallic bulk in the retarded regime, i.e. when we consider finite the speed of light. We then have

$$\frac{1}{\left(r^{TM}\right)^2} = e^{-2\kappa L} \xrightarrow{L\to\infty} \frac{1}{\left(r^{TM}\right)^2} = 0 \tag{3.3.33}$$

The solutions are therefore the poles of the TM reflection amplitude. The unique solution corresponds to two degenerate frequencies

$$\omega_{sp}^2[\mathbf{k}] = \frac{\omega_p^2 + 2\,|\mathbf{k}|^2 - \sqrt{\omega_p^4 + 4\,|\mathbf{k}|^4}}{2} \tag{3.3.34}$$

which is nothing but the retarded surface plasmons dispersion relation. In the electrostatic limit ($c \to \infty \Rightarrow |\mathbf{k}| \gg \omega_p$), we naturally recover for the surface plasmons frequencies the value $\omega_p/\sqrt{2}$.

To describe the connection between the evanescent modes behavior and the distance L let us introduce the parameterization

$$\kappa = \omega_p \sinh\left(\frac{\pi}{2}\tau\right) \quad \text{with } \tau \in [0, \infty] \tag{3.3.35}$$

This parametrization is the analytic continuation of the one used in the propagative sector with $t = \imath\tau$. The reflection coefficient then takes the form

$$r^{TM} = \frac{\kappa_m - \epsilon[\omega]\kappa}{\kappa_m + \epsilon[\omega]\kappa} = \frac{\cosh\left(\frac{\pi}{2}\tau\right) - \epsilon[\tau, s]\sinh\left(\frac{\pi}{2}\tau\right)}{\cosh\left(\frac{\pi}{2}\tau\right) + \epsilon[\tau, s]\sinh\left(\frac{\pi}{2}\tau\right)} \tag{3.3.36}$$

with the dielectric function

$$\epsilon[\tau, s] = 1 - \frac{1}{s^2 - \sinh^2\left(\frac{\pi}{2}\tau\right)}, \quad s = \frac{|\mathbf{k}|}{\omega_p} \tag{3.3.37}$$

Inserting these quantities into (3.3.33), we get two possible solutions $\frac{\kappa L}{\pi} = -\rho_{\pm}[\tau, s]$ corresponding to the double sign of the square root of $\left[r^{TM}\right]^2$ and therefore two possible modes in the evanescent sector:

$$\rho_+[\tau, s] = \frac{2}{\pi}\text{arctanh}\left[\epsilon[\tau, s]\tanh\left(\frac{\pi}{2}\tau\right)\right], \quad \rho_-[\tau, s] = \frac{2}{\pi}\text{arctanh}\left[\frac{1}{\epsilon[\tau, s]}\coth\left(\frac{\pi}{2}\tau\right)\right] \tag{3.3.38}$$

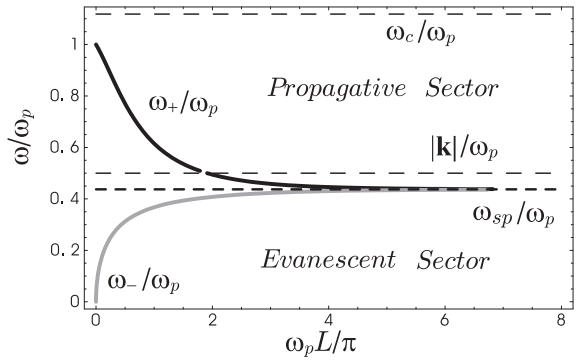

Figure 3.8 : Representation of the two evanescent modes ω_+ and ω_- through their frequency-length relation for $s = 0.5$. The mode ω_- lives exclusively in the evanescent region while the mode ω_+ crosses the evanescent/propagative frontier behaving as propagative or evanescent in function of the distance L. For $L \to \infty$ both modes coincide at the frequency ω_{sp} of the usual surface plasmons dispersion relation $\omega_{sp}[\mathbf{k}]$.

Those functions are defined only for

$$\rho_+ : \ -1 < \epsilon[\tau, s] \tanh\left(\frac{\pi}{2}\tau\right) < 0 \Rightarrow 0 < \tau < \tau_{sp} \tag{3.3.39a}$$

$$\rho_- : \ -1 < \frac{1}{\epsilon[\tau, s]} \coth\left(\frac{\pi}{2}\tau\right) < 0 \Rightarrow \tau_{sp} < \tau < \tau_- \tag{3.3.39b}$$

where

$$\tau_- = \frac{2}{\pi}\text{arcsinh}\,[s] \quad \text{and} \quad \tau_{sp} = \frac{2}{\pi}\text{arcsinh}\left[\sqrt{\frac{\sqrt{1+4s^4}-1}{2}}\right] \tag{3.3.39c}$$

It is not possible to give explicitly the frequencies $\omega_\pm$ of both solutions as a function of the cavity length L. Again, we use a representation in terms of a dimensionless frequency-length relation, which can be given in analogy with the parametrization used in the propagative sector:

$$x = \frac{\omega_p L}{\pi}, \quad y = \frac{\omega}{\omega_p} = \sqrt{\frac{|\mathbf{k}|^2}{\omega_p^2} - \frac{\kappa^2}{\omega_p^2}} \tag{3.3.40}$$

Our ensemble is now represented by

$$\left(x(t) = \frac{-\rho_\pm[\tau, s]}{\sinh\left(\frac{\pi}{2}\tau\right)}, \ y(t) = \sqrt{s^2 - \sinh^2\left(\frac{\pi}{2}\tau\right)}\right) \qquad s = \frac{|\mathbf{k}|}{\omega_p} \tag{3.3.41}$$

Both modes are represented via their frequency-length relation in figure 3.8. The mode ω_- corresponding to $\rho_-[\tau, s]$ totally lies in the evanescent sector. Its frequency tends to zero for $L \to 0$. For the forthcoming evaluation it will be labelled by the subscript "$-$". The mode ω_+ corresponding to the function $\rho_+[\tau, s]$ lies in the evanescent sector only for large distances. It crosses the barrier towards the propagative sector at $\omega_p = 2\left[\frac{1}{s^2} - 1\right]$ and dies in the propagative sector for $L \to 0$. It can be obtained from the TM propagative mode $n = 0$ through the analytic continuation $t = \imath\tau$. Here after we consider the two modes, the evanescent and the propagative $n = 0$, as a single mode, the frequency of which will be labeled by the subscript "$+$".

Both the modes ω_+ and ω_- show the same asymptotic behavior in the limit $L \to \infty$ where their frequencies degenerate are given by the surface plasmon dispersion relation

$$\omega_\pm \xrightarrow{L\to\infty} \sqrt{\frac{\omega_p^2 + 2\left|\mathbf{k}\right|^2 - \sqrt{\omega_p^4 + 4\left|\mathbf{k}\right|^4}}{2}} \tag{3.3.42}$$

3.4 Conclusion and comments

In this Chapter we have established the connection between the formulation of the Casimir effect via vacuum radiation pressure and the formulation using the sum over all cavity modes, as proposed by Casimir for perfectly reflecting mirrors. Here we have generalized the mode analysis of the Casimir effect for metallic mirrors described by plasma model. Starting from the expression of the Casimir force as a double integral over imaginary frequencies and transverse wavevector, we have expressed the Casimir energy as a sum over the modes of a real cavity. While for perfect mirrors only propagative cavity modes exist, we find for real mirrors two additional modes living in the evanescent sector.

The number of photonic mode can be estimated using condition (3.3.8) which imposes $\omega_c = \sqrt{\omega_p^2 + \left|\mathbf{k}\right|^2}$ as an upper frequency bound. Roughly speaking we can say that the propagative mode wavevectors are approximatively distributed within intervals equal to π/L. This means that the nth mode longitudinal wavevector is approximatively equal to $n\pi/L$ for large distances. If we traduce the frequency cutoff condition give in Eq.(3.3.8) into a condition for the longitudinal wavevector we get

$$\frac{n\pi}{L} \lesssim\Rightarrow n \lesssim n_c = \frac{\omega_p L}{\pi} \tag{3.4.1}$$

where the number n_c is then the number of photonic modes showing a frequency smaller or equal to ω_c.

We pointed out that the two polarizations TE and TM behave differently in the evanescent sector: only the TM polarization exhibits modes in this region. Furthermore the properties of those modes are very different from the propagative ones: they degenerate in the limit $L \to \infty$ in the surface plasmons frequencies in the non retarded limit only. One of the two modes, ω_-, belongs completely to the evanescent region. The other mode, ω_+, crosses the evanescent/propagative frontier. Properly speaking, for a fixed $|\mathbf{k}|$, therefore we can call it evanescent mode or propagative one only at a fixed cavity length L. In function of the further developments hereafter let us adopt the following classification:

- **plasmonic** modes are the cavity modes living in the evanescent sector at least for some particular value of their parameters. This ensemble contains only the two modes ω_+ and ω_-.
- **photonic** modes are the cavity modes propagating for all cavity length.

This analysis has be done taking into account retardation effects. For this reason it represents the generalization to all distances of the short distance formula for the Casimir

energy expressed as the Coulomb interaction between the mirrors surface plasmons. On the other hand, it represents also the generalization of Casimir formula, giving the Casimir energy as the sum over the cavity modes, to real mirrors described by a plasma model. Our analysis is therefore the interpolation between these two limiting cases.

It is worth to stress that the mathematical plasmonic modes properties drastically differs from the photonic ones. In the limit $L \to \infty$, all propagative modes coincide with the modes for the perfect mirrors. Their frequencies tends asymptotically to

$$\omega_m^p[\mathbf{k}] \xrightarrow{L\to\infty} \sqrt{|\mathbf{k}|^2 + \left(\frac{m\pi}{L}\right)^2} \tag{3.4.2}$$

In contrast, the plasmonic modes show a decreasing exponentially for $L \to \infty$ in the evanescent zone. This behavior will deserve particular attention when evaluating the asymptotic expression involved in the formula of the Casimir energy as sum over the modes.

However we have to remark that the plasmonic and photonic modes are not all the modes of our system. We also have a continuum of frequencies corresponding to the previously called bulk region ($\omega > \omega_c$) i.e. a to a free propagation inside the bulk. The properties of this continuous of modes can be directly reconnected to the discontinuity corresponding to the branch cut of κ_m. Those modes do not contribute to the expression of the Casimir as given in Eq.(3.2.16) because they cancel in the difference involved in the definition of $[\cdots]_{L\to\infty}^{L}$ (see Appendix C.2). Sometime however it is useful to reintroduce them for mathematical purposes (see Chapter.4).

CHAPTER 4

Plasmonic and Photonic Modes Contributions to the Casimir energy

In this chapter I evaluate separately the plasmonic and photonic contribution. I evaluate their asymptotic behaviors in the long distance and short distance limits and emphasize the change in sign of the plasmonic energy.

Contents

4.1 Introduction 69
4.2 Equation for the cavity modes 70
4.3 Photonic and Plasmonic modes contributions 74
4.4 The contribution of the Plasmonic modes to the Casimir energy 75
4.4.1 Convergence 75
4.4.2 Derivation of a simpler expression 76
4.4.3 Explicit calculation 77
4.5 Sum of the propagative modes and the bulk limit 83
4.6 Sum of the TE-propagative modes and asymptotic behavior . 85
4.7 The difference between the TM- and TE-propagative modes . 87
4.7.1 Recasting the first term of Eq.(4.7.10) 89
4.7.2 Recasting the second term of Eq.(4.7.10) 92
4.7.3 Result for $\Delta\eta_{ph}$ and asymptotic behaviors 92
4.8 Discussion of the results 94

4.1 Introduction

So far, we have shown that the Casimir energy can be written as a sum over all cavity modes for arbitrary non-dissipative dielectric mirrors. We have then calculated the explicit cavity modes for $\epsilon[\omega]$ given by the plasma model. This allowed us to distinguish two different mode ensembles, *plasmonic* (pl) modes corresponding to evanescent waves, and *photonic* (ph) modes describing propagating waves.

In this Chapter we will calculate the contribution of these two mode ensembles to the Casimir energy

$$E=\sum_{p,\mathbf{k}}\left[\sum_n\frac{\hbar\omega_n^p}{2}\right]_{L\to\infty}^{L}=\underbrace{\sum_{\mathbf{k}}\left[\frac{\hbar\omega_+}{2}+\frac{\hbar\omega_-}{2}\right]_{L\to\infty}^{L}}_{\text{Plasmonic Contribution}}+\underbrace{\sum_{p,\mathbf{k}}\left[\sum_n\frac{\hbar\omega_n^p}{2}\right]_{L\to\infty}^{L}}_{\text{Photonic Contribution}} \tag{4.1.1}$$

For simplicity we have used the definition

$$\sum_{\mathbf{k},p}\equiv cA\sum_p\int\frac{d^2\mathbf{k}}{(2\pi)^2},\quad p=TE,TM \tag{4.1.2}$$

At short distances, we already know that the Casimir energy is determined by the surface plasmon modes:

$$E\approx A\int\frac{d^2\mathbf{k}}{(2\pi)^2}\left(\frac{\hbar\omega_+}{2}+\frac{\hbar\omega_-}{2}-2\frac{\hbar\omega_s}{2}\right)\quad\text{with }\omega_\pm^2\approx\omega_s^2\left(1\pm e^{-|\mathbf{k}|L}\right),\quad\omega_s^2\approx\frac{\omega_p^2}{2} \tag{4.1.3}$$

Here we will generalize this calculation to arbitrary distances and find a somewhat surprising result, namely that the surface plasmon contribution suffers a change of sign when the distance increases.

The explicit calculation is lengthy, but nevertheless presented in detail. We will first rewrite the cavity mode equations of Chapter 3 in a form more suitable for the explicit calculation and define the photonic and plasmonic mode contributions to the Casimir energy. The main difficulty of this calculation resides in the fact that the mode frequency cannot be expressed as a combination of elementary function. Here we develop a technique which allows us to proceed with the analytical treatment of such quantities and the derivation of quite simple asymptotic behaviors.

The results are discussed in the end of the chapter, followed by a Letter which summarizes all physical important arguments, without lengthy calculations.

4.2 Equation for the cavity modes

To begin with we pass through a reanalysis of the cavity modes equations, in order to define the notations used for the explicit calculation of the Casimir energy. We also give in this section some features which are complementary to the one already obtained in Chapter 3.

As mentioned before, cavity modes are the poles of the closed loop cavity function. For two identical mirrors they are the solutions of

$$1-r^2e^{-2\kappa L}=0\Leftrightarrow\begin{cases}1-re^{-\kappa L}=0\\1+re^{-\kappa L}=0\end{cases}\qquad\text{with }\kappa=\sqrt{|\mathbf{k}|^2-\omega^2} \tag{4.2.1}$$

For a bulk mirror the reflection coefficient have a very simple form

$$r=\frac{1-Z^p}{1+Z^p} \tag{4.2.2}$$

where Z^p is the surface impedance of the mirror for p-polarization ($p = TE,\ TM$). In the bulk case, the equations for the cavity modes can be written as

$$Z^p = -\tanh[\frac{\kappa L}{2}], \quad Z^p = -\coth[\frac{\kappa L}{2}] \tag{4.2.3}$$

The mode frequencies are thus solutions of transcendental equations which cannot be written in terms of simple functions. The surface impedance has a different expression depending on the polarization of the electromagnetic field

$$Z^{TE} = \frac{\sqrt{|\mathbf{k}|^2 - \epsilon[\omega]\omega^2}}{\sqrt{|\mathbf{k}|^2 - \omega^2}}, \quad Z^{TM} = \epsilon[\omega]\frac{\sqrt{|\mathbf{k}|^2 - \omega^2}}{\sqrt{|\mathbf{k}|^2 - \epsilon[\omega]\omega^2}} \tag{4.2.4}$$

Again all the frequencies are measured as wavevectors, i.e. ω stands for $\frac{\omega}{c}$ and ξ stands for $\frac{\xi}{c}$.

For simplicity we define the dimensionless variables

$$\Omega = \omega L, \quad \Omega_p = \omega_p L, \quad |\mathbf{k}|\, L = k, \quad z = k^2 - \Omega^2 \tag{4.2.5}$$

Using the plasma model for $\epsilon[\omega]$, Eqs.(4.2.3) can be rewritten as

$$\frac{\sqrt{z + \Omega_p^2}}{\sqrt{z}} = \begin{cases} -\tanh[\frac{\sqrt{z}}{2}] \\ -\coth[\frac{\sqrt{z}}{2}] \end{cases} \quad \text{for TE polarization} \tag{4.2.6a}$$

$$\left(1 - \frac{\Omega_p^2}{k^2 - z}\right)\frac{\sqrt{z}}{\sqrt{z + \Omega_p^2}} = \begin{cases} -\tanh[\frac{\sqrt{z}}{2}] \\ -\coth[\frac{\sqrt{z}}{2}] \end{cases} \quad \text{for } TM \text{ polarization} \tag{4.2.6b}$$

With such a notation we recover the two distinct regions

- **the evanescent region**: is the region for which $z > 0 \Rightarrow |\mathbf{k}| > \omega$ and the e.m. field is evanescent (does not propagate) along the direction perpendicular to the mirror plane;
- **the propagative region**: is the region for which $z < 0 \Rightarrow |\mathbf{k}| < \omega$ and the e.m. field can also propagate along the direction perpendicular to the mirror plane.

So far, we have just rewritten the results obtained in Chapter 3. In order to calculate the Casimir energy as the sum of the cavity eigen-frequencies, we now need Ω as a function of all other variables. Formally we may write

$$\Omega^{TE}[k] = \sqrt{k^2 - z_s^{TE}}, \quad \Omega^{TM}[k] = \sqrt{k^2 - z_s^{TM}[k]} \tag{4.2.7}$$

where z_s^{TE} and z_s^{TM} denote respectively the solution of Eqs.(4.2.6) for TE- and TM- polarization. The problem of the characterization of the cavity mode frequencies is equivalent to knowing the solution of Eqs.(4.2.6). As those equations are transcendental, the solution

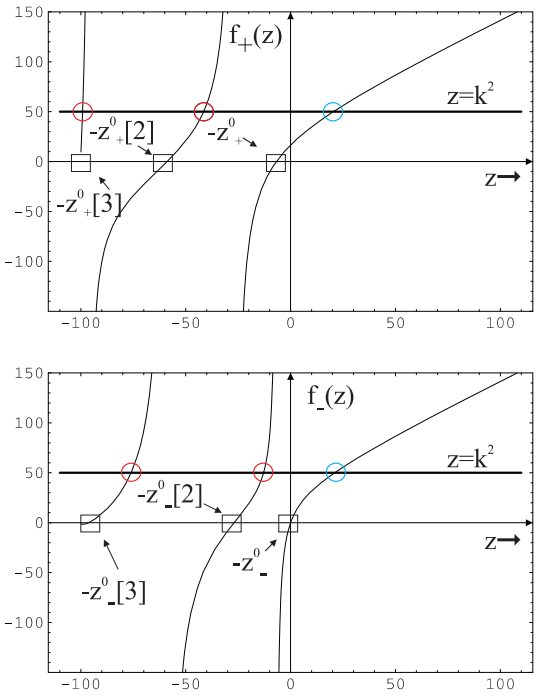

Figure 4.1 : A plot of $f_+(z)$ (top) and $f_-(z)$ (bottom) for $\Omega_p = 10$. The solutions of Eq.(4.2.8) are given by the intersections with $z = k^2$ (here we have fixed $k^2 = 50$). We can see that Eq.(4.2.8) allows solution both for $z > 0$ (evanescent domain) and $z < 0$ (propagative domain). Since $f_\pm$ are monodromic for $z > 0$ there is only one evanescent solution for each equation. For f_+ the evanescent solution becomes propagative depending on k^2. In the propagative domain $f_\pm$ are polydromic functions allowing several solutions.

z_s^{TE} and z_s^{TM} cannot be given explicitly. Let us remark, that for TE polarization, z_s^{TE} is independent of k while for TM polarization, z_s^{TM} is a function of k. The equations for TM polarization can be rewritten as follows

$$k^2 = f_\pm(z) \tag{4.2.8a}$$

where

$$f_+(z) = z + \frac{\Omega_p^2\,\sqrt{z}}{\sqrt{z} + \sqrt{z+\Omega_p^2}\tanh[\frac{\sqrt{z}}{2}]} \quad , f_-(z) = z + \frac{\Omega_p^2\,\sqrt{z}}{\sqrt{z} + \sqrt{z+\Omega_p^2}\coth[\frac{\sqrt{z}}{2}]} \tag{4.2.8b}$$

Inversion of Eq.(4.2.8) gives

$$z_s^{TM}[k] = f_\pm^{-1}[k^2] \tag{4.2.9}$$

Again $f_\pm^{-1}[k^2]$ cannot be expressed as combination of simple functions. We may however represent the solutions graphically by plotting the intersection between $f_\pm(z)$ and $z = k^2$.

Figure 4.1 shows a plot of $f_+(z)$ (top) and $f_-(z)$ (bottom) for $\Omega_p = 10$. The solutions of Eq.(4.2.8) are given by the intersections with $z = k^2$. We can see that Eqs.(4.2.8) allows solutions both for $z > 0$ (evanescent domain) and $z < 0$ (propagative domain). Since $f_\pm(z)$ are monodromic for $z > 0$ there exists only one evanescent solution for each equation.

For $f_+(z)$ the evanescent solution becomes propagative for small values of k^2. This happens for values $k < k_p$ where

$$k_p^2 = f_+(0) = \frac{2\Omega_p^2}{2+\Omega_p} > 0 \tag{4.2.10}$$

This shows that the evanescent solution of $f_+(z) = k^2$ always crosses the evanescent/propagative barrier ($\Omega_p > 0$). In the same way, since $f_-(0) = 0\ \forall\Omega_p$, the evanescent solution will never become propagative. Figure 4.1 shows that the first zero of $f_+(z)$ is in the propagative domain. Defining

$$-z_\pm^0 = f_\pm^{-1}[0] \quad \text{(the first value)} \tag{4.2.11}$$

and setting $y_+ = \sqrt{z_+^0}$, the equation describing the position of the zero as a function of Ω_p is given by

$$\Omega_p = \frac{y_+}{\cos[\frac{y_+}{2}]} \tag{4.2.12}$$

This allows to deduce that (see also fig.4.2)

$$y_+ \to \begin{cases} \Omega_p & \Omega_p \to 0 \\ \pi & \Omega_p \to \infty \end{cases} \Rightarrow z_+^0 \to \begin{cases} \Omega_p^2 & \Omega_p \to 0 \\ \pi^2 & \Omega_p \to \infty \end{cases} \tag{4.2.13}$$

We will come back to those limiting values in the following sections.

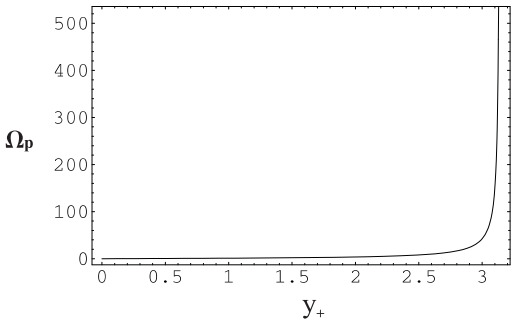

Figure 4.2 : A plot of $\Omega_p = \frac{y_+}{\cos[\frac{y_+}{2}]}$

For $f_-(z)$ the calculation of the first zero is very simple since

$$f_-(0) = 0\ \forall\ \Omega_p \Rightarrow z_-^0 = 0 \tag{4.2.14}$$

In the propagative domain ($z < 0$) $f_\pm(z)$ are polydromic functions and Eqs.(4.5.1) allow several solutions. Remark that for $z < -\Omega_p^2$ $f_\pm$ become a complex function and Eq.(4.2.8) never holds. The value $z = -\Omega_p^2 \Rightarrow \Omega = \Omega_c = \sqrt{\Omega_p^2 + k^2}$ is related to the high frequency transparency condition imposed by the plasma model and to the bulk approximation.

Figure 4.1 shows that in the propagative domain $f_\pm(z)$ exhibit divergences which occur at the solutions of the equations

$$\frac{1}{f_+(z)} = 0 \Rightarrow \sqrt{z} + \sqrt{z+\Omega_p^2}\tanh[\frac{\sqrt{z}}{2}] = 0 \tag{4.2.15a}$$

$$\frac{1}{f_-(z)} = 0 \Rightarrow \sqrt{z} + \sqrt{z+\Omega_p^2}\coth[\frac{\sqrt{z}}{2}] = 0 \tag{4.2.15b}$$

In view of the forthcoming calculations it is useful to define in the propagative region ($z \leq 0$)

$$-z_\pm^0[n] = f_\pm^{-1}[0], \quad -z_\pm^\infty[n] = f_\pm^{-1}[\infty] \tag{4.2.16}$$

In addition we have $z_\pm^0[1] = z_\pm^0$.

4.3 Photonic and Plasmonic modes contributions

We rewrite the expression of the Casimir energy (4.1.1) as

$$E = E_{ph} + E_{pl} \tag{4.3.1a}$$

As shown in Chapter 3 the plasmonic modes contribution (pl) to the Casimir energy is

$$E_{pl} = \left[\sum_{\mathbf{k}} \frac{\hbar}{2} \left(\omega_+[\mathbf{k}] + \omega_-[\mathbf{k}]\right)\right]_{L\to\infty}^{L} \tag{4.3.1b}$$

while the photonic modes contribution (ph) to the Casimir energy is

$$E_{ph} = \left[\sum_{\mathbf{k}} \frac{\hbar}{2} \sum_n \omega_n^{TE}[\mathbf{k}]\right]_{L\to\infty}^{L} + \left[\sum_{\mathbf{k}} \frac{\hbar}{2} \sum_n \omega_n^{TM}[\mathbf{k}]\right]_{L\to\infty}^{L} \tag{4.3.1c}$$

Let us remark that E_{pl} and E_{ph} may not necessarily be physical quantities when considered separately. Only their sum, the Casimir energy, is a physical observable. Each evaluation of the sums should thus pass through a checkup of the convergence properties. If one of both quantities shows the appropriate convergence properties, the other automatically does as well because of the convergence property of E.

For the forthcoming calculation it is useful to write E_{ph} as

$$E_{ph} = 2E^{TE} + \Delta E_{ph} \tag{4.3.1d}$$

where we ave defined

$$E^{TE} = \left[\sum_{\mathbf{k}} \frac{\hbar}{2} \sum_n \omega_n^{TE}[\mathbf{k}]\right]_{L\to\infty}^{L}, \quad \Delta E_{ph} = \left[\sum_{\mathbf{k}} \frac{\hbar}{2} \sum_n \left(\omega_n^{TM}[\mathbf{k}] - \omega_n^{TE}[\mathbf{k}]\right)\right]_{L\to\infty}^{L} \tag{4.3.1e}$$

The quantity E^{TE} is the TE polarization contribution to the Casimir energy. It is fully contained in the photonic mode contribution because we saw that this polarization does not allow for modes in the evanescent sector. In Appendix D.2 we show that this can also be seen from an invariance of the expression representing this quantity as a double integral over the frequency an the transverse wavevector (see Chapter 1). In the definition of ΔE_{ph} we have indicated the difference between the TM and TE photonic modes contributions.

The above decomposition of the Casimir energy entails that in the following we will concentrate on the calculation of three quantities:

- E_{pl}: the contribution of plasmonic modes to the Casimir energy
- E^{TE}: the TE-contribution of photonic modes to the Casimir energy
- ΔE_{ph}: the difference between TM- and TE- photonic modes contribution to the Casimir energy.

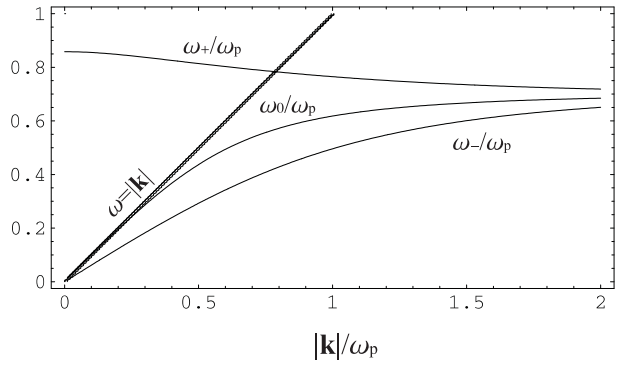

Figure 4.3 : A plot of $\frac{\omega_+}{\omega_p}$, $\frac{\omega_0}{\omega_p}$ and $\frac{\omega_-}{\omega_p}$ as function of $\frac{|\mathbf{k}|}{\omega_p}$ for $\frac{L}{\lambda_p} = 0.2$ ($\lambda_p = \frac{2\pi}{\omega_p}$).

4.4 The contribution of the Plasmonic modes to the Casimir energy

In this section we calculate the contribution of the plasmonic modes to the Casimir energy

$$E_{pl} = cA \int \frac{d^2\mathbf{k}}{(2\pi)^2} \frac{\hbar}{2} \left(\omega_+[\mathbf{k}, L] + \omega_-[\mathbf{k}, L] - 2\omega_{sp}[\mathbf{k}]\right) \tag{4.4.1}$$

For convenience we will call from now ω_0 the surface plasmon frequency (ω_{sp} so far).

Let us remind that for infinite distances $\omega_\pm$ obey the dispersion relation for the surface plasmons in a metallic bulk described by the plasma model

$$\omega_\pm[\mathbf{k}, L] \xrightarrow{L\to\infty} \omega_0^2[\mathbf{k}] = \frac{\omega_p^2 + 2\,|\mathbf{k}|^2 - \sqrt{\omega_p^4 + 4\,|\mathbf{k}|^4}}{2} \tag{4.4.2}$$

In the following paragraphs we show that the expression (4.4.1) is convergent and then transform it into a simpler form. We then recover the short distance asymptotic behaviors and study the long distance one.

4.4.1 Convergence

Here we check the convergence properties of Eq.(4.4.1) for large values of $|\mathbf{k}|$. The integrand is elsewhere a regular function $|\mathbf{k}|$.

From Chapter 3 we know that the mode $\omega_-[\mathbf{k}, L]$ lies totally in the evanescent sector while $\omega_+[\mathbf{k}, L]$ passes from the propagative to the evanescent sector with increasing $|\mathbf{k}|$.

Those modes are solutions of

$$Z^{TM}[\omega_+] = -\tanh[L\frac{\sqrt{|\mathbf{k}|^2 - \omega_+^2}}{2}], \quad Z^{TM}[\omega_-] = -\coth[L\frac{\sqrt{|\mathbf{k}|^2 - \omega_-^2}}{2}] \tag{4.4.3}$$

Figure 4.3 shows a plot of $\omega_\pm$ and ω_0 as a function of $|\mathbf{k}|$ (normalized to the plasma frequency). The frontier between the propagative and the evanescent sector is given by $\omega = |\mathbf{k}|$. In the limit $|\mathbf{k}| \to \infty$ all the functions are in the evanescent sector and $\omega_\pm, \omega_{sp} < \omega_p$. In this limit equations (4.4.3) take the form

$$\epsilon[\omega_\pm] \approx -(1 \mp 2e^{-|\mathbf{k}|L}) \Rightarrow \omega_\pm^2 \approx \frac{\omega_p^2}{2}\left(1 \pm e^{-|\mathbf{k}|L}\right) \tag{4.4.4}$$

from which we deduce

$$(\omega_+[\mathbf{k},L]+\omega_-[\mathbf{k},L]-2\omega_0[\mathbf{k}]) \xrightarrow{|\mathbf{k}|\to\infty} -\frac{\omega_p}{\sqrt{2}}\frac{e^{-2|\mathbf{k}|L}}{4} \tag{4.4.5}$$

This behavior ensures the convergence of the integral given in Eq.(4.4.1) and therefore of the other integrals involved in the definitions of Eqs.(4.3.1).

4.4.2 Derivation of a simpler expression

Eq.(4.4.1) is not the most suitable for a detailed evaluation of the contribution of the plasmonic modes to Casimir energy. In this section we manipulate them to obtain a simpler expression. The basic idea resides in the fact that the frequencies functions $\omega_i,\ i=0,\ \pm$ are solutions of simple equations. All the informations we need about the plasmonic modes are contained in ω_i as well as in the function f_i defined in Eqs.(4.2.8). In the next paragraphs we see that we can naturally define a function $f_0(z)$ in such a way that the frequency ω_0 arise as the solution of $k^2=f_0(z)$.

First of all it is useful to rewrite Eq.(4.4.1) as

$$E_{pl}=\eta_{pl}E_{Cas}, \qquad E_{Cas}=-\frac{\hbar c\pi^2 A}{720L^3} \tag{4.4.6a}$$

$$\eta_{pl}=-\frac{180}{\pi^3}\int_0^\infty k\left(\Omega_+[k]+\Omega_-[k]-2\Omega_0[k]\right)dk=-\frac{180}{\pi^3}\int_0^\infty \sum_i c_i k\Omega_i[k]d\mathbf{k} \tag{4.4.6b}$$

with $c_+=c_-=1, c_0=-2$. We defined a dimensionless surface plasmon frequency Ω_0

$$\Omega_0(k)=\sqrt{\frac{\Omega_p^2+2k^2-\sqrt{\Omega_p^4+4k^4}}{2}} \tag{4.4.6c}$$

expressed in terms of the dimensionless variables $\Omega_p=\omega_p L,\ \Omega=\omega L,\ k=|\mathbf{k}|\,L$.

The plasmonic contribution is therefore represented through the corrective factor η_{pl} with respect to the value of the Casimir energy in the perfect mirrors case E_{Cas}.

Note that

$$\eta_i=-\frac{180}{\pi^3}\int_0^\infty k\ \Omega_i[k]dk, \quad i=\pm,0 \tag{4.4.7}$$

is divergent despite the convergence of the whole expression given in Eq.(4.4.6b). Again this underlines that the meaningful physical quantity is the whole Eq.(4.4.6b). From the mathematical point of view this forbids us to invert sum and integral symbols in Eq.(4.4.6b). To bypass this mathematical difficulty it is convenient to introduce a regularizing factor $\nu_\gamma(k^2)$ such that

$$\eta_i^\gamma=-\frac{180}{\pi^3}\int_0^\infty \nu_\gamma(k^2)k\Omega_i[k]dk<\infty \quad \text{with} \lim_{\gamma\to0}\nu_\gamma(k^2)=1 \tag{4.4.8}$$

In such a way we can write

$$\eta_{pl}=\lim_{\gamma\to0}\sum_i c_i\eta_i^\gamma \tag{4.4.9}$$

This modification constitutes only a mathematical convenience and we shall prove in the end that it does not affect the final result.

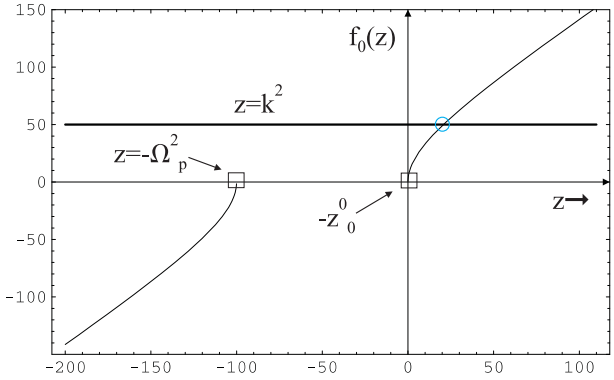

Figure 4.4 : A plot of $f_0(z)$. We can see that the solution of Eq.(4.4.11) besides in the evanescent region and it is unique.

4.4.3 Explicit calculation

In section 4.2 we showed that the frequencies $\Omega_\pm[k]$ are the solutions of equations

$$k^2 = f_\pm(z) \tag{4.4.10}$$

where $f_\pm(z)$ are defined in Eq. (4.2.8). A third equation must be added for $\Omega_0[k]$

$$k^2 = f_0(z) \quad \text{where} \quad f_0(z) = z + \frac{\Omega_p^2\sqrt{z}}{\sqrt{z} + \sqrt{z+\Omega_p^2}} = z + g_0^2[z] \tag{4.4.11}$$

Expression (4.4.11) can be obtained in two equivalent ways: either by starting directly from the explicit form of $\Omega_0[k]$ given in Eq.(4.4.6c) and solving for k^2 or by considering in the evanescent domain the limit $L \to \infty$ for the $f_\pm(z)$ function defined in Eqs.(4.2.8). With the dimensionless frequencies $\Omega_i[k]$ we may formally invert these equations:

$$k^2 = f_i(z) \Rightarrow \Omega_i[k] = \sqrt{k^2 - f_i^{-1}[k^2]} \quad i = 0,\ \pm \tag{4.4.12}$$

The previous expressions are the starting point of the following considerations.

Before going on we stress a feature concerning the behavior of the function $\Omega_+[k]$. We know that this function has the property

$$k = \Omega_+[k] \quad \text{for} \quad k = k_p = \frac{2\Omega_p^2}{2+\Omega_p} > 0 \tag{4.4.13}$$

This means that the corresponding plasmonic mode frequency $\omega_+[\mathbf{k}]$ crosses the evanescent/propagative frontier for $|\mathbf{k}| = k_p/L$. Moreover the definitions (4.4.12) imply that

$$y_+ = \Omega_+[0] \to \begin{cases} \Omega_p & \Omega_p \to 0 \\ \pi & \Omega_p \to \infty \end{cases} \tag{4.4.14}$$

while $\Omega_0[k],\ \Omega_-[k] < k\ \forall k$ and $\Omega_0[0] = \Omega_-[0] = 0$. These relations entail that for $\Omega_p \gg 1$

$$\Omega_+(0) \to \pi \neq 0 = \Omega_0(0) \tag{4.4.15}$$

This means that in the limit $\Omega_p \gg 1$ the function $\Omega_+[k]$ (describing the properties of the plasmonic mode frequency $\omega_+[\mathbf{k}]$) does not tend to the function $\Omega_0[k]$ (describing the surface plasmons dispersion low represented by $\omega_{sp}[\mathbf{k}]$).

Let us now come back to the term η_i^γ defined in Eq.(4.4.8) and make the following change of the variable in the integral

$$k^2 = f_i(z) = z + g_i^2(z) \tag{4.4.16}$$

Exploiting the definition of the function $\Omega_i[k]$ given in Eq.(4.4.12) one shows that

$$\begin{aligned} \eta_i^\gamma &= -\frac{180}{2\pi^3}\int_{f_i^{-1}[0]}^{f_i^{-1}[\infty]} f_i'(z)\nu_\gamma(f_i(z))g_i(z)dz \\ &= -\frac{180}{2\pi^3}\left[\int_{-z_i^0}^{\infty}\nu_\gamma(f_i(z))g_i(z)dz + 2\int_{-z_i^0}^{\infty}\nu_\gamma(f_i(z))g_i'(z)g_i^2(z)dz\right] \end{aligned} \tag{4.4.17}$$

where we have extended the definition (4.2.11) to $f_0(z)$ to obtain $-z_0^0 = f_0^{-1}[0]$.

Following the solutions in function of k^2 (see fig.4.1 and 4.4) we see that

$$z_0^0 = 0 \text{ and } f_i^{-1}[\infty] = \infty \tag{4.4.18}$$

Note that the second integral inside the square brackets of eq(4.4.17) is convergent even without the regularization factor. Taking the limit $\gamma \to 0$ we have indeed

$$\int_{-z_i^0}^{\infty} g_i'(z)g_i^2(z)dz = \frac{g_i^3(z)}{3}\Big|_{-z_i^0}^{\infty} = \frac{1}{3}\left[\left(\frac{\Omega_p}{\sqrt{2}}\right)^3 - \left(z_i^0\right)^{\frac{3}{2}}\right] \tag{4.4.19}$$

We have exploited the fact that Eqs.(4.2.8) and (4.4.11) and from $f_i(z) = z + g_i^2(z)$ we can deduce

$$f_i(-z_i^0) = 0 \Rightarrow g_i(-z_i^0) = \sqrt{z_i^0} \quad \text{and} \quad g_i(\infty) = \frac{\Omega_p}{\sqrt{2}} \tag{4.4.20}$$

Adding the three function η_i^γ weighted by the coefficients c_i and making some rearrangements one deduces that the corrective factor due to the plasmonic modes contribution to the Casimir energy defined in Eq.(4.4.6b) can be rewritten as

$$\eta_{pl} = -\frac{180}{2\pi^3}\left[\int_0^\infty \sum_i c_i g_i(z)dz + \int_{-z_+^0}^0 g_+(z)dz - \frac{2}{3}y_+^3\right] \tag{4.4.21}$$

We have already eliminated the regularizing function since all integrals of the previous expression are convergent. For the second integral this is evident because g_+ is a regular function for $z \in [-z_+^0, 0]$. The convergence holds also for the first integral because

$$\sum_i c_i g_i(z) \xrightarrow{z\to\infty} -\frac{\Omega_p}{\sqrt{2}}\frac{e^{-2\sqrt{z}}}{4} \tag{4.4.22}$$

In Eq.(4.4.21) we have also used

$$\int_{-z_+^0}^{\infty} g_+(z)dz = \int_0^{\infty} g_+(z)dz + \int_{-z_+^0}^{0} g_+(z)dz \tag{4.4.23}$$

and collected the first term in the sum. The sum and the integral symbols have been permuted again allowing to eliminate the regularizing function.

Eq.(4.4.21) basically involves the functions:

$$g_+(z) = \left[\frac{\Omega_p^2\ \sqrt{z}}{\sqrt{z}+\sqrt{z+\Omega_p^2}\tanh[\frac{\sqrt{z}}{2}]}\right]^{-\frac{1}{2}} \tag{4.4.24a}$$

$$g_-(z) = \left[\frac{\Omega_p^2\ \sqrt{z}}{\sqrt{z}+\sqrt{z+\Omega_p^2}\coth[\frac{\sqrt{z}}{2}]}\right]^{-\frac{1}{2}} \tag{4.4.24b}$$

$$g_0(z) = \left[\frac{\Omega_p^2\ \sqrt{z}}{\sqrt{z}+\sqrt{z+\Omega_p^2}}\right]^{-\frac{1}{2}} \tag{4.4.24c}$$

All those functions are real in the interval $[0,\infty]$. One can show that $g_+(z)$ is real too in the interval $\left[-z_+^0, 0\right]$ despite of the fact that $z<0$. This ensures that the corrective factor is a real quantity.

The corrective factor η_{pl} has a well defined structure: it is indeed decomposed into an integral over the positive real z-axis plus an integral over an interval of the negative z-axis plus a constant depending only on Ω_p. Moreover only one of the functions g_i, namely g_+, is involved in the last integral and in the constant. This particular structure can be traced back to the properties of the plasmonic modes analyzed in Chapter 3. We saw that the positive z-value domain coincides with the evanescent zone while the negative one describes the propagative zone. Now while the plasmonic mode ω_- and the dispersion frequency relation ω_0 are totally contained in the evanescent sector, the plasmonic mode ω_+ crosses the evanescent/propagative barrier. Therefore it appears that the functions g_0 and g_- describing the properties of ω_- and ω_0 are contained only in the first integral while the function g_+ describing ω_+ has to be evaluated in a wider range of z-values which includes at least a propagative interval. The second integral in Eq.(4.4.21) is thus nothing but the propagative part contribution of the plasmonic mode ω_+ while the constant the fact that the propagative value $\omega_+[\mathbf{k}=0] \neq 0$ still depends on L.

In Eq.(4.4.21) z_+^0 is still a quantity which has to be calculated numerically through the equation given in (4.2.12). Nevertheless this quantity depends only on Ω_p and represents only boundary: the integrand functions are all 'simple' functions. This will allow us to get asymptotic expressions over the whole domain of the variable Ω_p, the only variable on which the corrective factor η_{pl} depends after the integration. And since $\Omega_p = \omega_p L$ we will be able to discuss the behavior of E_{pl} as function of the distance L.

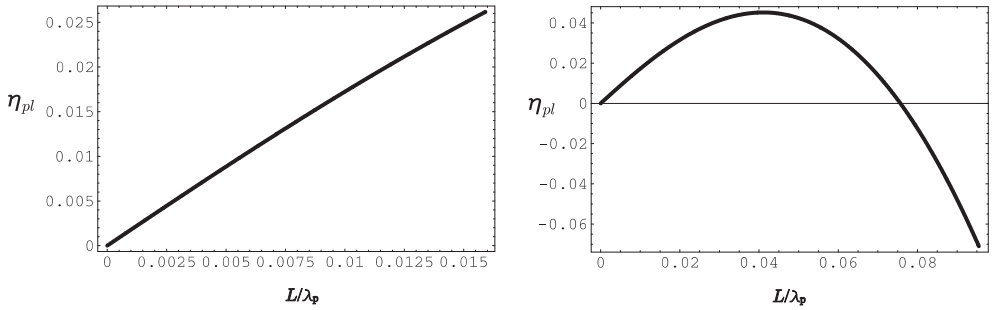

Figure 4.5 : A plot of η_{pl} as function of $\frac{L}{\lambda_p}$ on two different distance intervals

Fig.4.5 shows a plot of η_{pl} as function of $\frac{L}{\lambda_p} = \frac{\Omega_p}{2\pi}$ for two different distance intervals. The first graphic illustrates the short distance behavior of the plasmonic mode contribution, which is linear in $\frac{L}{\lambda_p}$. We thus recover exactly the correction factor known for the total Casimir energy.

To show this mathematically, we need to evaluate η_{pl} in the limit $\Omega_p \ll 1$ and compare it with the expression of the Casimir energy in the short distance limit. The limit is easily calculated by noting that, for $\Omega_p \ll 1$, $z_+^0 \approx \Omega_p^2 \ll 1$. To first order in Ω_p we have

$$g_+(z) \sim \Omega_p \sqrt{\frac{1}{1+\tanh[\frac{\sqrt{z}}{2}]}} = \frac{\Omega_p}{\sqrt{2}}\sqrt{1+e^{-\sqrt{z}}} \tag{4.4.25a}$$

$$g_-(z) \sim \Omega_p \sqrt{\frac{1}{1+\coth[\frac{\sqrt{z}}{2}]}} = \frac{\Omega_p}{\sqrt{2}}\sqrt{1-e^{-\sqrt{z}}} \tag{4.4.25b}$$

$$g_0(z) \sim \frac{\Omega_p}{\sqrt{2}} \tag{4.4.25c}$$

The propagative contribution of ω_+ is of third order in Ω_p

$$\int_{-z_+^0}^{0} g_+(z)dz - \frac{2}{3}y_+^3 \xrightarrow{\Omega_p \ll 1} g_+(0)\Omega_p^2 = k_p\Omega_p^2 \approx \Omega_p^3 \tag{4.4.26}$$

and can therefore be neglected in a linear approximation. The same argument holds for the term $y_+^3 = \left[z_+^0\right]^{\frac{3}{2}} \approx \Omega_p^3$. This entails that η_{pl} in the limit $\Omega_p \ll 1$ can be approximated by the first integral of Eq.(4.4.21). In other words the plasmonic contribution comes essentially from the evanescent sector ($z > 0$). Substituting the approximated expressions given in Eq.(4.4.25) and switching from z to κ^2 ($dz = 2\kappa\, d\kappa$) we find

$$\begin{aligned} \eta_{pl} &\approx -\frac{180}{2\pi^3}\int_0^\infty \sum_i c_i g_i(z)dz \\ &\approx -\frac{180}{\pi^3}\frac{\Omega_p}{\sqrt{2}}\int_0^\infty \kappa\left(\sqrt{1+e^{-\kappa}}+\sqrt{1-e^{-\kappa}}-2\right)d\kappa = \alpha_E\ \Omega_p \end{aligned} \tag{4.4.27}$$

$$\text{with} \quad \alpha_E = -\frac{180}{\sqrt{2}\pi^3}\int_0^\infty \kappa\left(\sqrt{1+e^{-\kappa}}+\sqrt{1-e^{-\kappa}}-2\right)d\kappa = 0.28489... \tag{4.4.28}$$

This last expression is exactly the same as the short distance correction factor of the Casimir energy, which is again equal to the interacting surface plasmons energy shift (see Chaps. 2 and 3). In particular we have

$$\alpha_E\ \Omega_p = \frac{3}{2}\alpha\frac{L}{\lambda_p} \quad \left(\Omega_p = 2\pi\frac{L}{\lambda_p}\right) \tag{4.4.29}$$

with $\alpha = 1.193...$ [90].

Note that to obtain the result in Eq.(4.4.27) we developed the expressions for $g_i(z)$ to first order in Ω_p. It is worth to stress that this method does not work for higher orders. The Taylor series obtained is not uniformly convergent in the variable z and we cannot interchange the integral and the summation. Moreover each integral obtained by this method is divergent except the first one given in Eq.(4.4.27). To avoid this problem an alternative method has to be developed. Despite this difficulty, the first order result coincides with Eq.(4.4.27) (see Appendix D.1).

The second graphics in figure 4.5 shows the plasmonic mode contribution η_{pl} at large distances. Surprisingly, it changes its sign for $\frac{L}{\lambda_p} \sim 0,08$. Mathematically this can be easily seen evaluating the expression given in Eq.(4.4.21) in the large distances limit $L \gg \lambda_p \Rightarrow \Omega_p \gg 1$.

One can check that the integrand of the first integral of Eq.(4.4.21) is significatively different from zero for $z \sim 1$. This allows therefore to consider the following approximated $\Omega_p \gg 1$ form of the function g_i

$$g_+[z] \approx \sqrt{\Omega_p}\sqrt{\sqrt{z}\coth[\frac{\sqrt{z}}{2}]} \tag{4.4.30a}$$

$$g_-[z] \approx \sqrt{\Omega_p}\sqrt{\sqrt{z}\tanh[\frac{\sqrt{z}}{2}]} \tag{4.4.30b}$$

$$g_0[z] \approx \sqrt{\Omega_p}\sqrt{\sqrt{z}} \tag{4.4.30c}$$

$$z_+^0 \approx \pi^2 \tag{4.4.30d}$$

Moreover since we saw that $0 \leq z_+^0 \leq \pi^2$ (see for example fig.4.2) the same approximated form for g_+ can be used in the second integral. At the same time since the z_+^0 is bounded in the limit $\Omega_p \gg 1$ we can neglect the constant term of Eq.(4.4.21). In the limit $\Omega_p \gg 1$ the corrective factor η_{pl} then takes the following approximated form:

$$\eta_{pl} \approx -\Gamma\sqrt{\Omega_p} \tag{4.4.31a}$$

$$\begin{aligned}\Gamma &= \frac{180}{2\pi^3}\int_0^\infty \sqrt[4]{z}\left(\sqrt{\coth[\frac{\sqrt{z}}{2}]}+\sqrt{\tanh[\frac{\sqrt{z}}{2}]}-2\right)dz \\ &+ \frac{180}{2\pi^3}\int_{-\pi^2}^0 \sqrt{\sqrt{z}\coth[\frac{\sqrt{z}}{2}]}dz\end{aligned} \tag{4.4.31b}$$

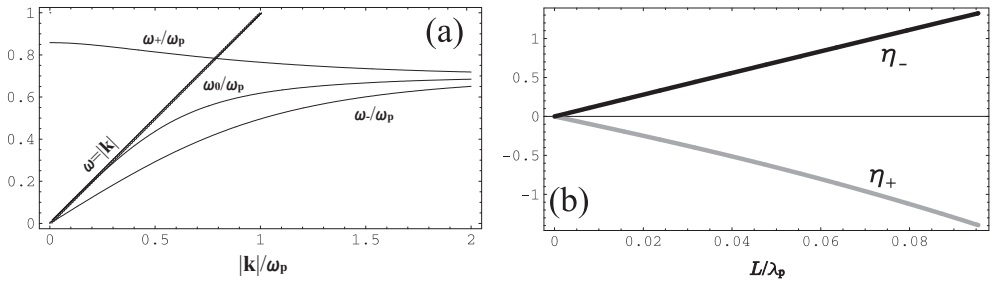

Figure 4.6 : A plot the two plasmonic frequencies ω_+ and ω_- compared to ω_0. The two separate mode contributions are plotted in fig. 4.6(b)

The last expression can be evaluated numerically giving as result $\Gamma = 29.7528$.

This last result confirms the behavior shown in fig. 4.5: the corrective coefficient describing the plasmonic mode contribution to the Casimir energy changes its sign for $\frac{L}{\lambda_p} \sim 0,08$ and then diverges in the long distances limit $L \gg \lambda_p$.

Now, the Casimir force is as usually the derivative with respect to the distance L of the Casimir energy. We may define in analogy the plasmonic Casimir force contribution F_{pl}

$$F_{pl} = \frac{d}{dL} E_{pl} \Rightarrow \begin{cases} F_{pl} > 0 & \text{for} L \ll \lambda_p \\ F_{pl} < 0 & \text{for} L \gg \lambda_p \end{cases} \tag{4.4.32}$$

This means that the plasmonic force F_{pl} contribution becomes repulsive with increasing distance between the mirrors or equivalently of the cavity length.

This change of sign can be understood plotting separately the contribution to the Casimir energy connected with $\omega_+[\mathbf{k}]$ and $\omega_-[\mathbf{k}]$. Figure 4.6(a) shows the two plasmonic frequencies ω_+ and ω_- compared to ω_0. While ω_- is always smaller than ω_0, ω_+ is always larger:

$$\sum_{\mathbf{k}} \frac{\hbar}{2} \left(\omega_-[\mathbf{k}, L] - \omega_{sp}[\mathbf{k}]\right) = E_- < 0, \quad \sum_{\mathbf{k}} \frac{\hbar}{2} \left(\omega_+[\mathbf{k}, L] - \omega_{sp}[\mathbf{k}]\right) = E_+ > 0 \tag{4.4.33a}$$

The energy related with the mode ω_+ always gives a repulsive contribution to the Casimir force. The convergence of the previous integral can be checked as in the paragraph 4.4.1. The two quantities E_- and E_+ correspond to a binding and anti-binding energies respectively [91]. We saw indeed that the short distance condition becomes a condition on the frequency and the wave vector

$$L \ll \lambda_p \ \Rightarrow \omega \ll |\mathbf{k}| \quad \text{(evanescent sector)} \tag{4.4.34}$$

which entails that $\omega_\pm[\mathbf{k}] = \omega_{sp}\sqrt{1 \pm e^{|\mathbf{k}|L}}$ and $\omega_{sp} = \omega_p/\sqrt{2}$. Graphically this asymptotic behavior can be recognized in fig. 4.6(a) in the region $|\mathbf{k}| > \omega_p$. Since we know that $\omega_\pm$, $\omega_{sp} < \omega_p$ the range $|\mathbf{k}| \gg \omega_p$ fits the short distance condition. Exploiting the approximated expressions one shows that

$$|\omega_-[\mathbf{k}, L] - \omega_{sp}[\mathbf{k}]| > |\omega_+[\mathbf{k}, L] - \omega_{sp}[\mathbf{k}]| \quad (\mathbf{k} \gg \omega_p) \tag{4.4.35}$$

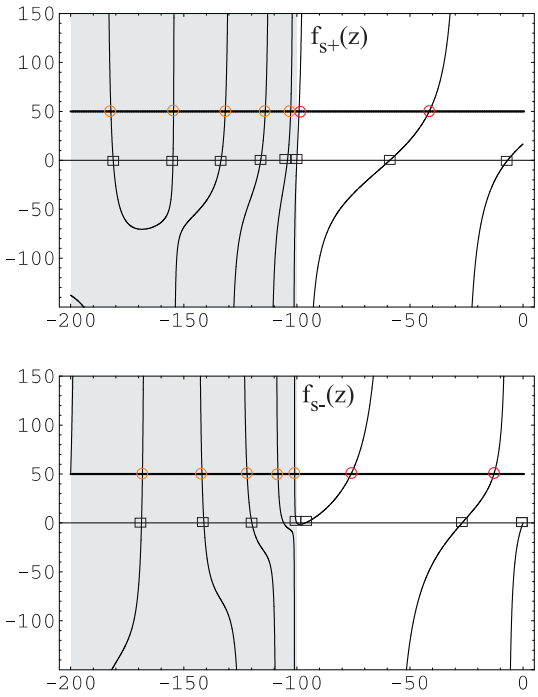

Figure 4.7 : A plot of $f_{s+}(z)$ (top) and $f_{s-}(z)$ (bottom) for $\Theta[x] = \coth[x]$ for $\Omega_p = 10$, $d = 1$. The solutions of Eq.(4.5.4a) are given by the intersections with $z = k^2$ (here we have fixed $k^2 = 50$). We can see that Eq.(4.5.4a) allows solution everywhere. The solutions gray zone are for $z < -\Omega_p^2$ and missed in the case of Eq.(4.2.8).

and therefore $|E_-| > |E_+|$. As a consequence, the ω_- mode contribution dominates and the total plasmonic mode contribution remains attractive.

For large distances we see from fig. 4.6(a) that for $|\mathbf{k}| \ll \omega_p$

$$|\omega_-[\mathbf{k}, L] - \omega_{sp}[\mathbf{k}]| < |\omega_+[\mathbf{k}, L] - \omega_{sp}[\mathbf{k}]| \qquad (\mathbf{k} \ll \omega_p) \tag{4.4.36}$$

Now, the ω_+ mode contribution becomes the dominant one resulting in a repulsive total plasmonic contribution. The two separate mode contributions are plotted in fig. 4.6(b).

Let us underline also that relaxing the short distance condition means from another point of view taking account of the retard-effects ($c < \infty$) in our treatment: therefore the change in the sign can be also seen as an implication of the finite speed of the light. We come back on this point in the following.

4.5 Sum of the propagative modes and the bulk limit

In the previous sections we have evaluated the Casimir energy contribution of the plasmonic modes directly in the bulk limit case. Unfortunately in the case of the pure propagative modes contribution working directly in the bulk limit rises up some mathematical problems. In the section 4.2, indeed, our discussions for the propagative zone focused on the interval $-\Omega_p^2 < z < 0$ which corresponds to mode frequencies inside the cavity, the lower bound being related to the high frequency transparency condition: the range $z < -\Omega_p^2$ corresponds to the frequency domain that we called in the Chapter 3 bulk region. Because of the bulk approximation those frequencies correspond to a field which

freely propagate inside the bulk. As we have said in Chapter 3 those frequencies do not contribute to the Casimir energy.

From a mathematical point of view the high frequency cutoff leads to a lack of solutions in the bulk region of the equations

$$k^2 = f_\pm(z) \quad \frac{1}{f_\pm(z)} = 0 \quad \forall\ z < -\Omega_p^2 \tag{4.5.1}$$

In this region indeed $f_\pm(z)$ become complex because of the square root $\sqrt{z+\Omega_p^2}(=\kappa_m L)$ in Eqs.(4.2.8) and since k^2 is real the previous equation never holds.

We therefore consider a mirror with finite thickness d to circumvent this problem and reintroduce the corresponding surface impedance Z_s^p:

$$Z_s^p = Z^p \coth[d\ \kappa_m] \tag{4.5.2}$$

Z^p is the surface impedance in the bulk limit corresponding to the polarization p. As before the subscript "s" denotes the mirrors of finite thickness (slab). Eqs.(4.5.1) then becomes

$$k^2 = f_{s\pm}(z), \quad \frac{1}{f_{s\pm}(z)} = 0 \tag{4.5.3}$$

Because of the modification introduced in Eq.(4.5.2) the functions $f_\pm$ defined in the previous section transform into

$$f_{s+}(z) = z + \frac{\Omega_p^2\ \sqrt{z}}{\sqrt{z} + \frac{\sqrt{z+\Omega_p^2}}{\coth[d\sqrt{z+\Omega_p^2}]}\tanh[\frac{\sqrt{z}}{2}]} = z + g_{s+}^2(z) \tag{4.5.4a}$$

$$f_{s-}(z) = z + \frac{\Omega_p^2\ \sqrt{z}}{\sqrt{z} + \frac{\sqrt{z+\Omega_p^2}}{\coth[d\sqrt{z+\Omega_p^2}]}\coth[\frac{\sqrt{z}}{2}]} = z + g_{s-}^2(z) \tag{4.5.4b}$$

The functions $f_{s\pm}(z)$ are real over the whole domain $z < 0$ and Eqs.(4.5.3) allow solutions everywhere on the negative real z-axis. The bulk solutions are obtained as the limit for $d \to \infty$ of the solutions in $z > -\Omega_p^2$.

Remark that instead of $\coth[d\ \kappa_m]$ we could introduce another function $\Theta[d\ \kappa_m]$ with the same parity and asymptotic characteristics

$$\Theta[-x] = -\Theta[x] \quad \text{and} \quad \lim_{d\to\infty} \Theta[d\ \kappa_m] = 1 \quad (Re\,[\kappa_m] > 0) \tag{4.5.5}$$

The introduction of such a function corresponds from a mathematical point of view to the elimination of the branch points due to the square root $\sqrt{z+\Omega_p^2}$ (for further details see ref. [111], Chap.3 and Appendix A.3). From a physical point of view it can be directly reconnected to the mirrors thickness. In the case of a lossless slab with a finite width, indeed, the system allows other modes with a frequency higher than the frequency cutoff $\omega_c = \sqrt{\omega_p^2 + |\mathbf{k}|^2}$ which oscillate principally in the inner of the slab (the solution in the

gray zone of figure 4.7). The respective frequency spectrum corresponds to a discretization of the continuous bulk region spectrum. Reintroducing a finite width for the mirror means that the photons which propagated freely in the bulk can now meet the end of the mirror and be reflected or transmitted. This leads to resonances which correspond to the frequency solutions of Eqs.(4.5.3) for $z < -\Omega_p^2$. Therefore, from this point of view, the bulk limit is equivalent to the infinite volume limit taken after the quantization of a field inside a finite volume (see for example [113, 120]).

To evaluate the photonic modes contribution to the Casimir energy we will apply the following procedure: we sum on the pure propagative modes which we can get from Eqs.(4.5.3) and we take the limit $d \to \infty$ at the end of the calculation. We will show that the final result does not depend on the function $\Theta[d\ \kappa_m]$ (see also App.C.2).

4.6 Sum of the TE-propagative modes and asymptotic behavior

In this section we evaluate the TE-modes contribution to the Casimir energy. As the TE-modes are purely propagative, this contribution is easily evaluated by using the formula

$$E^{TE} = \sum_{\mathbf{k}} \frac{\hbar}{2} \left[\sum_n \omega_n^{TE}[\mathbf{k}] \right]_{L\to\infty}^{L} = \frac{\hbar c A}{2\pi} \int \frac{d^2\mathbf{k}}{(2\pi)^2} \int_0^\infty \ln\left[1 - \rho_{\mathbf{k}}^{TE}[\imath\xi]\right]\ d\xi \tag{4.6.1}$$

The function $\rho_{\mathbf{k}}^{TE}[\imath\xi]$ is the open loop function for the TE-polarization

$$\kappa = \sqrt{|\mathbf{k}|^2 + \xi^2}, \quad Z_{\mathbf{k}}^{TE} = \frac{\sqrt{\kappa^2 + \omega_p^2}}{\kappa}, \quad r_{\mathbf{k}}^{TE} = \frac{1 - Z_{\mathbf{k}}^{TE}}{1 + Z_{\mathbf{k}}^{TE}}, \quad \rho_{\mathbf{k}}^{TE} = \left(r_{\mathbf{k}}^{TE}\right)^2 e^{-2\kappa L} \tag{4.6.2}$$

We change variables from ξ to $\kappa = \sqrt{|\mathbf{k}|^2 + \xi^2}$ leading to

$$\begin{aligned}
E^{TE} &= \frac{\hbar c A}{2\pi} \int_0^\infty |\mathbf{k}|\, d|\mathbf{k}| \int_0^\infty \ln\left[1 - \rho_{\mathbf{k}}^{TE}[\imath\xi]\right]\ d\xi \\
&= \frac{\hbar c A}{2\pi} \int_0^\infty |\mathbf{k}|\, d|\mathbf{k}| \int_{|\mathbf{k}|}^\infty \ln\left[1 - \rho^{TE}[\kappa]\right]\ \frac{\kappa}{\sqrt{\kappa^2 - |\mathbf{k}|^2}} d\kappa \\
&= \frac{\hbar c A}{2\pi} \int_0^\infty d\kappa\ \kappa \ln\left[1 - \rho^{TE}[\kappa]\right] \int_0^{|\mathbf{k}|} \frac{|\mathbf{k}|}{\sqrt{\kappa^2 - |\mathbf{k}|^2}} d|\mathbf{k}| \\
&= \frac{\hbar c A}{2\pi} \int_0^\infty d\kappa\ \kappa^2 \ln\left[1 - \rho^{TE}[\kappa]\right]
\end{aligned} \tag{4.6.3}$$

Remark that in the previous derivation we have exploited a particular property of the open loop function ρ^{TE} which can be expressed as a function of κ alone instead of $|\mathbf{k}|$ and ξ. This property will allow us to eliminate one of the integrations.

As for the plasmonic modes we define a corrective coefficient

$$E^{TE} = \eta^{TE} E_{Cas}, \qquad E_{Cas} = -\frac{\hbar c \pi^2 A}{720 L^3} \tag{4.6.4}$$

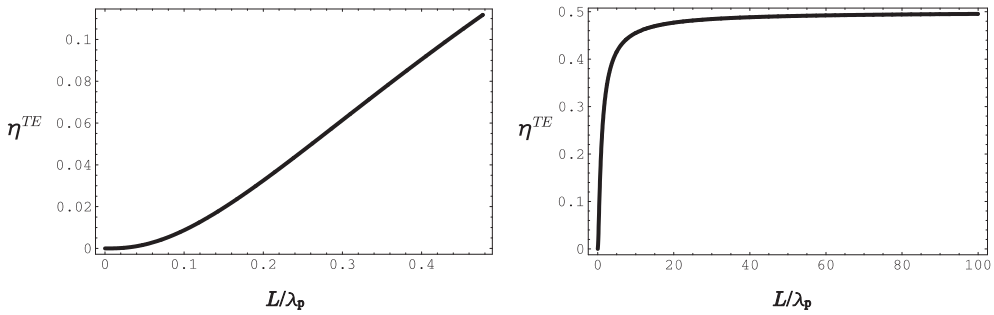

Figure 4.8 : A plot of η^{TE} as function of L/λ_p on two different distance intervals. η^{TE} scale as $(L/\lambda_p)^3$ for short distances ($L \ll \lambda_p$) and tends to 1/2 in the long distances limit ($L \gg \lambda_p$)

Using dimensionless variables

$$\Omega_p = \omega_p L, \quad K = \kappa L, \quad k = |\mathbf{k}|\, L \tag{4.6.5}$$

we get the expression

$$\eta^{TE} = -\frac{180}{\pi^4} \int_0^\infty dK\ K^2 \ln\left[1 - \rho^{TE}[K]\right] \tag{4.6.6}$$

Since $\rho^{TE}[K] < 0$ along the positive real K-axis, the corrective factor η^{TE} is always a positive quantity. In our case this means that in contrast to E_{pl} the corresponding energy E^{TE} always describes a binding force . η^{TE} is plotted in fig. 4.8 as a function of L/λ_p.

We now briefly discuss the long ($\Omega_p \gg 1$) and the short $\Omega_p \ll 1$ distances limit of the corrective coefficient η^{TE}. In the short distances limit ($\Omega_p \ll 1$), let us first remark that E^{TE} is finite at $L = 0$:

$$E^{TE}(L=0) = \frac{\hbar c A}{2\pi} \int_0^\infty d\kappa\ \kappa^2 \ln\left[1 - r^{TE}[\kappa]^2\right] < \infty \tag{4.6.7}$$

because of

$$r^{TE}[\kappa] \xrightarrow{\kappa\to\infty} -\frac{\omega_p^2}{4\kappa^2} \tag{4.6.8}$$

This means that $\eta^{TE} = E^{TE}/E_{Cas} \propto L^3$ for $L \to 0$ as can be seen in fig 4.8. Since η^{TE} is a dimensionless quantity and function of $\Omega_p = \omega_p L$ alone, we have

$$\eta^{TE} \propto \Omega_p^3 \quad \text{for} \quad \Omega_p \ll 1 \tag{4.6.9}$$

It is worth to stress that this behavior is not intuitive when starting directly from the expression for η^{TE} given in Eq.(4.6.6). For $\Omega_p \ll 1$ we would find

$$r^{TE} = \mathcal{O}^2[\Omega_p] \approx -\frac{\Omega_p^2}{4K^2} \Rightarrow \ln\left[1 - \rho_{TE}^2\right] = O^4[\Omega_p] \tag{4.6.10}$$

and would deduce $\eta^{TE} \propto \Omega_p^4$. However, because of the square root involved in the definition of r^{TE}, the power series leading to the previous approximated form for the reflection

coefficient is not convergent along the whole positive K-axis [129, 134]. This problem is similar to the one already encountered for the expansion in orders of Ω_p of η_{pl} (see paragraph 4.4.3 and Appendix D.1). Here the problem arises because of the branching points of $\sqrt{K^2+\Omega_p^2}$: passing in the complex K-plane, we see that the previous expansion is valid only for $|K|<\Omega_p$. Splitting the integral for η^{TE} in two we obtain

$$\eta^{TE}=-\frac{180}{\pi^4}\int_0^{\Omega_p} dK\ K^2\ln\left[1-\rho^{TE}[K]\right]-\frac{180}{\pi^4}\int_{\Omega_p}^{\infty} dK\ K^2\ln\left[1-\rho^{TE}[K]\right] \quad (4.6.11)$$

In the first integral since $K<\Omega_p\ll 1$, we can approximate $e^{-2K}\sim 1$ whereas we can expand the second integral into powers of $\left(r^{TE}\right)^2\ll 1$. Making the substitution $K=\Omega_p x$ we get

$$\begin{aligned}\eta^{TE} &\approx \Omega_p^3\left(-\frac{180}{\pi^4}\int_0^1 x^2\ln\left[1-r^{TE}[x]^2\right]dx+\frac{180}{\pi^4}\int_1^{\infty}x^2 r^{TE}[x]^2\ e^{-2x\Omega_p}dx\right)\\ &\propto \mathcal{O}^3[\Omega_p] \end{aligned} \quad (4.6.12)$$

The long distance limit was already discussed in Chapter 2. One can show that the principal contribution to the integral in Eq.(4.6.6) is

$$\left(r^{TE}\right)^2-1\approx-\frac{4K}{\Omega_p}\Rightarrow\ln\left[1-\rho^{TE}\right]\approx\ln\left[1-e^{-2K}\right]+\frac{4K}{\Omega_p}\frac{e^{-2K}}{1-e^{-2K}} \quad (4.6.13)$$

This entails that

$$\eta^{TE}\approx-\frac{180}{\pi^4}\int_0^{\infty}dK\ \left(K^2\ln\left[1-e^{-2K}\right]+\frac{4K^3}{\Omega_p}\frac{e^{-2K}}{1-e^{-2K}}\right)=\frac{1}{2}-\frac{3}{\Omega_p} \quad (4.6.14)$$

4.7 The difference between the TM- and TE-propagative modes

In this section we present the last step of our calculation, namely the evaluation of ΔE_{ph}. The main difficulty resides in taking into account only the pure TM-propagative modes and disregarding the two plasmonic modes. Both types of modes are solutions of the same equation (4.2.3) for the TM-polarization. We may follow two procedures to evaluate ΔE_{ph}:

- The first one is based on the residues technique. Following the same procedure as in section 4.6 we could sum over all TM-modes[1] and subtract E^{TE} and E_{pl}. This would be equivalent to take the analog of the expression given in Eq.(4.6.4) for TM-modes and subtracting the expression obtained in Eqs.(4.6.6) and (4.4.21).
- The second one consists in summing directly over the modes as we did for E_{pl}, the principal difficulties consisting in the great number of modes and in the necessity to disregard the plasmonic modes.

[1] A variant of this procedure could consist in adjusting the contour path to enclose only the TM-pure propagative modes. A similar trick has be exploited in Appendix D.2.

Despite the simplicity of the first solution it presents the inconvenient not to be independent of the calculation of E_{pl}. An independent calculation would prove and ensure the correctness of our result for E_{pl}. For those reasons here we follow the second procedure.

The term ΔE_{ph} represents the difference of the TM and the TE photonic modes contribution to the Casimir energy:

$$\Delta E_{ph} = \sum_{\mathbf{k}} \frac{\hbar}{2} \sum_{n} \left[\omega_n^{TM}[\mathbf{k}] - \omega_n^{TE}[\mathbf{k}]\right]_{L\to\infty}^{L} \tag{4.7.1}$$

From a mathematical point of view it is convenient to reintroduce the mirrors thickness as described in section 4.5 and to consider the previous expression as the bulk limit case

$$\Delta E_{ph} = \lim_{d\to\infty} \frac{\hbar c A}{4\pi} \left[\sigma_s\right]_{L\to\infty}^{L} \tag{4.7.2}$$

As shown in the previous sections the convergence of the plasmonic energy ensures that the integrals involved in the definition of ΔE_{ph} are convergent. The function $\sigma_s(L)$ is nothing but the sum over the difference between the modes evaluated at the distance L. In terms of dimensionless variables we can write

$$\sigma_s(L) = \frac{\Delta_s(L)}{L^3} \Rightarrow \Delta_s(L) = \sum_n I_n(L) \quad \text{with } I_n^s(L) = \int_0^\infty k \left[\bar{\Omega}_n^{TM}(k) - \bar{\Omega}_n^{TE}(k)\right] dk \tag{4.7.3}$$

The bar over the frequencies means that we are working in the finite width case. Unfortunately the properties of ΔE_{ph} do not give any guarantee of the convergence of $\sigma_s(L)$ alone. Such a problem can be resolved introducing a renormalizing function as we did in the plasmonic case and in the following we will disregard it.

We are going to show that $\Delta_s(L)$ can be written in a simpler form which allows to easily evaluate its asymptotic behavior.

Exploiting the result of section 4.2 and 4.5, the dimensionless frequencies can be written as

$$\bar{\Omega}_n^{TM}(k) = \begin{cases} \sqrt{k^2 - f_{s+}^{-1}[k^2]} \\ \\ \sqrt{k^2 - f_{s-}^{-1}[k^2]} \end{cases} , \quad \bar{\Omega}_n^{TE}(k) = \begin{cases} \sqrt{k^2 - f_{s+}^{-1}[\infty]} \\ \\ \sqrt{k^2 - f_{s-}^{-1}[\infty]} \end{cases} \tag{4.7.4}$$

Considering the functions introduced in the Eq.(4.5.4a) of section 4.5 let us define

$$-z_{s\pm}^0[n] = f_{s\pm}^{-1}[0], \quad -z_{s\pm}^\infty[n] = f_{s\pm}^{-1}[\infty] \tag{4.7.5}$$

The previous are nothing but the generalization of the definitions given in Eq.(4.2.16) to the finite width case. When taking the bulk limit $\forall z_{s\pm}^0[n], z_{s\pm}^\infty[n] < \Omega_p^2$ we have

$$\lim_{d\to\infty} (-z_{s\pm}^0[n], -z_{s\pm}^\infty[n]) = (-z_{\pm}^0[n], -z_{\pm}^\infty[n]) \tag{4.7.6}$$

The other values $\Omega_p^2 < z_{s\pm}^0[n], z_{s\pm}^\infty[n]$ become more and more dense reaching the continuum in the limit $d \to \infty$.

The ensemble of the $I_n^s(L)$ can be split in two sub-ensembles $I_n^{s+}(L)$ and $I_n^{s-}(L)$. In each one of those sub-ensembles we make respectively the following change of variable

$$k^2 = f_{s+}(z), \quad k^2 = f_{s-}(z) \tag{4.7.7}$$

From the definitions given in Eqs.(4.7.4) one shows that the terms $I_n^{s+}(L)$ can be rewritten as

$$\begin{aligned} I_n^{s\pm}(L) &= \frac{1}{2}\int_{-z_{s\pm}^0[n+1]}^{-z_{s\pm}^\infty[n]} f'_\pm(z)\left[g_{s\pm}(z) - \sqrt{f_\pm(z) + z_{s\pm}^\infty[n]}\right] dz \\ &= \frac{1}{2}\int_{-z_{s\pm}^0[n+1]}^{-z_{s\pm}^\infty[n]} g_{s\pm}(z)dz + \frac{1}{3}\left[g_{s\pm}^3(z) - \left(f_{s\pm}(z) + z_{s\pm}^\infty[n]\right)^{\frac{3}{2}}\right]_{-z_{s\pm}^0[n+1]}^{-z_{s\pm}^\infty[n]} \end{aligned} \tag{4.7.8}$$

From eqs.(4.5.4a) we have $g_{s\pm}^2(z) = f_{s\pm}(z) - z$ and exploiting the definitions given in eqs.(4.7.5), the last term of the previous equation can be rewritten as

$$\begin{aligned} &\left[g_{s\pm}^3(z) - \left(f_{s\pm}(z) + z_{s\pm}^\infty[n]\right)^{\frac{3}{2}}\right]_{-z_{s\pm}^0[n+1]}^{-z_{s\pm}^\infty[n]} \\ &= \left[(f_{s\pm}(z) - z)^{\frac{3}{2}} - \left(f_{s\pm}(z) + z_{s\pm}^\infty[n]\right)^{\frac{3}{2}}\right]_{-z_{s\pm}^0[n+1]}^{-z_{s\pm}^\infty[n]} = -\left(z_{s\pm}^0[n+1]^{\frac{3}{2}} - z_{s\pm}^\infty[n]^{\frac{3}{2}}\right) \end{aligned} \tag{4.7.9}$$

We then write

$$\Delta_s(L) = \underbrace{\sum_i \sum_{n=1}^{\infty} \frac{1}{2}\int_{-z_{si}^0[n+1]}^{-z_{si}^\infty[n]} g_{si}(z)dz}_{\text{1st term}} - \underbrace{\frac{1}{3}\sum_i \sum_{n=1}^{\infty}\left(z_{si}^0[n+1]^{\frac{3}{2}} - z_{si}^\infty[n]^{\frac{3}{2}}\right)}_{\text{2nd term}} \tag{4.7.10}$$

Here our expression looks like an extension to the propagative domain of the expression reached in Eq.(4.4.21) for the plasmonic modes. There are however some important differences. First, all the integrations are defined over some intervals of the real negative z axis ($z < 0$). Figure 4.7 shows that for $z < 0$ the functions $f_{s\pm}$ behave in a complicated way and in particular they become negative entailing that the functions $g_{s\pm} = \sqrt{f_{s\pm}(z) - z}$ may become purely imaginary. Pay attention however to the definitions of integration domain one can show that $g_{s\pm}(z)$ are real over the interval $\mathcal{I}_n^{s\pm} \equiv \left[-z_{s\pm}^0[n+1], -z_{s\pm}^\infty[n]\right]$.

The second difference is that here we deal with more than two modes and, because of the particular convergence properties of the propagative modes, we cannot directly write down the asymptotic expression for each mode but have to do this for the whole expression.

In the following paragraph we show how to cast the first and the second term of expression (4.7.10) in a more compact form, of which we can evaluate the asymptotic behavior in the limit $L \to \infty$.

4.7.1 Recasting the first term of Eq.(4.7.10)

Let us look for a function which is equal to $g_{s\pm}(z)$ for $z \in \mathcal{I}_n^{s\pm} \equiv \left[-z_{s\pm}^0[n+1], -z_{s\pm}^\infty[n]\right]$ and zero elsewhere and define

$$\tilde{g}_{s\pm}(z) = Im\left[\imath g_{s\pm}(z) - \frac{2g_{s\pm}(z)}{\pi}\text{arctanh}[\frac{\sqrt{-z}}{g_{s\pm}(z)}]\right] \tag{4.7.11a}$$

We prove that

$$\tilde{g}_{\pm}(z) = \begin{cases} g_{\pm}(z) & \forall z \in \mathcal{I}_n^{s\pm} \\ 0 & \forall z \notin \mathcal{I}_n^{s\pm} \end{cases} \Rightarrow \sum_{n=1}^{\infty} \frac{1}{2} \int_{-z_{s\pm}^{0}[n+1]}^{-z_{s\pm}^{\infty}[n]} g_{s\pm}(z)dz = \int_{-\infty}^{-z_{s\pm}^{0}} \tilde{g}_{s\pm}(z)dz \quad (4.7.11b)$$

The demonstration consists in showing that the function proportional to the hyperbolic arctangent deletes the first term on the right-hand side of Eq.(4.7.11a). In other words we have to show that

$$Im\left[\text{arctanh}[\frac{\sqrt{-z}}{g_{s\pm}(z)}]\right] = \begin{cases} 0 & \forall z \in \mathcal{I}_n^{s\pm} \\ \imath\frac{\pi}{2} & \forall z \notin \mathcal{I}_n^{s\pm} \end{cases} \quad \text{or} \quad \frac{\sqrt{-z}}{g_{s\pm}(z)} = \begin{cases} < 1 & \forall z \in \mathcal{I}_n^{s\pm} \\ > 1 & \forall z \notin \mathcal{I}_n^{s\pm} \end{cases} \quad (4.7.12)$$

When its argument is greater the imaginary part of the hyperbolic arctangent becomes equal to $\pm\imath\frac{\pi}{2}$. The sign depends from which side we approach the real axis in the complex plane. Moving the values of z in $Im\,[z] < 0$ of a vanishing quantity we reach the right result. This means that instead of z we should consider $\tilde{z} = z - \imath 0^{+}$. Nevertheless we continue to use z where the result cannot be ambiguous. Now let us note that (see for example the figure 4.7)

$$f_{s\pm}(z) \geq 0 \Rightarrow g_{s\pm}^2(z) > -z > 0 \quad \forall z \in \mathcal{I}_n^{s\pm}\ (z < 0) \quad (4.7.13a)$$

This leads to the fact that

$$f_{s\pm}(z) = z + g_{s\pm}^2(z) \geq 0 \Rightarrow \frac{-z}{g_{s\pm}^2(z)} \leq 1 \Rightarrow \frac{\sqrt{-z}}{g_{s\pm}(z)} \leq 1 \quad \forall z \in \mathcal{I}_n^{s\pm}\ (z < 0) \quad (4.7.13b)$$

This ensures that $\tilde{g}_{s\pm}(z)$ is equal to $g_{s\pm}(z)$ inside the intervals $\mathcal{I}_n^{s\pm}$.

Elsewhere we have

$$f_{s\pm}(z) \leq 0 \text{ but } g_{s\pm}^2(z) \lesseqgtr 0 \quad \forall z \notin \mathcal{I}_n^{s\pm}\ (z < 0) \quad (4.7.13c)$$

When $g_{s\pm}^2(z) > 0$

$$f_{s\pm}(z) = z + g_{s\pm}^2(z) \leq 0 \Rightarrow \frac{-z}{g_{s\pm}^2(z)} \geq 1 \Rightarrow \frac{\sqrt{-z}}{g_{s\pm}(z)} \geq 1 \quad \forall z \notin \mathcal{I}_n^{s\pm}\ (z < 0) \quad (4.7.13d)$$

The case $g_{s\pm}^2(z) < 0$ is more subtle. We have indeed that

$$Re\,[g_{s\pm}(z)] = 0 \Rightarrow Re\left[\frac{\sqrt{-z}}{g_{s\pm}(z)}\right] = 0 \Rightarrow Im\left[\frac{2g_{s\pm}(z)}{\pi}\text{arctanh}[\frac{\sqrt{-z}}{g_{s\pm}(z)}]\right] = 0 \quad (4.7.13e)$$

We have exploited the fact that the arctangent of an imaginary number is an imaginary number.

Using the properties of $\tilde{g}_{s\pm}(z)$ the first term of Eq.(4.7.10) can be rewritten as

$$\sum_i \sum_{n=1}^{\infty} \frac{1}{2} \int_{-z_{si}^{0}[n+1]}^{-z_{si}^{\infty}[n]} g_{si}(z)dz = \sum_i \frac{1}{2} \int_{-\infty}^{-z_{si}^{0}} Im\left[\imath g_{si}(z) - \frac{2g_{si}(z)}{\pi}\text{arctanh}[\frac{\sqrt{-z}}{g_{si}(z)}]\right] dz \quad (4.7.14a)$$

We now perform a Wick rotation in the complex plane similar to the one performed in Chapter 1 to deduce the expression of the Casimir energy as an integral over the imaginary frequencies. Writing

$$\int_{-\infty}^{-z_{si}^{0}} dz = \int_{-\infty}^{0} dz - \int_{-z_{s\pm}^{0}}^{0} dz \tag{4.7.14b}$$

and reintroducing $\tilde{z} = z = (z - \imath 0^{+}) = -y^{2}$ we get

$$\int_{-\infty}^{0} \tilde{g}_{s\pm}(z)dz = \int_{\imath 0^{+}}^{\infty+\imath 0^{+}} \tilde{g}_{s\pm}(-y^{2})dy^{2} \tag{4.7.14c}$$

The function $\tilde{g}_{s\pm}(-y^{2})$ has its poles on the real positive y-axis. This means that for the appropriate sign of the square root, $\tilde{g}_{s\pm}(-y^{2})$ is analytic in the first quadrant of the complex y-plane. Taking a path C which contours this quadrant we have

$$\oint_{C} dy^{2}\tilde{g}_{s\pm}(-y^{2}) = \left(\int_{\imath 0^{+}}^{\infty+\imath 0^{+}} dy^{2} + \int_{\gamma} dy^{2} + \int_{\imath\infty}^{\imath 0^{+}} dy^{2} \right) \tilde{g}_{s\pm}(-y^{2}) = 0 \tag{4.7.14d}$$

The path C has been decomposed in a path vanishing near the real y-axis plus the imaginary y-axis and a curve γ which connects the two axes at infinity. Since in the first quadrant of the complex y-plane we have

$$\tilde{g}_{s\pm}(-y^{2}) \xrightarrow{|y|\to\infty} 0 \tag{4.7.14e}$$

this last integral can be neglected. This entails that

$$\int_{\imath 0^{+}}^{\infty+\imath 0^{+}} \tilde{g}_{s\pm}(-y^{2})dy^{2} = \int_{\imath 0^{+}}^{\imath\infty} \tilde{g}_{s\pm}(-y^{2})dy^{2} \tag{4.7.14f}$$

These manipulations allow to recast the first term

$$\begin{aligned}
\int_{-\infty}^{0} \tilde{g}_{s\pm}(z)dz &= \int_{\imath 0^{+}}^{\imath\infty} Im\left[\imath g_{s\pm}(-y^{2}) - \frac{2g_{s\pm}(-y^{2})}{\pi} \text{arctanh}\left[\frac{y}{g_{s\pm}(-y^{2})} \right] \right] dy^{2} \\
&= -\int_{0}^{\infty} Im\left[\imath g_{s\pm}(x^{2}) - \frac{2\imath g_{s\pm}(x^{2})}{\pi} \arctan\left[\frac{x}{g_{s\pm}(x^{2})} \right] \right] dx^{2} \\
&= -\int_{0}^{\infty} \left(g_{s\pm}(x^{2}) - \frac{2g_{s\pm}(x^{2})}{\pi} \arctan\left[\frac{x}{g_{s\pm}(x^{2})} \right] \right) dx^{2} \\
&= -\int_{0}^{\infty} \left(g_{s\pm}(z) - \frac{2g_{s\pm}(z)}{\pi} \arctan\left[\frac{\sqrt{z}}{g_{s\pm}(z)} \right] \right) dz
\end{aligned} \tag{4.7.14g}$$

where we have changed the variable $y = \imath x$ and posed $x = \sqrt{z}$. Reintroducing the second integral in the right hand side of Eq.(4.7.14b) we can now take the bulk limit to get the expression

$$\begin{aligned}
&\lim_{d\to\infty} \sum_{i} \sum_{n=1}^{\infty} \frac{1}{2} \int_{-z_{si}^{0}[n+1]}^{-z_{si}^{\infty}[n]} g_{si}(z)dz = \\
&\qquad \sum_{i} \left(-\frac{1}{2} \int_{-z_{i}^{0}}^{\infty} g_{i}(z)dz + \int_{0}^{\infty} \frac{g_{i}(z)}{\pi} \arctan\left[\frac{\sqrt{z}}{g_{i}(z)} \right] dz \right)
\end{aligned} \tag{4.7.14h}$$

4.7.2 Recasting the second term of Eq.(4.7.10)

To write the second term of Eq.(4.7.10) in a more compact form, it is convenient to change $z = y^2$. Exploiting the logarithmic argument theorem [129] (see also Appendix A.3) and definition (4.7.5) we can write

$$\sum_{n=1}^{\infty}\left(y_{s+}^{0}[n+1]^3 - y_{s+}^{\infty}[n]^3\right) = \frac{1}{2\pi\imath}\oint_C y^3\partial_y \ln[f_{s+}(-y^2)]dy - y_{s+}^{0}[1]^3 \tag{4.7.15a}$$

$$\sum_{n=1}^{\infty}\left(y_{s-}^{0}[n+1]^3 - y_{s-}^{\infty}[n]^3\right) = \frac{1}{2\pi\imath}\oint_C y^3\partial_y \ln[f_{s-}(-y^2)]dy \tag{4.7.15b}$$

where C is a path in the complex y-plane enclosing the half plane $Re\,[y] > 0$, closed in counterclockwise sense. This path includes all relevant zeros but in the first case also $y_{s+}^{0}[1]$. It is not included in the left side corresponding summation and therefore it has to be eliminated by hand. Indeed, even if it lies in the propagative region in the bulk limit this zero corresponds to the value

$$\lim_{d\to\infty} = y_{s+}^{0}[1] = y_+ = \sqrt{z_+^0} = \Omega_+[k=0] \tag{4.7.15c}$$

defined in the treatment of the plasmonic modes.

Collecting the above equations and making the substitution $y = \imath x$ we can take now the bulk limit to get

$$\begin{aligned}\lim_{d\to\infty}\sum_i\sum_{n=1}^{\infty}\left(z_{si}^{0}[n+1]^{\frac{3}{2}} - z_{si}^{\infty}[n]^{\frac{3}{2}}\right) &= -\frac{1}{2\pi}\oint_C x^3\partial_x \ln[f_{s-}(x^2)f_{s+}(x^2)]dx - y_{s+}^{0}[1]^3 \\ &= \left(\Omega_p^3 - y_+^3\right)\end{aligned} \tag{4.7.15d}$$

where we have used the identities

$$f_+(x^2)f_-(x^2) = f_0^2(x^2), \quad f_0^2(z) = z(z+\Omega^2), \quad -\frac{1}{2\pi}\oint_C x^3\partial_x \ln[f_0^2(x^2)]dx = \Omega_p^3 \tag{4.7.15e}$$

The last identity comes directly from the logarithmic argument theorem.

4.7.3 Result for $\Delta\eta_{ph}$ and asymptotic behaviors

Collecting the result of the previous paragraphs, expression (4.7.10) can now be rewritten in the bulk limit as

$$\Delta(L) = \sum_i\left(-\frac{1}{2}\int_{-z_i^0}^{\infty} g_i(z)dz + \int_0^{\infty}\frac{g_i(z)}{\pi}\arctan\left[\frac{\sqrt{z}}{g_i(z)}\right]dz\right) - \frac{1}{3}\left(\Omega_p^3 - y_+^3\right) \tag{4.7.16}$$

Let us stress again that it may happen that all the expressions defined in the previous paragraph may need the introduction of a renormalizing function to be finite. Here we

neglected this point, formally proceeding as if all the integrals were convergent. We will see that the role of the renormalizing function in the total expression (4.7.1) will be played by the limit $L \to \infty$. This means that

$$\Delta E_{ph} = \lim_{d\to\infty} \frac{\hbar c A}{4\pi} [\sigma_s]_{L\to\infty}^{L} = \frac{\hbar c A}{4\pi} [\sigma(L) - \sigma(L \to \infty)] \tag{4.7.17}$$

is going to be convergent in any case.

To evaluate the asymptotic expression $\sigma(L \to \infty)$ we have to come back to the dimensional variables

$$z = \kappa^2 L^2, \quad \Omega_p = \omega_p L \tag{4.7.18}$$

From Eq.(4.7.16) we have

$$\begin{aligned} \sigma(L) &= \frac{\Delta(L)}{L^3} = \sum_i \left(-\frac{1}{2} \int_{-\frac{z_i^0}{L^2}}^{\infty} G_i(\kappa^2 L^2) d\kappa^2 + \int_0^{\infty} \frac{G_i(\kappa^2 L^2)}{\pi} \arctan\left[\frac{\sqrt{\kappa^2}}{G_i(\kappa^2 L^2)}\right] d\kappa^2 \right) \\ &- \frac{1}{3}\left(\omega_p^3 - \frac{y_+^3}{L^3}\right) \end{aligned} \tag{4.7.19a}$$

The functions G_i can be derived directly form the expression of the functions g_i given in Eqs.(4.4.24)

$$G_+^2(\kappa^2 L^2) = \frac{g_+^2(\kappa^2 L^2)}{L^2}, \quad G_-^2(\kappa^2 L^2) = \frac{g_-^2(\kappa^2 L^2)}{L^2} \tag{4.7.19b}$$

Evaluating the asymptotic behaviors of all functions we have

$$G_i^2(\kappa^2 L^2) \xrightarrow{L\to\infty} G_0^2(\kappa^2 L^2) = \frac{\omega_p^2 \sqrt{\kappa^2}}{\sqrt{\kappa^2} + \sqrt{\kappa^2 + \omega_p^2}} = \frac{g_0^2(\kappa^2 L^2)}{L^2}, \quad \frac{z_i^0}{L^2} \xrightarrow{L\to\infty} 0 \tag{4.7.19ca}$$

The last relation is essentially due to the fact that $0 < z_i^0 < \pi$.

Therefore coming back to the dimensionless variable we can write that

$$\sigma(L \to \infty) = \frac{2}{L^3}\left(-\frac{1}{2}\int_0^{\infty} g_0(z) dz + \int_0^{\infty} \frac{g_0(z)}{\pi} \arctan\left[\frac{\sqrt{z}}{g_0(z)}\right] dz \right) - \frac{1}{3}\frac{\Omega_p^3}{L^3} \tag{4.7.19d}$$

The factor two on the right hand side is due to the fact that both, G_+ and G_- have as asymptotic expression G_0.

We may now give the final result in terms of the correction coefficient $\Delta\eta_{ph}$

$$\begin{aligned} \Delta\eta_{ph} &= \frac{180}{2\pi^3}\left(\int_0^{\infty} \sum_i c_i \left(g_i(z) - 2\frac{g_i(z)}{\pi} \arctan\left[\frac{\sqrt{z}}{g_i(z)}\right]\right) dz + \int_{-z_+^0}^{0} g_+(z) dz - \frac{2}{3} y_+^3 \right) \\ &= \frac{180}{2\pi^3}\left(\frac{2}{\pi}\int_0^{\infty} \sum_i c_i \; g_i(z) \arctan\left[\frac{g_i(z)}{\sqrt{z}}\right] dz + \int_{-z_+^0}^{0} g_+(z) dz - \frac{2}{3} y_+^3 \right) \end{aligned} \tag{4.7.4}$$

with $c_+ = c_- = 1,\ c_0 = -2$.

All the integrals in the previous expression are convergent. Because of $\lim_{z\to\infty} g_i(z) = \Omega_p/\sqrt{2}$ we have indeed

$$\sum_i c_i g_i(z) \arctan\left[\frac{g_i(z)}{\sqrt{z}}\right] \xrightarrow{z\to\infty} \sum_i c_i \frac{g_i^2(z)}{\sqrt{z}} \tag{4.7.5}$$

which goes to zero faster than $1/z$. The other integral has already been discussed in the calculation of the plasmonic contribution. The function is plotted in figure 4.9 as a function of L/λ_p. It tends towards zero for vanishing mirrors separation.

From Eq.(4.7.4) is quite simple to see that in the long distance limit ($\Omega_p \gg 1$) the function $\Delta\eta_{ph}$ shows the same asymptotic behavior than η_{pl}. It is sufficient to note that, as for the plasmonic case, the first integral of Eq.(4.7.4) is significatively different from zero for $z \sim 1$ and that

$$\arctan\left[\frac{g_i(z)}{\sqrt{z}}\right] \xrightarrow{\Omega_p\gg 1} = \frac{\pi}{2} \tag{4.7.6}$$

This means that in this limit $\Delta\eta_{ph}$ and η_{pl} have exactly the same expression except for the sign (see Eq.(4.4.21)). This means that in the long distance limit, $\Delta\eta_{ph}$ has the asymptotic form

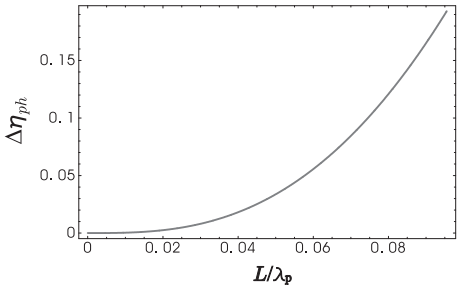

Figure 4.9 : A plot of $\Delta\eta_{ph}$ and as function of $\frac{L}{\lambda_p}$.

$$\Delta\eta_{ph} \approx \Gamma\sqrt{\Omega_p} \quad (\Gamma = 29.7528.....) \tag{4.7.7}$$

The short distance limit ($\Omega_p \ll 1$) is more complicated for the same reason as in the case of η_{pl} and η^{TE}. As for the TE mode contribution η^{TE}, splitting the integration domain in $z < \Omega_p^2$ and $z > \Omega_p^2$ one can show that (see the last paragraph in Appendix D.1)

$$\int_0^\infty \sum_i c_i \; g_i(z) \arctan\left[\frac{g_i(z)}{\sqrt{z}}\right] dz = \mathcal{O}^3\left[\Omega_p\right] \tag{4.7.8}$$

Taking into account the results (paragraph 4.4.3) for the short distance behavior of the other components of $\Delta\eta_{ph}$, we find that in the limit $\Omega_p \ll 1$

$$\Delta\eta_{ph} = \mathcal{O}^3\left[\Omega_p\right] \tag{4.7.9}$$

4.8 Discussion of the results

In this chapter we have calculated the contribution to the Casimir energy coming from plasmonic and photonic modes

$$E = E_{ph} + E_{pl} = \left(\eta_{ph} + \eta_{pl}\right) E_{Cas} = \eta E_{Cas} \tag{4.8.1}$$

where we have indicated with E_{pl} the plasmonic modes contribution and with E_{ph} the photonic one. We have expressed our results in terms of correction coefficients which

describe E_{ph} and E_{pl} with respect to the Casimir energy in the perfect mirrors case. Those coefficient are described in Eqs.(4.4.21),(4.6.6) and (4.7.4).

The asymptotic behavior of the global correction coefficient is

$$\eta \approx \frac{3}{4\pi}\alpha\ \Omega_p, \quad \Omega_p \ll 1 \quad \text{and} \quad \eta \approx 1 - \frac{4}{\Omega_p}, \quad \Omega_p \gg 1 \tag{4.8.2}$$

where $\alpha = 1.193..$ [90]. It is plotted as the dashed line in fig.4.10. Separation of the two mode ensembles leads to plasmonic and photonic contribution as shown also in fig.4.10. Their sum reproduces of course the global coefficient. However, their individual behavior is very different.

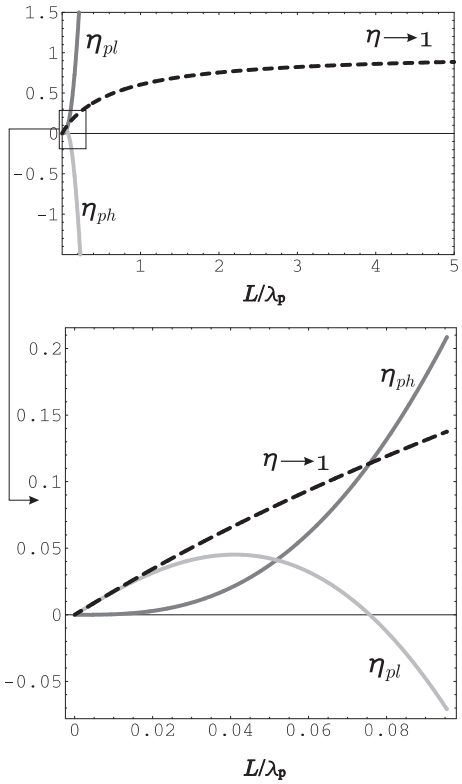

Figure 4.10 : A plot of η, η_{pl} and $\eta_{ph} = 2\eta^{TE} + \Delta\eta_{ph}$ on two different ranges of L/λ_p. In the limit $L \ll \lambda_p$ η is well approximated by η_{pl}. For $L \gg \lambda_p$ despite the divergence of both η_{pl}(negatively) and η_{ph}(positively) the net result given by η is finite and tends to unity (perfect mirrors case).

In particular the plasmonic modes contribution η_{pl} while being positive at small distances, changes its sign at intermediate distances $L/\lambda_p \sim 0.08$. For large cavity lengths it becomes repulsive and tends to $-\infty$ for infinite mirrors separations. In contrast the photonic modes contribution is always positive, corresponding to an attractive force, and tends to $+\infty$ at infinite distances. This means that at infinite distances, the separate contributions are each much larger than the Casimir energy.

In the long distances limit ($L \gg \lambda_p \Rightarrow \Omega_p \gg 1$) plasmonic and photonic contribution may be approximated by

$$\eta_{pl} \approx -\Gamma\sqrt{\Omega_p} \tag{4.8.3}$$

$$\eta_{ph} = 2\eta^{TE} + \Delta\eta_{ph} \approx \Gamma\sqrt{\Omega_p} \tag{4.8.4}$$

with $\Gamma = 29.7528....$

This clearly shows that plasmonic modes are much more important for Casimir effect than usually anticipated. They do not only dominate in the short distances limit, but also give a repulsive contribution at large distances which is necessary to counterbalance the much too large (positive) photonic contribution to the Casimir energy.

We showed that the repulsive contribution of the plasmonic modes may be attributed to the ω_+ mode, which dominates for intermediate and large distances. We will discuss this point in the conclusion.

Here, the mode ω_+ which crosses the border between the evanescent and propagative sector, was completely attributed to the plasmonic ensemble. If we consider only the evanescent contribution (η_{ev}), i.e. forgetting the propagative part of the mode ω_+, we would obtain a

similar result (see Appendix D.2)

$$\eta_{ev} \approx -\beta\sqrt{\Omega} \quad (\Omega_p \gg 1) \tag{4.8.5}$$

The coefficient β differs from Γ because it does not contains that integral which take account of the propagative part of the mode ω_+. Its numerical value is different

$$\beta = -\frac{180}{\pi^3}\int_0^\infty \kappa^{\frac{3}{2}}\left(\sqrt{\coth[\frac{\kappa}{2}]}+\sqrt{\tanh[\frac{\kappa}{2}]}-2\right)d\kappa = 1.65987 \tag{4.8.6}$$

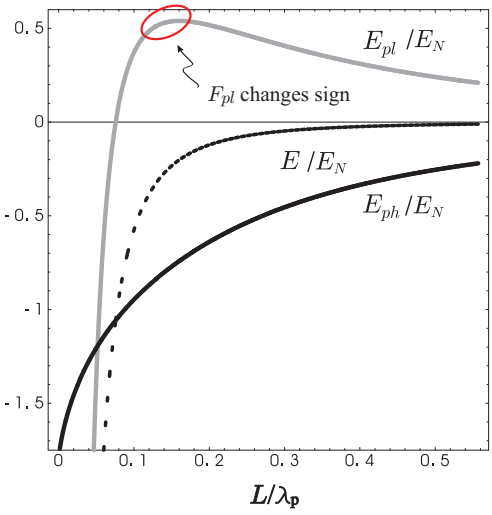

Figure 4.11 : A plot of plasmonic E_{pl}, photonic E_{ph} and Casimir E energy normalized to $E_N = (2\pi)^3\frac{\hbar c\pi^2 A}{720\lambda_p^3}$ as function of L/λ_p. We see that E_{pl} show a maximum for $L/\lambda_p \sim 0.16$ (F_{pl} changes its sign) while E_{ph} monotonically tends to zero (F_{ph} is always attractive).

In Appendix D.2 we derive the same result exploiting a method different from the one used in the text.

Up to now, we have discussed the results with respect to the correction factors η, which means that all quantities are normalized by the ideal Casimir energy

$$E_{Cas} = -\frac{\hbar\pi^2 cA}{720L^3} \tag{4.8.7}$$

It may also be useful to briefly discuss the variation of the energies E_{pl} and E_{ph} normalized by a constant energy $E_N = (2\pi)^3\frac{\hbar c\pi^2 A}{720\lambda_p^3}$. The corresponding result is shown in fig.4.11. The total Casimir energy E/E_N (dashed line) is negative, corresponding to an attractive force at all distances. The same is true for E_{ph}/E_N . However for E_{pl}/E_N is negative only for short distances. For $L \gtrsim 0.08\lambda_p$ it becomes positive and has a maximum at $L \sim 0.16\lambda_p$, corresponding then to a change in the sign of the force and to a repulsive Casimir force contribution for distances larger than this last value.

Reprint from **Physical Review Letters**

PRL **94**, 110404 (2005) PHYSICAL REVIEW LETTERS week ending 25 MARCH 2005

Surface Plasmon Modes and the Casimir Energy

F. Intravaia and A. Lambrecht

Laboratoire Kastler-Brossel UPMC/ENS/CNRS case 74, Campus Jussieu, F75252 Paris CEDEX 05, France

(Received 13 December 2004; published 23 March 2005)

We show the influence of surface plasmons on the Casimir effect between two plane parallel metallic mirrors at arbitrary distances. Using the plasma model to describe the optical response of the metal, we express the Casimir energy as a sum of contributions associated with evanescent surface plasmon modes and propagative cavity modes. In contrast to naive expectations, the plasmonic mode contribution is essential at all distances in order to ensure the correct result for the Casimir energy. One of the two plasmonic modes gives rise to a repulsive contribution, balancing out the attractive contributions from propagating cavity modes, while both contributions taken separately are much larger than the actual value of the Casimir energy. This also suggests possibilities to tailor the sign of the Casimir force via surface plasmons.

DOI: 10.1103/PhysRevLett.94.110404 PACS numbers: 03.70.+k, 42.50.Pq, 73.20.Mf

When Casimir first predicted the existence of a force between neutral mirrors in vacuum [1], he considered two plane parallel perfect reflectors and found an interaction energy E_{Cas} depending only on geometrical parameters, the mirrors distance L and surface $A \gg L^2$, and two fundamental constants, the speed of light c and Planck constant $\hbar$:

$$E_{\mathrm{Cas}} = -\frac{\hbar c \pi^2 A}{720 L^3}. \tag{1}$$

The signs have been chosen to fit the thermodynamical convention with the minus sign of the energy E_{Cas} corresponding to a binding energy. The Casimir energy for perfect mirrors is usually obtained by summing the zero-point energies $\frac{\hbar\omega}{2}$ of the cavity eigenmodes, subtracting the result for finite and infinite separation, and extracting the regular expression (1) by inserting a formal high-energy cutoff and using the Euler-McLaurin formula [2].

In his seminal paper [1], Casimir noticed that the energy should be a finite expression, without the need of any regularization, provided one takes into account the high-frequency transparency of real mirrors. The idea was implemented by Lifshitz, who calculated the Casimir energy for mirrors characterized by dielectric functions [3]. For metallic mirrors, he recovered expression (1) for separations L much larger than the plasma wavelength λ_{p} associated with the metal, as metals are very good reflectors at frequencies much smaller than the plasma frequency ω_{p}. At shorter separations, in contrast, the Casimir effect probes the optical response of metals at frequencies where they are poor reflectors and the Casimir energy is reduced with respect to (1). This reduction has been studied in great detail recently ([4,5], and references therein) since it plays a central role in the comparison of theoretical predictions ([6], and references therein) with experimental results [7].

In the limit of small separations $L \ll \lambda_{\mathrm{p}}$, the Casimir effect has another interpretation establishing a bridge between quantum field theory of vacuum fluctuations and condensed matter theory of forces between two metallic bulks. It can indeed be understood as resulting from the Coulomb interaction between surface plasmons, that is, the collective electron excitations propagating on the interface between each bulk and the intracavity vacuum [8–10]. The corresponding field modes are evanescent waves and have an imaginary longitudinal wave vector. We will call them plasmonic modes at arbitrary distances as they coincide with the surface plasmon modes at small distances. Plasmonic modes have to be seen in contrast to ordinary propagating cavity modes, which have a real longitudinal wave vector. For simplicity, we will call those photonic modes in the following. Photonic modes are usually considered in the quantum field theory of the Casimir effect [2] and are thought to determine the Casimir effect at large distances where the mirrors can be treated as perfect reflectors. At short distances, plasmonic modes are known to dominate the interaction [11,12].

The purpose of the present Letter is to show the singular behavior of one of the two plasmonic modes, which gives rise to a repulsive contribution to the Casimir energy at all distances, ensuring in this way that the correct value for the Casimir energy is recovered, in particular, the ideal Casimir energy at large distances. Plasmonic modes therefore have a much greater importance than usually appreciated. To show this, we will use the decomposition of the Casimir energy as a sum of zero-point energies $\frac{\hbar\omega}{2}$ over the whole set of modes of the cavity with its two mirrors described by a plasma model. This set contains plasmonic as well as photonic modes. As expected from [11,12], the contributions of plasmonic modes will be found to dominate the Casimir effect for small separations corresponding to Coulomb interaction between surface plasmons. But, contrary to naive expectations, they do not vanish for large separations. For distances larger than about $\lambda_{\mathrm{p}}/4\pi$ ($\sim$10 nm for typical metals), they even give rise to a contribution having simultaneously a negative sign and a too large magnitude with respect to the Casimir formula

PRL **94,** 110404 (2005) PHYSICAL REVIEW LETTERS week ending 25 MARCH 2005

(1). The repulsive character can be attributed to one of the two plasmonic modes. The photonic modes as well as the second plasmonic mode give rise to an attractive contribution much larger than (1). It is therefore the repulsive contribution of a single plasmonic mode which renders the total plasmonic mode contribution to the Casimir energy repulsive outside the short distance limit, while assuring at the same time that the sum over all modes reproduces (1) at large distances. This repulsive character may open interesting possibilities to tailor surface plasmons via nanostructuration of metallic surfaces in order to change the sign of the total Casimir force.

In this Letter, we restrict our attention to the situation of two infinitely large plane mirrors at zero temperature so that the only modification of Casimir formula (1) is due to the metals finite conductivity. This modification is calculated by evaluating the radiation pressure of vacuum fields upon the two mirrors [5]:

$$E = \sum_{\epsilon} \sum_{\mathbf{k}} \sum_{\omega} -\frac{i\hbar}{2} \ln(1 - r_{\mathbf{k}}^{\epsilon}[\omega]^2 e^{2ik_z L}) + \text{c.c.}, \qquad (2)$$

$$\sum_{\mathbf{k}} \equiv A \int \frac{d^2\mathbf{k}}{4\pi^2}, \qquad \sum_{\omega} \equiv \int_0^{\infty} \frac{d\omega}{2\pi}.$$

The energy E is obtained by summing over polarization $\epsilon = (\text{TE, TM})$, transverse wave vector $\mathbf{k} \equiv (k_x, k_y)$ (with z the longitudinal axis of the cavity), and frequency ω; k_z is the longitudinal wave vector associated with the mode. The reflection amplitudes $r_{\mathbf{k}}^{\epsilon}$, here supposed to be the same for both mirrors, are causal retarded functions obeying high-frequency transparency.

We now calculate the Casimir energy as a sum over the cavity modes using the plasma model for the mirrors dielectric function

$$\varepsilon[\omega] = 1 - \frac{\omega_p^2}{\omega^2}, \qquad (3)$$

with ω_p the plasma frequency and $\lambda_p = \frac{2\pi c}{\omega_p}$ the plasma wavelength, of the order of 100 nm for metals used in experiments [13]. In this case, the zeros of the argument of the integrand in (2) lie on the real axis. In fact, they have to be pushed slightly below this axis by introducing a vanishing dissipation parameter in order to avoid any ambiguity in expression (2) [5]. We may then rewrite (2) as a sum over the solutions $[\omega_{\mathbf{k}}^{\epsilon}]_m$ of the equation labeled by an integer index m,

$$r_{\mathbf{k}}^{\epsilon}[\omega]^2 e^{2ik_z L} = 1. \qquad (4)$$

Simple algebraic manipulations exploiting residues theorem and complex integration techniques [10] then lead to the Casimir energy expressed as sums over these modes:

$$E = \sum_{\epsilon,\mathbf{k}} \Big[\sum_{m}{}' \frac{\hbar[\omega_{\mathbf{k}}^{\epsilon}]_m}{2} \Big]_{L\to\infty}^{L}. \qquad (5)$$

The prime in the sum over m signifies as usual that the term $m = 0$ has to be multiplied by $1/2$. The sum over the modes is to be understood as a regularized quantity as it involves infinite quantities. This result is well known for perfect mirrors and is not changed by the choice of the plasma model for the mirrors reflection coefficients. The upper expression contains as limiting cases at large distances the Casimir expression with perfect mirrors and at short distances the expression in terms of surface plasmon resonances. For arbitrary distances, photonic modes as well as plasmonic modes are important.

We will now discuss the structure of TE and TM modes inside the cavity formed by the two mirrors. The different modes have been obtained by writing explicitly all solutions of (4), using the standard expressions for the reflection coefficients. Figure 1 shows the phase shift acquired by the TE modes through the influence of imperfect reflection. They are represented through their longitudinal wave vector as a function of kL. The TE polarization admits only photonic modes which can be written under the standard form $k_z L = m\pi - \delta$, where the integer $m = 1, 2, \ldots, \infty$ is the order of the cavity mode and δ the phase shift of the mode on a mirror. Perfect mirrors lead to cavity modes plotted as dotted lines corresponding to $\delta^{\text{TE}} = 0$. With the plasma model, the photonic modes are displaced compared to the perfect cavity modes as a direct consequence of the phase shift δ acquired by vacuum fields upon reflection. The limit of perfect reflection corresponds to the large distances limit. The high-frequency transparency of metallic mirrors imposes an upper bound to their longitudinal wave vector $ck_z < \omega_p$, where all photonic modes coincide.

For TM polarization, similar photonic modes are obtained, labeled also by a positive integer m. They are accompanied by two additional modes, which we label $[\omega_{\mathbf{k}}^{\text{pl}}]_{\pm}$ as they tend to the frequencies of surface plasmon

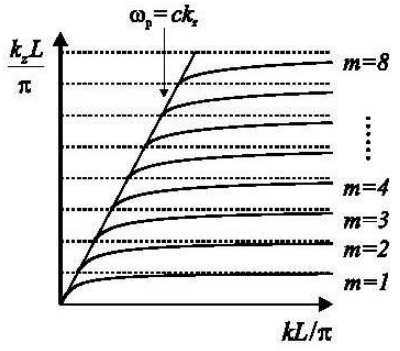

FIG. 1. Mode plot of the first photonic TE modes ($m = 1, 2, \ldots, 8$) with the plasma model for $ck = 0.5\omega_p$. Modes are presented through their longitudinal wave vector as a function of kL/π. The dotted lines correspond to the cavity modes with perfect mirrors.

modes [9] in the limit of small distances. These plasmonic modes are shown as solid black lines in Fig. 2, while photonic modes correspond to gray lines. In order to make the plasmonic modes with their imaginary wave vector visible, the modes are now represented through their frequency as a function of kL. Plasmonic and photonic modes lie, respectively, in the sector $\omega < ck$ and $\omega > ck$. In the limit of infinite mirrors separation, the plasmonic modes are given by the usual dispersion relation for the surface plasmons in a metallic bulk [9]:

$$[\omega_{\mathbf{k}}^{\mathrm{pl}}]_{\pm} \overset{L\to\infty}{\longrightarrow} \frac{\omega_{\mathrm{p}}^2 + 2|\mathbf{k}|^2 - \sqrt{\omega_{\mathrm{p}}^4 + 4|\mathbf{k}|^4}}{2}. \tag{6}$$

For the photonic modes the phase shift δ tends towards zero for infinite distances where they obey the dispersion relation for perfect mirrors $[\omega_{\mathbf{k}}^{\epsilon}]_m = \sqrt{|\mathbf{k}|^2 + k_z^2}$, with the longitudinal wave vector $k_z = m\pi/L$. For $L \to \infty$, the sum over m in (5) becomes a continuous integral and the mode contribution of photonic modes corresponds to the one of free field vacuum which is subtracted from the contribution at finite distances.

Let us now discuss in more detail the behavior of the two plasmonic modes. $\omega_{\mathbf{k}}^{-}$ is restricted to the plasmonic mode sector, while $\omega_{\mathbf{k}}^{+}$ lies in the plasmonic mode sector for large distances, but crosses the barrier $\omega = ck$ and dies in the photonic mode sector for $kL/\pi \to 0$. In the present calculation, the whole mode was attributed to the plasmonic mode contribution as its frequency tends to the surface plasmon contribution at short distances. The qualitative results do not change if the part of the mode lying in the photonic modes sector is attributed to the photonic modes contribution.

Obviously, when decreasing the distance L, the plasmonic mode $\omega_{\mathbf{k}}^{+}$ acquires a phase shift with the same sign as the TM photonic modes below the plasma frequency. Its frequency at short distances is always larger than the one in the large distance limit. In contrast, the frequency of $\omega_{\mathbf{k}}^{-}$ is decreased at short distances compared to long distances. When now performing the difference (5) of the contributions at finite and infinite distances, the Casimir energy contribution turns out to be negative for photonic modes, as the mode contribution in free vacuum ($L \to \infty$) exceeds the one inside the cavity, in accordance with an attractive force. It is also negative for the plasmonic mode $\omega_{\mathbf{k}}^{-}$. However, the difference is positive for the plasmonic mode $\omega_{\mathbf{k}}^{+}$. An immediate consequence is that the contribution of $\omega_{\mathbf{k}}^{+}$ to the Casimir energy is repulsive.

To assess quantitatively the effect of the plasmonic modes to the Casimir energy, we have computed separately the energies associated with photonic modes $[\omega_{\mathbf{k}}^{\epsilon}]_m$ and plasmonic modes $[\omega_{\mathbf{k}}^{\mathrm{pl}}]_{\pm}$. All energies in the following will be presented as a reduction factor η [13]:

$$E = \eta E_{\mathrm{Cas}}. \tag{7}$$

As the ideal Casimir energy is negative corresponding to attraction, positive and negative reduction factors mean, respectively, attractive or repulsive interaction. The reduction factor due to imperfect reflection described with the plasma model is shown as a solid line in Fig. 3 as a function of the ratio L/λ_{p}. We also introduce reduction factors corresponding to contributions of the different modes to the Casimir energy:

$$\eta_{\mathrm{ph}} = E_{\mathrm{ph}}/E_{\mathrm{Cas}}, \qquad \eta_{\mathrm{pl}} = E_{\mathrm{pl}}/E_{\mathrm{Cas}}.$$

Their sum corresponds to the whole Casimir energy $\eta = \eta_{\mathrm{ph}} + \eta_{\mathrm{pl}}$. The contribution η_{pl} of plasmonic modes (dashed line) dominates at short distances $L \ll \lambda_{\mathrm{p}}$, which confirms the interpretation of the Casimir effect as resulting in this regime from the Coulomb interaction of surface plasmons. There, a simple expression may be given for the

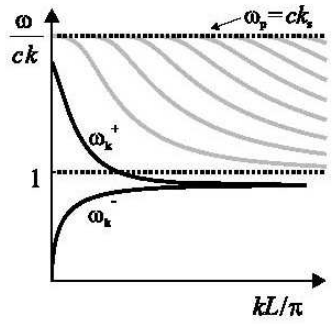

FIG. 2. Mode plot of the two plasmonic modes $\omega_{\mathbf{k}}^{-}$ and $\omega_{\mathbf{k}}^{+}$ (black lines) in the sector $\omega < ck$ and of photonic modes (gray lines) in the sector $\omega > ck$ for $ck = 0.5\omega_{\mathrm{p}}$. Modes are presented through their frequency as a function of kL/π.

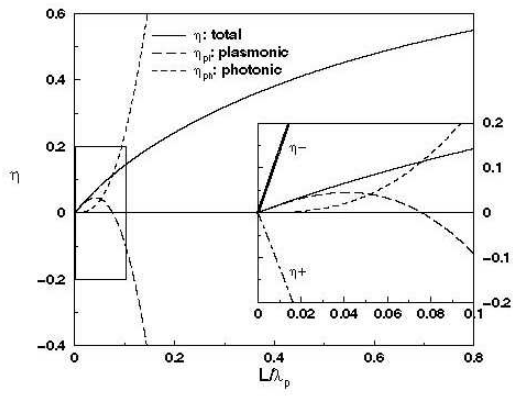

FIG. 3. Contributions to Casimir energy normalized to (1) of photonic modes (dotted line) and plasmonic modes (dashed line) to the total Casimir energy (solid line) as functions of L/λ_{p}. The inset shows the separate contributions of $\omega_{\mathbf{k}}^{-}$ and $\omega_{\mathbf{k}}^{+}$.

reduction factor [11,14]:

$$\eta \underset{L\ll\lambda_p}{\simeq} \frac{3\alpha}{2}\frac{L}{\lambda_p}, \qquad \alpha \simeq 1.193. \tag{8}$$

The power law dependence of E then goes from L^{-3} at large distances to $L^{-2}\lambda_p^{-1}$ at short distances [3]. The contribution of photonic modes η_{ph} scales as $(L/\lambda_p)^4$, and its contribution may be neglected at the 1% level up to $L/\lambda_p \sim 0.2$. At larger distances, η_{ph} increases, while η_{pl} becomes negative at a distance of the order $\lambda_p/4\pi$. This clearly comes from the behavior of $\omega_{\mathbf{k}}^{+}$, shown in the inset, which gives a repulsive contribution at all distances. For example, the photonic and the plasmonic contribution to the Casimir energy at $\lambda_p/L \sim 1$ are both about 36 times larger than the total Casimir energy between metallic mirrors. They are of opposite sign while the photonic contribution slightly dominates. For large separations $L/\lambda_p \gg 1$, η_{ph} tends to $+\infty$, while η_{pl} tends to $-\infty$. The sum of the two contributions reproduces the known value for η, which is positive and increasing over all separations going from (8) to unity for large distances, where the Casimir formula (1) is recovered. This feature results from a compensation between the large positive value of η_{ph} and the large negative value of η_{pl}. More precise asymptotic laws for the two contributions are

$$\eta_{ph} - 1 \underset{L\gg\lambda_p}{\simeq} -\eta_{pl} \underset{L\gg\lambda_p}{\simeq} \beta\sqrt{\frac{L}{\lambda_p}}, \qquad \beta \simeq 74.58. \tag{9}$$

The behavior of the whole reduction factor is also recovered, $\eta \underset{L\gg\lambda_p}{\simeq} 1 - 2\lambda_p/(\pi L)$.

These results clearly show the crucial importance of the surface plasmon contribution, not only for short distances where it dominates the Casimir effect but also for long distances. For metallic mirrors the existence of surface plasmons are not an additional correction to the Casimir effect, but inherent to it. A single plasmonic mode $\omega_{\mathbf{k}}^{+}$ ensures consistency with the Casimir energy between metallic mirrors at intermediate distances and with the Casimir formula (1) for perfect mirrors. If we had calculated the Casimir effect by accounting only for the photonic modes, we would have found a result much too large. The photonic modes and one of the plasmonic modes are displaced by the phase shifts which induce a systematical deviation towards a larger magnitude of Casimir energy. The discrepancy which would be obtained in this manner is cured only by the contribution of the $\omega_{\mathbf{k}}^{+}$ plasmonic mode. The whole Casimir energy turns out to be the result of a fine balance between the large attractive photonic contribution and the large repulsive plasmonic contribution. As already known from discussions of arbitrary dielectric mirrors [5], the outcome of this balance keeps the sign of a binding energy. However, this result relies heavily on the symmetry of the Casimir geometry with two plane mirrors. One might thus hope to change this behavior by enhancing the contribution of plasmonic modes, by changing the geometry, using, for example, the hole arrays used to enhance the transmission of light through metallic structures [15] or nanostructured metallic surfaces. This could then play a role in microelectromechanical systems in which the Casimir force is known to have a great influence [16].

Many thanks are due to S. Reynaud, C. Genet, M.-T. Jaekel, and P. A. Maia Neto for discussions. F. I. thanks the Foundation Angelo della Riccia for financial support.

[1] H. B. G. Casimir, Proc. K. Ned. Akad. Wet. **51**, 793 (1948).
[2] C. Itzykson and J. B. Zuber, *Quantum Field Theory* (McGraw-Hill, New York, 1985), Sect. 3-2-4.
[3] E. M. Lifshitz, Sov. Phys. JETP **2**, 73 (1956).
[4] M. T. Jaekel and S. Reynaud, J. Phys. (Paris) I **1**, 1395 (1991).
[5] C. Genet, A. Lambrecht, and S. Reynaud, Phys. Rev. A **67**, 043811 (2003).
[6] M. Bordag, U. Mohideen, and V. M. Mostepanenko, Phys. Rep. **353**, 1 (2001).
[7] S. K. Lamoreaux, Phys. Rev. Lett. **78**, 5 (1997); U. Mohideen and A. Roy, *ibid.* **81**, 4549 (1998); B. W. Harris, F. Chen, and U. Mohideen, Phys. Rev. A **62**, 052109 (2000); Th. Ederth, *ibid.* **62**, 062104 (2000); H. B. Chan, V. A. Aksyuk, R. N. Kleiman, D. J. Bishop, and F. Capasso, Science **291**, 1941 (2001); G. Bressi, G. Carugno, R. Onofrio, and G. Ruoso, Phys. Rev. Lett. **88**, 041804 (2002); R. S. Decca, D. López, E. Fischbach, and D. E. Krause, *ibid.* **91**, 050402 (2003).
[8] N. G. Van Kampen, B. R. A. Nijboer, and K. Schram, Phys. Lett. **26A**, 307 (1968); J. Heinrichs, Phys. Rev. B **11**, 3625 (1975); F. Forstmann and H. Stenschke, *ibid.* **17**, 1489 (1978).
[9] G. Barton, Rep. Prog. Phys. **42**, 65 (1979).
[10] K. Schram, Phys. Lett. **43A**, 282 (1973).
[11] C. Genet, F. Intravaia, A. Lambrecht, and S. Reynaud, Ann. Fond. L. de Broglie **29**, 311 (2004); quant-ph/0302072.
[12] C. Henkel, K. Loulain, J-Ph. Mulet, and J.-J. Greffet, Phys. Rev. A **69**, 023808 (2004).
[13] A. Lambrecht and S. Reynaud, Eur. Phys. J. D **8**, 309 (2000).
[14] C. Genet, A. Lambrecht, and S. Reynaud, Phys. Rev. A **62**, 012110 (2000).
[15] T. W. Ebbensen, H. J. Lezec, H. F. Ghaemi, T. Thio, and P. A. Wolff, Nature (London) **391**, 667 (1998); L. Martin-Moreno, F. J. García-Vidal, H. J. Lezec, K. M. Pellerin, T. Thio, J. B. Pendry, and T. W. Ebbesen, Phys. Rev. Lett. **86**, 1114 (2001); E. Altewischer, M. P. van Exter, and J. P. Woerdman, Nature (London) **418**, 304 (2002).
[16] H. B. Chan, V. A. Aksyuk, R. N. Kleiman, D. J. Bishop, and F. Capasso, Phys. Rev. Lett. **87**, 211801 (2001); E. Buks and M. L. Roukes, Europhys. Lett. **54**, 220 (2001).

Conclusion

As we have explained in the introduction, we have started our calculations with the idea to generalize the original Casimir calculation, in which the Casimir energy is evaluated by summing the zero point energies of the cavity eigenmodes, subtracting the result for finite and infinite mirror separation and extracting the regular expression by inserting a formal high frequency cutoff. We have applied this procedure to metallic mirrors described by the plasma model.

We will here shortly resume the essential of our work. We have first introduced the basic theories our work relies on, that is first two formulations of the Casimir effect, the original one with its regularization procedures and the Quantum Optical Networks theory, which is divergence free. We have then introduced the hydrodynamic model and the plasma model to describe the metallic mirrors material properties. We have shown that the use of the plasma model naturally leads to the appearance of two plasmonic modes, that is the generalization of surface plasmon modes, defined at short distances, to arbitrary distances. Plasmonic modes do not have a counterpart in the perfect mirror case, where only propagating cavity modes - or photonic modes - exist. As metallic mirrors become perfectly reflecting in the large distance limit, one might be tempted to deduce in a first inspection that the short distances behavior of the Casimir energy is dominated by surface plasmons and photonic modes are negligible, while the long distance behavior is dominated by photonic modes and in contrary plasmonic modes may be neglected.

In the first chapter we showed that the first deduction is indeed correct. Propagation effects do not play a role in the short distance behavior of the Casimir force and the Casimir energy is very well approximated as the Coulomb interaction energy between the two surface plasmons. The study of the behavior at arbitrary distances, and especially the long distance limit, needed much longer and complicated calculations. We first performed the complete decomposition of the Casimir energy between metallic mirrors into cavity eigenmodes, which led to the appearance of the two plasmonic modes $\omega_{-}[\mathbf{k}]$ and $\omega_{+}[\mathbf{k}]$ as well as to a set of photonic modes. $\omega_{-}[\mathbf{k}]$ turned out to be restricted to the plasmonic mode sector, while $\omega_{+}[\mathbf{k}]$ lies in the plasmonic mode sector for large distances, but crosses the barrier $\omega = c|\mathbf{k}|$ and dies in the photonic mode sector for $|\mathbf{k}|L/\pi \to 0$. We attributed the whole mode to the plasmonic mode contribution as its frequency tends to the surface plasmon contribution at short distances. In appendix D.2, we showed that the qualitative results do not change if the part of the mode lying in the photonic modes sector is attributed to the photonic modes contribution.

An inspection of the dephasing of the modes between metallic mirrors with respect to one between perfect mirrors (recovered at large distances) has shown that, when decreasing the distance L the plasmonic mode $\omega_+ [\mathbf{k}]$ acquires a phase shift with the same sign as the TM photonic modes below the plasma frequency. Its frequency at short distances is always larger than the one in the large distance limit. In contrast, the frequency of $\omega_- [\mathbf{k}]$ is decreased at short distances compared to long distances. When performing the difference of the contributions at finite and infinite distances, the Casimir energy contribution turns out to be negative for photonic modes, as the mode contribution in free vacuum ($L \to \infty$) exceeds the one inside the cavity, in accordance with an attractive force. It is also negative for the plasmonic mode $\omega_- [\mathbf{k}]$. However, the difference is positive for the plasmonic mode $\omega_+ [\mathbf{k}]$ with the immediate consequence that its contribution to the Casimir energy is repulsive.

To asses quantitatively the effect of the plasmonic modes to the Casimir energy, we have then computed separately the energies associated with photonic modes $\omega_m^p [\mathbf{k}]$ and plasmonic modes $\omega_\pm [\mathbf{k}]$. Since these frequencies cannot be expressed in terms of a combination of elementary, to reach an analytic result we developed a particular mathematical technique, the key point of which is the possibility to express in a particular simple form the equations which have $\omega_\pm [\mathbf{k}]$ as solutions. This technique works very well with plasma model but it is easily generalizable to all dielectric functions which lead to modes equations having an analog simple form.

The contribution of plasmonic modes dominates at short distances $L \ll \lambda_p$, which confirms the interpretation of the Casimir effect as resulting in this regime from the Coulomb interaction of surface plasmons. There, the power law dependence of E goes from L^{-3} at large distances to $L^{-2}\lambda_\mathrm{p}^{-1}$ at short distances. The contribution of photonic modes scales as $(L/\lambda_\mathrm{p})^3$ and its contribution may be neglected at the 1% level up to $L/\lambda_\mathrm{p} \sim 0.2$. At larger distances, the photonic mode contribution increases while the plasmonic one becomes negative at a distance of the order $\lambda_p/4\pi$. We have clearly attributed this to the behavior of ω_+, which gives a repulsive contribution at all distances. For large separations $L/\lambda_p \gg 1$, both contribution remain of equal order of magnitude but of opposite sign. The photonic contribution slightly dominates. The sum of the two contributions reproduces the known value for the Casimir energy going from the short distance approximation to the usual Casimir formula for large distances.

These results clearly show the crucial importance of the surface plasmon contribution, not only for short distances where it dominates the Casimir effect but also for long distances.

For metallic mirrors the existence of surface plasmons are not an additional correction to the Casimir effect as it had been suggested in [92]. In contrary, surface plasmons are inherent to it. A single plasmonic mode ω_+ ensures consistency with the Casimir energy between metallic mirrors at intermediate distances and with the Casimir formula for perfect mirrors. If we had calculated the Casimir effect by accounting only for the photonic modes, we would have found a result much too large. The photonic modes and one of the plasmonic modes are displaced by the phase shifts which induce a systematical deviation towards a larger magnitude of Casimir energy. The discrepancy which would

be obtained in this manner is only cured by the contribution of the ω_+ plasmonic mode. The whole Casimir energy turns out to be the result of a fine balance between the large attractive photonic contribution and the large repulsive plasmonic contribution.

In [84] it had been shown that the Casimir force between two flat, plane parallel dielectric mirrors is always attractive, and the outcome of the fine balance keeps the sign of a binding energy. However, this result relies heavily on the symmetry of the Casimir geometry with two plane mirrors. One might thus hope affecting this behavior by enhancing the contribution of plasmonic modes, by changing the geometry. One could think of using non-planar mirror, metallic surfaces with nanostructures graved into it or even hole arrays used recently to enhance the transmission of light through metallic structures [93,94,95]. A change of sign in the Casimir force would certainly be important for micro-electro-mechanical systems (MEMS) in which the Casimir force is known to have a great influence [42,43], as it may produce the sticking between the tiny metallic elements integrated in the MEMS. This could be avoided if one finds means to reverse the sign of the Casimir force. However, for the time being, a possible change of sign remains an open question, which will be interesting to study in the future.

APPENDIX A

Complement on the general derivation of the Casimir effect

A.1 Regularization in Casimir's approach

To understand way the "zero" can be obtained from $\mathcal{E}(L)$ taking the asymptotic function in the limit $L \to \infty$ we can claim the fact that in this manner we automatically set that the (Casimir) energy shift be null for $L = \infty$ [113]. In this case, indeed, the two vacuum energy configurations (with or "without" the mirrors) are identical. Another look to the Casimir force, however, gives a clearer explication [113]. The idea here is that the vacuum photons like the classical e.m. field carry a linear momentum $\frac{1}{2}\hbar\mathbf{K}$. The reflection off the plates of the zero-point field outside the plates act to push the plates together,while the reflection of the field confined between the plates push them apart. Generally speaking one can show in our case[1] that the modulo of e.m. pressure exerted on a plate can be written as

$$P(L) = \frac{\hbar}{2\pi}\sum_p \int_{\mathbb{R}^2} \frac{d^2\mathbf{k}}{(2\pi)^2} \int_0^\infty d\omega k_z g^p_{\mathbf{k}}[\omega] \tag{A.1.1}$$

where $g^p_{\mathbf{k}}[\omega]$ is a function connected with the e.m. vacuum spectral density. As the vacuum energy in Eq.(1.2.8) the pressure expression given in Eq.(A.1.1) is a divergent quantity. For example for free vacuum outside the cavity we simply have $g^p_{\mathbf{k}}[\omega] = 1$.

Anyways the force on a mirror can be written as

$$F(L) = A\frac{\hbar}{2\pi}\sum_p \int_{\mathbb{R}^2} \frac{d^2\mathbf{k}}{(2\pi)^2} \int_0^\infty d\omega k_z \left(1 - g^p_{\mathbf{k}}[\omega]\right), \tag{A.1.2}$$

$$k_z = \sqrt{\frac{\omega^2}{c^2} - |\mathbf{k}|^2} \tag{A.1.3}$$

[1] The calculation has be given with some detail in section 1.5 of the Chapter 1 (see also Appendix A.2).

This force is the net result of the action of the radiation pressure on the two sides (internal and external) of one mirror forming the cavity. The term $k_z g^p_{\mathbf{k}}[\omega]$ summarizes indeed the magnitude of the radiation pressure due to the electromagnetic field inside the cavity while the term k_z represents the magnitude of vacuum radiation pressure on the external face of the mirror.

Because of the boundary condition upon the mirrors for a perfect cavity we have

$$g^p_{\mathbf{k}}[\omega] = \lim_{\gamma\to 0^+} \frac{1}{L} \sum_{n=-\infty}^{\infty} \frac{1}{\frac{\gamma}{L} + \imath\left(\frac{n\pi}{L} - k_z\right)} = \frac{\pi}{L} \sum_{n=0}^{\prime} \delta\left(\frac{n\pi}{L} - k_z\right), \quad k_z = \sqrt{\frac{\omega^2}{c^2} - |\mathbf{k}|^2} \tag{A.1.4}$$

Introduction of the previous expression in Eq.(A.1.2) with the help of the cutoff function and of the application of the Euler-Maclaurin summation formula (Eq.(1.2.13)) leads to the Casimir result [113]

$$F(L) \equiv F_{Cas}(L) = \frac{\hbar c \pi^2}{240} \frac{A}{L^4} \tag{A.1.5}$$

It is interesting to have a look at this from another side. We could equivalently say, indeed, that Eq.(A.1.2) represents the net effect we have if we replace with the cavity an equivalent volume of vacuum. k_z is also the magnitude of the pressure which a volume of vacuum equivalent to cavity volume should exert to be in equilibrium with the surrounding vacuum. This point of view that we could call (with the opportune precautions) Archimedean sets the Casimir effect as a quantum filed theory version of the Archimede's principle. The interesting feature is that through we see immediately the physical property

$$\lim_{L\to\infty} F_{Cas}(L) = 0 \tag{A.1.6}$$

is due to the fact that[2]

$$\lim_{L\to\infty} g^p_{\mathbf{k}}[\omega] = 1 \tag{A.1.7}$$

This last relation is more general then the perfect mirror case because reposes on the fact that at infinity the mirror can be considered isolated in the vacuum which, by the space isotropy principle, must exert the same pressure on both sides of the mirror. Exploiting this last property we can write the force as

$$F_{Cas}(L) = \mathcal{F}(L) - \mathcal{F}(L\to\infty) \equiv [\mathcal{F}]^L_{L\to\infty} \quad \mathcal{F}(L) = -A\frac{\hbar}{2\pi} \sum_p \int_{\mathbb{R}^2} \frac{d^2\mathbf{k}}{(2\pi)^2} \int_0^\infty d\omega k_z g^p_{\mathbf{k}}[\omega] \tag{A.1.8}$$

where we have introduced the symbol $[\cdots]^L_{L\to\infty}$ which means that we have to evaluate the difference between the function inside the square brackets at a distance L and its asymptotic expression for $L\to\infty$. The energy is defined by

$$E(L) = -\int_L^\infty F(l)dl \tag{A.1.9}$$

[2]The following it would be totally justified by the argumentations in the following paragraph.

Inverting the square brackets and the integral symbols[3]

$$E_{Cas}(L) = [\mathcal{E}]_{l\to\infty}^{l} \Big|_{l=\infty}^{l=L} = [\mathcal{E}]_{L\to\infty}^{L} = \mathcal{E}(L) - \mathcal{E}(L\to\infty) \tag{A.1.10}$$

The term $\mathcal{E}(L\to\infty)$ is therefore connected with the work done by the free vacuum (for this reason $L\to\infty$) to carry a mirror from L to infinity.

A.2 Radiation pressure on a plane mirror

The Poynting theorem states

$$\frac{d}{dt}\left(\mathbf{P}_{mec} + \mathbf{P}_{field}\right) = \oint_S \mathbb{T}\cdot\mathbf{n}da \tag{A.2.1}$$

where $\mathbf{P}_{mec}$ and $\mathbf{P}_{field}$ are the mechanical and the field momentum contained in the volume V enclosed by the closed surface S. $\mathbf{n}$ is the normal vector to the surface element da oriented outside the volume V. $\mathbf{P}_{mec}$ is defined starting from the Lorentz's force on a particle

$$\mathbf{F} = q\left(\mathbf{E} + \mathbf{v}\times\mathbf{B}\right) \tag{A.2.2}$$

generalized to the volume V with a charge density ρ and a current $\mathbf{j}$

$$\frac{d}{dt}\mathbf{P}_{mec} = \int_V \left(\rho\mathbf{E} + \mathbf{j}\times\mathbf{B}\right) d^3\mathbf{r} \tag{A.2.3}$$

$\mathbf{P}_{field}$ is the momentum carried by the electromagnetic field and enclosed in the volume V

$$\mathbf{P}_{field} = \frac{1}{c^2}\int_V \mathbf{S}d^3\mathbf{r} \tag{A.2.4}$$

where $\mathbf{S}$ is the Poynting's vector [85].

$\mathbb{T}$ is the Maxwell'stress tensor [85] defined by

$$T_{i,j} = \frac{1}{Z_{vac}}\left[E_iE_j + c^2B_iB_j - \frac{1}{2}\left(E^2 + c^2B^2\right)\delta_{i,j}\right], \qquad Z_{vac} = c\mu_0 = \frac{1}{c\epsilon_0} \tag{A.2.5}$$

The Poynting's theorem is an extension of the momentum conservation law to the fields. The product $\mathbb{T}\cdot\mathbf{n}$ represents the momentum vector flux which enters into the volume through the surface element ds oriented along the direction $\mathbf{n}$ [85]. The tensor has the dimension of a pressure can be used to determine the module of the pressure exerted by the system (charges+fields) on the surface element da

$$P(\mathbf{r},t) = \mathbf{n}\cdot\mathbb{T}(\mathbf{r},t)\cdot\mathbf{n} \tag{A.2.6}$$

[3] The exchange of the order of integral/square bracket symbol require a bit of justification and it will be discussed in detail in a more general context in Chapters 3.

A.2.1 Pressure on a Mirror oriented in the (x, y)*-plane.*

We will now consider a mirror placed orthogonally to the z-axis and calculate what is the pressure exerted by the vacuum field upon its surface (the left one). Of course this is given by the stress tensor defined in the previous paragraph.

$$P = T_{z,z} = -\frac{1}{2Z_{vac}}\left(\mathbf{E}\cdot\mathbb{G}\cdot\mathbf{E} + c^2\mathbf{B}\cdot\mathbb{G}\cdot\mathbf{B}\right) \tag{A.2.7}$$

where $\mathbb{G} = 1 - 2\mathbf{zz}$ (dyadic notation). The electric and magnetic field can be written as

$$\mathbf{E} = \sqrt{cZ_{vac}}\sum_{m,\phi}\sqrt{\frac{\hbar\omega}{2}}\boldsymbol{\epsilon}_m^\phi \hat{e}_m^\phi e^{\imath(\omega t - \mathbf{k}\cdot\boldsymbol{\rho} - \phi|k_z|z)} + h.c. \tag{A.2.8}$$

$$\mathbf{B} = \sqrt{\frac{Z_{vac}}{c}}\sum_{m,\phi}\sqrt{\frac{\hbar\omega}{2}}\boldsymbol{\beta}_m^\phi \hat{e}_m^\phi e^{\imath(\omega t - \mathbf{k}\cdot\boldsymbol{\rho} - \phi|k_z|z)} + h.c. \tag{A.2.9}$$

where $\boldsymbol{\rho} \in (x, y)$, $m \equiv (\omega, \mathbf{k}, p)$ and $\phi = \pm 1$ depending on the propagation z-direction. $\hat{e}_m^\phi$ is the field annihilation operator.

For simplicity we can write

$$\mathbf{E} = \underbrace{\mathbf{E}^{\leftarrow}}_{\phi=1} + \underbrace{\mathbf{E}^{\rightarrow}}_{\phi=-1} \tag{A.2.10}$$

$$\mathbf{B} = \underbrace{\mathbf{B}^{\leftarrow}}_{\phi=1} + \underbrace{\mathbf{B}^{\rightarrow}}_{\phi=-1} \tag{A.2.11}$$

Therefore we have

$$\begin{aligned} P \;\propto\; & \mathbf{E}^{\leftarrow}\cdot\mathbb{G}\cdot\mathbf{E}^{\leftarrow} + c^2\mathbf{B}^{\leftarrow}\cdot\mathbb{G}\cdot\mathbf{B}^{\leftarrow} \\ + \; & \mathbf{E}^{\rightarrow}\cdot\mathbb{G}\cdot\mathbf{E}^{\rightarrow} + c^2\mathbf{B}^{\rightarrow}\cdot\mathbb{G}\cdot\mathbf{B}^{\rightarrow} \\ + \; & \mathbf{E}^{\leftarrow}\cdot\mathbb{G}\cdot\mathbf{E}^{\rightarrow} + c^2\mathbf{B}^{\leftarrow}\cdot\mathbb{G}\cdot\mathbf{B}^{\rightarrow} \\ + \; & \mathbf{E}^{\rightarrow}\cdot\mathbb{G}\cdot\mathbf{E}^{\rightarrow} + c^2\mathbf{B}^{\leftarrow}\cdot\mathbb{G}\cdot\mathbf{B}^{\leftarrow} \end{aligned} \tag{A.2.12}$$

We can regroup the previous terms in two ensembles: 1) diagonal terms and 2) non-diagonal terms. The following step is to do the quantum average on the vacuum state, and over the mirror surface

$$\overline{P} = \lim_{a\to\infty,\; b\to\infty}\frac{1}{ab}\int_{-a}^{a}dx\int_{-b}^{b}dyP(\mathbf{r}, t) \tag{A.2.13}$$

first on the diagonal terms then on the non-diagonal ones.

A.2.2 Diagonal terms

All the diagonal terms show the same behavior. For example let us calculate the quantum vacuum average of the following term

$$p^{\leftarrow\leftarrow} = -\frac{1}{2Z_{vac}}\left(\mathbf{E}^{\leftarrow}\cdot\mathbb{G}\cdot\mathbf{E}^{\leftarrow} + c^2\mathbf{B}^{\leftarrow}\cdot\mathbb{G}\cdot\mathbf{B}^{\leftarrow}\right) \tag{A.2.14}$$

Taking the 'sandwich' on the vacuum state we get

$$\langle p^{\leftarrow\leftarrow}\rangle = -\sum_m \sum_{m'} \frac{\hbar\sqrt{\omega\omega'}}{2}\pi^{\leftarrow\leftarrow}_{m,m'} \frac{\langle \hat{e}^{\leftarrow}_m \left(\hat{e}^{\leftarrow}_{m'}\right)^\dagger\rangle e^{-\imath[(\omega-\omega')t-(\mathbf{k}-\mathbf{k}')\cdot\mathbf{r}-(|k_z|-|k'_z|)z]}}{2} \tag{A.2.15}$$

with

$$\begin{aligned}\pi^{\leftarrow\leftarrow}_{m,m'} &= \frac{\boldsymbol{\epsilon}^{\leftarrow}_m \cdot \mathbb{G} \cdot \boldsymbol{\epsilon}^{\leftarrow}_{m'} + \boldsymbol{\beta}^{\leftarrow}_m \cdot \mathbb{G} \cdot \boldsymbol{\beta}^{\leftarrow}_{m'}}{2} \\ &= \delta_{m,m'} - (\boldsymbol{\epsilon}^{\leftarrow}_m \cdot \mathbf{z})(\boldsymbol{\epsilon}^{\leftarrow}_{m'} \cdot \mathbf{z}) - (\boldsymbol{\beta}^{\leftarrow}_m \cdot \mathbf{z})(\boldsymbol{\beta}^{\leftarrow}_{m'} \cdot \mathbf{z})\end{aligned} \tag{A.2.16}$$

We have already eliminated the terms proportional to

$$\langle (\hat{e}^{\leftarrow})^\dagger_m \, \hat{e}^{\leftarrow}_{m'}\rangle = \langle \hat{e}^{\leftarrow}_m \hat{e}^{\leftarrow}_{m'}\rangle = (\langle \hat{e}^{\leftarrow})^\dagger_m \, (\hat{e}^{\leftarrow}_{m'})^\dagger\rangle = 0 \tag{A.2.17}$$

Now since we have in general

$$[\hat{e}^{\leftarrow}_m, (\hat{e}^{\leftarrow}_{m'})^\dagger] = \delta\left(\omega - \omega'\right) g(\omega) \tag{A.2.18}$$

and taking the average on the whole plane (x, y) we get

$$\overline{\langle p^{\leftarrow,\leftarrow}\rangle} = -\sum_m \frac{\hbar\omega}{4} g(\omega)\cos\theta_m \tag{A.2.19}$$

where we have used the relations

$$\pi^{\leftarrow\leftarrow}_{m,m} = \frac{\boldsymbol{\epsilon}^{\leftarrow}_m \cdot \mathbb{G} \cdot \boldsymbol{\epsilon}^{\leftarrow}_{m'} + \boldsymbol{\beta}^{\leftarrow}_m \cdot \mathbb{G} \cdot \boldsymbol{\beta}^{\leftarrow}_{m'}}{2} = 1 - (\boldsymbol{\epsilon}^{\leftarrow}_m \cdot \mathbf{z})^2 - (\boldsymbol{\beta}^{\leftarrow}_m \cdot \mathbf{z})^2 = (\frac{\mathbf{K}}{K} \cdot \mathbf{z})^2 = \cos\theta_m \tag{A.2.20}$$

for which the following closure relation holds

$$\frac{\mathbf{K}}{K}\frac{\mathbf{K}}{K} + \boldsymbol{\epsilon}^{\leftrightarrows}_m \boldsymbol{\epsilon}^{\leftrightarrows}_m + \boldsymbol{\beta}^{\leftrightarrows}_m \boldsymbol{\beta}^{\leftrightarrows}_m = 1 \tag{A.2.21}$$

and

$$\frac{\omega^2}{c^2} = k^2 + k_z^2 \quad \text{to set} \quad |k_z| = \left|k'_z\right| \tag{A.2.22}$$

One can easily show that

$$\overline{\langle p^{\leftarrow\leftarrow}\rangle} = \overline{\langle p^{\rightarrow\rightarrow}\rangle} \tag{A.2.23}$$

A.2.3 Non-diagonal terms

Let us calculate the non-diagonal term

$$p^{\leftarrow\rightarrow} = -\frac{1}{2Z_{vac}}\left(\mathbf{E}^{\leftarrow} \cdot \mathbb{G} \cdot \mathbf{E}^{\rightarrow} + c^2 \mathbf{B}^{\leftarrow} \cdot \mathbb{G} \cdot \mathbf{B}^{\rightarrow}\right) \tag{A.2.24}$$

Taking the 'sandwich' on the vacuum state we get

$$\langle |p|^{\leftarrow\rightarrow} \rangle = \sum_m \sum_{m'} \frac{\hbar\sqrt{\omega\omega'}}{2} \pi^{\leftarrow\rightarrow}_{m,m'} \frac{\langle \hat{e}^{\leftarrow}_m \left(\hat{e}^{\rightarrow}_{m'}\right)^\dagger \rangle e^{-\imath[(\omega-\omega')t-(\mathbf{k}-\mathbf{k}')\cdot\mathbf{r}-(|k_z|+|k'_z|)z]}}{2} \tag{A.2.25}$$

with

$$\begin{aligned} \pi^{\leftarrow\rightarrow}_{m,m'} &= \frac{(\boldsymbol{\epsilon}^{\leftarrow}_m \cdot \boldsymbol{\epsilon}^{\rightarrow}_{m'}) + (\boldsymbol{\beta}^{\leftarrow}_m \cdot \boldsymbol{\beta}^{\rightarrow}_{m'})}{2} - (\boldsymbol{\epsilon}^{\leftarrow}_m \cdot \mathbf{z})(\boldsymbol{\epsilon}^{\rightarrow}_{m'} \cdot \mathbf{z}) - (\boldsymbol{\beta}^{\leftarrow}_m \cdot \mathbf{z})(\boldsymbol{\beta}^{\rightarrow}_{m'} \cdot \mathbf{z}) \\ &= \pi^{\rightarrow\leftarrow}_{m',m} \end{aligned} \tag{A.2.26}$$

Now since

$$[\hat{e}^{\leftarrow}_m, (\hat{e}^{\rightarrow}_{m'})^\dagger] = \delta\left(\omega - \omega'\right) d(\omega) \tag{A.2.27}$$

averaging on the surface we get

$$\overline{\langle p^{\leftarrow\rightarrow} \rangle} = -\sum_m \frac{\hbar\omega}{4} \pi^{\leftarrow\rightarrow}_{m,m} d(\omega) e^{+2\imath|k_z|z} \tag{A.2.28}$$

In the same manner

$$p^{\rightarrow\leftarrow} = -\frac{1}{2Z_{vac}} \left(\mathbf{E}^{\rightarrow} \cdot \mathbb{G} \cdot \mathbf{E}^{\leftarrow} + c^2 \mathbf{B}^{\rightarrow} \cdot \mathbb{G} \cdot \mathbf{B}^{\leftarrow}\right) \tag{A.2.29}$$

gives

$$\langle p^{\rightarrow\leftarrow} \rangle = -\sum_m \sum_{m'} \frac{\hbar\sqrt{\omega\omega'}}{2} \pi^{\rightarrow\leftarrow}_{m,m'} \frac{\langle \hat{e}^{\rightarrow}_m \left(\hat{e}^{\leftarrow}_{m'}\right)^\dagger \rangle e^{-\imath[(\omega-\omega')t-(\mathbf{k}-\mathbf{k}')\cdot\mathbf{r}+(|k_z|+|k'_z|)z]}}{2} \tag{A.2.30}$$

and since

$$[\hat{e}^{\rightarrow}_m, (\hat{e}^{\leftarrow}_{m'})^\dagger] = \delta\left(\omega - \omega'\right) d^*(\omega) \tag{A.2.31}$$

averaging on the surface gives

$$\overline{\langle p^{\rightarrow\leftarrow} \rangle} = \sum_m \frac{\hbar\omega}{4} \pi^{\rightarrow\leftarrow}_{m,m} d^*(\omega) e^{-2\imath|k_z|z} = \overline{\langle p^{\leftarrow\rightarrow} \rangle}^* \tag{A.2.32}$$

The last passage is due to the property in Eq.(A.2.26).

A.2.4 Evaluation of $\pi^{\rightarrow\leftarrow}_{m,m'}$

Let us have a more detailed look to the term $\pi^{\rightarrow\leftarrow}_{m,m'}$. From the definition of $\mathbb{G} = (1 - 2\mathbf{zz})$ this geometrical term can be rewritten as

$$\pi^{\leftarrow\rightarrow}_{m,m'} = \frac{(\boldsymbol{\epsilon}^{\leftarrow}_m \cdot \mathbb{G} \cdot \boldsymbol{\epsilon}^{\rightarrow}_{m'}) + (\boldsymbol{\beta}^{\leftarrow}_m \cdot \mathbb{G} \cdot \boldsymbol{\beta}^{\rightarrow}_{m'})}{2} \tag{A.2.33}$$

In our symmetry (a mirror orthogonal to the z-direction) the reflection process connects the vector $\mathbf{K}^{\leftarrow}$, $\boldsymbol{\epsilon}_m^{\leftarrow}$, $\boldsymbol{\beta}_m^{\leftarrow}$ as it follows

$$\mathbf{K}^{\leftarrow} = \mathbb{G} \cdot \mathbf{K}^{\rightarrow} \tag{A.2.34}$$

$$\boldsymbol{\epsilon}_m^{\leftarrow} = \mathbb{G} \cdot \boldsymbol{\epsilon}_m^{\rightarrow} \tag{A.2.35}$$

$$\boldsymbol{\beta}_m^{\leftarrow} = -\mathbb{G} \cdot \boldsymbol{\beta}_m^{\rightarrow} \tag{A.2.36}$$

The transformation produced by $\mathbb{G}$ changes the sign of the z-component of a vector. The minus sign in the last equality arises from the face that $\boldsymbol{\beta}$ is defined by

$$\boldsymbol{\beta} = \mathbf{K} \times \boldsymbol{\epsilon} \tag{A.2.37}$$

to form a right hand frame[4].

Exploiting the property $\mathbb{G}^2 = 1$ we get

$$\pi_{m,m'}^{\leftarrow\rightarrow} = \frac{(\boldsymbol{\epsilon}_m^{\rightarrow} \cdot \boldsymbol{\epsilon}_{m'}^{\rightarrow}) - (\boldsymbol{\beta}_m^{\rightarrow} \cdot \boldsymbol{\beta}_{m'}^{\rightarrow})}{2} = \frac{\delta_{m,m'} - \delta_{m,m'}}{2} = 0 \tag{A.2.38}$$

Therefore the geometric factor $\pi_{m,m'}^{\leftarrow\rightarrow}$ is zero and as a consequence the diagonal terms in Eq.(A.2.12) are automatically equal to zero.

Coming back to the expression of the pressure in terms of the stress tensor and collecting all the results of the previous sections we obtain

$$\overline{\langle P \rangle} = -\sum_m \frac{\hbar\omega}{2} \cos\theta_m g(\omega) \tag{A.2.39}$$

getting the usual form for the radiation pressure.

A.3 The Logarithmic argument theorem

In this section we sketch a demonstration of a corollary of the residue theorem called logarithmic argument theorem.

A.3.1 Demonstration

Hypothesis

Let $f(z)$ be a meromorphic function in a domain D and $\varphi(z)$ an analytic function in the same domain. Let Γ be a closed path contained in the domain D.

Thesis

$$\frac{1}{2\pi\imath} \oint_\Gamma \varphi(z) \frac{f'(z)}{f(z)} dz = \sum_n \alpha_n \varphi(z_n^0) - \sum_m \beta_m \varphi(z_m^\infty) \tag{A.3.1}$$

[4]The change of the sigh can be obtained directly from the definition of the vector product

where $z_n^0,\ z_m^\infty$ are in the domain contoured by Γ and

$$f(z_n^0) = 0, \quad \frac{1}{f(z_m^\infty)} = 0$$

α_n and β_m being the multiplicity of the zero an the order of the pole respectively.

Demonstration
Since $\varphi(z)$ is analytic in the domain contoured by Γ we have just to show that $z_n^0,\ z_m^\infty$ are first order poles of the function

$$\frac{f'(z)}{f(z)}$$

By the definition of zero and pole we have

$$\lim_{z\to z_n^0} \frac{f(z)}{(z-z_n^0)^{\alpha_n}} = k_1 < \infty \qquad \lim_{z\to z_m^\infty} f(z)(z-z_n^\infty)^{\beta_m} = k_2 < \infty \tag{A.3.2}$$

By the application of the De l'Hospital's theorem we have also

$$\lim_{z\to z_n^0} \frac{f'(z)}{(z-z_n^0)^{\alpha_n-1}} = \alpha_n k_1 < \infty \tag{A.3.3}$$

$$\lim_{z\to z_m^\infty} \frac{(z-z_n^\infty)^{\beta_m-1}}{\frac{d}{dz}\frac{1}{f(z)}} = \lim_{z\to z_m^\infty} -\frac{f^2(z)}{f'(z)}(z-z_n^\infty)^{\beta_m-1} = \frac{k_2}{\beta_m} < \infty \tag{A.3.4}$$

Therefore

$$\lim_{z\to z_n^0} \frac{f'(z)}{f(z)}(z-z_n^0) = \lim_{z\to z_n^0} \frac{f'(z)}{(z-z_n^0)^{\alpha_n-1}} \frac{(z-z_n^0)^{\alpha_n}}{f(z)} = \alpha_n \tag{A.3.5a}$$

And also

$$\lim_{z\to z_m^\infty} \frac{f'(z)}{f(z)}(z-z_n^0) = \lim_{z\to z_m^\infty} \frac{f'(z)}{f^2(z)(z-z_n^0)^{\beta_m-1}} f(z)(z-z_n^0)^{\beta_m} = -\beta_m \tag{A.3.5b}$$

C.Q.F.D.

A.3.2 Some mathematical considerations: the branching points

A connection between Lifshitz's theory of Casimir effect an the sum of the modes of the cavity electromagnetic filed, was deeply investigate by Van Kampen and, in a more general form, by Schram. This last one pointed out that when the retard effects are included in the calculation we have to confront to the branch cuts which occurs in integral given in Eq.(3.2.1a) or equivalently in the expression of the Casimir energy given in Eq.(3.2.1b). The previous attempts [143] which claimed to have bring to light the link between Lifshitz formula in retarded case and the sum over the modes were "mathematically incorrect

because contour integrations were performed in the ω- complex plane without taking account of branch points of non-analytic functions which occur in integrals" [111].

Let illustrate those difficulties with more details. The mathematical calculation besides on the application of a corollary of residues theorem, the *logarithmic argument theorem* [129] (see the previous paragraph), which states

$$\frac{1}{2\pi\imath}\oint_C \phi(z)\frac{d}{dz}\ln\left[f(z)-A\right]dz = \sum_{j=1}^{m} a_j\phi(x_j^z) - \sum_{j=1}^{n} b_j\phi(x_j^p) \tag{A.3.6}$$

$$f(x_j^z) - A = 0, \quad \frac{1}{f(x_j^p)} = 0 \tag{A.3.7}$$

where $f(z)$ is a monodromic function on a domain G which does not contains singular points except poles (i.e. $f(z)$ is a meromorphic function), A is a generic complex number, $\phi(z)$ an analytic and monodromic function in the same domain and C a closed Jordan's path contained in G which does not pass through x_j^z and x_j^p. The a_j and b_j are the multiplicity of the zeros and the order of the poles respectively.

It should be stressed here that the meromorphic property of $f(z)$ is an essential constraint for the application of the theorem. To be more explicit let us consider the following example.

$$I = \frac{1}{2\pi\imath}\oint_{|z|=R}\frac{d}{dz}\ln\left[exp(\sqrt{z})\right]dz \tag{A.3.8}$$

Since $exp(\sqrt{z}), exp(-\sqrt{z}) \neq 0, \forall z$ the corollary should state $I = 0$. Conversely we have

$$I = \frac{1}{2\pi\imath}\oint_{|z|=R}\frac{1}{2\sqrt{z}}dz = -\frac{\sqrt{R}}{\imath\pi} \tag{A.3.9}$$

This result can be explained as it follows: $\sqrt{z}$ is not a monodromic function in al complex plane. There is in fact no way to choose $\sqrt{z}$ so that it is continuous for all complex values of z. There has to be a *branch cut* - a line in the complex plane across which the function $\sqrt{z}$ is discontinuous. In Eq.(A.3.9), indeed, we have made two choices: (i) we have placed the branch cut along the positive real semiaxe starting in $z = 0$ -*branching point* for the function $\sqrt{z}$ [129]. In the domain obtained $(\mathbb{C} - \{Im\,[z] = 0, Re\,[z] \geq 0\})$ it is possible to isolate one monodromic branch of the root. We (ii) have chosen one particular determination (branch) for the square root fixing $\sqrt{\imath} = \frac{1+\imath}{\sqrt{2}}$.

Because of the branch cut the path $|z| = R$ is not a closed path contained in the domain where $\sqrt{z}$ is a monodromic function. Therefore in the case of Eq.(A.3.8) the formula given in Eq.(A.3.6) does not apply.

Generally speaking, before applying the logarithmic argument theorem we need to correctly individuate the domain where $f(z)$ is a meromorphic function. When a root is involved in the expression of $f(z)$ we have to choice a monodromic domain for the root and consequently associate a determination (isolating a particular branch). Unique values, indeed, have to be chosen for the function. The choices cannot be made continuous over the whole complex plane. Instead, lines of discontinuity, or branch cuts, must occur.

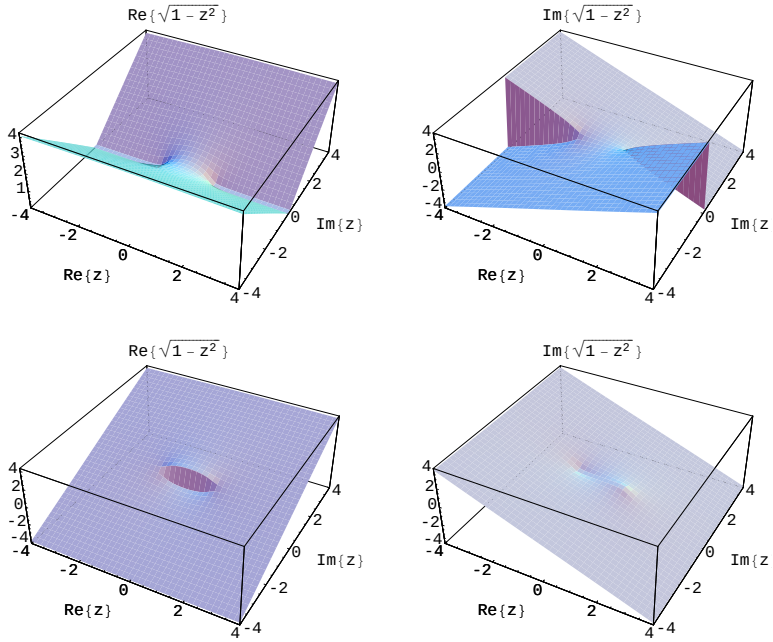

Figure A.1 : Two typical positions of branch cuts in for $\sqrt{1-z^2}$.In the first case the branch points are connected with a (infinite) 'segment' of the real axe passing through the point $z=\infty$. In the second one the branch points are connected with a finite segment of the real axe. In both cases we have selected the branch fixing $\sqrt{1-z^2}>0\ \forall Im\left[z\right]>0$.

The positions of these branch cuts are often quite arbitrary. For example in defining $\sqrt{z}$ in Eq.(A.3.9) we have decided to place the cut along the positive real axe but we can equivalently chose another semiaxe starting in $z=0$. For example choosing $Im\left[z\right]=0, Re\left[z\right]\leq 0$ and the same branch we get

$$I=\frac{\sqrt{R}}{\pi} \tag{A.3.10}$$

Another example about the branch points/cuts and on the monodromic definition domains is given $\sqrt{1-z^2}$ (such an example will be useful in the forthcoming calculation). This function has two branching points: $z=\pm 1$. The are several domain where it is possible isolate a branch of the square root. They can be obtained by placing the branch cut along a generic path connecting the branching points.

Two typical conventions are represented in fig.A.1. In the first case the branch points are connected with a (infinite) 'segment' of the real axe passing through the point $z=\infty$. In the second one the branch points are connected with a finite segment of the real axe. In both cases we have selected the branch fixing $\sqrt{1-z^2}>0\ \forall Im\left[z\right]>0$.

Different choices do not show the same continuity properties, which can lead to a 'privilegiate choice' for a given problem.

APPENDIX B

The hydrodynamic model with boundary conditions

B.1 Bulk shape

Let us consider that our electronic fluid with its positive background extends throughout the half-space $z \leq 0$. This imposes the following boundary condition of the displacement field

$$\zeta_z(z=0) = 0 \quad \text{and} \quad \zeta_z(z \to -\infty) < \infty \tag{B.1.1}$$

namely that the normal component of the displacement (and hence the velocity since $\mathbf{v} = \partial_t \boldsymbol{\zeta}$) vanishes on the interface of the bulk with the vacuum and the displacement remains finite to (minus) infinite.

Now if the fluid is irrotational ($\nabla \times \mathbf{v} = 0$) [134] it is convenient to represent the displacement as the gradient of a scalar potential

$$\boldsymbol{\zeta} = -\nabla\Psi \Rightarrow \nabla \cdot \boldsymbol{\zeta} = -\nabla^2\Psi \tag{B.1.2}$$

If we consider the electrostatic limit $c \to \infty$, the electric field can be derived from a scalar potential $\Phi(\mathbf{r}, t)$ through

$$\mathbf{E} = -\nabla\Phi \Rightarrow \nabla^2\Phi = -4\pi\langle\varrho_e\rangle\nabla^2\Psi \quad \text{inside the plasma } (z \leq 0) \tag{B.1.3}$$

Outside the plasma bulk we have

$$\nabla^2\Phi = 0 \quad (z > 0) \quad \text{with} \quad \Phi(z \to \infty) < \infty \tag{B.1.4}$$

The boundary conditions for the the electric field and potential [85] impose that across the interface metal/vacuum Φ and $E_z = \partial_z\Phi$ are continuous functions

$$\Phi(z = 0^-) = \Phi(z = 0^+), \quad \partial_z\Phi(z = 0^-) = \partial_z\Phi(z = 0^+). \tag{B.1.5}$$

Now the vectorial wave equation given in Eq.(2.2.8) can be rewritten as a scalar one

$$\nabla\left(\beta^2\nabla^2\Psi - \partial_t^2\Psi - \omega_p^2\Psi\right) = 0 \quad (z \leq 0) \tag{B.1.6}$$

and from the equation of motion (2.2.8) we get

$$\nabla\left(\frac{e}{m_e}\Phi + \beta^2\nabla^2\Psi - \partial_t^2\Psi\right) = 0 \quad (z \leq 0) \tag{B.1.7}$$

Going in the frequency domain (by Fourier transformation) and taking the divergence of both sides we obtain

$$\nabla^2\left(\beta^2\nabla^2 + \omega^2 - \omega_p^2\right)\Psi = 0 \quad (z \leq 0) \tag{B.1.8a}$$

$$\Phi = -\frac{m_e}{e}\left(\beta^2\nabla^2 + \omega^2\right)\Psi \quad (z \leq 0) \tag{B.1.8b}$$

Because of the symmetry of our system the solution $\Psi[\mathbf{r},\omega]$ has to be invariant with respect to a translation in the (x,y) plane. This means that $\Psi[\mathbf{r},\omega]$ assumes the form

$$\Psi[\mathbf{r},\omega] = \psi(z)e^{\imath\mathbf{k}\cdot\boldsymbol{\rho}}, \quad \Phi[\mathbf{r},\omega] = \phi(z)e^{\imath\mathbf{k}\cdot\boldsymbol{\rho}} \tag{B.1.9}$$

with $\boldsymbol{\rho} = (x,y)$ and $\mathbf{k} = (k_x,k_y)$. Inserting Eq.(B.1.9) in Eqs. (B.1.4) and (B.1.8b) and we derive

$$\phi = -\frac{m_e}{e}\left(-\beta^2\left|\mathbf{k}\right|^2 + \beta^2\partial_z^2 + \omega^2\right)\psi \quad (z \leq 0) \qquad -\left|\mathbf{k}\right|^2 + \partial_z^2\phi \quad (z > 0) \tag{B.1.10}$$

The equation for $\psi(z)$ is obtained inserting Eq.(B.1.9) in Eq.(B.1.8a)

$$\left(-\left|\mathbf{k}\right|^2 + \partial_z^2\right)\left(\beta^2\partial_z^2 + \omega^2 - \omega_p^2 - \beta k^2\right)\psi = 0 \quad (z \leq 0) \tag{B.1.11}$$

The solution of the previous equation is give by linear superposition of function having the form

$$\psi_n(z) \propto e^{\imath k_z} \tag{B.1.12}$$

where k_z is the nth root of the quartic equation

$$\begin{aligned}
&\left(-\left|\mathbf{k}\right|^2 - k_z^2\right)\left(-\beta^2k_z^2 + \omega^2 - \omega_p^2 - \beta^2\left|\mathbf{k}\right|^2\right) = 0 \\
\Rightarrow \quad k_z = \pm\imath\left|\mathbf{k}\right|, \quad k_z &= \pm\imath\frac{\sqrt{\omega_p^2 + \beta\left|\mathbf{k}\right|^2 - \omega^2}}{\beta} = \pm\imath\kappa_{sp}[\omega]
\end{aligned} \tag{B.1.13}$$

The boundary conditions given in Eqs.(B.1.1) and (B.1.5) impose restrictions to the value that the frequency ω can assume. The ensemble of the solutions splits into two ensembles depending on whether $\omega^2 < \omega_p^2 + \beta\left|\mathbf{k}\right|^2$ or $\omega^2 > \omega_p^2 + \beta\left|\mathbf{k}\right|^2$. We may analyze both ensembles separately.

Surface modes: $\omega^2 < \omega_p^2 + \beta\,|\mathbf{k}|^2$.

In this case all the solutions of equation (B.1.13) are imaginary. Because of the second condition given in Eq.(B.1.1) we have to rule out the solution which increases exponentially ($k_z = -\imath k$ and $k_z = -\imath\kappa_{sp}$). Imposing also the first condition in Eq.(B.1.1) we find

$$\psi_{|\mathbf{k}|}(z) = N_{|\mathbf{k}|}\left(\kappa_{sp}[\omega]\; e^{|\mathbf{k}|z} - |\mathbf{k}|\;\; e^{\kappa_{sp}[\omega]z}\right) \quad (z \leq 0) \tag{B.1.14}$$

where $N_{|\mathbf{k}|}$ is a constant. Note that when the previous function is inserted in Eq.(B.1.9) the function Ψ describes oscillations of the plasma which propagate parallel to the interface, strongly localized close to the interface and which exponentially decreases when moving away from it.

The electric potential inside the bulk can be univocally determined inserting the previous expression in Eq.(B.1.10). We then derive the form of the electric potential outside the bulk

$$\phi_k(z) = C_{|\mathbf{k}|}e^{-|\mathbf{k}|z} \tag{B.1.15}$$

Supposing β fixed the unknown variables of our system are $N_{|\mathbf{k}|}$, $C_{|\mathbf{k}|}$, ω, $|\mathbf{k}|$. The constant $N_{|\mathbf{k}|}$ can be fixed imposing normalization of $\psi_{|\mathbf{k}|}(z)$ (see the quantification of the plasma oscillation in Chapter 2). The remaining two other boundary conditions in Eq.(B.1.5) leave only one unfixed variable, the others being defined in function of it. In particular if we chose $|\mathbf{k}|$ as the free variable we have univocally that

$$\omega = \omega_{sp}[\mathbf{k}] \tag{B.1.16}$$

defining the dispersion relation for these modes.

In particular, applying the boundary conditions in Eq.(B.1.5)

$$\begin{cases} \phi_{|\mathbf{k}|}(0^-) = -\frac{m_e}{e}N_{|\mathbf{k}|}\left(\kappa_{sp} - |\mathbf{k}|\right)\left[\omega^2 - \beta^2\,|\mathbf{k}|\left(\kappa_{sp} + |\mathbf{k}|\right)\right], \\ \phi_{|\mathbf{k}|}(0^+) = \phi_{|\mathbf{k}|}(0^-) \Rightarrow C_{|\mathbf{k}|} = \phi_k(0^-) \\ \partial_z\phi(0^-) = \partial_z\phi(0^+) \Rightarrow -\frac{m_e}{e}\beta^2 N_{|\mathbf{k}|}\kappa_{sp}\,|\mathbf{k}|\left(|\mathbf{k}|^2 - \kappa_{sp}^2\right) = -\,|\mathbf{k}|\,\phi_k(0^+) \end{cases} \tag{B.1.17}$$

leads to the following equation

$$\left(\kappa_{sp} - |\mathbf{k}|\right)\left[\omega^2 - \beta^2\left(\kappa_{sp} + |\mathbf{k}|\right)^2\right] = 0 \tag{B.1.18}$$

Together to the definition for $\kappa_{sp}[\omega]$ given in Eq.(B.1.13) we obtain the dispersion relation

$$\omega_{sp}^2[\mathbf{k}] = \frac{\omega_p^2 + \beta^2\,|\mathbf{k}|^2 + \beta\,|\mathbf{k}|\sqrt{2\omega_p^2 + \beta^2\,|\mathbf{k}|^2}}{2} \xrightarrow{\beta\to 0} \frac{\omega_p^2}{2} \tag{B.1.19}$$

for the surface modes.

Bulk modes: $\omega^2 > \omega_p^2 + \beta\,|\mathbf{k}|^2$.

In this case $\kappa_{sp} = \imath k_B$ is a pure imaginary quantity ($k_z = \pm k_B$ where k_B is definite non-negative). Therefore we have that $\omega^2 = \omega_p^2 + \beta^2\,|\mathbf{k}|^2 + \beta^2 k_B^2$. Imposing the second boundary of the Eq.(B.1.1) the solution for $\psi(z)$ has therefore the following form

$$\psi_{|\mathbf{k}|,k_B}(z) = A_{|\mathbf{k}|,k_B}\cos\left[k_B z + \varphi_{|\mathbf{k}|,k_B}\right] + B_{|\mathbf{k}|,k_B}e^{|\mathbf{k}|z} \tag{B.1.20}$$

where the phase $\left|\varphi_{|\mathbf{k}|,k_B}\right| < \frac{\pi}{2}$. Inserting the previous expression in Eq.(B.1.9) the function Ψ now describe oscillations which propagate inside the metal.

Let calculate the number of free variables versus the number of boundary conditions. Since the expression for the electric potential outside the bulk is still given by Eq.(B.1.15) we have six free variables and, adding the normalization constraint only, four boundary conditions to apply. Therefore all undeterminate constants will be expressed as function of two free variables[1]. In particular we can write

$$\omega = \omega_B[\mathbf{k}, k_B] \tag{B.1.21}$$

If we suppose that the bulk has a finite thickness $\zeta_z(z = -d) = 0,\ d \gg 1$ we find also

$$\omega^2 = \omega_B^2[\mathbf{k}, n] \equiv \omega_p^2 + \beta^2\,|\mathbf{k}|^2 + \left(\beta\frac{n\pi}{d} - \beta\frac{\varphi_{|\mathbf{k}|,n}}{d}\right)^2 \quad n = 1, 2.... \tag{B.1.22}$$

i.e. a infinite but discrete number of frequency modes. In the Chapters 3 and 4 we shall see it can be mathematically advantageous to deal with a finite bulk thickness and take the the limit $d \to \infty$ only at the end of the calculation. In this case we have a discrete number of modes becoming continuous in the limit $d \to \infty$.

Since $\left|\varphi_{|\mathbf{k}|,n}\right| < \frac{\pi}{2}$ we see from Eq.(B.1.22)

$$\omega_B^2[\mathbf{k}, n] \xrightarrow{\beta \to 0} \omega_p^2 \tag{B.1.23}$$

Evidently the result remains valid also in the limit $d \to \infty$.

B.2 Two facing bulks

Let us consider now two metallic bulks facing each other in the electrostatic limit. The bulk on the left ($Left$) extends for $-\infty \le z \le -L/2$ while the one on right ($Right$) for $L/2 \le z \le \infty$.

Because of the translational symmetry of the whole system the specular symmetry with respect to the plane $z = 0$ we have

$$\phi^{\pm}_{|\mathbf{k}|}(z) = C^{\pm}_{|\mathbf{k}|}\left(e^{|\mathbf{k}|z} \pm e^{-|\mathbf{k}|z}\right) \quad (|z| \le \frac{L}{2}) \tag{B.2.1}$$

[1] It is for this reason that anticipating the final result we write $\psi_{|\mathbf{k}|,k_B}(z)$

The even (+) and odd (-) solution corresponds to a particular $\psi^{\pm}_{|\mathbf{k}|}(z)$ in the left bulk and in the right one. Again because of the specular symmetry it is sufficient to consider solutions only in one half space, say, the left half-space ($z \leq -\frac{L}{2}$) and the mode solutions split into two classes depending on whether $\beta\kappa_{\pm} = \sqrt{\omega_p^2 + \beta^2 |\mathbf{k}|^2 - \omega^2}$ is a real or a pure imaginary number.

For the **coupled surface modes** we have that

$$\psi^{\pm}_{k}(z) = N^{\pm}_{|\mathbf{k}|}\left(\kappa_{\pm}\, e^{|\mathbf{k}|\left(z+\frac{L}{2}\right)} - |\mathbf{k}|\;\, e^{\kappa_{\pm}\left(z+\frac{L}{2}\right)}\right) \quad (z \leq -\frac{L}{2}) \tag{B.2.2}$$

In this case the application of the boundary conditions lead to (I have dropped the subscript $|\mathbf{k}|$ for simplicity)

$$\begin{cases} \phi^{\pm}(-\frac{L}{2}^{-}) = -\frac{m_e}{e} N^{\pm}\left(\kappa_{\pm} - |\mathbf{k}|\right)\left[\omega^2 - \beta^2 |\mathbf{k}|\left(\kappa_{\pm} + |\mathbf{k}|\right)\right], \\ \phi^{\pm}(-\frac{L}{2}^{+}) = \phi^{\pm}(-\frac{L}{2}^{-}) \Rightarrow C^{\pm}\left(e^{-|\mathbf{k}|\frac{L}{2}} \pm e^{|\mathbf{k}|z\frac{L}{2}}\right) = \phi^{\pm}(-\frac{L}{2}^{-}) \\ \partial_z\phi^{\pm}(-\frac{L}{2}^{-}) = \partial_z\phi^{\pm}(-\frac{L}{2}^{+}) \Rightarrow -\frac{m_e}{e}\beta^2 N^{\pm}\kappa_{s\pm}|\mathbf{k}|\left(|\mathbf{k}|^2 - \kappa_{\pm}^2\right) = -\frac{|\mathbf{k}|\phi^{\pm}(-\frac{L}{2}^{-})}{h_{\pm}} \end{cases} \tag{B.2.3}$$

where we have defined

$$h_{-} = \tanh\left[|\mathbf{k}|\,\frac{L}{2}\right] \quad \text{and} \quad h_{+} = \coth\left[|\mathbf{k}|\,\frac{L}{2}\right] \tag{B.2.4}$$

The conditions in Eq.(B.2.3) lead to

$$\left(\kappa_{sp} - |\mathbf{k}|\right)\left[\omega^2 - \beta^2\left(\kappa_{\pm} + |\mathbf{k}|\right)\left(h_{\pm}\kappa_{\pm} + |\mathbf{k}|\right)\right] = 0 \tag{B.2.5}$$

Disregarding spurious solutions which do not satisfy the boundary conditions we get

$$\beta\kappa_{\pm} = \frac{-\beta|\mathbf{k}| + \sqrt{\left(1+h_{\pm}\right)\omega_p^2 + \beta^2|\mathbf{k}|^2}}{\left(1+h_{\pm}\right)} \tag{B.2.6}$$

$$\omega^2_{\pm}[\mathbf{k}] \xrightarrow{\beta\to 0} \omega_p^2\frac{h_{\pm}}{1+h_{\pm}} = \frac{\omega_p^2}{2}\left(1 \pm e^{-|\mathbf{k}|L}\right) \tag{B.2.7}$$

where for simplicity at the end we consider only the non-dispersive limit for the frequency mode.

With similar a argument on the symmetry properties we get for the **coupled bulk modes**

$$\psi^{\pm}_{|\mathbf{k}|,k_B^{\pm}}(z) = A^{\pm}_{|\mathbf{k}|,k_B^{\pm}}\cos\left[k_B^{\pm}\left(z+\frac{L}{2}\right) + \varphi^{\pm}_{|\mathbf{k}|,k_B^{\pm}}\right] + B^{\pm}_{|\mathbf{k}|,k_B^{\pm}}e^{|\mathbf{k}|\left(z+\frac{L}{2}\right)} \tag{B.2.8}$$

Again the insufficient number of boundary conditions and the infiniteness of the bulks lead to a continuum of modes with frequencies given by $\omega_B^{\pm}\left[|\mathbf{k}|, k_B^{\pm}\right]$.

The discretization of the bulk modes is now obtained imposing that $\zeta_{Left}(z = -d) = 0$ $\zeta_{Right}(z = d) = 0$ For large enough d we get

$$k_B^{\pm} d + \varphi^{\pm}_{|\mathbf{k}|,k_p^{\pm}} = n\pi \Rightarrow k_B^{\pm} = \frac{n\pi}{d} - \frac{\varphi^{\pm}_{|\mathbf{k}|,n}}{d} \quad n = 1, 2.... \tag{B.2.9}$$

and consequently

$$\omega^2 \equiv \omega_B^{\pm}[\mathbf{k}, n]^2 = \omega_p^2 + \beta^2 |\mathbf{k}| + \left(\beta \frac{n\pi}{d} - \beta \frac{\varphi^{\pm}_{|\mathbf{k}|,n}}{d} \right)^2 \quad n = 1, 2.... \tag{B.2.10}$$

i.e. infinite but discrete number of frequency modes.

APPENDIX C

Complements to the mode decomposition

C.1 The propagative and the evanescent waves

Let us make a step backwards to the expressions of the field operators given in Eqs.(1.5.1). There we chosen to expand the field over a particular base of the three-dimensional space functions, i.e. the plane waves. Of course generally speaking we could have expanded over another orthogonal base, i.e. spherical waves for instance, but our choice derive from the fact that the plane waves are easy to hand in the plane-plane geometry because of the translational invariance along each direction in the plane (x, y). This particular symmetry property is responsible for example of the definition given in Eqs.(1.4.16) for the reflection an the transmission coefficients (interface field dynamic properties [85]) as well as of the conservation of the transverse wavevector in passing through the interface between two dielectric

$$(\mathbf{K}\cdot\mathbf{x})_i = (\mathbf{K}\cdot\mathbf{x})_r = (\mathbf{K}\cdot\mathbf{x})_t \tag{C.1.1}$$

Those relations traduce in the equality of the incidence (θ_i) and of the reflection (θ_r) angles[1] as well as in the snell reflection law involving the incoming and the transmitted wave

$$\frac{K_t}{K_i} = \frac{\sin\theta_i}{\sin\theta_t} \tag{C.1.2}$$

The monochromatic plane waves have to satisfy the corresponding Helmotz equation in function of the medium where they propagate

$$A_{\mathbf{K}}(\mathbf{r}) = e^{-\imath(\mathbf{k}\cdot\boldsymbol{\rho}+k_z z)} \rightarrow \nabla^2 A_{\mathbf{K}}(\mathbf{r}) - \left(n\frac{\omega}{c}\right)^2 A_{\mathbf{K}}(\mathbf{r}) \Rightarrow K^2 = \mathbf{k}^2 + k_z^2 = \left(n\frac{\omega}{c}\right)^2 \tag{C.1.3}$$

where we have defined the two-dimensional vector $\boldsymbol{\rho} \equiv (x, y)$.

Remark that from the previous equation we can get

$$k_z = \pm\sqrt{\left(n\frac{\omega}{c}\right)^2 - \mathbf{k}^2} \tag{C.1.4}$$

[1] The usual convention states that all those angles are measured between the z-direction (normal to the interface) and the relative wavevector of the incoming, reflected or transmitted wave.

Now the previous expression can generate two possible situations

- $n\frac{\omega}{c} \geq \mathbf{k}$: in this case the k_z component of the wave vector is real; $A_{\mathbf{K}}(\mathbf{r})$ is a propagative wave in the z-direction. The sign of k_z specify the direction of propagation.
- $n\frac{\omega}{c} < \mathbf{k}$: in this case the k_z component of the wave vector is complex. Mathematically speaking this correspond to an attenuation/amplification of $A_{\mathbf{K}}(\mathbf{r})$ in the z-direction. The sign specify the direction of the attenuation/amplification

While the amplification is not physically admissible[2] the attenuation corresponds to a precise physical situation.

For simplicity let us place at the interface between the vacuum and a dielectric characterized by the index $n > 1$ and suppose that a plane wave coming from the dielectric arrives at the interface. From the Snell's law (Eq.(C.1.1)) we get

$$\sin\theta_t = n\sin\theta_i \tag{C.1.5}$$

In this case k_z of the transmitted wave is given by

$$k_z = \frac{\omega}{c}\cos\theta_t = \pm\frac{\omega}{c}\sqrt{1 - n^2\sin^2\theta_i} \tag{C.1.6}$$

Now since $n > 1$ it may happen

$$n^2\sin^2\theta_i \lessgtr 1 \Rightarrow\ \theta_i \lessgtr \theta_0 = \arcsin\frac{1}{n} < \frac{\pi}{2} \tag{C.1.7}$$

In the first two cases ($\theta_i \leqq \theta_0$) k_z is real leading to a propagative wave. The last case corresponds to an incoming plane wave propagating in the dielectric medium with $\theta_0 < \theta_i < \frac{\pi}{2}$ which is a physical realizable situation. The transmitted wave has an imaginary k_z and it should show an attenuation away from the interface. Therefore if the incoming plane wave has the expression

$$A_n(\mathbf{r},t) = e^{-\imath(\mathbf{k}\cdot\boldsymbol{\rho}+k_z z-\omega t)}, \quad k_z = \sqrt{\left(n\frac{\omega}{c}\right)^2 - k^2}, \quad n\frac{\omega}{c} > k \tag{C.1.8}$$

for an incidence angle larger then the limit angle θ_0 ($\theta_0 < \theta_i < \frac{\pi}{2}$) the transmitted wave is described by

$$A_0(\mathbf{r},t) = e^{-\imath(\mathbf{k}\cdot\boldsymbol{\rho}-\omega t)-\kappa z}, \quad \kappa = \sqrt{k^2 - \left(\frac{\omega}{c}\right)^2}, \quad \frac{\omega}{c} < k \tag{C.1.9}$$

$A_0(\mathbf{r},t)$ is still a propagative wave but in the (x,y) plane only, i.e. on the interface surface. For this reason it is sometime called surface wave. Its characteristic feature is however its damping behavior and for this wave like $A_0(\mathbf{r},t)$ have been baptized evanescent waves.

Of course all the precedent results can be generalized to a generic interface between two dielectric media. In this case the evanescent waves appears in the medium with the lower dielectric index if a plane wave arrives at the interface from the higher index medium

[2] We place in a framework where only passive elements are involved.

and with an angle larger then the limit angle corresponding to this particular dielectric configuration.

I want to stress that those waves are physical solutions of Maxwell equations when we deal with well specified real boundary conditions[3] (the interface discontinuity in this case) which introduce an asymmetry in the system. Their presence is necessary in order to take account of the structure in the current distribution which is finer than a wavelength [146]. This last feature is the reason for which the evanescent waves properties are at the same time central subject of interest and an essential tool of the a whole optics domain, namely the near field optics.

Remark that the evanescent behavior arises even when the dielectric is non-dissipative. Moreover it is worth to point out that despite some similarities the dissipative and evanescent attenuation are two different phenomena. Basically this is obvious in the case of dielectric/vacuum interface the evanescent waves lay in the vacuum which is lossless. In a generic dissipative situation the wavevector shows also an imaginary part but it is in general a complex number with a non zero real part. For this reason attenuation and propagation can have the same direction. Conversely as we have seen the evanescent wave always propagate on the interface and attenuate along the orthogonal direction to this surface.

C.1.1 Polarization of the evanescent and propagative waves.

Until now we have discussed the "scalar" features of the solutions of the Maxwell equations. We have shown that in plane-plane geometry, in function of the boundary conditions, those solutions may correspond to propagative or evanescent waves representing some well defined physical situations. The vectorial nature of e.m. field, however, implies some treatment of the polarization properties. For brevity and simplicity we place in the simple case of dielectric/vacuum interface which is the base configuration we deal with in this thesis. Moreover we only interest in the field in the vacuum where both evanescent and propagative waves exist. In the previous section we saw that the transversality condition led us to

$$\mathbf{K} \cdot \boldsymbol{\epsilon}^p[\mathbf{K}] = 0 \tag{C.1.10}$$

for the electric polarization vector $\boldsymbol{\epsilon}^p(\mathbf{K})$. The normalization and the TE and TM polarizations definition lead us to the expressions given in the table C.1. At the same time we saw that an evanescent wave born when the cosines of the transmission angle becomes a pure imaginary number, i.e.

$$\cos\theta_{ev} = \sin\bar{\theta}_{ev} = \imath \sinh\alpha_{ev} \quad \text{with } \alpha_{ev} \in \mathbb{R} \tag{C.1.11}$$

where we have substituted the subscript t to precise that we are now working with evanescent waves. The angle $\bar{\theta}_{ev}$ is the complemental of θ_{ev}

$$\bar{\theta}_{ev} = \frac{\pi}{2} - \theta_{ev} = \imath\alpha_{ev} \Rightarrow \theta_{ev} = \frac{\pi}{2} - \imath\alpha_{ev} \tag{C.1.12}$$

[3] One can evidently asks what about the quantization of the evanescent waves. This question finds a clear answer in ref. [144, 145].

Wavevector	**Transversal Electric**	**Transversal Magnetic**
$k_x = \frac{\omega}{c}\sin\theta\cos\varphi$	$\epsilon_x^{TE} = -\sin\varphi$	$\epsilon_x^{TM} = \cos\theta\cos\varphi$
$k_y = \frac{\omega}{c}\sin\theta\sin\varphi$	$\epsilon_y^{TE} = \cos\varphi$	$\epsilon_y^{TM} = \cos\theta\sin\varphi$
$k_z = \frac{\omega}{c}\cos\theta$	$\epsilon_z^{TE} = 0$	$\epsilon_z^{TM} = -\sin\theta$

Table C.1 : A scheme of the definition of the wavevector and TE and TM polarizations vectors for **propagative waves**.

Wavevector	**Transversal Electric**	**Transversal Magnetic**
$k_x = \frac{\omega}{c}\cosh\alpha_{ev}\cos\varphi$	$\epsilon_x^{TE} = -\sin\varphi$	$\epsilon_x^{TM} = \imath\sinh\alpha_{ev}\cos\varphi$
$k_y = \frac{\omega}{c}\cosh\alpha_{ev}\sin\varphi$	$\epsilon_y^{TE} = \cos\varphi$	$\epsilon_y^{TM} = \imath\sinh\alpha_{ev}\sin\varphi$
$k_z = \imath\frac{\omega}{c}\sinh\alpha_{ev}$	$\epsilon_z^{TE} = 0$	$\epsilon_z^{TM} = -\cosh\alpha_{ev}$

Table C.2 : A scheme of the definition of the wavevector and TE and TM polarizations vectors for the **evanescent waves**.

One can show that choosing the definitions given in the table C.2 we fulfill the transversality condition given in Eq.(C.1.10) as well the normalization condition give in Eq.(1.5.4b) and the orthogonality between the TE and the TM polarization.

The table C.2 put in evidence some quite interesting features: of course the evanescent wavevector is a complex vector. The TE-polarization is still defined by a real vector: the evanescent wave generated be a TE plane wave conserve this polarization, i.e. it still has a linear polarization. Conversely the TM-polarization vector is complex. Moreover if for simplicity we look for a propagation along the y-direction ($\varphi = \pi/2$) we can see that the electric field show a component in this direction (see table C.2).The fact that this component is imaginary means that it is dephased with respect the others, i.e. in this case respect the z-component. This means that the whole electric field vector rotates in in the (y, z) plane propagating in the y-direction, i.e. the electric field has an elliptic polarization. Of course the polarization is a concept which is totally meaningful only for the propagative waves and it loses part of its sense in the evanescent domain. Nevertheless introducing the generalized concept of degree of polarization [120, 146] we can talk about the polarization degree of a surface wave.

One can show that those properties are inverted for the magnetic: the evanescent magnetic field has a linear polarization for TM plane waves and elliptical polarization for TE waves.

C.1.2 Reflection and transmission coefficients

Reflection and transmission coefficients are strongly connected with energetic balancing and energetic considerations for evanescent waves are a quite complicate matter. Whether for the propagative waves we can reason as in paragraph 1.4.1 some difficulties need a more careful interpretation of evanescent results. For this reason here we do some general remarks.

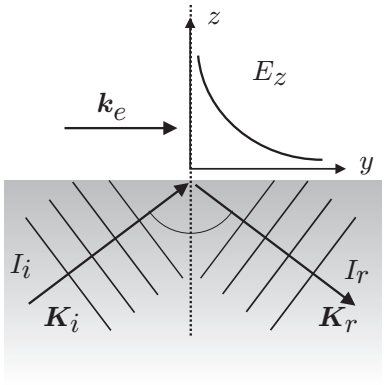

Figure C.1 : The phenomenon of the total internal reflection at the interface between two dielectric media. If the incoming wave comes form the higher index medium with an incidence angle larger then the limit angle for this media-configuration, the reflected and the incident waves will have the same intensities, i.e. $I_i = I_r$. The transmitted field however is non-null: It take the form of an evanescent wave which attenuate as far as we move from the surface and which propagate along the interface.

First of all even if a no zero electric field is associate with an evanescent waves this does not correspond to a an energetic transfer through the interface a this can easily see evaluating the time average of the Poynting vector immediately near the interface on the low index side [85]. This however as we have already seen does not imply that there is no transmitted wave because the necessity of satisfy boundary conditions to the interface. Those last allow indeed to still define a reflection an transmission coefficient which are nothing but the extension to the case $\frac{\omega}{c} < |\mathbf{k}|$ of the reflection and the transmission coefficients given for the propagative wave in Eqs.(1.4.16). From the mathematical point of view this corresponds to a well defined analytical continuation [129] of the function involved in Eqs.(1.4.16) which fulfill the appropriate physical constraints. It means for example that the analytical continuation should lead to an attenuation instead of an amplification.

It is interesting to note that in the non dissipative case we have that r_{int} for evanescent waves is a complex number with unit modulo which means that the intensity of the reflected wave is equal to the incoming one [85, 147] and for this reason the generation of the evanescent waves is intimately related with the phenomenon of the total internal reflection [85, 147]. A unit modulo for the reflection coefficient implies again that although there must be a transmitted wave it cannot, on the average, carry energy across the boundary. A more extensive treatment would show that the energy actually circulate back and forth across the interface, resulting on the average in a zero net flow of energy through the boundary [147].

Despite those considerations evanescent waves cannot be disregarded in the description of any optical system because they show some peculiar properties some of which are for example exploited in the near field optics. In particular if we consider a Fabry-Perot like configuration when an evanescent wave is produced in the inner of the cavity it may extend with non negligible amplitude across the vacuum from a mirror to the other. Here the

evanescent field can couple with the electron inside the distant mirror generating a propagative wave. This process as a whole is remarkably similar to the quantum mechanical phenomenon of tunneling [147]. In this case there is a flow of energy through the vacuum and disregarding evanescent waves will lead to the suppression of a large physical domain of frequency where to a propagative wave incoming on a Fabry-perot cavity correspond a propagative wave out going from the fabry perot cavity.

More over as we have see in the text the evanescent waves contribute to the radiation pressure balancing on a mirror of a Fabry-Perot cavity and then to the Casimir force.

C.2 The bulk approximation

The expression given in Eq.(3.2.1b) connects the Casimir energy to a unique physical concept: the mirrors reflection coefficients and in particular the reflection coefficients seen from inside the cavity. Supposing that we are dealing with identical mirror those coefficient degenerate in one unique quantity. Despite the linearity of this connection the reflection amplitude is involved in expression in Eq.(3.2.1b) in a quite complicate manner and it has in general by itself a non-simple algebraical expression (see for example Chap.1). For this reasons to simplify all sort of mathematical developments the reflection coefficient is evaluated making the so called bulk approximation. Physically speaking this approximation leads to consider infinite the mirrors thickness d passing to a configuration where the Casimir energy and force has to be evaluated between two identical semi-infinite facing bulks (see Chap.2). Differently from the calculation reported in Chapter 2 this time the bulk approximated form of Eq.(3.2.1b) takes account of the retardation effects due to the finite value of the light speed.

We already pointed up that the bulk approximation is a quite delicate approximation which reveals some some non-senses in the non-dissipative case or where in general the z-component of the wavevector vanishes. Nevertheless all those difficulties disappear we evaluate the Casimir effect as an integral over the imaginary frequencies. In this case indeed the quantity

$$\kappa_m = \sqrt{|\mathbf{k}|^2 + \epsilon[\imath\xi]\xi^2} \tag{C.2.1}$$

is a real number and the exponential factor which represent the field propagation across the mirror medium is a real quantity too avoiding the problem dues to its complex expression as function of real frequencies. In the limit of the mirror infinite thickness we can therefore approximate in Eq.(3.2.1b) the intracavity reflection coefficient with the expression of the reflection amplitude on the vacuum/metal interface [48, 85] (see also Chap.1)

$$r^p_{\mathbf{k}}[\imath\xi] = \frac{1 - Z^p_{\mathbf{k}}[\imath\xi]}{1 + Z^p_{\mathbf{k}}[\imath\xi]} \tag{C.2.2}$$

It is worth to stress however that this result can be obtained from an infinity of mirror internal configurations. We mean, the expression in Eq.(C.2.2) is not only the result of the limit $d \to \infty$ for a homogenous slab: we would reach the same result indeed for example taking the limit $d \to \infty$ for the first layer thickness in a multi-layer mirror supposing of course that the first layer properties is described by $\epsilon[\imath\xi]$. Mathematically with the help

of the Quantum Optical network formalism this can easy seen considering the following T-matrix

$$T = \underbrace{\begin{pmatrix} a_{int} & b_{int} \\ c_{int} & d_{int} \end{pmatrix}}_{\text{Interface}} \underbrace{\begin{pmatrix} p & 0 \\ 0 & \frac{1}{p} \end{pmatrix}}_{\text{Propagation}} \underbrace{\begin{pmatrix} a_x & b_x \\ c_x & d_x \end{pmatrix}}_{\text{The rest of the mirror}} = \begin{pmatrix} a_{int}a_x p + \frac{b_{int}c_x}{p} & a_{int}b_x p + \frac{b_{int}d_x}{p} \\ c_{int}a_x p + \frac{d_{int}c_x}{p} & c_{int}b_x p + \frac{d_{int}d_x}{p} \end{pmatrix} \tag{C.2.3}$$

The first matrix corresponds to the intracavity interface T-matrix; the second represent the propagation inside the intracavity interface layer ($p = e^{\alpha_m}$- see Chap.1); the third describe the rest of the mirror structure. The intracavity reflection coefficient can be obtained

$$r = \frac{c_{int}a_x p + \frac{d_{int}c_x}{p}}{a_{int}a_x p + \frac{b_{int}c_x}{p}} \xrightarrow{p\to\infty} = \frac{c_{int}}{a_{int}} = r_{int} \tag{C.2.4}$$

This characteristic feature can easily resumed saying that in the bulk approximation the mirror loses all the informations about its structure far away from its intracavity interface. At the same time this behavior reveal particularly useful in mathematical computations. We could evaluate for example the Casimir force using a reflection coefficient with particular mathematical properties but which admits expression in Eq.(C.2.2) as limit.

C.2.1 The contribution of the bulk region

In sections 4.6 and 4.7 we consider the sum of the propagative modes of a Fabry-Perot cavity. I mentioned that it is mathematically convenient to introduce the thickness of the mirrors and consider the bulk case as the limit of an infinite width at the end of the calculation (see section 4.5). However, the finite width case has shows a particular mode structure (see the figure 4.7). In the case of a lossless slab with a finite width, indeed, the system allows modes with a frequency higher then the high frequency cut off and which oscillate principally inside of the slab.

Here we analyze how those modes are involved in the modes sum expression of the Casimir energy trying to evaluate their role when we take the bulk limit.

To sum over the propagative modes we consider a modification of the surface impedance. Using dimensionless variables

$$\Omega = \omega L, \quad k = |\mathbf{k}|\, L, \quad \Omega_p = \omega_p L \tag{C.2.5}$$

we have

$$Z_s^p = Z^p \Theta[d\, \sqrt{z + \Omega_p^2}] \tag{C.2.6}$$

where

$$z = k^2 - \Omega^2 \tag{C.2.7}$$

$$Z^{TE} = \frac{\sqrt{z+\Omega_p^2}}{\sqrt{z}}, \quad Z^{TM} = \left(1 - \frac{\Omega_p^2}{k^2 - z}\right) \frac{\sqrt{z}}{\sqrt{z+\Omega_p^2}} \tag{C.2.8}$$

The function $\Theta[x]$ is a generic function having the following properties

$$\Theta[x], \quad \lim_{d\to\infty}\Theta[x] = 1 \ (Re\,[x] > 0) \tag{C.2.9}$$

The mode equations are

$$Z_s^p = -\tanh\left[\frac{\sqrt{z}}{2}\right], \quad Z_s^p = -\coth\left[\frac{\sqrt{z}}{2}\right] \tag{C.2.10}$$

We now choose a particular expression for $\Theta[x]$, for example as Schram [111]

$$\Theta[x] = \coth[x] \tag{C.2.11}$$

The modes equations can then be recast as it follows

$$\tanh[d\,\sqrt{z+\Omega_p^2}] = -Z^p\coth\left[\frac{\sqrt{z}}{2}\right], \quad \tanh[d\,\sqrt{z+\Omega_p^2}] = -Z^p\tanh\left[\frac{\sqrt{z}}{2}\right] \tag{C.2.12}$$

Therefore the Casimir energy as sum over all modes $\omega_{sn}^p[\mathbf{k}]$, which are solutions of those equations can be written as

$$\begin{aligned} E &= \sum_{\mathbf{k},p}\left[\lim_{d\to\infty}\sum_{n=0}^{\infty}\frac{\hbar}{2}\omega_{sn}^p[\mathbf{k}]\right]_{L\to\infty}^{L} \\ &= \sum_{\mathbf{k},p}\left[\lim_{d\to\infty}\underbrace{\sum_{n=0}^{N}\frac{\hbar}{2}\omega_{sn}^p[\mathbf{k}]}_{z>-\Omega_p^2}\right]_{L\to\infty}^{L} + \sum_{\mathbf{k},p}\left[\lim_{d\to\infty}\underbrace{\sum_{m=0}^{\infty}\frac{\hbar}{2}\omega_{sm}^p[\mathbf{k}]}_{z<-\Omega_p^2}\right]_{L\to\infty}^{L} \end{aligned} \tag{C.2.13}$$

where we have distinct two class of modes

- the bulk limit modes ($z > \Omega_p^2$): those modes tend for $d \to \infty$ to the modes we would get from the bulk case modes equation already discussed in section 4.2

$$\lim_{d\to\infty}\omega_{sn}^p[\mathbf{k}] = \omega_n^p[\mathbf{k}] \tag{C.2.14}$$

  For all them we have $\omega_{sn}^p[\mathbf{k}] < \omega_h[\mathbf{k}]$ where $\omega_c[\mathbf{k}] = \sqrt{\omega_p^2 + |\mathbf{k}|^2}$ is the high frequency transparency cutoff.

- the 'spurious modes' ($z < -\Omega_p^2$): those modes are introduced by the modification of the surface impedance given in Eq.(C.2.6). They obey $\omega_{sm}^p[\mathbf{k}] > \omega_c[\mathbf{k}]$.

Let concentrate our attention on this second class and calculate the solution of Eqs.(C.2.12). We can write

$$d\sqrt{z+\Omega_p^2} = \imath m\pi - \frac{\sqrt{z}}{2} - \delta_i^p, \quad i = \pm\ m = 0, \pm1, \pm2, ... \tag{C.2.15}$$

where

$$\delta_+^p = \operatorname{arctanh}\left[Z^p \coth\left[\frac{\sqrt{z}}{2}\right]\right] - \frac{\sqrt{z}}{2} = \operatorname{arccoth}\left[\frac{(Z^p-1)\coth\left[\frac{\sqrt{z}}{2}\right]}{1-Z^p\coth^2\left[\frac{\sqrt{z}}{2}\right]}\right] \tag{C.2.16}$$

$$\delta_-^p = \operatorname{arctanh}\left[Z^p \tanh\left[\frac{\sqrt{z}}{2}\right]\right] - \frac{\sqrt{z}}{2} = \operatorname{arctanh}\left[\frac{(Z^p-1)\tanh\left[\frac{\sqrt{z}}{2}\right]}{1-Z^p\tanh^2\left[\frac{\sqrt{z}}{2}\right]}\right] \tag{C.2.17}$$

We are interested in the solutions for $z < -\Omega_p^2 < 0$. In this range the phase shift δ_i^p are pure imaginary numbers. Even if eq.(C.2.15) can be cast in the form $z = F[z,k,d]$ where $F[z,k,d]$ has a very complicate expression we will consider the solutions in the limit $d \to \infty$. One can show that in this case, independently of p and i, we have

$$z \approx -\left[\Omega_p^2 + \left(\frac{m\pi}{d}\right)^2\right] \Rightarrow \Omega_m = \sqrt{k^2 + \left[\Omega_p^2 + \left(\frac{m\pi}{d}\right)^2\right]} \tag{C.2.18}$$

Coming back to dimensional variables this translates into

$$\omega_{sm}^p[\mathbf{k}] = \sqrt{|\mathbf{k}|^2 + \left[\omega_p^2 + \left(\frac{m\pi}{Ld}\right)^2\right]} \tag{C.2.19}$$

The limit for $d \to \infty$ allows to pass from the sum to an integral and write

$$\lim_{d\to\infty} \sum_{m=0}^{\infty} \frac{\hbar}{2}\omega_{sm}^p(|\mathbf{k}|) = Ld\frac{\hbar}{2\pi}\int_0^\infty \sqrt{|\mathbf{k}|^2 + \left[\omega_p^2 + k_z^2\right]}dk_z \tag{C.2.20}$$

Now remembering that $L \to \infty$ stays for the asymptotic expression in the variable L and remarking that in this case the asymptotic form of the previous expression is nothing but itself we get

$$\left[\lim_{d\to\infty} \underbrace{\sum_{m=0}^{\infty} \frac{\hbar}{2}\omega_{sm}^p(|\mathbf{k}|)}_{z<-\Omega_p^2}\right]_{L\to\infty}^{L} = 0 \tag{C.2.21}$$

In conclusion despite the modifications entailed by the eq.(C.2.6) (introduction of the spurious modes) in limit $d \to \infty$ the Casimir energy is given only by the modes we get from the bulk case modes equation

$$E = \sum_{\mathbf{k},p}\left[\sum_{n=0}\frac{\hbar}{2}\omega_n^p(|\mathbf{k}|)\right]_{L\to\infty}^{L} \tag{C.2.22}$$

APPENDIX D

Complements to the photonic and plasmonic mode contribution

D.1 Higher orders developments in Ω_p

In the first part of this appendix we analyze the development of the function η_{pl} in powers of Ω_p

$$\eta_{pl} = \eta_{ev} + \eta_{+} \tag{D.1.1}$$

where

$$\eta_{ev} = -\frac{180}{2\pi^3}\int_0^\infty \sum_i c_i g_i(z)dz \tag{D.1.2}$$

$$\eta_{+} = -\frac{180}{2\pi^3}\left[\int_{-z_+^0}^0 g_+(z)dz - \frac{2}{3}z_+^{\frac{3}{2}}\right] \tag{D.1.3}$$

These two terms have a clear interpretation: η_{ev} is the evanescent waves contribution ($z > 0$) to the plasmonic energy while η_+ is the contribution of the propagative part of the mode ω_+ (see sections 4.2, 4.4 and figure 4.3).

In particular in this annex we calculate the development up to the third order in Ω_p^3. The principal problems arise from η_{ev}. Since $z_+ = \Omega_p^2 + \mathcal{O}^3[\Omega_p]$ we get, indeed,

$$\eta_{+} \approx -\frac{180}{2\pi^3}\left[g_+(0)\Omega_p^2 - \frac{2}{3}\Omega_p^3\right] \approx -\frac{180}{6\pi^3}\Omega_p^3 = -d\ \Omega_p^3 \tag{D.1.4}$$

with $d = 0.9675...$

In the last paragraph we study the small distances behavior of $\Delta\eta_{ph}$.

D.1.1 Analysis of the integrand of η_{ev}

From a general point of view the functions $g_i(z)$ can be written as

$$g_i(z) = \sqrt{\frac{\Omega_p^2\sqrt{z}}{\sqrt{z}+\sqrt{z+\Omega_p^2}\ A_i(z)}} \tag{D.1.5}$$

with

$$A_+(z) = \tanh[\frac{\sqrt{z}}{2}], \quad A_-(z) = \coth[\frac{\sqrt{z}}{2}], \quad A_0(z) = 1 \tag{D.1.6}$$

One can easily see that all the previous functions are regular except at $z = 0$ where $g_+(z)$ and $g_0(z)$ have an eliminable discontinuity.

Even if the whole integrands are regular functions, the Taylor's series in powers of Ω_p is not uniformly convergent in z. This is particularly evident for $g_0(z)$

$$g_0(z) = \frac{\Omega_p}{\sqrt{2}} + \Omega_p^3\frac{1}{8\sqrt{2}z} + \mathcal{O}^4[\Omega_p] \tag{D.1.7}$$

The series development is valid only if

$$\left|\frac{\Omega_p^2}{8z}\right| \ll 1 \Rightarrow \ |z| \gg \left|\frac{\Omega_p^2}{8}\right| \tag{D.1.8}$$

This entails that we cannot interchange the integral and the Taylor's summation. This is problem is deeply related the branching points of $\sqrt{z+\Omega_p^2}$ contained in all the expression of $g_i(z)$: passing in the complex z-plane, we see that the previous square root can be expanded in powers of z/Ω_p^2 only where $|z| < \Omega_p^2$.

As mentioned in section 4.4.3 this problem dos not arise when we consider the first term of the development. We then have

$$g_i(z) = \Omega_p\sqrt{\frac{1}{1+A_i(z)}} \tag{D.1.9}$$

which is always well defined for $z = 0$

D.1.2 Alternative method

To bypass the problem we need to use another development of the integrand. First we note that

$$g_\pm(z) = g_0(z)\sqrt{\frac{1\pm e^{-\sqrt{z}}}{1\pm\rho}} \tag{D.1.10}$$

with

$$\rho = -\frac{g_0^4(z)}{z\Omega_p^2}e^{-\sqrt{z}} = r^{TE}e^{-\sqrt{z}} \tag{D.1.11}$$

Exploiting

$$\frac{1}{\sqrt{1+x}} = \sum_{n=0} \frac{\sqrt{\pi}}{\Gamma(\frac{1}{2}-n)} \frac{x^n}{n!} \tag{D.1.12}$$

we get

$$g_{\pm}(z) = g_0(z)\sqrt{1 \pm e^{-\sqrt{z}}} \sum_{n=0} \frac{\sqrt{\pi}}{\Gamma(\frac{1}{2}-n)} \frac{(\pm\rho)^n}{n!} \tag{D.1.13}$$

This series of functions converges uniformly in z. One can easily show that

$$\sup_{\Omega_p} |\rho| = e^{-\sqrt{z}} \tag{D.1.14}$$

and then that series

$$\sum_n \frac{e^{-n\sqrt{z}}}{n!\Gamma(\frac{1}{2}-n)} \tag{D.1.15}$$

converges uniformly. We can write

$$(g_+(z) + g_-(z) - 2g_0(z)) = \sum_{n=0} f_n(z) \tag{D.1.16}$$

$$f_n(z) = \begin{cases} g_0(z)\left(\sqrt{1+e^{-\sqrt{z}}} + \sqrt{1-e^{-\sqrt{z}}} - 2\right) & \text{for } n = 0 \\ \sqrt{\pi} 2 g_0(z) \frac{\sqrt{1+e^{-\sqrt{z}}} + (-1)^n \sqrt{1-e^{-\sqrt{z}}}}{\Gamma(\frac{1}{2}-n)} \frac{\rho^n}{n!} & \text{for } n > 0 \end{cases} \tag{D.1.17}$$

It is then possible to interchange the sum and the integral symbols. The series obtained converges for $\Omega_p < \infty$ and we can approximate it with its firsts terms. All the integrals obtained are convergent. For the first term we find

$$g_0(z)\left(\sqrt{1+e^{-\sqrt{z}}} + \sqrt{1-e^{-\sqrt{z}}} - 2\right) \xrightarrow{z\to\infty} -g_0(z)\frac{e^{-2\sqrt{z}}}{4} \tag{D.1.18}$$

which ensures the convergence of the first integral.

Since $g_0(z) = \mathcal{O}[\Omega_p]$ and $\rho = \mathcal{O}^2[\Omega_p]$ developing the series into two orders is equivalent to an approximation up to $\mathcal{O}^3[\Omega_p]$.

D.1.3 Improving calculations

To go further in our calculation it is convenient to change $z = \Omega_p^2\, x^2$. Let us note that

$$g_0(\Omega_p^2 x^2) = -\frac{\imath\Omega_p}{\sqrt{2}}\sqrt{x^2 + \imath x} + c.c. \tag{D.1.19}$$

$$g_0^5(\Omega_p^2 x^2) = -\frac{\imath\Omega_p^5 x^2}{\sqrt{2}}(4x^2 + 2\imath x + 1)\sqrt{x + \imath x} + c.c. \tag{D.1.20}$$

Let us develop the series (D.1.13) to second order and taking into account that

$$\sqrt{1 \pm e^{-\kappa}} = \sum_n \frac{\sqrt{\pi}}{2\Gamma[\frac{3}{2}-n]} \frac{(\pm 1)^n}{n!} e^{-n\kappa} \tag{D.1.21}$$

we have

$$\left[g_+(\Omega_p^2\, x^2)+g_-(\Omega_p^2\, x^2)-2g_0(\Omega_p^2\, x^2)\right]\approx\sum_{n=1}\frac{\sqrt{\pi}}{\Gamma[\frac{3}{2}-2n]}\frac{e^{-2n\kappa}}{(2n)!}\left[g_0(\kappa^2)+\frac{g_0^5(\kappa^2)}{2\kappa^2\Omega_p^2}\frac{n}{\frac{3}{2}-2n}\right]$$
$$=-\frac{\imath\Omega_p}{\sqrt{2}}\sum_{n=1}\frac{\sqrt{\pi}}{(2n)!\Gamma(\frac{3}{2}-2n)}\left[1+\left(1-2\imath x+4x^2\right)\frac{n}{\frac{3}{2}-2n}\right]e^{-2n\Omega_p x}\sqrt{x^2+\imath x}+c.c. \tag{D.1.22}$$

We then have to solve integrals of the form[1]

$$\int_0^\infty t^m(t^2+\imath t)^{\frac{1}{2}}e^{-2\mu t}dt=\imath\frac{\pi}{4}(-\frac{1}{2})^{m+1}\frac{d^m}{d\mu^m}\left(\frac{e^{\imath\mu}}{\mu}H_1^{(2)}[\mu]\right)=\imath\frac{\pi}{4}\mathcal{H}^{(m)}[\mu] \tag{D.1.23}$$

where $H_\nu^{(2)}[\Omega_p]$ is the Hankel function of 2nd kind. In our case $m=1,2,3$. Collecting all the previous results leads to

$$\eta_{ev}\approx-\frac{45}{\pi^2}\Omega_p^3\sum_{n=1}\frac{\sqrt{\pi/2}}{(2n)!\Gamma(\frac{3}{2}-2n)}F_n(\Omega_p)+c.c. \tag{D.1.24}$$

$$F_n(\Omega_p)=\left[\mathcal{H}^{(1)}[n\Omega_p]+\left(\mathcal{H}^{(1)}[n\Omega_p]-2\imath\mathcal{H}^{(2)}[n\Omega_p]+4\mathcal{H}^{(3)}[n\Omega_p]\right)\frac{n}{\frac{3}{2}-2n}\right] \tag{D.1.25}$$

The previous expression can be further simplified until it contains only $H_0^{(2)}[\Omega_p]$ and $H_1^{(2)}[\Omega_p]$.

$$\eta_{ev}=-\frac{45}{\pi^2}\sum_{n=1}\frac{\sqrt{\pi/2}}{(2n)!\Gamma(\frac{3}{2}-2n+1)}\left[A_n(\Omega_p)H_0^{(2)}[n\Omega_p]+\frac{B_n(\Omega_p)}{\Omega_p}H_1^{(2)}[n\Omega_p]\right]\frac{3e^{\imath n\Omega_p}}{n^3}+c.c. \tag{D.1.26}$$

where

$$A_n(\Omega_p)=n\left(1-\imath n\Omega_p+\left(\frac{1}{2}-\frac{7}{3}n\right)\frac{n\Omega_p^2}{4}\right) \tag{D.1.27a}$$

$$B_n(\Omega_p)=-2(1-\imath n\Omega_p)-\left(1-\frac{17n}{3}\right)\frac{n\Omega_p^2}{4}+\imath\left(\frac{1}{2}-\frac{7}{3}n\right)\frac{n^2\Omega_p^3}{4} \tag{D.1.27b}$$

A very good approximation can be obtained if we develop the previous series up to $n=10$. If we develop we obtain

$$\eta_{ev}\approx a\Omega_p+(b+c\ln\Omega_p)\Omega_p^3 \tag{D.1.28}$$

with

$$a=-\frac{45}{\pi^3}\sum_{n=1}\frac{\sqrt{\pi/2}}{(2n)!\Gamma(\frac{3}{2}-2n)}\frac{1}{n^2}=-\frac{180}{\pi^3}\int_0^\infty\frac{\kappa}{\sqrt{2}}\left(\sqrt{1+e^{-\kappa}}+\sqrt{1-e^{-\kappa}}-2\right)d\kappa=0.284... \tag{D.1.29a}$$

[1] Int. 3.388-3, Table of integrals, Gradshteyn/Ryzhik, Alan Jeffrey Edition [114]

$$
\begin{aligned}
b &= -\frac{45}{\pi^3}\sum_{n=1}\frac{\sqrt{\pi/2}}{(2n)!\Gamma(\frac{3}{2}-2n+1)}\left[\left(\frac{3}{4}-2n\right)\left[1+\gamma+\ln\frac{n}{2}\right]-\left(\frac{1}{2^3}-\frac{n}{30}\right)\right] \\
&= (1+\gamma)c+\frac{45}{\pi^3}\left[\frac{1-\sqrt{2}}{60}+\frac{1}{10\sqrt{2}}\int_0^\infty e^{-\kappa}\left(\sqrt{1+e^{-\kappa}}-\sqrt{1-e^{-\kappa}}\right)d\kappa\right] \\
&- \frac{45}{\pi^3}\sum_{n=1}\frac{\sqrt{\pi/2}}{(2n)!\Gamma(\frac{3}{2}-2n+1)}\left(\frac{3}{4}-2n\right)\ln\frac{n}{2} \\
&= (1+\gamma)c+\frac{3}{4\pi^3}(9-5\sqrt{2}) \\
&- \frac{45}{\pi^3}\sum_{n=1}\frac{\sqrt{\pi/2}}{(2n)!\Gamma(\frac{3}{2}-2n+1)}\left(\frac{3}{4}-2n\right)\ln\frac{n}{2} = 2.208... \qquad \text{(D.1.29b)}
\end{aligned}
$$

$$
\begin{aligned}
c &= -\frac{45}{\pi^3}\sum_{n=1}\frac{\sqrt{\pi/2}}{(2n)!\Gamma(\frac{3}{2}-2n+1)}\left(\frac{3}{4}-2n\right) \\
&= -\frac{45}{\pi^3}\left[1-\sqrt{2}-\frac{3}{4\sqrt{2}}\int_0^\infty e^{-\kappa}\left(\sqrt{1+e^{-\kappa}}-\sqrt{1-e^{-\kappa}}\right)d\kappa\right] \\
&= \frac{45}{\pi^3\sqrt{2}} = 1.026... \qquad \text{(D.1.29c)}
\end{aligned}
$$

where $\gamma = 0.577...$ is the Euler's gamma constant.

Note that the first order term in eq.(D.1.28) is identical to the expression given in eq.(4.4.27) which was obtained doing a Taylor expansion. Furthermore the fact that eq.(D.1.28) contains a logarithm is directly connected to the impossibility to use from the begin the Taylor's expansion for the terms higher then the first one.

D.1.4 Comparison with the previous results

Adding the contribution of η_+ we get

$$\eta_{pl} = a\Omega_p + (b' + c\ln\Omega_p)\Omega_p^3 \qquad b' = b + d \qquad \text{(D.1.30)}$$

It is interesting to note that when we pass from the Casimir energy to the force, an approximation of η_{pl}^F to the same order leads to

$$\eta_{pl}^F = \eta_{pl} - \frac{\Omega_p}{3}\dot{\eta}_{pl} = \frac{2}{3}a\Omega_p - \frac{c}{3}\Omega_p^3 \qquad \text{(D.1.31)}$$

which, at this order, is independent on b' and of the logarithm.

Furthermore we have

$$\frac{2}{3}a = 0.189..., \quad \frac{c}{3} = 0.342... \qquad \text{(D.1.32)}$$

The first result which matches exactly with the value previously found in [90] while the second give the coefficient of the third order.

D.1.5 On the small distances behavior of $\Delta\eta_{ph}$

Let us consider the expression for $\Delta\eta_{ph}$ obtained in Chapter 4

$$\Delta\eta_{ph} = \frac{180}{2\pi^3}\left(\frac{2}{\pi}\int_0^\infty \sum_i c_i\, g_i(z)\arctan\left[\frac{g_i(z)}{\sqrt{z}}\right]dz + \int_{-z_+^0}^0 g_+(z)dz - \frac{2}{3}y_+^3\right) \quad \text{(D.1.33)}$$

with $c_+ = c_- = 1,\ c_0 = -2$.

We have already seen that the last two terms give a contribution proportional to Ω_p^3. Let us concentrate on the first integral changing the variable $z = \Omega_p^2 y^2$ and splitting the integration domain in $y < 1$ and $y > 1$.

Since $\Omega_p \ll 1$ in the first interval ($y < 1$) we can make the following approximation

$$g_+(\Omega_p^2y^2) \approx \Omega_p, \quad g_-(\Omega_p^2y^2) \approx \Omega_p y\sqrt{\frac{\Omega_p}{\sqrt{y^2+1}}}, \quad g_0(\Omega_p^2y^2) = \Omega_p\sqrt{\frac{y}{y+\sqrt{y^2+1}}} \quad \text{(D.1.34)}$$

The function g_- can be neglected in comparison with g_+ and g_0. We have for the first interval the following result

$$\frac{360}{\pi^4}\int_0^1 \Omega_p^3 y\left(\arctan\left[\frac{1}{y}\right] - 2\sqrt{\frac{y}{y+\sqrt{y^2+1}}}\arctan\left[\frac{1}{y}\sqrt{\frac{y}{y+\sqrt{y^2+1}}}\right]\right)dy \propto \Omega_p^3 \quad \text{(D.1.35)}$$

The proportional coefficient can be evaluated to 0.277714....

In the interval $z > \Omega_p^2$ since $\frac{g_i(z)}{\sqrt{z}} < \infty$ we can write

$$\sum_i c_i\ \left(\frac{g_i^2(z)}{\sqrt{z}} + \mathcal{O}^2\left[g_i^2(z)\right]\right) \quad \text{(D.1.36)}$$

One can show that

$$\sum_i c_i\ \frac{g_i^2(z)}{\sqrt{z}} = \mathcal{O}^4[\Omega_p], \quad g_i^2(z) = \mathcal{O}^2[\Omega_p] \Rightarrow \sum_i c_i\ \mathcal{O}^2\left[g_i^2(z)\right] = \mathcal{O}^4[\Omega_p] \quad \text{(D.1.37)}$$

This means that the integral on the interval $z > \Omega_p^2$ is of the order $\mathcal{O}^4[\Omega_p]$ and that globally $\Delta\eta_{ph}$ is of the order $\mathcal{O}^3[\Omega_p]$ at small distances.

D.2 Evanescent and Propagative contribution

In Chapter 3 we showed that cavity modes split into two classes, that it two plasmonic modes, ω_+ and ω_-, and propagative photonic modes. We also established that ω_- is totally contained on the evanescent sector, while ω_+ crosses the barrier and is propagative for small $|\mathbf{k}|$ and evanescent for large $|\mathbf{k}|$. In the calculation of the mode contribution to the Casimir energy, the whole mode ω_+ was in some sense attributed to the evanescent

sector. Here we calculated the evanescent and the ordinary contributions to the Casimir energy attributing ω_+ to the evanescent or the ordinary sector, depending on the value of $|\mathbf{k}|$. Instead of the separation in plasmonic an photonic contribution we evaluate the evanescent (ev) and the ordinary (ord) ones and write

$$\eta^p = \eta^p_{ev} + \eta^p_{ord} \tag{D.2.1}$$

This will confirm the statement in Chapter 4 that if we consider only the evanescent contribution (η_{ev}), i.e. forgetting the propagative part of the mode ω_+, we would obtain a result similar to η_{pl}.

D.2.1 TE-modes: no evanescent contribution

The TE-contribution to Casimir energy has the form

$$E^{TE} = \sum_{\mathbf{k}} \frac{\hbar}{2} \left[\sum_n \omega_n^{TE}(\mathbf{k}) \right]_{L\to\infty}^{L} \tag{D.2.2}$$

From the mode analysis in Chapter 3 we already know, that all TE-modes lie in the ordinary (propagative) sector. This means that the TE-contribution should be totally included in OMC. To confirm this result here we show that

$$\eta^{TE} = \eta^{TE}_{ord} \Rightarrow \eta^{TE}_{ev} = 0 \tag{D.2.3}$$

$$E^{TE} = \eta^{TE} E_{Cas} \qquad E_{Cas} = -\frac{\hbar c \pi^2 A}{720 L^3} \tag{D.2.4}$$

Using dimensionless variables

$$\imath\Xi = \Omega = \frac{\omega}{c} L \qquad k = |\mathbf{k}|\, L \tag{D.2.5}$$

we find

$$\eta^{TE} = -\frac{180}{\pi^4} \int_0^\infty dk \int_0^\infty d\Omega Im \left[k \ln[1 - \rho^{TE}[\Omega]^2] \right] \tag{D.2.6}$$

It is possible to show that (Wick rotation)

$$\begin{aligned} \eta^{TE}_{ord} &= -\frac{180}{\pi^4} \int_0^\infty dk \int_k^\infty d\Omega Im \left[k \ln[1 - \rho^{TE}[\Omega]^2] \right] \\ &= -\frac{180}{\pi^4} Re \left[\int_0^\infty dk \int_0^\infty d\Xi k \ln[1 - \rho^{TE}[\imath(\Xi + \imath k)]^2] \right] \end{aligned} \tag{D.2.7}$$

Defining

$$\kappa^2 = \Xi^2 + 2\imath k \Xi \tag{D.2.8}$$

and switching from Ξ to κ we can write

$$\eta^{TE}_{ord} = -\frac{180}{\pi^4} Re \left[\int_0^\infty dk \int_0^\infty d\kappa \frac{\kappa}{\sqrt{\kappa^2 - k^2}} \ln[1 - \rho^{TE}[\kappa]^2] \right] \tag{D.2.9}$$

Inverting the order of integration between k and κ we have

$$\eta_{ord}^{TE} = -\frac{180}{\pi^4}\int_0^\infty d\kappa \ln[1-\rho^{TE}[\kappa]^2] Re\left[\int_0^\infty dk \frac{k\kappa}{\sqrt{\kappa^2-k^2}}\right] \tag{D.2.10}$$

Now we have

$$Re\left[\int_0^\infty dk \frac{k\kappa}{\sqrt{\kappa-k^2}}\right] = \kappa^2 \tag{D.2.11}$$

And the formula we obtain is

$$\begin{aligned}\eta_{ord}^{TE} &= \frac{-180}{\pi^4}\int_0^\infty d\kappa\kappa^2 \ln[1-\rho_{\mathbf{k}}^{TE}[\kappa]^2] \\ &= -\frac{180}{\pi^4}\int_0^\infty dk \int_0^\infty d\Omega Im\left[k\ln[1-\rho^{TE}[\Omega]^2]\right] \\ &= \eta^{TE}\end{aligned} \tag{D.2.12}$$

Therefore $\eta_{ev}^{TE} = 0$.

D.2.2 TM-modes: evanescent and ordinary contribution

In this section we will give the exact behavior of the evanescent (E_{ev}) and ordinary (E_{ord}) contributions to the Casimir energy.

$$E_{ord}^{TE} = \frac{\hbar A}{4\pi}\int \frac{d^2\mathbf{k}}{(2\pi)^2}\int_{-\infty}^\infty d\xi \ln[1-\rho_{\mathbf{k}}^{TE}[\imath\xi]^2] \tag{D.2.13}$$

$$E_{ev} + E_{ord}^{TM} = \frac{\hbar A}{4\pi}\int \frac{d^2\mathbf{k}}{(2\pi)^2}\int_{-\infty}^\infty d\xi \ln[1-\rho_{\mathbf{k}}^{TM}[\imath\xi]^2] \tag{D.2.14}$$

We have shown that the TE polarization has no poles in evanescent zone and then gives contributes only to the ordinary part. We have therefore to concentrate our attention only on polarization TM separating evanescent from ordinary part.

It is straightforward to show that

$$\begin{aligned}\ln[1-\rho_{\mathbf{k}}^{TM}[\imath\xi]^2] &= \ln\left(1-\rho^2[\kappa]\right) \\ &+ \ln\left[\frac{\frac{\xi^2}{c^2\kappa^2}+a_+^2[\kappa]}{\frac{\xi^2}{c^2\kappa^2}+a_0^2[\kappa]}\right] + \ln\left[\frac{\frac{\xi^2}{c^2\kappa^2}+a_-^2[\kappa]}{\frac{\xi^2}{c^2\kappa^2}+a_0^2[\kappa]}\right]\end{aligned} \tag{D.2.15}$$

where we put

$$z = \sqrt{1+\frac{\omega_p^2}{c^2\kappa^2}} \tag{D.2.16a}$$

$$\rho[\kappa] \equiv \rho_{\mathbf{k}}^{TE} = e^{-\kappa L}\frac{\kappa-\sqrt{\kappa^2+\frac{\omega_p^2}{c^2}}}{\kappa+\sqrt{\kappa^2+\frac{\omega_p^2}{c^2}}} \tag{D.2.16b}$$

$$a_0[\kappa] = \sqrt{z-1} \tag{D.2.16c}$$

$$a_\pm[\kappa] = a_0[\kappa]\sqrt{\frac{1\pm e^{-\kappa L}}{1\pm\rho[\kappa]}} \tag{D.2.16d}$$

Since the first term on the righthand side of equation (D.2.15) is identical to the TE contribution, E_{ev} is contained exclusively in the second term. Integrating this second

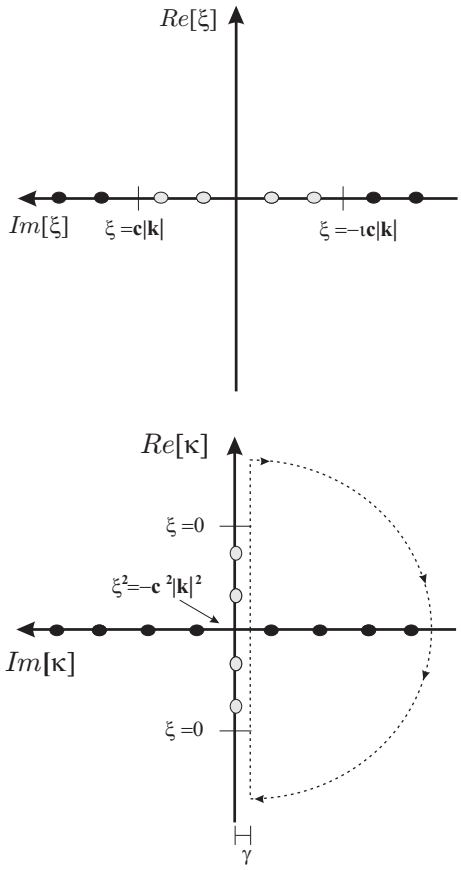

Figure D.1 : Position of zeros. The figure shows the position of the zeros of $1-\rho_{\mathbf{k}}^{TM}$ when we switch the variable from ξ to κ. The gray point indicate zero whose frequency in in the evanescent wave domain.

term over κ in the complex plane along the path shown in fig.D.1 we extract the remaining ordinary waves contribution for the TM polarization. Exploiting the decomposition given in Eq.(D.2.15) and changing again the variable from ξ to $\kappa = \sqrt{\frac{\xi^2}{c^2} + |\mathbf{k}|^2}$ we have

$$\begin{aligned} E_{ord}^{TM} &= \frac{c\hbar A}{(2\pi)^2}\int_0^\infty d\kappa\ \kappa^2 \ln\left(1-\rho^2[\kappa]\right) \\ &+ \frac{c\hbar A}{2\pi}\frac{1}{2}\int \frac{d\mathbf{k}^2}{(2\pi)^2}\oint_C d\kappa \sqrt{\frac{\kappa^2}{\kappa^2-|\mathbf{k}|^2}}\sum_i c_i \ln\left[1-\frac{|\mathbf{k}|^2}{\kappa^2}+a_i^2[\kappa]\right] \end{aligned} \quad \text{(D.2.17)}$$

where C the semicircular path of figure D.1 of radius $R\to\infty$ closed in the clockwise sense. The coefficients $a_i[\kappa]$ are the extensions in κ of a_+,a_- and a_0 and $c_+ = c_- = 1, c_0 = -2$. Note that the path does not touch the axis $Im\,[\kappa] = 0$ to exclude the evanescent contribution. It is separated from it by the positive quantity γ, which will be taken $\gamma \to 0$ only at the end.

The path C
It is worst to stop a second to understand how we have chosen the path C in the previous formula. Suppose we have $z_k \geq 0$.

$$\frac{\hbar}{2}\sum_k z_k = \frac{\hbar}{2}\sum_k \frac{1}{2\pi\imath}\oint_{C_{c.c.s.}} \frac{z}{z-z_k}dz$$

where $C_{c.c.s.}$ is a path which contours the half-plane $\Re z \geq 0$ and which is closed in the counterclockwise sense. We can write further

$$\begin{aligned}\frac{\hbar}{2}\sum_k z_k &= \frac{\hbar}{2}\frac{1}{2\pi\imath}\oint_{C_{c.c.s.}} z\partial_z \ln\prod_k (z-z_k)dz \\ &= \frac{\hbar}{2}\frac{1}{2\pi\imath}\oint_{C_{c.c.s.}} z\partial_z \ln G(z)dz = -\frac{\hbar}{2}\frac{1}{2\pi\imath}\oint_{C_{c.c.s.}} \ln G(z)dz\end{aligned}$$

where $G(z)$ is a generic function that $G(z_k)=0$.We can then write

$$-\frac{\hbar}{2}\frac{1}{2\pi\imath}\oint_{C_{c.c.s.}} \ln G(z)dz = \frac{\hbar}{2}\frac{1}{2\pi}\oint_{C_{c.s.}} \ln G(\imath\xi)d\xi$$

where $C_{c.s.}$ is a path closed in the clockwise sense contouring the half-plane $Im\,[\xi] \leq 0$. Because the transformation $z = \imath\xi$, indeed, the points z_k have been moved from the axis $Re\,[z] \geq 0$ on the axis $Im\,[\xi] \leq 0$.

Exploiting that $a_i[\kappa] \xrightarrow{|\kappa|\to\infty} 0$, the integral over the semicircular part of C vanishes in the limit $R \to \infty$. Inverting the order of integration of $|\mathbf{k}|$ and κ and integrating by part we obtain

$$\begin{aligned}E_{ord}^{TM} &= \frac{c\hbar A}{(2\pi)^2}\int_0^\infty d\kappa\kappa^2 \ln\left(1-\rho^2[\kappa]\right) \\ &- \frac{c\hbar A}{(2\pi)^2}\int_{-\imath\gamma}^{\infty-\imath\gamma} d\kappa \sum_i c_i\kappa^2 \left[\sqrt{1-\frac{|\mathbf{k}|^2}{\kappa^2}}\ln\left[1-\frac{|\mathbf{k}|^2}{\kappa^2}+a_i^2[\kappa]\right]\right]_{|\mathbf{k}|=0}^{|\mathbf{k}|=\infty} \\ &+ \frac{c\hbar A}{(2\pi)^2}\int_{-\imath\gamma}^{\infty-\imath\gamma} d\kappa \sum_i c_i\kappa^2 \left[2\sqrt{1-\frac{|\mathbf{k}|^2}{\kappa^2}}\right]_{|\mathbf{k}|=0}^{|\mathbf{k}|=\infty} \\ &- \frac{c\hbar A}{(2\pi)^2}\int_{-\imath\gamma}^{\infty-\imath\gamma} d\kappa \sum_i c_i\kappa^2 \left[2a_i[\kappa]\arctan[\frac{\sqrt{1-\frac{|\mathbf{k}|^2}{\kappa^2}}}{a_i[\kappa]}]\right]_{|\mathbf{k}|=0}^{|\mathbf{k}|=\infty}\end{aligned} \tag{D.2.18}$$

Using

$$(1+a_+^2[\kappa])(1+a_-^2[\kappa]) = (1+a_0^2[\kappa])^2 \tag{D.2.19}$$

and inserting the value of the coefficients c_i, we obtain

$$E_{ord}^{TM} = \frac{c\hbar A}{(2\pi)^2}\int_0^\infty d\kappa\kappa^2 \ln\left(1-\rho^2[\kappa]\right) + \frac{c\hbar A}{2\pi^2}\int_0^\infty d\kappa\ \kappa^2\left[\phi(a_+)+\phi(a_+)-2\phi(a_0)\right] \tag{D.2.20}$$

with $\phi(a)$ defined as

$$\phi(a) = a\arctan\left[\frac{1}{a}\right] - \frac{\pi}{2}a = -a\arctan\left[a\right] \tag{D.2.21}$$

Here we have taken the limit $\gamma \to 0$ (none of the functions involved in the expression of E_{ord}^{TM} shows singularities on the real axis).

Finally we have that

$$\begin{aligned} E_{ord} &= E_{ord}^{TE} + E_{ord}^{TM} = \frac{c\hbar A}{2\pi^2}\int_0^\infty d\kappa\kappa^2 \ln\left(1-\rho^2[\kappa]\right) \\ &+ \frac{c\hbar A}{2\pi^2}\int_0^\infty d\kappa\kappa^2\left[\phi(a_+)+\phi(a_+)-2\phi(a_0)\right] \end{aligned} \tag{D.2.22}$$

The expression for E_{ev} can easily be obtained by the difference with respect to the expression of E obtained in the previous papers which can be put in a form similar to E_{ord} making the change

$$\phi(a) \to \psi(a) = a\arctan\frac{1}{a}. \tag{D.2.23}$$

This procedure leads to the following expressions for $E_{ev} = E - E_{ord}$

$$E_{ev} = \frac{cA}{2\pi}\int_0^\infty \frac{\hbar\kappa^2}{2}\left(a_+ + a_- - 2a_0\right)d\kappa = \eta_{ev}E_{Cas} \tag{D.2.24}$$

Where η_{ev} can be written as

$$\eta_{ev} = -\frac{180}{2\pi^3}\int_0^\infty \sum_i c_i g_i(z)dz \tag{D.2.25}$$

Bibliography

[1] M. Planck, Verh. Deutsch. Phys. Ges. **2** (1900), 237.

[2] P. W. Milonni and M. L. Shih, *Zero-point energy in early quantum theory*, Am. J. Phys. **59** (1991), 684.

[3] A. Einstein and O. Stern, Ann. Physik **40** (1913), 551.

[4] P. Debye, Ann. Physik **43** (1914), 49.

[5] R. Mulliken, Nature **114** (1924), 349.

[6] W. Nernst, Verh. Deutsch. Phys. Ges. **18** (1916), 83.

[7] R. J. Adler, B. Casey, and O. C. Jacob, *Vacuum catastrophe: An elementary exposition of the cosmological constant problem*, Am. J. Phys. **63** (1995), 620.

[8] L. Abbott, *The Mystery of the Cosmological Constant*, Sci. Am. **258** (1988), 106.

[9] S. Weinberg, *The cosmological constant problem*, Rev. Mod. Phys. **61** (1989), 1.

[10] J. van der Waals Academisch Proefschrift, 1873 (Leiden).

[11] F. London, *Zur Theorie und Systematik der Molekularkräfte*, Z. Physik **63** (1930), 245.

[12] E. Verweey and J. Overbeek, *Theory of the Stability of Lyophobic Colloids*, Elsevier Science Publishers, 1948.

[13] M. Sparnaay, *Physics in the Making*, Elsevier Science Publishers, 1989.

[14] H. B. G. Casimir and D. Polder, *The Influence of Retardation on the London-van der Waals Forces*, Phys. Rev. **73** (1948), 360.

[15] H. Casimir, J. Chimie Phys. **46** (1949), 407.

[16] ———, *On the attraction between two perfectly conducting plates*, Proc. kon. Ned. Ak. Wet **51** (1948), 793.

[17] P. Causse *L'album du marin* Mante, Charpentier, 1836.

[18] S. L. Boersma, *A maritime analogy of the Casimir effect*, Am. J. Phys. **64** (1996), 539.

[19] J. Overbeek and M. Sparnaay, Proc. Kon. Ned. Akad. Wetenschap **54** (1951), 387.

[20] B. Derjaguin, I. Abrikosova, and E. Lifshitz, Quart. Revs. **10** (1956), 33.

[21] B. Derjaguin and I. Abrikosova, Sov. Phys. JETP **3** (1957), 819.

[22] M. Sparnaay, Nature **180** (1957), 334.

[23] B. Derjaguin and I. Abrikosova, J. Phys. Chem. Solid **5** (1958), 1.

[24] ———, Sci. Am. **203** (1960), 47.

[25] W. Black, J. D. Jongh, J.Th.G.Overbeek, and M. Sparnaay, Trans. Faraday Soc. **56** (1960), 1597.

[26] D. Tabor and R. Winterton, Nature **219** (1968), 1120.

[27] G. Rouweler and J. Overbeek, J. Chem. Soc. Faraday Transactions **I 67** (1971), 2117.

[28] J. Israelachvili and D. Tabor, Proc. Roy. Soc. Lond. **A331** (1972), 19.

[29] S. Hunklinger, H. Geisselmann, and W. Arnold, Rev. Sci. Instr. **43** (1972), 584.

[30] E. Sabisky and C. Anderson, *Verification of the Lifshitz Theory of the van der Waals Potential Using Liquid-Helium Films*, Phys. Rev. A **7** (1973), 790.

[31] L. White, J. Israelachvili, and B. Ninham, J. Chem. Soc. Faraday Transactions **72** (1976), 2526.

[32] P. van Blokland and J. Overbeek, J. Chem. Soc. Faraday Transactions **I 74** (1978), 2637.

[33] B. Derjaguin, Y. Rabinovich, and N. Churaev, Nature **272** (1978), 313.

[34] W. Arnold, S. Hunklinger, and K. Dransfeld, *Influence of optical absorption on the Van der Waals interaction between solids*, Phys. Rev. B **19** (1979), 6049.

[35] B. Derjaguin, N. Churaev, and V. Muller, *Surface Forces*, Plenum, 1987.

[36] S. Lamoureaux, *Demonstration of the Casimir Force in the 0.6 to 6 μm range*, Phys. Rev. Lett. **78** (1997), 5.

[37] U. Mohideen and A. Roy, *Precision Measurement of the Casimir Force from 0.1 to 0.9 μm*, Phys. Rev. Lett. **81** (1998), 4549.

[38] A. Roy, C. Lin, and U. Mohideen, *Improved precision measurement of the Casimir force*, Phys. Rev. D **60** (1999), 111101.

[39] B. Harris, F. Chen, and U. Mohideen, *Precision measurement of the Casimir force using gold surfaces*, Phys. Rev. A **62** (2000), 052109.

[40] T. Ederth, *Template-stripped gold surfaces with 0.4-nm rms roughness suitable for force measurements: Application to the Casimir force in the* $20 \div 100$*-nm range*, Phys. Rev. A **62** (2000), 062104.

[41] H. Chan, V. Aksyuk, R. Kleiman, D. Bishop, and F. Capasso, *Quantum Mechanical Actuation of Microelectromechanical Systems by the Casimir Force*, Science **291** (2001), 1941.

[42] H. B. Chan, V. A. Aksyuk, R. N. Kleiman, D. J. Bishop, and F. Capasso, *Nonlinear Micromechanical Casimir Oscillator*, Phys. Rev. Lett. **87** (2001), 211801.

[43] E. Buks and M. L. Roukes, *Metastability and the Casimir effect in micromechanical systems*, EuroPhys. Lett. **54** (2001), 220.

[44] G. Bressi, G. Carugno, R. Onofrio, and G. Ruoso, *Measurement of the Casimir Force between Parallel Metallic Surfaces*, Phys. Rev. Lett. **88** (2002), 041804.

[45] M. Bordag, U. Mohideen, and V. Mostepanenko, *New Development in the Casimir Effect*, Phys. Rep. **353** (2001), 1.

[46] A. Lambrecht and S. Reynaud, *Recent experiments on the casimir effect: Description and analysis*, in Poincaré Seminar 2002. Vacuum Energy, (B. . V. Rivasseau, ed.) Birkhauser, 2003, p. 109 (http://xxx.lanl.gov/abs/quant-ph/0302073).

[47] E. Lifshitz, Sov. Phys.-JETP (USA) **2** (1956), 73.

[48] L. Landau, E. Lifshitz, and L. Pitaevskii, *Course of Theoretical Physics: Electrodinamics in Continuous Media*, Butterworth-Heinmann, Oxford, 1980.

[49] G. Plunien, B. Müller, and W. Greiner, *The Casimir effect*, Phys. Rep. **134** (1986), 87.

[50] V. Mostepanenko and N. Trunov, *The Casimir effect and its application*, Clarendon, 1997.

[51] E. Elizalde and A. Romeo, *Essentials of the Casimir effect and its computation*, Am. J. Phys. **59** (1991), 711.

[52] S. Lamoreaux, *Resource Letter CF-1: Casimir Force*, Am. J. Phys. **67** (1999), 850.

[53] B. Duplantier and V. Rivasseau Séminaire Poincaré du 9 mars 2002, 2002.

[54] G. Carugno, Z. Fontana, R. Onofrio, and C. Rizzo, *Limits on the existence of scalar interactions in the submillimeter range*, Phys. Rev. D **55** (1997), 6591.

[55] E. Fischbach and C. Talmadge, *The Search for Non Newtonian Gravity*, AIP Press/Springer Verlag, 1998.

[56] M. Bordag, B. Geyer, G. Klimchitskaya, and V. Mostepanenko, *Stronger constraints for nanometer scale Yukawa-type hypothetical interactions from the new measurement of the Casimir force*, Phys. Rev. D **60** (1999), 055004.

[57] E. Fischbach and D. Krause, *New Limits on the Couplings of Light Pseudoscalars from Equivalence Principle Experiments*, Phys. Rev. Lett. **82** (1999), 4753.

[58] J. Long, H. Chan, and J. Price, Nucl. Phys. B **539** (1999), 23.

[59] C. D. Hoyle, U. Schmidt, B. R. Heckel, E. G. Adelberger, J. H. Gundlach, D. J. Kapner, and H. E. Swanson, *Submillimeter Test of the Gravitational Inverse-Square Law: A Search for "Large" Extra Dimensions*, Phys. Rev. Lett. **86** (2001), 1418.

[60] E. Adelberger, *Sub-mm tests of the gravitational inverse-square law*, *preprint*.

[61] J. C. Long, H. W. Chan, A. B. Churnside, E. A. Gulbis, M. C. M. Varney, and J. C. Price, *New Experimental Limits on Macroscopic Forces Below 100 Microns*, *preprint*.

[62] A. Lambrecht and S. Reynaud, *Casimir force between metallic mirrors*, Euro. Phys. J. D **8** (2000), 309.

[63] M. Boström and B. E. Sernelius, *Thermal Effects on the Casimir Force in the* $0.1 \div 5$ *μm Range*, Phys. Rev. Lett. **84** (2000), 4757.

[64] V. Svetovoy and M. Lokhanin, *Linear temperature correction to the Casimir force* , Phys. Lett. A **280** (2001), 177.

[65] M. Bordag, B. Geyer, G. Klimchitskaya, and V. Mostepanenko, *Casimir Force at Both Nonzero Temperature and Finite Conductivity*, Phys. Rev. Lett. **85** (2000), 503.

[66] S. Lamoreaux, *Comment on "Thermal Effects on the Casimir Force in the* $0.1 \div 5$ *μm Range"*, Phys. Rev. Lett. **87** (2001), 139101.

[67] B. E. Sernelius, *Sernelius Replies*, Phys. Rev. Lett. **87** (2001), 139102.

[68] B. E. Sernelius and M. Boström, *Comment on "Casimir Force at Both Nonzero Temperature and Finite Conductivity"*, Phys. Rev. Lett. **87** (2001), 259101.

[69] M. Bordag, B. Geyer, G. Klimchitskaya, and V. Mostepanenko, *Bordag, Geyer, Klimchitskaya, and Mostepanenko Reply*, Phys. Rev. Lett. **87** (2001), 259102.

[70] G. Klimchitskaya and V. Mostepanenko, *Investigation of the temperature dependence of the Casimir force between real metals*, Phys. Rev. A **63** (2001), 062108.

[71] V. Bezerra, G. Klimchitskaya, and V. Mostepanenko, *Thermodynamical aspects of the Casimir force between real metals at nonzero temperature*, Phys. Rev. A **65** (2002), 052113.

[72] J. Torgerson and S. Lamoreaux, *The Low-Frequency Character of the Thermal Correction to the Casimir Force between Metallic Films*, *preprint*.

[73] C. Genet, *La Force de Casimir entre deux mirroirs métalliques à température non nulle*, PhD thesis, Univ. Paris VI, 2002.

[74] V. M. M. B. V. Derjaguin and Y. P. Toporov, *Effect of contact deformations on the adhesion of particles*, J. of Colloid and Interface Science **53** (1975), 314.

[75] D. Langbein, J. Phys. Chem. Solids **32** (1971), 1657.

[76] J. K. et al., J. Colloid and Interface Sci. **67** (1978), 140.

[77] R. Balian and B. Duplantier, *Electromagnetic waves near perfect conductors. II. Casimir effect* , Annals of Phys. **112** (1978), 165.

[78] C. Genet, A. Lambrecht, P. M. Neto, and S. Reynaud, *The Casimir force between rough metallic plates*, Europhys. Lett. **62** (2003), 484.

[79] P. A. M. Neto, A. Lambrecht, and S. Reynaud, *Roughness correction to the Casimir force: Beyond the Proximity Force Approximation*, Europhys. Lett. **69** (2005), 924.

[80] P. M. Neto, A. Lambrecht, and S. Reynaud, *preprint*.

[81] C. Itzykson and J.-B. Zuber, *Quantum Fielf Theory*, McGraw-Hill, New York, 1985.

[82] M. Abramowitz and I. Stengun, *Handbook of Mathematical Functions*, Dover Books, New York, 1971.

[83] M.-T. Jaekel and S. Reynaud, *Casimir force between partially transmitting mirrors*, J. de Phys. **I-1** (1991), 1395.

[84] C. Genet, A. Lambrecht, and S. Reynaud, *Casimir force and the quantum theory of lossy optical cavities*, Phys. Rev. A **67** (2003), 043811.

[85] J. Jackson, *Classical Electrodynamics*, John Wiley and Sons Inc., New York, 1975.

[86] G. Barton, *Some surface effects in the hydrodynamic model of metals*, Rep. Prog. Phys. **42** (1979), 963.

[87] J. Heinrichs, *Theory of van der Waals interactions between metal surfaces*, Phys. Rev. B **11** (1975), 3625.

[88] N. Van Kampen, B. Nijboer, and K. Schram, *On the macroscopic theory of Van Der Waals forces*, Phys. Lett. **26A** (1968), 307.

[89] S. Raimes, *The theory of plasma oscillations in metals*, Rep. Prog. Phys. **20** (1957), 1.

[90] C. Genet, F. Intravaia, A. Lambrecht, and S. Reynaud, *Electromagnetic vacuum fluctuations, Casimir and van der Waals forces*, Ann. Fond. L. de Broglie **29** (2004), 311.

[91] C. Henkel, K. Joulain, J.-P. Mulet, and J.-J. Greffet, *Coupled surface polaritons and the Casimir force*, Phys. Rev. A **69** (2004), 023808.

[92] F. Chen, G. Klimchitskaya, U. Mohideen, and V. Mostepanenko, *Theory confronts experiment in the Casimir force measurements: Quantification of errors and precision*, Phys. Rev. A **69** (2004), 022117.

[93] T. Ebbesen, H. Lezec, H. Ghaemi, T. Thio, and P. Wolff, *Extraordinary optical transmission through sub-wavelength hole arrays*, Nature **391** (1998), 667.

[94] L. Martín-Moreno, F. J. García-Vidal, H. J. Lezec, K. M. Pellerin, J. B. P. T. Thio, and T. W. Ebbesen, *Theory of Extraordinary Optical Transmission through Subwavelength Hole Arrays*, Phys. Rev. Lett. **86** (2001), 1114.

[95] E. Altewischer, M. van Exter, and J. Woerdman, *Plasmon-assisted transmission of entangled photons*, Nature **418** (2002), 304.

[96] M. Planck, Verh. Deutsch. Phys. Ges. **13** (1911), 138.

[97] D. Sciama, *The Philosophy of Vacuum*, Clarendon, 1991, p. 137.

[98] E. Gunzig and S. Diner, *Le vide : univers du tout ou du rien*, Editions Complexe, 1998.

[99] O. Darrigol, Ann. Physik **9** (2000), 951.

[100] A. Einstein, Am. J. Phys. **33** (1965), 367 ((Translation)).

[101] ———, Phys. Z. **10** (1909), 185.

[102] ———, Phys. Z. **18** (1917), 121.

[103] E. Wolf Opt. News, 1979 (Winter issue).

[104] S. Bose, Z. Phys. **26** (1924), 178.

[105] A. Einstein, Sitzungsber, Berlin, 1924, Chap. Phys. Math. Kl., p. 261.

[106] ———, Sitzungsber, Berlin, 1925, Chap. Phys. Math. Kl., p. 3.

[107] P. Dirac, *The Principles of Quantum Mechanics*, Oxford University Press, 1958.

[108] ———, Proc. Roy. Soc. Lond. **114** (1927), 243.

[109] W. Heisenberg, Z. Phys. **43** (1927), 172.

[110] M. Demianski, *History of the Cosmological Constant*, Ann. Phys. (Leipzig) **9** (2000), 278.

[111] K. Schram, *On the macroscopic theory of retarded Van Der Waals forces*, Phys. Lett. **43A** (1973), 282.

[112] T. H. Boyer, *Quantum Electromagnetic Zero-Point Energy of a Conducting Spherical Shell and the Casimir Model for a Charged Particle*, Phys. Rev. **174** (1968), 1764.

[113] P. W. Milonni, *The Quantum Vacuum*, Academic Press Inc., San Diego, 1994.

[114] I. Gradshteyn and I. Ryzhik, *Table of Integrals, Series and Products*, Fifth edition, Academic Press, San Diego, 1994.

[115] R. Balian and B. Duplantier, *Geometry of the Casimir Effect*, *preprint*, 2004.

[116] M. Schaden and L. Spruch, *Classical Casimir effect: The interaction of ideal parallel walls at a finite temperature*, Phys. Rev. A **65** (2002), 034101.

[117] C. Genet, A. Lambrecht, and S. Reynaud, *Temperature dependence of the Casimir effect between metallic mirrors*, Phys. Rev. A **62** (2000), 012110.

[118] S. Barnet, C. Gilson, B. Huttner, and N. Imoto, *Field Commutation Relations in Optical Cavities*, Phys. Rev. Lett. **77** (1996), 1739.

[119] F. Grassia, *Fluctuations quantiques et thermiques dans le transducteurs electro-mecaniques*, PhD thesis, Université Pierre et Marie Curie, 1998.

[120] L. Mandel and E. Wolf, *Optical Coherence and Quantum Optics*, Cambridge University Press, New York, 1995.

[121] S. Haroche, *New Trends in Atomic Physics*, North Holland, 1984, p. 193.

[122] H. Breuer and F. Petruccione, *The Theory of Open Quantum Systems*, Oxford University Press, Oxford, 2002.

[123] J. Paz and W. Zurek, *Lecture Notes in Physics*, Vol. 587, Springer-Verlag GmbH, 2002, p. 77.

[124] G. Ford and M. Kac, *On the Quantum Langevin Equation*, Journal of Stat. Phys. **46** (1987), 803.

[125] A. O. Caldeira and A. J. Leggett, *Influence of Dissipation on Quantum Tunneling in Macroscopic Systems*, Phys. Rev. Lett. **46** (1981), 211.

[126] F. Intravaia, S. Maniscalco, and A. Messina, *Density-matrix operatorial solution of the non-Markovian master equation for quantum Brownian motion*, Phys. Rev. A **67** (2003), 042108.

[127] S. Maniscalco, J. Piilo, F. Intravaia, F. Petruccione, and A. Messina, *Lindblad- and non-Lindblad-type dynamics of a quantum Brownian particle*, Phys. Rev. A **70** (2004), 032113.

[128] A. Lambrecht, M.-T. Jaekel, and S. Reynaud, *The Casimir force for passive mirrors*, Phys. Lett. A **225** (1997), 188.

[129] A. I. Markusevic, *Elements of Theory of Analytic Functions*, Mir, Moscow, 1988.

[130] A. Eguiluz, *Density response function and the dynamic structure factor of thin metal films: Nonlocal effects*, Phys. Rev. B **19** (1979), 1689.

[131] A. Eguiluz, S. C. Ying, and J. J. Quinn, *Influence of the electron density profile on surface plasmons in a hydrodynamic model*, Phys. Rev. B **11** (1975), 2118.

[132] G. Feinberg and J. Sucher, *General Theory of the van der Waals Interaction: A Model-Independent Approach*, Phys. Rev. A **2** (1970), 2395.

[133] R. H. Ritchie, *Plasma Losses by Fast Electrons in Thin Films*, Phys. Rev. **106** (1957), 874.

[134] P. M. Morse and H. Feshbach, *Methods of Theoretical Physics*, McGraw-Hill Publishing Company, New York, 1953.

[135] R. Esquivel and V. B. Svetovoy, *Correction to the Casimir force due to the anomalous skin effect*, Phys. Rev. A **69** (2004), 0162102.

[136] R. Esquivel, C. Villarreal, and W. L. Mochán, *Exact surface impedance formulation of the Casimir force: Application to spatially dispersive metals*, Phys. Rev. A **68** (2003), 0152103.

[137] ———, *Erratum: Exact surface impedance formulation of the Casimir force: Application to spatially dispersive metals [Phys. Rev. A 68, 052103 (2003)]*, Phys. Rev. A **71** (2005), 029904(E).

[138] R. Balian, *Du micorscopique au macroscopique*, Seventh edition, Ecole Politechnique - Ellipses, Paris, 1982.

[139] C. Kittel, *Introduction to Solid State Physics*, Fourth edition, John Wiley and Son Inc.

[140] W. Barnes, *Quantum physics: Survival of the entangled*, Nature **418** (2002), 281.

[141] G. L. Klimchitskaya, A. Roy, U. Mohideen, and V. M. Mostepanenko, *Complete roughness and conductivity corrections for Casimir force measurement*, Phys. Rev. A **60** (1999), 3487.

[142] K. A. Milton, *The Casimir effect: Recent controversies and progress*, J. Phys. A.: Math. Gen. **37** (2004), R209.

[143] E. Gerlach, *Equivalence of van der Waals Forces between Solids and the Surface-Plasmon Interaction*, Phys. Rev. B **4** (1971), 393.

[144] C. K. Carniglia and L. Mandel, *Quantization of Evanescent Electromagnetic Waves*, Phys. Rev. D **3** (1971), 280.

[145] I. Bialynicki-Birula and J. B. Brojan, *Completeness of Evanescent Waves*, Phys. Rev. D **5** (1972), 485.

[146] M. Born and E. Wolf, *Principles of Optics*, Seventh edition, Cambridge University Press, Cambridge, 1999.

[147] E. Hecht, *Optics*, Second edition, Addison-Wesley Publishing Company, Amsterdam, 1989.